学位論文

# A study on extrasolar cometary source populations with the AKARI far-infrared all-sky survey

(『あかり』遠赤外線全天観測データを用いた系外彗星雲の研究)

平成 26 年 12 月博士 (理学)　申請

東京大学大学院理学系研究科

天文学専攻

有松 亘

# Abstract

This thesis describes a search for cometary source populations (CSPs), corresponding to the scattered disk (SD) and the Oort cloud (OC), in extrasolar systems, using far-infrared all-sky map obtained with the Far-Infrared Surveyor (FIS) onboard the *AKARI* satellite.

The SD and the OC are proposed for the origin of comets, and are thought to constitute major building blocks of the solar system. Objects resided in these CSPs are thought to be remnants of the planetesimals originally in the protoplanetary disk, which are scattered by giant planets during early stages of the planetary system formation. Unveiling analogues of these populations in extrasolar systems is fundamental to understanding an unknown nature of the outer (astrocentric distances of $> 1000$ AU) solar and extrasolar systems, and formation and evolution scenarios of typical stellar systems. One of the most effective diagnostic methods for the extrasolar CSP (exo-CSP) detection is infrared radiometry. The spatial and spectral properties of the far-infrared (FIR) emission around stars provide a direct evidence for the existence of the exo-CSPs. However, there has been lack of observational constraints on the FIR emission from the exo-CSPs so far, especially at larger astrocentric distances ($10^3 - 10^4$ AU). Therefore I have carried out a search for the infrared emission from the CSPs around nearby stars with the far-infrared all-sky map taken by the *AKARI*/FIS. The sensitivity of the *AKARI*/FIS survey is still insufficient to detect the exo-CSPs around arbitral types of stars. Therefore I have selected nearby A-type stars for the targets, where the FIR emission is expected to be strong. In addition, I have carried out a stacking analysis to search for the emission from the exo-CSPs fainter than detection-limits.

The *AKARI*/FIS all-sky maps are calibrated only for diffuse sources. Therefore additional calibrations for point sources are carried out in order to perform accurate spatial and spectral studies of the exo-CSPs. Radial brightness profiles (RBPs) of point spread functions (PSFs) are determined using the stacked images of infrared standard stars, and are confirmed to be stable within the investigated flux range $(0.06 - 12$ Jy) at the $90\,\mu$m band. Furthermore, aperture photometry of faint infrared standard stars is performed, and measured fluxes are compared with emission model values to derive photometric calibration factors. I have checked whether the calibration factors of the stacked point sources depend on the fluxes of the sources or not. Any flux dependence in the calibration factors with amplitude larger than $\sim 20\%$ is not seen on the investigated flux ranges of $0.1 - 19, 0.06 - 12$, and $0.02 - 3.7$ Jy at the 65, 90, and $140\,\mu$m bands, respectively.

Based on a data set of 3583 A-type stars located inside 158 pc from the Sun, stacking analyses have been performed with three appropriate distance bins ($15.8 - 39.8$ pc, $39.8 - 100$ pc, and $100 - 158$ pc bins) using the *AKARI*/FIS all-sky map at the 65, 90, and $140\,\mu$m bands. The photometry of the stacked image presents a FIR excess emission that comes from closer than 2600 AU from the parent stars, and corresponds a $\sim 120$ K blackbody with a fractional luminosity (the energy contribution of the excess to the stellar photospheric emission) of $\sim 5 \times 10^{-5}$. These properties are in agreement with the average properties of known debris disks around A-type stars. In addition to the debris disk component, a colder excess component corresponding to the $\sim 23$ K modified blackbody emission with a fractional luminosity of an order of $10^{-5}$ is seen in the annulus corresponding physical radii of $2600-6600$ AU. In order to make a constraint on a spatial distribution of the cold excess component, RBPs are derived from the stacked images at the $90\,\mu$m band. The RBPs indicate that the emission structure extends to approximately 5000 AU, which is larger than the typical debris-disk sizes (smaller than 1000 AU).

In order to evaluate the significance of the present detection, I have performed four tests. First, I have carried out a median stacking analysis that is thought to be more robust to contamination from background point sources. The median stack and average stack to the same sample give consistent results of the cold excess fluxes. I thus found no evidence of the cold excess emission from the background objects. Second, I have performed a stacking analysis of sub-groups of the sample and found that the observed cold excess fluxes are not due to anomalous contribution from minor samples. For the third test, the cold excess fluxes are compared with those derived from stacks of randomly selected blank regions, and are found to be above the statistical background fluctuations with significances of up to $\sim 2.5\sigma$. Finally, I have derived the RBPs of four sub-regions of the stacked image, and found no evidence of the contamination of local background inhomogeneities to the observed profile.

Assuming the observed cold excess comes from the circumstellar dust grains around the stacked stars, the excess can be explained by the thermal emission from micron-sized grains with the mass of $\sim 0.1\,\mathrm{M_{earth}}$. Taking interstellar diffusion timescales of the grains into consideration, these grains can be supplied form object groups with the total mass of $\sim 10-100\,\mathrm{M_{earth}}$, which is comparable to the OC of the solar system, via several possible replenish processes. The present results indicate that the

CSPs are not exceptional products of typical stellar system formations.

# Contents

Chapter1

# Introduction

Figure1.1 An example of the long-period comets, C/2013 R1 (Lovejoy). The spherical atmosphere, "coma", is seen as a green spot at the image center, whereas the blue, straight tail is streaming from the coma to the upper left of the image. This image is taken by the author from Kiso Observatory, Japan, on December 4th 2013. Image details: camera: Olympus EM-5 + 45mm F1.8 (F2.2), gain: ISO1600, 65 × 3 second exposure.

## 1.1 Cometary source populatins

### 1.1.1 Comets and their origins

The solar system comprises the Sun, eight planets, five dwarf planets, moons and rings around the planets, and other small bodies and dust including zodiacal dust particles, asteroids, Kuiper Belt objects, and comets, according to the latest definitions and knowledge. Most comets have larger orbits (i.e., larger semimajor axes) with wider ranges of inclinations and eccentricities, compared with those of the known major and minor planets. When they approach to the Sun at their perihelia, the comets usually inhabit atmospheric spheres (called as "comas") and tails, which are seen at optical (see Figure 1.1) and other wavelengths. These coma and tail structures are formed with gas and dust that are ejected by the sublimation of volatile ices from a cometary nucleus, and are illuminated by the Sun. These comets are thought to supply the volatile materials and the dust grains in the interplanetary space and the planets including the Earth (e.g., Greenwood et al. 2011).

Comets are sorted according to their orbital characteristics and classified into two groups. Comets with semimajor axes larger than $\sim 40$ AU are referred to as "Long Period Comets" (LPCs), and the other comets are sorted to be "Short Period Comets" (SPCs). Most of the LPCs have orbits with isotropic inclinations. These LPCs have been thought to come from a shell-like reservoir called "Oort cloud" (OC). The idea of the OC was postulated by Oort (1950), who investigated the orbital characteristics of the comets. Figure 1.2 presents the distribution of the orbital energies of the LPCs, which is reproduced from Dones et al. (2004). Figure 1.2a shows the "osculating" orbital energies, which are derived from the semimajor axes of the LPCs measured during their perihelion passages, i.e., when the comets are orbiting with the heliocentric distances of about $< 5$ AU. The majority of the osculating energies distribute below zero; these comets are apparently weakly unbound, and seem to come from outside the solar system. In fact, this trend results from the gravitational perturbation by the major planets located within 40 AU from the Sun (the inner solar system). The "original" orbital energies, which are shown in Figure 1.2b, are the energies of the comets before the perturbations by the planets during the latest

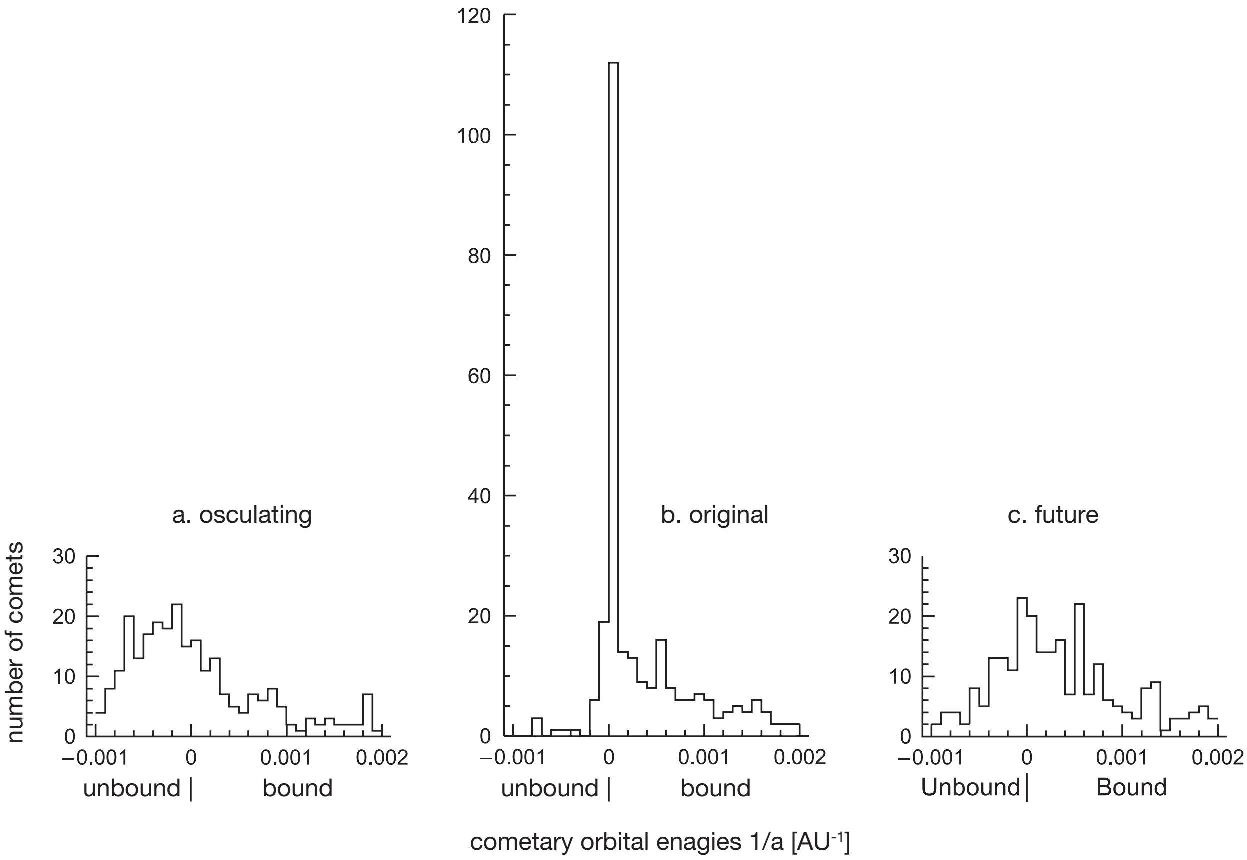


Figure1.2 Histgram of the number of known LPCs as a function of the orbital energies, $E \equiv 1/a$, the inverse of their orbital semimajor axes in AU. If $E < 0$, comets are weakly unbound to the solar system, and have hyperbolic orbits. On the other hand, comets with $E > 0$ are weakly bounded, and have elliptic orbits. Each panel shows the orbital energies of comets directly derived from the observed semimajor axis ("osculating", a), energies derived by correcting the gravitational effects ("original", b), and energies after passing through the inner solar system ("future", c), respectively. The orbital energies are quoted from the *Catalogue of Cometary Orbits*, and the figure reproduced from Dones et al. (2004).

perihelion passages, which are derived by orbital integration. The original energy distribution has a sharp peak at the corresponding semimajor axis of $\sim 27000\,\mathrm{AU}$. Oort thought that this spike represents the typical orbital energy of the source of the LPCs, i.e., the OC. The orbital energies after passing through the inner solar system are derived by orbital integration, and their distribution is shown in Figure 1.2c. This "future" orbital distribution does not show the peak seen in the original distribution, and indicates that the most of the comets will never go back to their original source; comets with negative energy values will be ejected from the solar system, whereas those with larger positive values will be more tightly bound orbits with smaller aphelia.

Since they are weakly bounded to the Sun, objects in the OC can be perturbed by nearby passing stars and molecular clouds, as well as long-term effects of nearby galactic matter ("Galactic tides"; Holmberg & Flynn 2000). Several perturbed objects reduce the perihelion distances and enter into the inner solar system. Dynamical simulations indicate that the comets represent the outermost of the cloud, where the gravitational perturbations much more effectively disrupt the orbits (Hills, 1981). Therefore, the sharp peak of the original cometary semimajor axis distribution (see Figure 1.2b) does not represent the real distribution of the OC objects, but is due to the selection effect. The properties of the inner-side of the OC (the inner OC) remains unknown; the comets in the inner OC do not enter the inner solar system via usual perturbations because they are more tightly bound to the Sun.

The SPCs are sorted into two groups according to their semimajor axes. The SPCs having relatively larger semimajor axes ($7.4 \leq a \leq 40$AU) are called as Halley-type comets (HTCs). On the other hand, comets with their semimajor axes smaller than 7.4 AU are classified as Jupiter-family comets (JFCs). The HTCs have nearly isotropic inclinations (median $i \sim 64^\circ$, Dones et al. 2004), and are thought to arise from the OC (Levison et al., 2001). On the other hand, the JFCs have smaller inclinations (median $i \sim 11^\circ$, Dones et al. 2004), and are suggested to come from a different origin that contains low-inclination sources. As the source of the JFCs, a low inclination source called Edgeworth-Kuiper belt was firstly proposed (Joss, 1973; Fernández, 1980; Duncan et al., 1988). However, recent dynamical simulations suggest that these "classical" Kuiper-belt objects, objects with lower inclinations and eccentricities, are not the primary source of the JFC (Duncan et al., 2004). Currently, these comets are thought to come from the scattered disk (SD, Duncan & Levison 1997; Duncan et al. 2004; Volk & Malhotra 2008) rather than the classical Kuiper belt. Objects in the SD are thought to have relatively higher eccentricity (i.e., aphelion distances) and higher inclinations than the classical Kuiper belt objects. From the SD, the JFCs can be supplied much more efficiently than the classical Kuiper belt (Duncan et al., 2004).

### 1.1.2 Origins of the CSPs

The cometary objects in the "cometary source populations" (CSPs), such as the OC and the SD, could not have formed in situ, because objects are not thought to have grown bigger than meter-sized beyond $\sim 50$ AU from the Sun (Weidenschilling, 2003). According to theoretical calculations (Duncan et al., 1987; Dones et al., 2004), these objects are thought to be originally formed in the inner solar system, and ejected into the present locations through gravitational perturbations by the major planets.

The early stages of the solar systems are thought to consist of the planets and many remaining planetesimals in the planetesimal disk with semimajor axes less than 50 AU (Weidenschilling, 2003). These planetesimals are gravitationally perturbed by giant planets. Through the perturbations, a fraction of the scattered planetesimals gained larger aphelion distances. Then, perturbations from passing stars and giant molecular clouds, and the tidal force from the Galactic disk ("Galactic tide") change the orbital characteristics of the planetesimals passing their aphelia; these perturbations increase perihelion distances of the planetesimals, and randomize their inclination distributions. Dynamical simulations indicate that the Galactic tide is the major perturber for the planetesimals with larger aphelia (Harrington, 1985; Heisler

& Tremaine, 1986). Since the perturbations of the planetesimal disk are initially required to achieve the extended orbital distributions of the CSPs, giant planets are thought to be essential for the CSP formations.

The numerical simulations of the CSP formations infer the present properties of the OC (and SD). According to the simulations, the objects in the OC are expected to distribute with heliocentric distances of $\sim 10^5$ AU, where the gravitational force of the Sun becomes comparable to the interstellar gravitational effects. On the other hand, these simulations indicate that the inner OC is expected to contain a large number of cometary objects equivalent to (Dones et al., 2004), or larger than that of the outer OC (Duncan et al., 1987), which are concentrated on an inner edge of the cloud located at $\sim$ a few thousand AU. According to the simulations by Duncan et al. (1987), the radial number density of the OC objects is expected to proportional to a power-law function of radius $r$, $r^{-\eta}$ with an index $\eta$ of $\eta \sim 3.5$. This result suggests that the mass of the cometary objects with semimajor axes of $< 20000$ AU are expected to be about 5 times larger than that of the objects with larger semimajor axes. According to Weissman (1996), based on the influx rate of the observed LPCs, the total mass of the observable OC cometary objects (objects with sizes typically $> 1$km) with semimajor axes of $> 20000$ AU is deduced to be $\sim 7 M_{\rm earth}$ ($M_{\rm earth}$ is the mass of the Earth, $M_{\rm earth} = 5.97 \times 10^{27}$g). The Duncan et al. (1987) result thus gives the total mass of the OC to be $\sim 40 \rm M_{earth}$. Another work by Dones et al. (2004) reported that the model that is approximated by the power-law with the index of $\eta \sim 3$. In this case, the total OC mass is deduced to be $\sim 15 M_{\rm earth}$. As a transitional phase of the OC, objects with relatively smaller perihelia ($< 50$ AU) and high eccentricities are expected to be emerged (Dones et al., 2004). The characteristics of these objects are similar to that of the SD objects. These objects are thought to be supplied into the OC, even in the present day (Fernández, 2004).

According to the simulations, SD contains objects resided at heliocentric distances of $< 4000$ AU, and the number of the objects containing in the SD is comparable to that of the inner OC until $\sim$ a few 100 Myr after the planet formation (Dones et al., 2004).

### 1.1.3 Observations of the CSPs in the solar system

After the discovery of the first candidate of the classical Kuiper belt objects (Jewitt & Luu, 1993), several serendipitous surveys for the outer solar system objects have been performed with optical ground-based and space telescopes (Trujillo & Brown, 2003; Brown et al., 2008; Schwamb et al., 2009, 2010). As of late 2014, more than 1500 bodies called trans-Neptunian objects (TNOs) are found outside the neptunian orbit. Firgure 1.3 plots the distributions of the eccentricities and inclinations against semimajor axes of known TNOs. Most TNOs have the semimajor axes between 30 AU and 50 AU, and low eccentricities and inclinations. In addition, about 200 SD objects have been found, and many of them have large sizes (with radius $r$ of more than 100 km). If one extrapolates the size distribution down to $\sim$ km-sized, there are expected to be extremely large number ($\sim 10^{10}$) of kilometer-sized objects resided in the SD (Gomes et al., 2008).

Though several candidates of the inner OC objects have been found with the semimajor axes of $500-1000$ AU and the perihelia of $> 40$ AU (orange dots in Figure 1.3), such as the large TNO Objects Sedna (Brown et al. 2004, a red circle in Figure 1.3), their belonging is still controversial because they seem to be more like transitional ("detached") SD objects between the outer SD and the inner edge of the OC (Jewitt & Delsanti, 2006), than the native inner OC objects. Since the objects in the outer SD and the OC region is expected to be extremely faint (see Figure 1.3), direct detection of these objects located at $> 1000$ AU are impossible with the current and near-future observational instruments.

## 1.2 Search for extra-solar CSPs

### 1.2.1 Motivations

As reviewed above, there seem to be CSPs in the solar system containing a huge amount of primitive small bodies originally formed inside $\sim 50$ AU from the Sun, and then scattered into the outer regions. However, lack of direct observational evidences for the CSPs hampers us to understand the nature of the populations, especially those at larger distances from the Sun. It is worth studying the existence of similar populations around the extrasolar systems in the context of the planetary astronomy; unveiling the analogues of the CSPs in extrasolar systems are not only fundamental to understanding the unknown nature of the outer solar and extrasolar systems, but also to addressing the question of the universality of the solar system.

In addition, the existence of the OC and the SD analogues around the extrasolar systems is fundamental to understanding the general formation and evolution processes of stellar systems. Since the existence of the OC and the SD are indicative of orbital evolutions of planetesimals occurred in the early phase of the solar system, the evidence for CSP analogues would infer a similar evolutional history of the extrasolar systems. In the solar system, the OC and SD are signatures of the gravitational scattering of the protoplanetary disk by the giant planets. If extrasolar systems have CSP analogues, they are expected to have experienced similar planetesimal-scattering history. The study of the CSPs' analogues in the extrasolar systems thus should provide valuable information of the evolution scenarios of the typical stellar systems.

Protoplanetary disks around low- and intermediate-mass stars are known to have outer-edge radii of smaller than 1000 AU (Mannings & Sargent, 1997; Vicente &

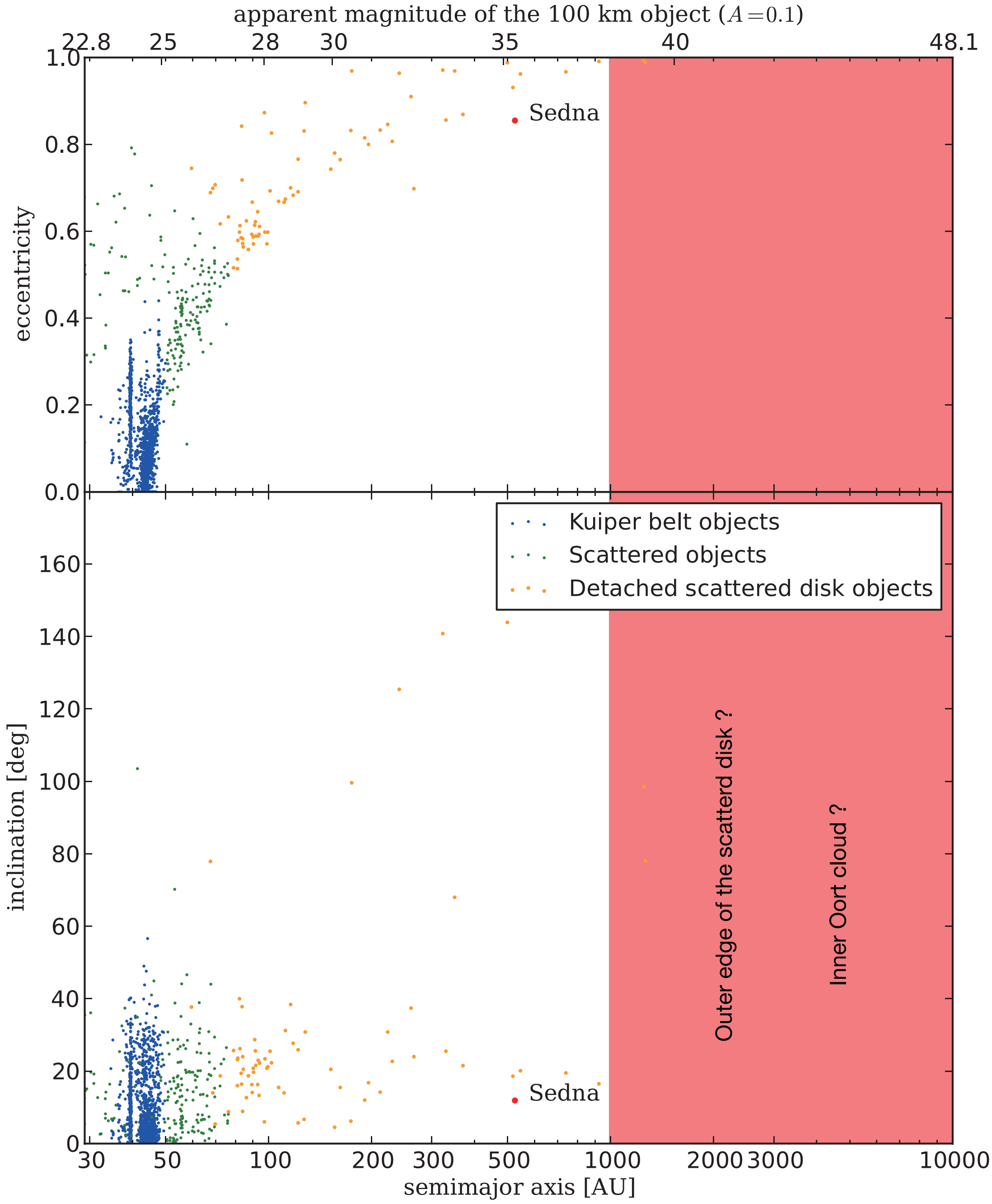


Figure1.3 Distribution of orbital elements (semimajor axis, inclination, and eccentricity) of TNOs with known orbits. Blue and green dots indicate the orbital elements of the Kuiper belt objects and scattered disk objects, respectively. Orange dots are "detached" SD objects; objects having a perihelion distances of $q > 40$AU, where perturbation by the giant planets does not affect. A red circle indicates the largest detached SD object, Sedna. The pink area indicates the outer edge of the SD and the inner OC regions, where observational constraints are not obtained due to instrumentation. The orbital information is obtained from *the international Astronomical Union/Minor Planet Center*.

Alves, 2005; Andrews & Williams, 2007). Therefore, if a population containing small bodes is located beyond $\sim 1000$ AU from the stars after their formation phase, it can have been generated through similar formation pathways that generated the OC and SD in the solar system. I therefore search for evidences of populations extended more than $\sim 1000$ AU as candidates of the extrasolar CSPs (exo-CSPs).

### 1.2.2 Infrared observations of the exo-CSPs

Infrared observations should be a prospective method for a search of the exo-CSPs. Whatever is in the exo-CSPs around the stars, such as debris and dust grains, would emit far-infrared (FIR; $\lambda = 50 - 200\,\mu$m) radiation (Stern et al., 1991). The exo-CSPs would thus appear as extended circumstellar FIR emission around the parent stars. Therefore the detection of the corresponding FIR emission would be a direct observational evidence for the exo-CSPs.

As well as the exo-CSPs, the debris disks and the parent stars' photospheres will emit FIR radiation. In order to surely extract the exo-CSP emission from the other emission components, the exo-CSPs should be spatially resolved. For example, if the extrasolar CSPs have a radius of 3000 AU, comparable to the outer SD (with radius up to 4000 AU) or the inner edge of the OC ($1000 - 5000$ AU), the angular diameter of these exo-CSPs within $\sim 40$ pc to the sun are about $75''$, which can be resolved with the recent FIR instruments (angular resolutions typically smaller than $100''$; Werner et al. 2004; Kawada et al. 2007; Poglitsch et al. 2010).

The expected emission intensity from the exo-CSPs is determined by their unknown optical depth $\tau$, which highly depends on the radial density profiles and size distributions of the exo-CSPs' objects. If a exo-CSP consists only of comet-sized (meter-to-kilometer sized) objects, the expected $\tau$ is smaller than $\tau < 10^{-9}$, and such a cloud is too faint to be detected by recent and latest FIR observations. However, smaller dust particles are expected to be supplied from the larger objects via several possible processes (Stern et al. 1991; Yamamoto & Mukai 1998; Howe & Rafikov 2014; see details in Chapter 5). The expected $\tau$ of the exo-CSPs can thus reach to $\tau \sim 10^{-5} - 10^{-7}$ (Stern et al., 1991).

The exo-CSP's intensity also depends on the luminosity of the parent star. The exo-CSPs around more luminous stars would be more luminous at FIR, and thus can be more detectable with FIR observations. For example, expected fluxes of the CSPs with $\tau = 10^{-6}$ extending to 3000 AU from solar type (G2V) main-sequence (MS) stars at 40 pc are less than 10 mJy at $\sim$ 100 $\mu$m. On the other hand, the corresponding intensity around A-type stars ($5 - 50$ times brighter than the solar luminosity) is expected to be more than 100 mJy (see details in Chapter 2). The exo-CSP emission thus may be more detectable, if the luminous stars are selected as the targets for the present study.

### 1.2.3 Space infrared observations

Since the infrared emissions are vulnerable to the emission and absorption from the atmosphere, only space-borne infrared observations can reveal the properties of the dust emission with a wide wavelength coverage and sufficient sensitivities. There are several infrared missions that are performed in space, which are shortly reviewed in the following paragraphs.

The first space telescope to perform infrared all-sky observations is the Infra-Red Astronomy Satellite (IRAS; Neugebauer et al. 1984), which was a joint mission by the United States, the United Kingdom and Netherlands, and was launched on January 26th 1983. The IRAS survey discovered the mid-infrared (MIR) to FIR thermal dust emission from the debris disks associated with nearby main-sequence stars (Aumann et al., 1984; Oudmaijer et al., 1992; Mannings & Barlow, 1998).

The IRAS data was also used for a pioneering study of the exo-OCs. Stern et al. (1991) searched for the extended excess emission that are spatially associated with nearby main-sequence stars and extended more than $10^3$ AU. They selected 17 A to K-type stars located within 17 pc from the Sun for the target objects, and used IRAS survey maps at 60 and 100 $\mu$m, where the intensity of the thermal emission from the exo-OCs is expected to appear. The radial brightness profiles (RBPs) were compared with the point spread functions (PSFs), to find an evidence for the extended emission. In this IRAS study, no evidence of extended emission associated with these stars was found. The obtained upper limits of the optical depth $\tau$ of the CSP emission around stars at 100 $\mu$m were typically $\tau \sim 10^{-3} - 10^{-5}$ at astrocentric distances of $3000 - 10000$ AU.

Observations with the Spitzer space telescope (Werner et al., 2004) have progressed the studies of the circumstellar environment of the main-sequence stars, owing to higher sensitivities and angular resolutions than IRAS. The *Spitzer* MIR to FIR observations had been performed during about two years (July 2004 - March 2009). Through the statistical studies of the emission characteristics, the Spitzer data made constraints on the formation and evolutions of the debris disks (Su et al., 2006; Wyatt, 2008). However, since the *Spitzer* FIR detector was also sensitive to near-infrared photons, an artifact signals due to the reflection of near-infrared light within the optical instrument severely contaminated with the data at a longer wavelength (160 $\mu$m) band (Stansberry et al., 2007), where the intensity of the thermal emission from the CSPs is expected to be maximal. This artifact is clearly seen in the data of the nearby stars (Tanner et al., 2009), and hampers us from the search for the faint CSPs' emission accurately.

Latest observations performed with the *Herschel* space telescope (Pilbratt et al., 2010) have evolutionised debris disk studies, owing to its unprecedented spatial resolutions and sensitivities for point sources. Two key programs of *Herschel*, Cold Disks around Nearby Stars (DUNES) and Disc Emission via a Bias-free Reconnaissance in the Infrared/Submillimetre (DEBRIS), especially dedicated to the study of debris disks around nearby stars. These observations began in 2009, and were completed in 2013. Among these key programs, *Herschel* observed more than 200 nearby stars located at distances of $\sim$ 40 pc from the solar system, and enabled to investigate spatial and spectral characteristics of the debris disks (Morales et al., 2011; Eiroa et al., 2013; Marshall et al., 2014). However, both DUNES and DEBRIS surveys only gave the maps covering the rectangular area only about $\sim 200''$ high for most of the targets. Since the outer populations of the stellar systems, if exist, would extend more than $300''$ for the DEBRIS sample, it is difficult to recognize it due to small field coverage. Furthermore, strong low-frequency thermal noise from the detector system dominates the PACS data with the angular scale of more than $\sim 1'$ (Ibar et al., 2010). Owing to this low-frequency noise confusion, the studies of debris disks and other circumstellar characteristics usually performed with the data that subtracts large angular scale components through the standard data reduction procedures (e.g., Eiroa et al. 2013). As a result of these procedures, faint and extended structures that are seen with other instruments were reported to be undetected in the Herschel data (Kerschbaum et al., 2010). Recent data reduction pipelines for the Herschel data offer techniques that enable us to restore low-frequency component with several image reconstruction methods (Cantalupo et al., 2010; Roussel, 2013). However, even if we use these procedures, it seems to be difficult to faithfully restore sources extended comparable to the map size, because the strong low frequency noise and real emission structures would be degenerated in the data. Therefore, it is controversial to perform investigations of the tenuous emission from the exo-CSPs using the Herschel data.

### 1.2.4 *AKARI* all-sky survey

*AKARI* is the first Japanese satellite that carried out MIR to FIR all-sky survey (Murakami et al., 2007). The *AKARI* all-sky survey in FIR wavelengths were performed from May 8 2006 to August 28 2007 with the Far-Infrared Surveyor (FIS, Kawada et al. 2007) in four bands, covering 50-180 $\mu$m wavelength range. The FIS scanned more than 98 % of the sky, and provides the FIR all-sky dataset with the highest spatial resolutions and sensitivities (Kawada et al., 2007). Thanks to its high-performance cooling system, *AKARI* could maintain the system temperature down to $\sim$ 6 K. Therefore the *AKARI* all-sky observation is not overwhelmed by thermal emission from the instruments, and is sensitive to emission on arcminute to degree scales (Doi et al. in prep.), which is wider spatial scale than that of any other existing FIR wide-field observation.

From the FIS all-sky data, the FIR bright source catalogue (BSC) is released (Yamamura et al., 2010). In addition, the all-sky maps will be available from the data archive server. The all-sky maps will enable us to perform studies of an arbitrary set of objects.

### 1.2.5 Detection algorithm: stacking analysis

The sensitivity of the FIS all-sky survey (550 mJy at the 90 $\mu$m; Kawada et al. 2007) is still insufficient to search for the emission from the exo-CSPs around the individual stars. ($\sim$ 100 mJy for 3000 AU exo-CSP with $\tau = 10^{-6}$ at 40 pc from the Sun, see Chapter 2). Therefore, I have adopted a stacking analysis for the present study. Stacking analysis is a analytic method that is averaging the images at the locations of the targets to obtain an aggregate signal from the targets. The background random noise of the stacked image would decreases against the signal as the number of the stacked images increases (approximately proportional to the square root of the number of stacked images, assuming the random noise). With the stacked image, one can perform the FIR photometry and the study of spatial structures of the sample with higher sensitivities than that performed with individual images. Therefore the stacking technique has been extensively adopted for the statistical FIR studies for faint sources, such as known normal galaxies and quasars (Kashiwagi et al., 2012), galaxy clusters (Giard et al., 2008), and mid-infrared extragalactic sources in deep field survey areas (Jauzac et al., 2011). These studies have succeeded in investigating FIR spectral and spatial features of the faint sources with fluxes even below the detection limits. Therefore, application of the stacking analysis to the *AKARI* FIR all-sky data would give us the opportunity of the detection, photometry, and studies of spatial properties of the emission from the CSPs (see Chapter 2).

### 1.2.6 Technical issues for the present study

The present study intends to measure radial brightness profiles (RBPs) of the stacked images to derive radial properties of the circumstellar FIR emission. In order to measure accurate RBPs of the CSP emission with angular sizes comparable to the PSFs, a subtraction of the component from the central point sources is required. This subtraction procedure requires information of the PSF in the FIS map. Furthermore, in order to carry out accurate detection and photometry of the FIR emission from the exo-CSPs with angular sizes comparable to the PSF, photometric calibrations for point sources are required. The FIS all-sky map is calibrated by diffuse sources, such as zodiacal light and interstellar dust emission (Matsuura et al., 2011; Doi et al., 2012). Additional flux calibrations for the point sources are thus needed. The present study plans to perform photometry and the RBP studies with fluxes down to about one order of magnitude below the detection limits by applying the stacking analysis. The PSFs and calibration factors should be determined for objects with the faint fluxes. However, response functions of the FIS detectors in pointed-mode observations are known to be incoming-flux dependent (Shirahata et al., 2009); Output signal intensities relative to the true fluxes can decrease as a function of point source fluxes (see Figure 1.4). One has to check whether the calibrations for point sources in the all-sky maps are valid to the faint sources or not.

## 1.3 Aim and outline of this thesis

The aim of this thesis is to reveal an evidence for the FIR emission around nearby stars with astrocentric distances characteristics of the CSPs (a few $10^3$ to $10^4$ AU). I use the *AKARI*/FIS all-sky map for the present study. In order to detect circumstellar FIR emission with sufficient sensitivities, I selected nearby A-type stars for targets, where the circumstellar FIR emission is expected to be $\sim 10$ times stronger than solar-type stars. I also adopt a stacking analysis technique that enhances signal-to-noise ratios by summing fluxes. In order to perform accurate photometry and radial distributions of the circumstellar FIR emission, the PSFs are determined and photometric calibration factors for point sources are estimated in a faint flux ranges. The rest of the thesis is organized as follows. Chapter 2 describes the instrumentation of the *AKARI* satellite, and the outline of the FIS all-sky observations. Also, Chapter 2 presents expected spectra of the FIR circumstellar emission from the exo-CSPs with different optical depths and with different stellar types of the parent stars, and potential applications of the stacking analysis. Chapter 3 shows results of the PSF determination and the photometric calibration of infrared standard stars in the *AKARI* all-sky map. By stacking infrared standard stars with different ranges of the fluxes, the flux-dependences of the RBPs and of the calibration factors of the point sources are checked. In Chapter 4, results of the exo-CSP search are presented. From the stacked images of the nearby A-type stars, the spectral energy distributions and the radial brightnesses profiles of the possible extended emission are derived. Chapter 5 offers some discussions of the origin of the observed extended emissions. I have checked the possibilities of the contamination with the background objects by several tests. In this chapter, I also show that the observed excess can be explained by the thermal emission from micrometer-sized dust grains around the target stars, assuming the detected emission is the real circumstellar emission. This chapter also focuses on possible processes that can supply the dust grains from larger-sized objects in the exo-CSPs, and discusses possible properties of the exo-CSPs. Chapter 6 summarizes the present thesis.

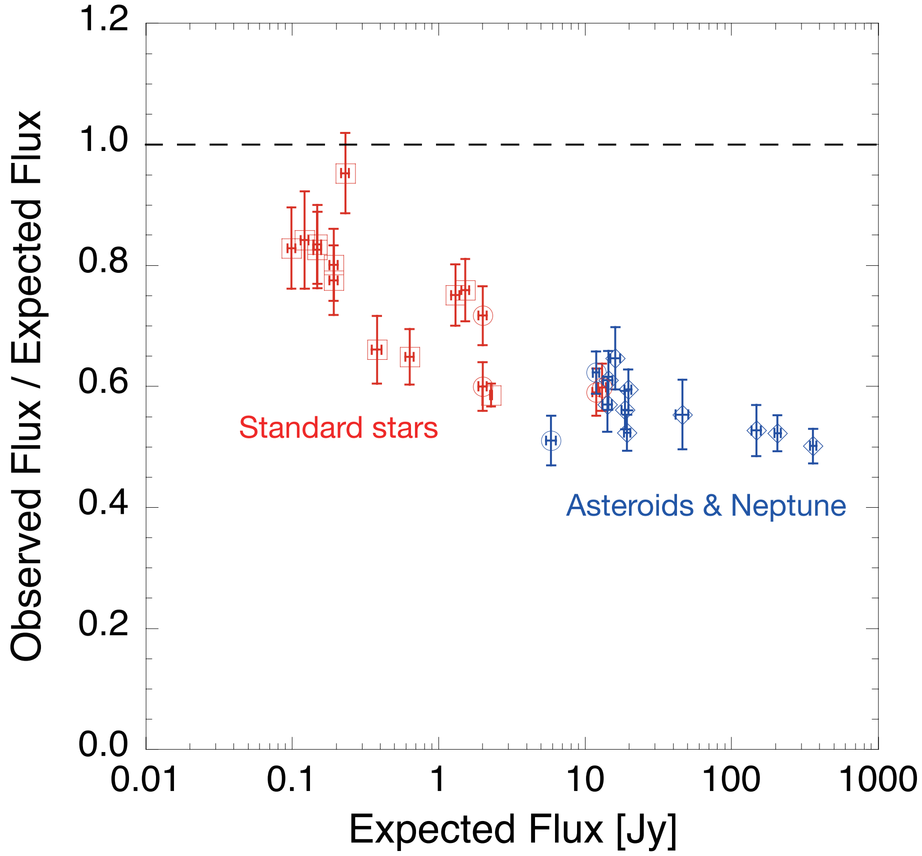


Figure1.4 The observed-to-expected flux ratio as a function of the expected flux derived from the spectral models. The observed fluxes are derived from data obtained in pointed-mode observation with the *AKARI*/FIS. Note that the results are derived from pointed observations, not from the all-sky observations used for the present study (see Chapter 3 for details). Figure reproduced from Shirahata et al. (2009).

# Chapter2

# Data sets and search concept

# 2.1 *AKARI*

## 2.1.1 the *AKARI* satellite

*AKARI* (ASTRO-F) is the second Japanese space mission for infrared astronomy (Murakami et al., 2007), developed and operated by the Institute of Space and Astronautical Science (ISAS), and other collaborators. It was launched on February 21, 2006 (UT) by M-V-8 rocket, which was developed by the Japan Aerospace Exploration Agency (JAXA). The main purpose of the mission is to create the all-sky catalogue of the infrared sources with better angular resolutions, and a wider spectral range than the first catalogues produced by the IRAS (Neugebauer et al., 1984). The satellite was brought into a Sun-synchronous polar orbit with an altitude of 700 km and an inclination of 98°.2. The period of the orbit was about 100 min.

In order to reduce the thermal noise from the instruments, the whole system must be cooled. *AKARI* is equipped with a cooling system consisting of hybrid cryogenic system combining of cryogen and mechanical coolers. This unique system enabled to maintain the telescope temperature down to $\sim$ 6 K in a long cryogenic mission lifetime with only 170 litters of liquid helium. The observations with *AKARI* begun on May 8, 2006, and the liquid helium boiled off on August 26, 2007. After the liquid helium was exhausted, the telescope system is kept at about 40 K by the mechanical cooler and observations at near-infrared wavelengths had been continued until May 24, 2011. The operation of the *AKARI* spacecraft was finished on Novevmber 24, 2011. Figure 2.1 shows the overall structure of the *AKARI* spacecraft. The spacecraft is about 5.5m height after deployment in orbit, and weighs 952 kg as launched.

*AKARI* is equipped with a Ritchey-Chretien type telescope with an effective aperture size of 68.5 cm and an $f/6$ system, and two focal plane instruments (FPI), The

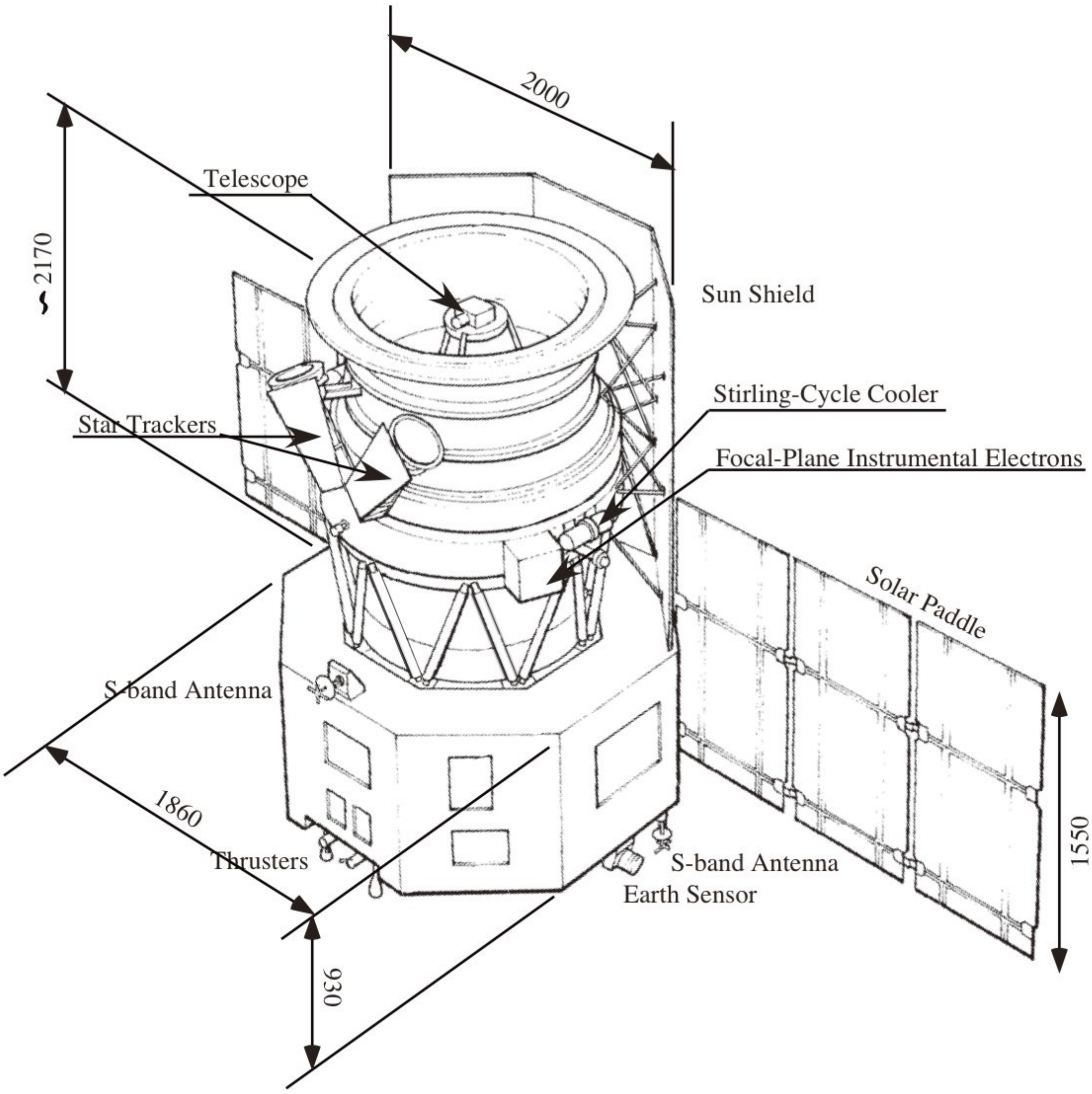


Figure2.1 An overall view of the AKARI spacecraft (*ASTRO-F Observer's Manual*, scales are in mm).

Infrared Camera (IRC) and the Far-Infrared Surveyor (FIS). In addition to the FPIs, two units of the Focal-Plane Star Sensor (FSTS) are equipped at the focal plane to obtain accurate position information during scanning observations. Figure 2.2 shows the focal-plane layout projected onto the sky. While the IRC and FIS share the focal plane near the telescope optical axis, they are disposed in different areas. The field

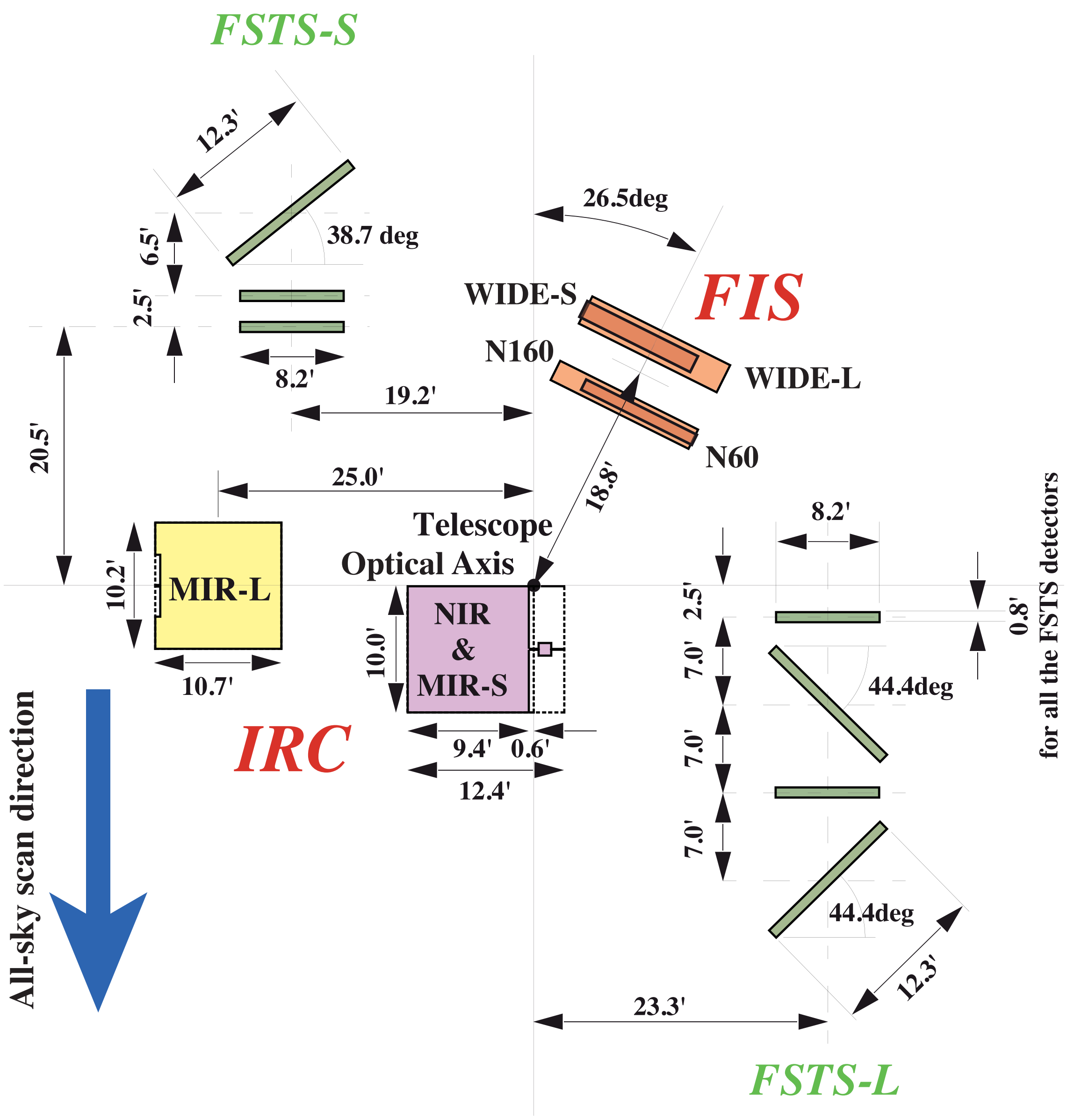


Figure2.2 Focal-Plane layout of the *AKARI* telescope FPI. The IRC fields of view are shown as purple and yellow areas, whereas the fields of view of the FIS are shown as orange areas. The scan direction in the all-sky survey is indicated as a blue arrow at the bottom left. Figure reproduced from *the ASTRO-F Observer's Manual*.

of view of the FIS is offset from the telescope optical axis by about 19′ and is rotated by 26°.5 from the scanning direction.

A major goal of the mission is to carry out an all-sky survey with the FIS at the four bands and additionally with the IRC at 9 and 18 $\mu$m. *AKARI* also carried out dedicated pointed observations with both the FIS and IRC.

The schematic view of the in-orbit attitude of the AKARI observations is shown in Figure 2.3. During the all-sky survey, *AKARI* always points the telescope in the direction perpendicular to the Sun-Earth line, and revolved in a Sun-synchronous polar orbit with an angular speed of $3'.6\,\mathrm{sec}^{-1}$. Therefore the detector sweeps the sky with the same angular speed in a direction almost perpendicular to the ecliptic latitude and to the direction of the Sun. Since the direction of the orbit axis rotates as the Earth revolves about the Sun, the scan path moves with a rate of $4'.1$ to the ecliptic between successive orbits, and thus the survey can cover the whole sky in half a year. On the other hand, in the pointed observations, the telescope was pointed towards the target for about 10 minutes. These pointed observations were inserted into the survey operations. As well as during the pointed observations, the all-sky survey operation was halted during the presence of the South Atlantic Anomaly (SAA, see Murakami et al. 2007) and the Moon.

### 2.1.2 The Far-Infrared Surveyor (FIS)

FIS (Kawada et al., 2007) was designed for the all-sky survey observation, but was also used for pointed observations in a slow-scan mode. It is also equipped with a Fourier Transform Spectrometer (FTS) that enables imaging spectroscopy over the full FIS wavelength range. The detector system of the FIS consists of two kinds of Ge:Ga extrinsic photoconductors, one is a monolithic Ge:Ga array detector, the Short Wavelength array (SW), covering the wavelength range of $50-110\,\mu$m, and the other is a stressed Ge:Ga array detector, the Long Wavelength array (LW), covering $110-180\,\mu$m, with four photometric FIR bands, N60 (65 $\mu$m), WIDE$-$S (90 $\mu$m), WIDE$-$L (140 $\mu$m), and N160 (160 $\mu$m). The characteristics of the FIS photometric

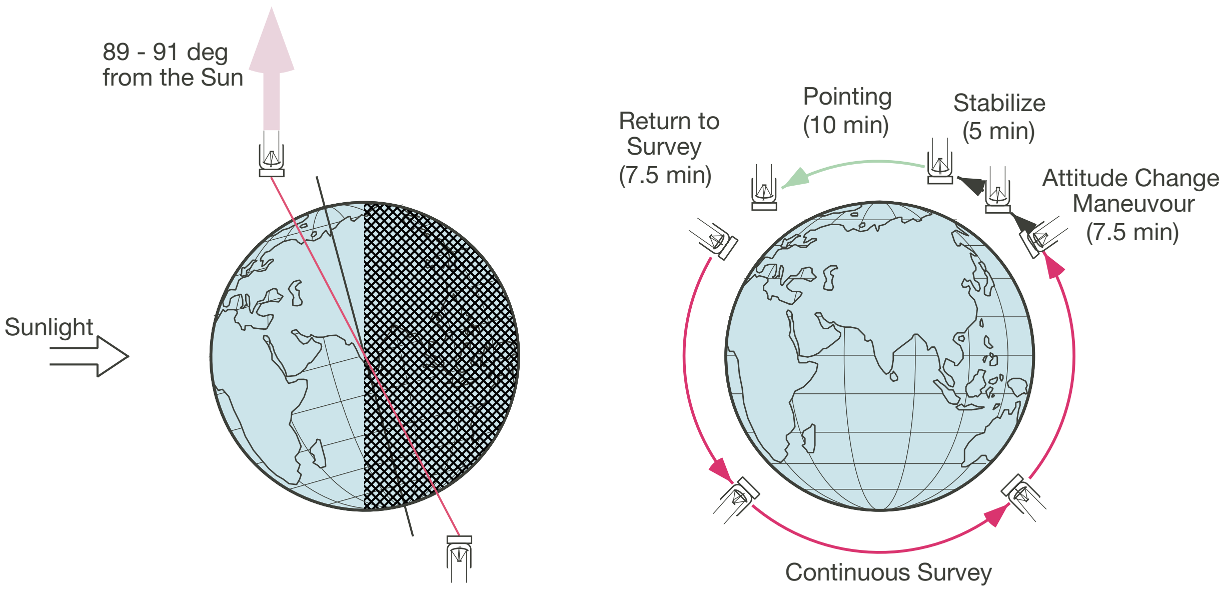


Figure2.3 Schematic view of the in-orbit attitude of the *AKARI* observations (from *ASTRO-F Observer's Manual version 3.2*, Murakami et al. 2007).

Table2.1 The specification of the FIS photometric bands (Kawada et al., 2007)

| Channel | SW | | LW | |
|---|---|---|---|---|
| Detector | Monolithic Ge:Ga | | Stressed Ge:Ga | |
| Band | N60 | WIDE-S | WIDE-L | N160 |
| Covering wavelength [$\mu$m] | 50-80 | 60-110 | 110-180 | 140-180 |
| Central wavelength [$\mu$m] | 65 | 90 | 140 | 160 |
| Bandwidth [$\mu$m] | 21.7 | 37.9 | 52.4 | 34.1 |
| Array size | $20 \times 2$ | $20 \times 3$ | $15 \times 3$ | $15 \times 2$ |
| Field of view | $10' \times 1'.0$ | $10' \times 1'.5$ | $12' \times 2'.5$ | $12' \times 1'.6$ |
| $5\sigma$ detection limit [Jy] | 2.4 | 0.55 | 1.4 | 6.3 |

bands are summarized in Table 2.1 and the spectral responses of the four photometric bands are shown in Figure 2.4. Since each FIS band is sensitive to a fairly broad wavelength range, one should apply a color correction depending on the spectrum of the sources to the observed fluxes in order to obtain the monochromatic flux at the band center wavelength.

As shown in Figure 2.2, the WIDE−S and WIDE−L bands share the same field-

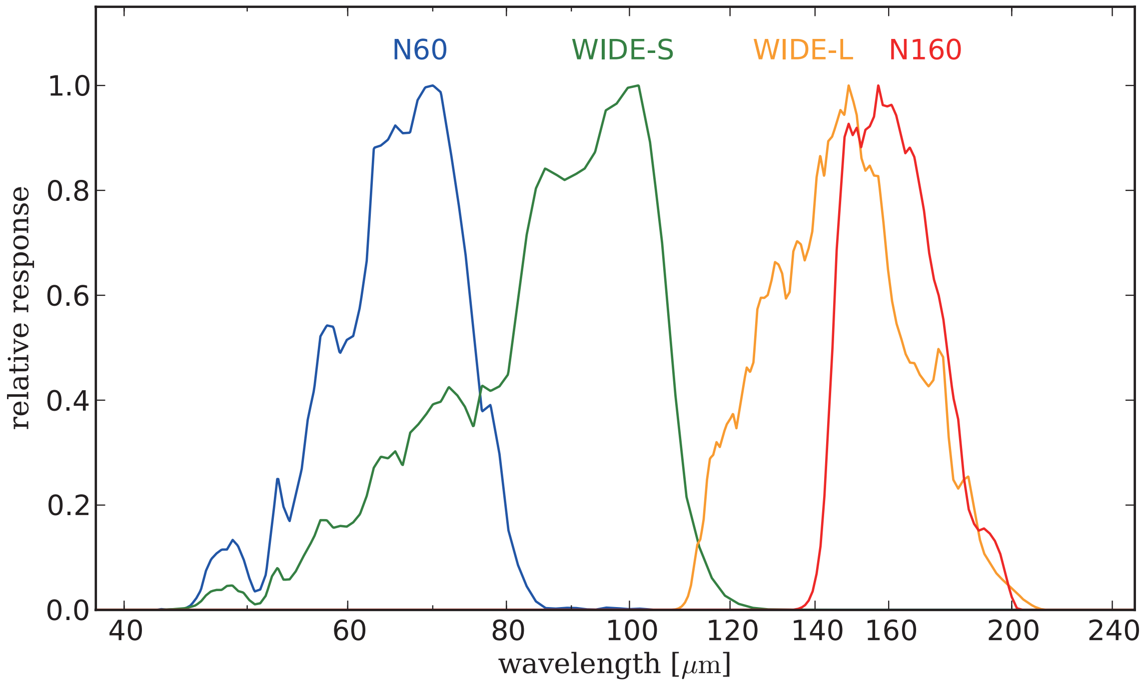


Figure2.4 Spectral response of the FIS photometric bands, each normalized at its peak.

of-view (FOV), whereas the N60 and N160 bands share the other FOV. Pixel sizes of detectors are $26.8'' \times 26.8''$ and $44.2'' \times 44.2''$ for the SW and LW detectors, respectively. These scales are comparable with the diffraction limit of the telescope at each wavelength ($24''$ and $51''$ at 65 $\mu$m and 140 $\mu$m, respectively). To achieve a Nyquist sampling with the diffraction limited spatial resolution, the arrays are rotated by 26.5 degrees from the scanning direction (see Figure 2.2). In this configuration, the angular intervals between the neighboring scan-line paths of the detector pixels are $13''$ and $22''$ for the SW and LW detectors, respectively.

The optical layout of the FIS is shown in Figure 2.5. The incident beam comes from the entrance aperture ((a) in Figure 2.5) below the folding mirror (b) and paralleled by the collimator mirror (c). At the entrance aperture, there is a cold shutter to measure the instrumental dark current. The collimated beam goes to the filter wheel

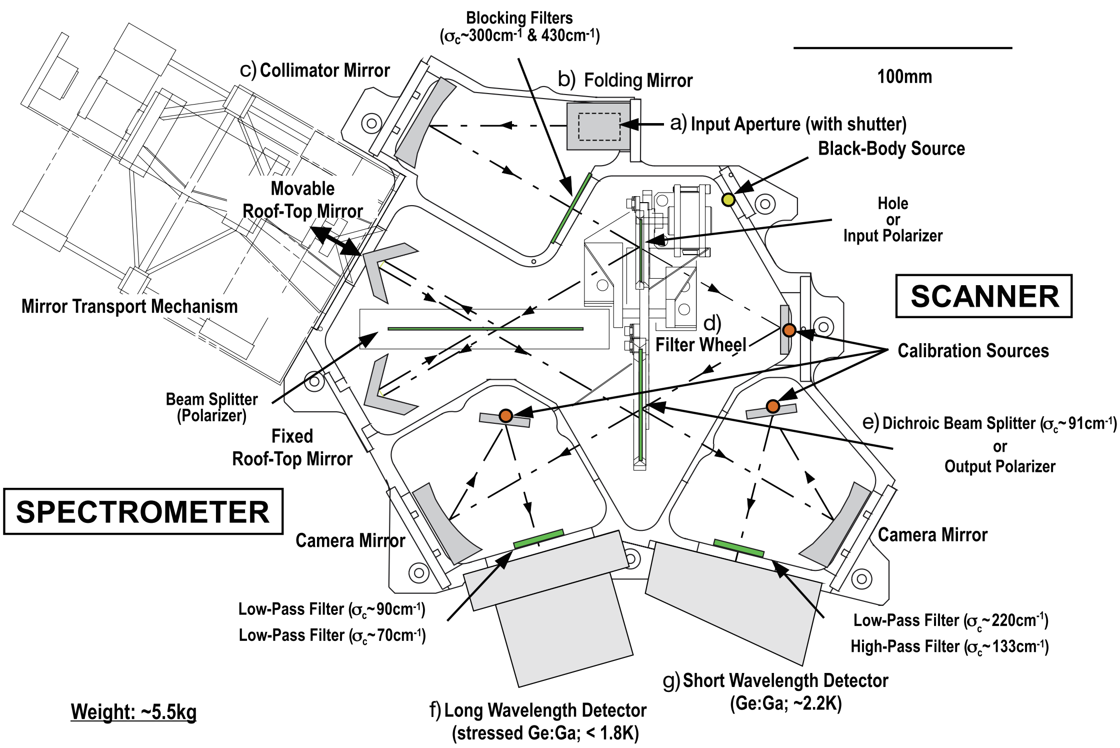


Figure2.5 Optical configuration of the FIS. Figure reproduced from *the FIS data user manual*.

(d), which selects the observation mode. The scanner mode (photometric imaging mode) or the spectrometer mode is selected by rotating the filter wheel and selecting the combination of filters. In the scanner mode, the beam goes to the dichroic beam splitter (e). Photons of wavelengths longer than 110 $\mu$m goes through the splitter and is concentrated onto the LW detector module (f), while shorter wavelength photons are reflected by the beam splitter and sent to the SW module (g).

### 2.1.3 *AKARI*/FIS all-sky survey

As noted in the previous section, the primary purpose of the *AKARI* mission is to achieve the infrared all-sky survey. The AKARI all-sky observations in FIR wavelengths were performed from 2006 May 8 to 2007 August 28 with the FIS in the four bands. During the period, the FIS observed more than 98 % of the sky. In the survey observations, the detector sweeps the sky in a direction almost perpendicular to the ecliptic latitude with a scan speed of $3'.6$ sec$^{-1}$. During the scan, the integrated detector signals are continuously read out as time-series data with cadences of 25.28 Hz (65, 90 $\mu$m bands) and 16.86 Hz (140, 160 $\mu$m bands). These sampling timescales correspond to about three samples in a pixel crossing time of a point source (Kawada et al., 2007). Detectors are reset to discharge the stacked photo-electrons at intervals of about 2 seconds, nominally, 0.5 seconds for bright sky regions (regions with surface brightnesses greater than 60 MJy sr$^{-1}$ at 140 $\mu$m), except for the galactic plane (regions with surface brightnesses greater than 210 MJy sr$^{-1}$ at 140 $\mu$m), where the reset intervals are about 26 and 45 ms for the SW and LW detectors, respectively, not to saturate. In order to trace the detector responsivity, calibration pulse flashes with illuminator lamps are inserted every minute. Also, the cold shutter is closed for 1 minute at every 150 minutes or 3/2 revolution of the satellite to monitor the instrumental dark current.

From the FIS all-sky survey data, the FIS Bright Source Catalogue (BSC) was released in 2010 March (Yamamura et al., 2009, 2010). The FIS-BSC contains 18638, 290209, 69092, 26631 sources detected at the 65, 90, 140, 160 $\mu$m bands, respectively. According to Kawada et al. (2007), the $5\sigma$ detection limits for the 65, 90, 140, 160 $\mu$m bands are 2.4, 0.55, 1.4, 6.3 Jy, respectively (see also table 2.1). Comparing to the $5\sigma$ detection limits of the previous IRAS survey at the two FIR bands (0.45 and 1.5 Jy at the 60 and 100 $\mu$m bands; Neugebauer et al. 1984), sensitivity for point sources is improved at $\sim 100\,\mu$m by a factor of three.

### 2.1.4 FIS all-sky map

In the preset study, I have used the FIS all-sky maps version 130401, which went through data reduction procedures that apply to the publicly released dataset. The all-sky maps are produced from time-series scan data obtained during the all-sky observations. To construct maps from the time-series data, the following two pipelines are carried out. First of all, the obtained data are pre-processed with the FIS pipeline tool originally optimized for bright point source extraction (Yamamura et al., 2009, 2010). The procedures exerted in this pipeline are as follows: Firstly, linearity is corrected by referring the intermittently inserted calibration pulses. Then the data that is affected by high-energy particles (Suzuki et al., 2008), and the saturation effect is rejected. The dark current signals are also subtracted in this pipeline using the data obtained during the shutter closed. Direction of the detector FOV is determined referring the data taken by the FSTS.

Following the pre-processing, an additional pipeline is used for depicting diffuse emission structures accurately (Doi et al., 2009, 2012). In the resultant data after pre-processing, the slow-transient response of the detector severely affects the signal structures. Therefore the effect of the transient response is empirically corrected using in-flight time-sequence data of the detector response to a step function of internal calibration lamp illuminations. This procedure corresponds a high-pass filtering in principle, and amplifies high-frequency noise as well as true signals. Therefore the maps are convolved with a Gaussian filter with $\sigma = 13''$ in order to surpass the high-frequency part. Through the procedure, the maps can depict the diffuse signals accurately. However, the transient response is not corrected perfectly, especially for the point sources (see chapter 3). The zodiacal light (ZL) is the dominant emission source at the FIS bands, and the brightness strongly depends on the direction and time. Therefore we have subtracted the smooth component of the ZD from the time-series data using the model proposed by Gorjian et al. (2000). The resultant image shows stripe-like patterns with typical angular scales of several degrees. These patterns are thought to be emerged due to imperfect flat-fielding caused by long-term sensitivity variations of the detector. We empirically subtracted these patterns from the images (Tanaka et al. in preparation).

Through these procedures, the all-sky map is produced with a sample scale of $15''$ and units of surface brightness in $\mathrm{MJy\,sr^{-1}}$. The derived map is compared with the COBE/DIRBE Zodi-Subtracted Mission Average data. The correction factor is derived from the comparison and adopted for the procedures recursively. The final maps obtained with the procedures are shown in Figure 2.6. The final map is confirmed to be well calibrated for the diffuse emission (Takita et al. in preparation).

## 2.2 Search concept

### 2.2.1 Expected FIR emission from exo-CSPs

In order to search for an evidence of the FIR emission surrounding nearby stars at astrocentric distances of the present interest ($10^3$ to $10^4$ AU), one has to select targets of parent stars that enable us to detect the exo-CSP emission spatially resolved from the emission from the stellar photospheres and circumstellar debris disks. The apparent angular radius $\theta$ of an exo-CSP with a radius $R$ is derived by

$$\theta = \tan^{-1}\left(\frac{R}{d_{\mathrm{star}}}\right) \sim \frac{R}{d_{\mathrm{star}}}, \tag{2.1}$$

where $d_{\mathrm{star}}$ is the distance to a star from the Sun. Figure 2.7 shows how $\theta$ changes with $R$ and $d_{\mathrm{star}}$. The angular resolution of the AKARI/FIS 90 $\mu$m band map (the

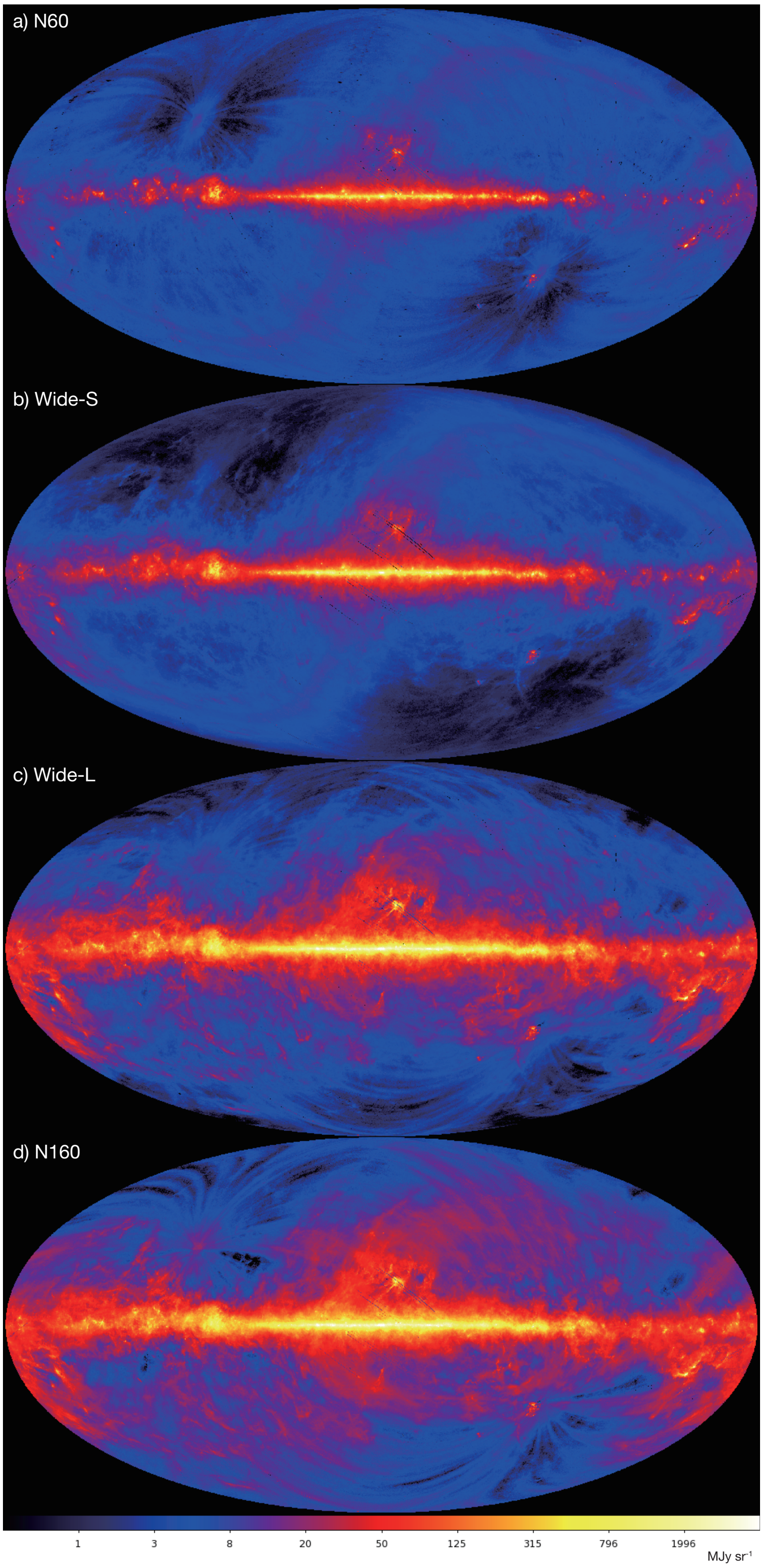


Figure2.6 FIS all-sky maps at the 65, 90, 140, 160 $\mu$m bands. Figure reproduced from Doi et al. (2012).

cross-scan FWHM of 55″; Arimatsu et al. 2014, see Chapter 3) is also shown for comparison. If $R$ is $10^3 - 10^4$ AU, exo-CSPs surrounding the stars located within 20-200 pc of the Sun can be spatially resolved in the FIS map.

In the following, I provide an estimate of expected emission spectra from dust grains in the exo-CSPs. For simplicity, I assume a simple optical condition; the emissivity (= absorption cross section) of the grain with a typical radius $a$ at the wavelengths $\lambda > \lambda_0$ is $(\lambda/\lambda_0)^{-1}\pi a^2$, and $(1 - A)\pi a^2$ at $\lambda < \lambda_0$, where $A$ is the typical albedo of the grains (assuming $A$ is independent of the wavelength) and $\lambda_0$ is a reference wavelength. In the following, $\lambda_0$ is set to be $\lambda_0 \sim 1.5\,a$, which is permissible for dirty ice grains (Stern et al., 1991). In the dust grains located at the distance from the parent star greater than $R > 1000$ AU, the ambient interstellar radiation should be taken into consideration, because the radiation from the parent star becomes relatively weak. If the grain is assumed to be in radiation equilibrium, the equilibrium temperature $T_{\rm eq}$ is derived by the following equation (Stern et al., 1991);

$$T_{\rm eq} = 5.2\left[(1 - A)\left(\frac{\lambda_0}{1\,\mu{\rm m}}\right)^{-1}\left(T_{\rm bkg}^4 + \frac{L_*}{16\pi\sigma_{\rm SB}R^2}\right)\right]^{1/5}\ [{\rm K}], \qquad (2.2)$$

where $\sigma_{\rm SB}$ is the Stefan-Boltzmann constant, $L_*$ is the luminosity of the parent star and $T_{\rm bkg}$ is the effective radiative temperature of the interstellar radiation field. This equation is applicable when $\lambda_0$ is larger than the wavelengths of incoming radiation, and is smaller than the reradiating wavelengths. In the following, $A$ is assumed to be $A = 0.03$ (comparable to the albedo of the comet nuclei), and the intensity of the interstellar radiation field is comparable to the solar neighborhood interstellar radiation field (i.e., $T_{\rm bkg} = 3.5\,{\rm K}$; Spitzer 1978). Assuming the exo-CSP is optically thin spherical shell with an optical depth at $100\,\mu$m, $\tau$, the expected spectrum $F_\nu^{\rm CSP}(\lambda)$

is derived by the following equation

$$F_\nu^{\rm CSP}(\lambda) = 4\pi\tau\left(\frac{R}{d_{\rm star}}\right)^2 B_\nu(\lambda, T_{\rm eq})\left(\frac{\lambda}{100\,\mu{\rm m}}\right)^{-1}, \tag{2.3}$$

where $B_\nu(\lambda, T)$ is the Planck function of temperature $T_{\rm eq}$ at a wavelength $\lambda$.

Figure 2.8 shows expected infrared spectra of the exo-CSPs with $R$ = 3000 AU and different optical thickness $\tau$ surrounding solar type (G2V) and Delta Leonis-type (A4V) stars, located at 40 pc from the Sun; the $5\sigma$ detection limits of the FIS all-sky observations at each band (Kawada et al., 2007) is also shown for comparison. Since the stars with later spectral types (F, G, K, and M-types) have relatively lower stellar illuminates, they are incapable of heating grains in the zones of the present interest ($R = 10^3 - 10^4$ AU) to the temperatures observable at the FIS bands ($T > 20$ K, see Figure 2.8a). On the other hand, A-type stars, are enough luminous ($5 - 50$ solar luminosity) to heat-up grains with the temperature of $\sim$ 20 K. The corresponding thermal emission would have a peak at $\sim 150\,\mu$m and be detectable with the FIS $90\,\mu$m (WIDE-S) or the $140\,\mu$m (WIDE-L) bands (see Figure 2.8b). Furthermore, the intensity of the FIR emission from the exo-CSPs with the same $\tau$ becomes an order of magnitude brighter at the FIS bands. Therefore nearby A-type stars are favorable targets for the present study.

As shown in Figure 2.8, the expected detection limit at the $160\,\mu$m (N160) band is insufficient to derive a nontrivial constraint on the exo-CSPs' emission intensity, compared to the other bands. Therefore the $160\,\mu$m data is not used for the following study. The sensitivity of the $65\,\mu$m (N60) band data is also insufficient to detect the exo-CSPs' emission. However, the $65\,\mu$m band is expected to be useful to understand spectral properties of the FIR emission from the debris disks, which typically has its spectral peak at $\sim 70\,\mu$m (Su et al., 2006). Therefore I use the FIS 65, 90, and $140\,\mu$m maps in the following study.

### 2.2.2 Stacking analysis

Even if one makes photometry for the individual nearby A-type stars, the expected sensitivity for the FIR emission from the exo-CSPs is insufficient for the detection, because the exo-CSPs are expected to be very optically thin ($\tau < 10^{-5}$, Stern et al. 1991), and their expected fluxes would be below the detection limits (Figure 2.8b). Therefore I adopted a stacking analysis to the set of nearby stars for the present study. A stacking analysis is a analysis that is averaging images of the targets with known positions to obtain an aggregate signal from the targets. If one assumes the noise in the images is random, the noise decreases as the square root of the number of the samples. According to the Hipparcos catalogue (Perryman et al., 1997), the number of the A-type stars within 40 pc from the Sun is about 100. If one stacks 100 stars, the S/N ratio can be improved by $\sim \sqrt{100} = 10$. The stacking analysis thus allows us to gain the constraints on $\tau$ of the exo-CSPs' emission by an order of magnitude smaller (see Figure 2.8b). The expected $5\sigma$ upper-limit on the optical depth $\tau$ of the exo-CSP surrounding A-type stars at $R = 3000\,\mathrm{AU}$ is $\tau \sim 10^{-6}$ at the $90\,\mu$m band. The combination of the *AKARI*/FIS all-sky data with the stacking analysis of the A-type stars can make significantly deeper constraint of the evidence for the exo-CSPs than the previous study performed with IRAS ($\tau = 10^{-3} - 10^{-5}$; Stern et al. 1991). On the other hand, the number of G-type MS stars within 50 pc is about 1000, and sensitivity would be improved by a factor of $\sim \sqrt{1000} = 30$, if stacking. However, the $5\sigma$ sensitivity of the stacked 1000 G-type stars would be still low ($\tau \sim 10^{-5}$, see Figure 2.8a), compared to that from the stacked A-type stars ($\tau \sim 10^{-6}$). Taking the high luminosity and sufficient abundance for the stacking analysis into consideration, the A-type stars are the most favorable targets for the present study.

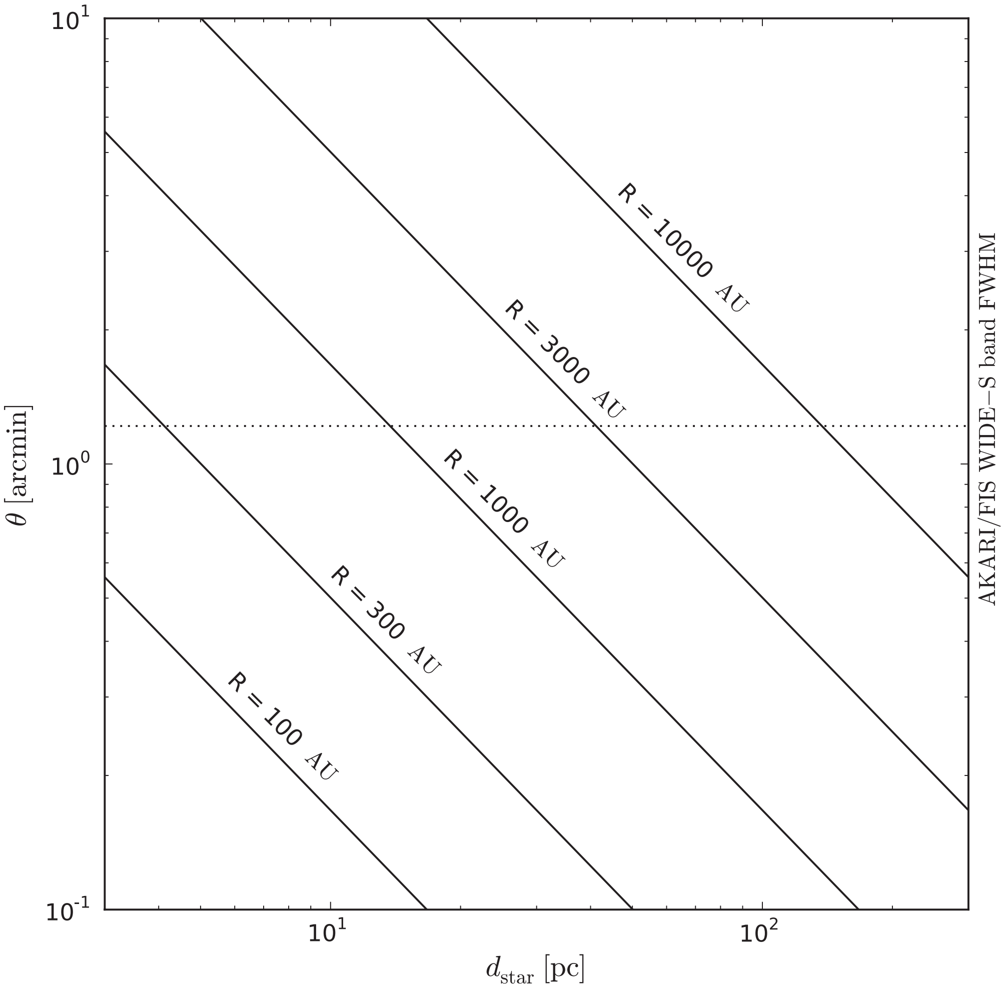


Figure2.7 Angular radius of an exo-CSP with a geometrical radius $R$ observed from the distance $d_{\rm star}$. The cross-scan FWHM of the *AKARI*/FIS 90 $\mu$m band (55″ ;Arimatsu et al. 2014, see Chapter 3) is also plotted as the dotted line.

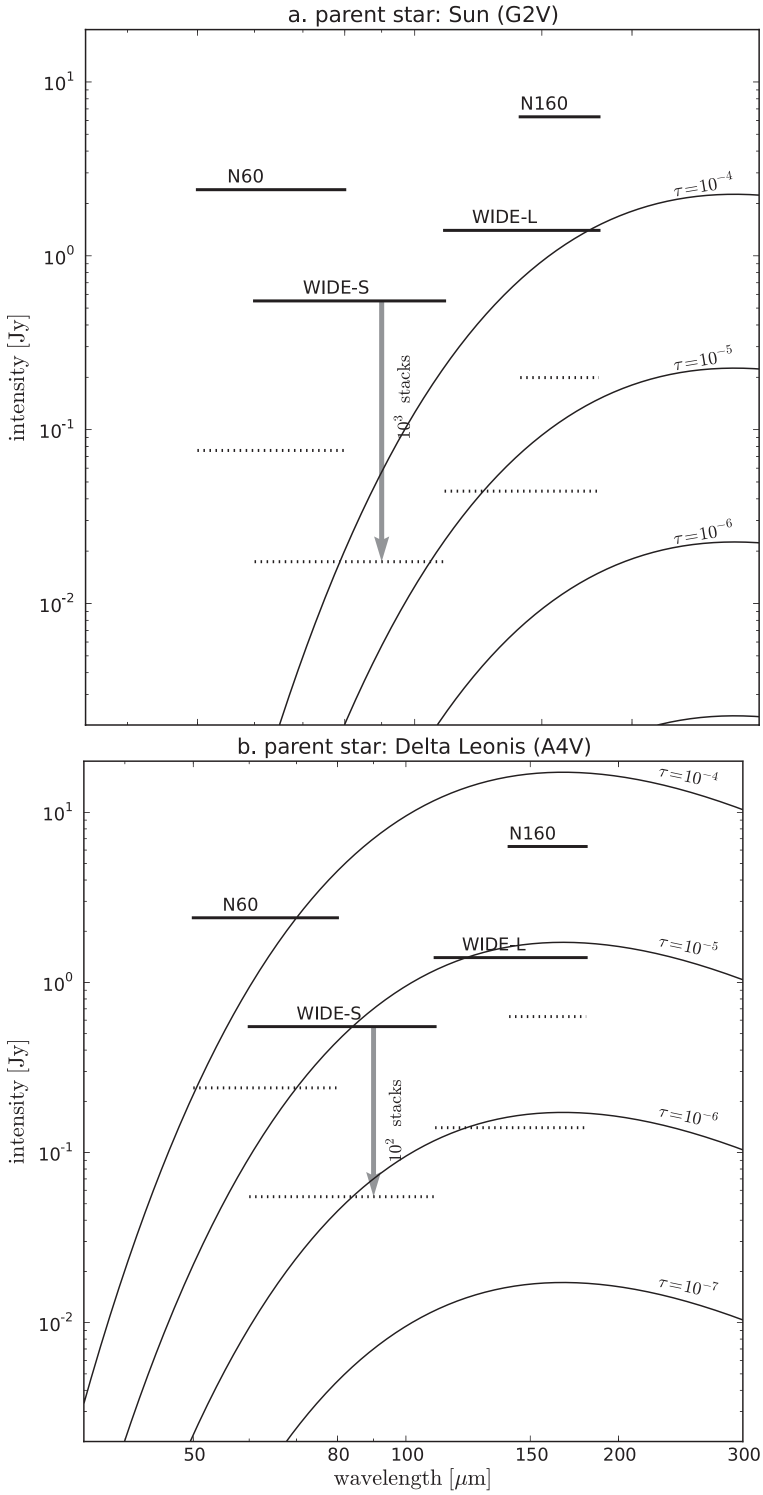


Figure2.8 The expected spectra of the assumed $R = 3000$ AU exo-CSPs with different optical depths $\tau = 10^{-4} - 10^{-7}$ around a) the Sun (G2V: $L_* = 1L_\odot$), and b) an A-type star, Delta Leonis (A4V :$L_* = 16L_\odot$; Akeson et al. 2009), located at 40 pc from the Sun. The solid horizontal bars indicate the $5\sigma$ detection limits of the FIS all-sky survey (Kawada et al., 2007), and the dashed bars indicate those expected when stacking analyses of a) 1000, and b) 100 stars are performed, respectively. The radius of the CSPs' grain $a$ is assumed to be $a = 5\,\mu$m. The corresponding $T_{\rm eq}$ is a) 13.2 and b) 22.1 K, respectively.

# Chapter3

# Point source calibrations of the AKARI/FIS all-sky maps

Part of this chapter is published as: Ko Arimatsu, Yasuo Doi, Takehiko Wada, Satoshi Takita, Mitsunobu Kawada, Shuji Matsuura, Takafumi Ootsubo, & Hirokazu Kataza
"Point source calibration of the AKARI/FIS all-sky survey maps for stacking analysis"
Publications of the Astronomical Society of Japan, Volume 66, issue 2, id 47

## 3.1 Introduction

The present study intends to search for exo-CSPs by investigating spatial and spectral properties of the FIR emission from the stacked images of nearby A-type stars. The spatial and spectral studies are performed by deriving radial brightness profiles (RBPs) and carrying out photometry. In order to extract accurate RBP of the FIR emission, a subtraction of the extended component from the central unresolved sources are needed, because the angular sizes of the exo-CSPs are comparable to that of the PSFs. This subtraction procedure requires the information of the RBP of the PSF (e.g., Arimatsu et al. 2011a), which was not determined in previous studies for the FIS maps. Furthermore, in order to carry out photometry of the exo-CSP emission, photometric calibrations for point sources are required. The FIS all-sky map is calibrated only by diffuse sources with angular scales greater than degree-scale, such as zodiacal and interstellar dust emission (Matsuura et al. 2011, Takita et al. in prep.). Additional flux calibrations for point sources are thus required. Since the present study intends to perform the photometry and the RBP analyses of the exo-CSPs with fluxes down to an order of magnitude lower than the detection limits, by applying the stacking analysis, one has to check whether the calibrations and the radial properties of the PSF can be applied to the faint sources or not.

This chapter focuses on the post-launch calibrations for point sources in the *AKARI*/FIS diffuse maps. For the calibrations, I adopt infrared standard stars proposed by Cohen et al. (1999) with a flux range from 0.06 to 12 Jy at 90 $\mu$m. To investigate PSFs and photometric properties of the faint standard stars, I use a stacking analysis for the present study. By stacking the FIS maps at the locations of standard stars, signals from the faint standard stars are statistically investigated.

I present RBPs of the point sources in the FIS maps with fluxes down to about ten times lower than the detection limits. Also, I compare fluxes of the stacked sources derived with aperture photometry to average fluxes that are expected from model spectral templates (Cohen et al., 1999). From the comparison, calibration factors for point sources are calculated. I also check flux-dependence of the calibration factors by comparing the calibration factors calculated between stacked stars of different flux ranges.

In this chapter, section 2 describes a selection method of the stacked targets and the stacking method used for the present study. In section 3, I report radial properties of point sources obtained by the stacking method and calibration factors for point source fluxes. Our results are discussed in section 4, and section 5 offers a short summary.

## 3.2 Data analysis

### 3.2.1 Selection of the data sets and stacking method

Calibration stars are selected from the infrared standard star catalogue proposed by Cohen et al. (1999). This catalogue includes 422 giant stars with spectral types of K0 to M0. These stars have been studied extensively using the optical and infrared observation data. Cohen et al. (1999) confirmed that the catalogued stars are well isolated, and the flux of each star is more than 20 times higher than the total flux from nearby sources located within a radius of $6'$ at the mid-infrared wavelengths. The infrared model spectrum is derived for each star based on the photosphere emission templates scaled by photometric observation results, which are concluded to be reliable with accuracies better than 6 %. However, these stars were checked in the FIR wavelengths range only with the IRAS data. These stars may have excess emission from their circumstellar dust at FIR that could not be detected with IRAS. I thus reject stars with possible FIR excesses by the following criteria.

For the calibration stars with their model fluxes less than 1.0 Jy at 90 $\mu$m, information of the variability is extracted from the SIMBAD database (`http://simbad.u-strasbg.fr/simbad/`); the stars with the stellar types identified as variable stars are rejected from the sample. Several positions of the stars are severely contaminated with background interstellar dust emission, and I exclude positions with the background surface brightnesses of more than 20 M Jy sr$^{-1}$ at the FIS 90 $\mu$m band. Aperture photometry is performed at the individual positions of the stars on the 90 $\mu$m maps with an aperture radius of $90''$. I compare the observed fluxes with those expected from the model spectrum by Cohen et al. (1999), and five stars with fluxes $5\sigma$ higher than the expected fluxes are rejected. A search of the Cohen catalogue that satisfied these criteria produces 353 stars. I then exclude the images that contaminates with stripe-like patterns (thought to be due to anomalous output signals after the detector reset; Doi et al. in preparation) or speckles (thought to be due to high-energy particle hitting; Kawada et al. 2007) with surface brightness of larger than $\sim 6, 2, 4$ M Jy sr$^{-1}$ at the 65, 90, and 140 $\mu$m, respectively. Therefore 15, 2, 16 stars are excluded from standards at the 65, 90, and 140 $\mu$m, respectively.

The number of the selected stars in each expected flux bin is presented in table 3.1. The expected flux is derived by convolving the model spectrum of each star with the spectral responsivity function for the FIS bands. The expected fluxes range from 0.1 to 19, 0.06 to 12, and 0.02 to 3.7 Jy in the 65, 90, and 140 $\mu$m bands, respectively.

### 3.2.2 Stacking Analysis

I stack the all-sky map at the locations of the selected stars over their appropriate flux bins. In this procedure, I evaluate values on finer pixels ($3''.75 \times 3''.75$ grids) over

Table3.1 Number of selected standard stars in each flux bin.

| flux range [Jy] | 60 $\mu$m | 90 $\mu$m | 140 $\mu$m |
|---|---|---|---|
| used for the PSF | 49 | 97 | 9 |
| $-3.98$ | 7 | 4 | 0 |
| $3.98 - 1.58$ | 29 | 16 | 2 |
| $1.58 - 0.63$ | 41 | 43 | 11 |
| $0.63 - 0.25$ | 89 | 39 | 34 |
| $0.25 - 0.1$ | 172 | 182 | 37 |
| $0.1-$ | 0 | 67 | 253 |

$24' \times 24'$ image by the cloud-in-cell interpolation; an output pixel value is derived by weighted averaging of the nearest four pixel values in an input image in accordance with the area of the overlap of the output pixel. The vertical axis of each image is aligned with the scan-direction of the survey. Then the median value of all pixel values in an image is estimated as a background pixel value. This background pixel value is subtracted from all pixels. After that, these images are combined by averaging to make a stacked image. In order to eliminate the contamination with the bright background objects in the stacked image, pixels with pixel values of more than $4\sigma$ above the r.m.s. of the background fluctuations are masked before stacking. This procedure is performed for all of the sample images, except for the image center. In the image center, a scaled PSF normalized to the central pixel value, is subtracted from the image in order to avoid masking signals from the central targets, and then the masking procedure is performed.

## 3.3 Results

### 3.3.1 Point Spread Functions

Firstly, in order to measure the PSFs for bright sources at the 65, 90, and 140 $\mu$m bands, I stack 49, 97, and 9 selected standard stars with their fluxes brighter than 1.2, 0.28, and 0.7 Jy, respectively (see Table 3.1). These thresholds correspond to the typical 2.5$\sigma$ detection limits of the all-sky surey (Kawada et al., 2007). The stacked images are shown in Figure 3.1. The r.m.s. fluctuations of the surface brightnesses in the background of the stacked images relative to the central peak intensity are 4, 2, and 9 % at the 65, 90, and 140 $\mu$m bands, respectively. The background fluctuation contaminates relatively stronger at the 140 $\mu$m band (Figure 3.1c). This is because the standard stars become faint due to the Rayleigh-Jeans distribution of the stellar photospheric spectra; expected fluxes at the 140 $\mu$m band are about 2.5 times fainter than those at the 90 $\mu$m band. At the 65 and 90 $\mu$m bands (Figures 3.1a and b), PSFs are elongated in the in-scan direction (corresponds to the vertical direction of Figure 3.1).

The full widths at the half maximum (FWHMs) of the in-scan, and the cross-scan directions are derived from the stacked images, which are listed in table 3.2. The cross-scan FWHMs are less than 70$''$ at the three bands. Especially at the 65 and 90 $\mu$m bands, the in-scan FWHMs are about two times larger than the cross-scan FWHMs. A possible reason of this asymmetry is that the transient response of the FIS detector is not perfectly corrected in the data reduction procedure (Doi et al. 2009, 2012, see Chapter 2), and the latency of the signal is detected as the prolonged PSF features. I should note that the all-sky maps are constructed from the observations performed with two different scan directions, from North ecliptic

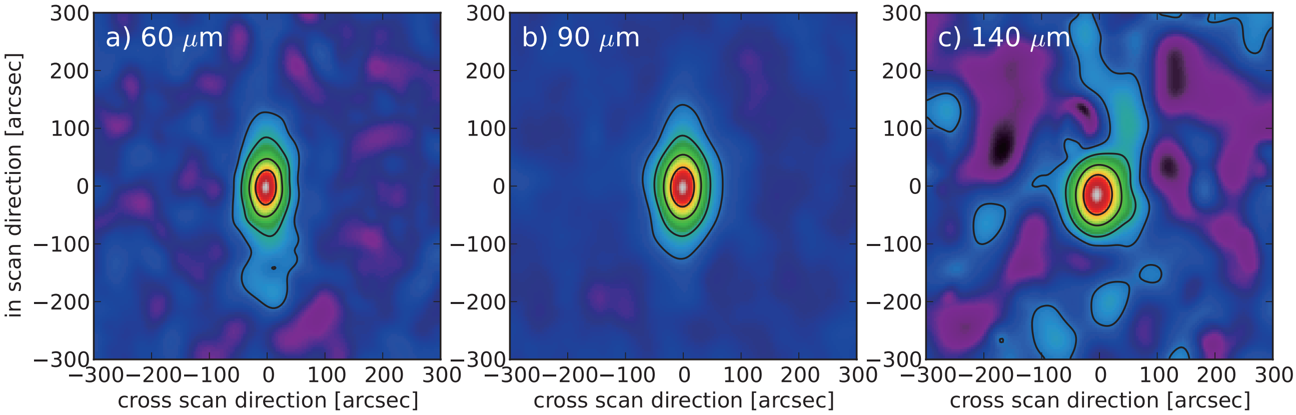


Figure3.1 Stacked images used to measure the PSFs for the FIS 65, 90, and 140 $\mu$m bands. Contours are at 75%, 50%, 25% and 10% of the peak pixel value.

Table3.2 In-scan and cross-scan FWHMs of stacked PSFs for the FIS all-sky map.

| wavelength | 60 $\mu$m | 90 $\mu$m | 140 $\mu$m |
|---|---|---|---|
| In-scan FWHM*1 | $81.7'' \pm 0.5''$ | $98.2'' \pm 0.3''$ | $101.0'' \pm 1.5''$ |
| Cross-scan FWHM*1 | $33.0'' \pm 0.3''$ | $54.76'' \pm 0.14''$ | $70.4'' \pm 1.3''$ |

pole to South ecliptic pole and vice versa. The prolonged feature can thus be axially asymmetric and be different for individual sources in the maps, because the number of the scans of either direction used for the reconstruction of a signal at a pixel is different from location to location. The stacked images are made by simply averaging all observation data, and the asymmetry can be missed in the present study.

The RBPs of the PSFs are also derived from the stacked images by azimuthally averaging the surface brightnesses, which are shown in Figure 3.2. A continuous decline that is expected to be due to extended signals from the point source is seen at radial distances of up to $\sim 150 - 200''$ at the three bands.

*1 Uncertainties are derived by taking the error-bars of the RBPs of the PSFs (see Figure 3.2).

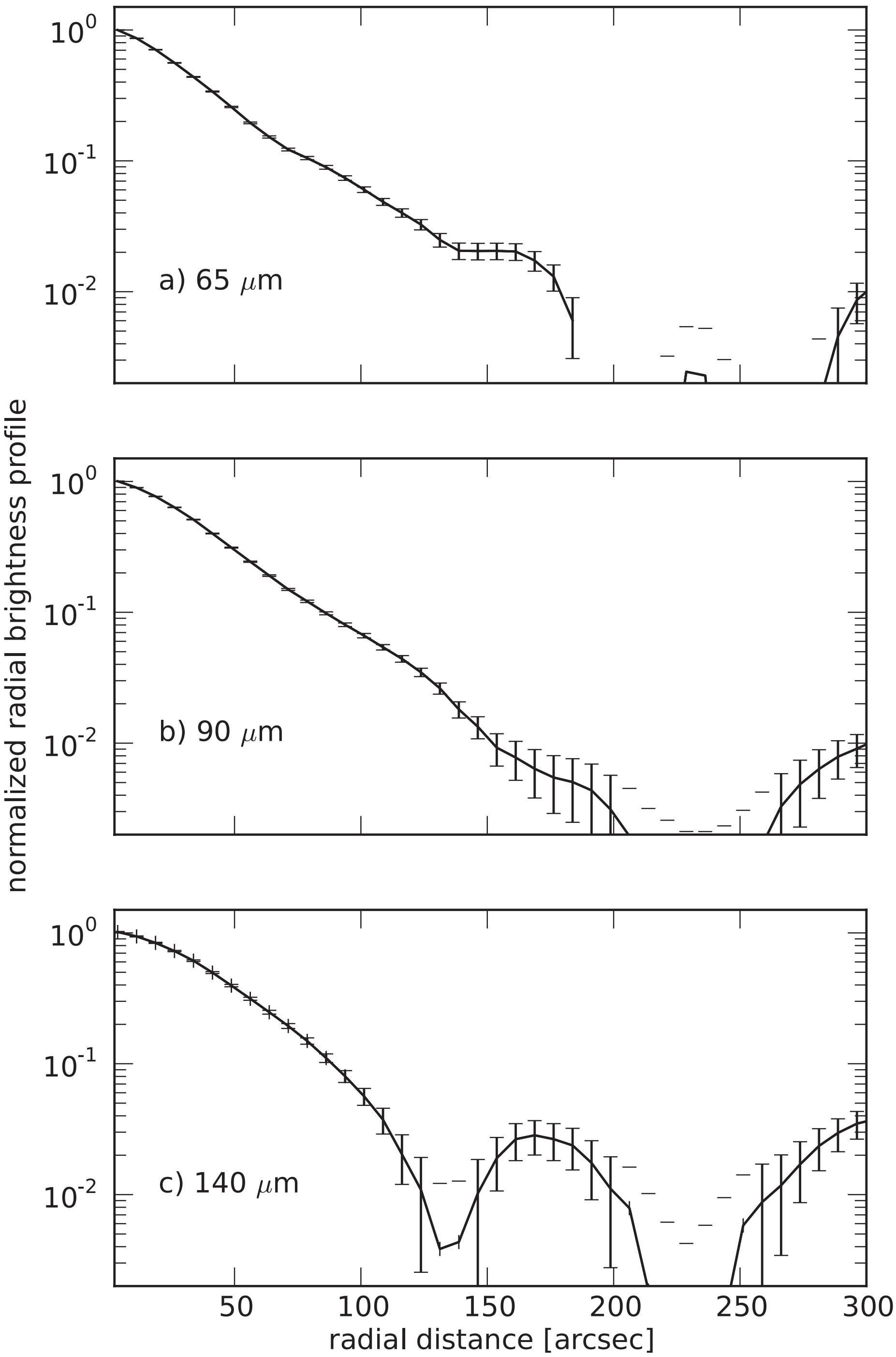


Figure3.2 RBPs of the stacked images used to measure the PSFs at the FIS a) 65, b) 90, c) 140 $\mu$m bands (see Figure 3.1). All profiles are normalized at the central peak. The error-bar corresponds to the $1\sigma$ r.m.s. fluctuations of the profiles in the background region (radial distances of $200'' - 300''$) The horizontal bar corresponds to the $1\sigma$ upper-limit at the radius.

Table3.3 Aperture correction factor for the 226″ aperture

| aperture correction factors | 60 $\mu$m | 90 $\mu$m | 140 $\mu$m |
|---|---|---|---|
| $A(226'')^{*1}$ | $0.810 \pm 0.024$ | $0.856 \pm 0.054$ | $0.97 \pm 0.21$ |

### 3.3.2 Aperture correction factor

In the following, aperture photometry for the standard stars is performed with an aperture radius of 90″ and a background annulus between radii 120 − 300″ in order to reduce contaminations of the background fluctuation. However, as shown in Figure 3.2, the signals from the point sources extend to ∼ 200″. To correct the underestimation of the signals outside the small aperture, aperture correction factors should be applied to the measured fluxes. Two sets of aperture photometry on the stacked images are performed with different apertures; the 90″ aperture, and an aperture with a radius of 226″ and with a background annulus of 251″ − 703″. The aperture correction factor $A(226'')$ is derived from the 90″ aperture flux normalized by the 226″ aperture flux, which is shown in Table 3.3. If one assumes that the 226″ aperture is enough large to sum the total signals from the point source, one can deduce total signals by dividing the 90″ aperture fluxes by $A(226'')$.

### 3.3.3 Stacked point sources with different fluxes

To investigate radial properties of the PSFs for sources with fainter fluxes, I stack the standard sources over their appropriate flux bins. Panels in Figures 3.3, 3.4, and 3.5 show the stacked images of standard sources with different flux bins at

*1 Uncertainties correspond to the deviations of the values measured by aperture photometry with the same aperture radius in four selected areas in the background annulus.

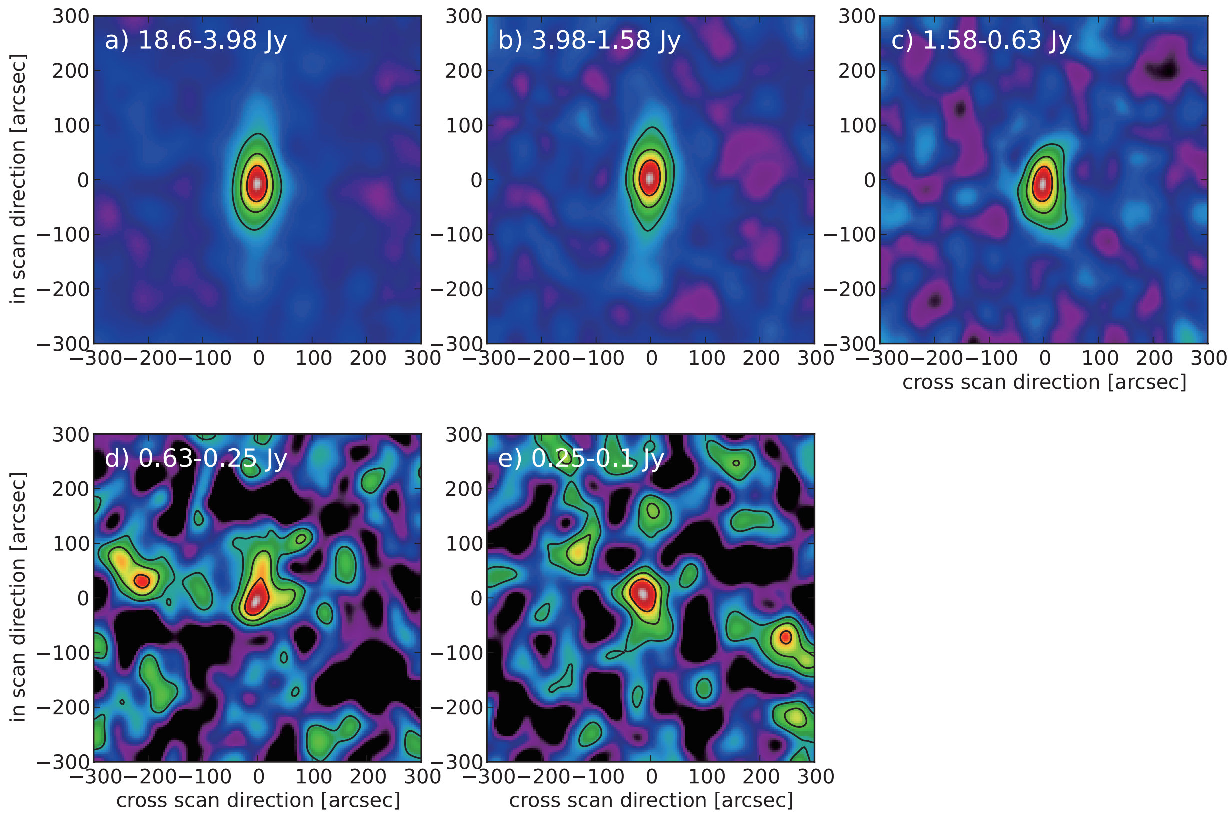


Figure3.3 Stacked images of standard sources for the FIS 65 $\mu$m band with different flux ranges. Contours are at 70%, 50%, and 30% of the central pixel value. Stacked sources in the panels d and e are severely contaminated with background fluctuations. The $1\sigma$ background fluctuation levels are 2.3, 4.6, 7.3, 25, and 27% of the peak intensity of the central stacked source for a, b, c, d, and e, respectively.

the 65, 90, and 140 $\mu$m bands, respectively. Note that a flux range of a bin at the 140 $\mu$m (Figure 3.5c, 0.8 dex) is different from the other bins (0.4 dex) in order to stack sufficient sources. All of the panels at the 90 $\mu$m (Figure 3.4) clearly show the stacked sources at the image center. At the 90 $\mu$m band, the shape of stacked sources for each flux bin seems to follow the stacks for the PSF determination (figure 3.1b). On the other hand, the intensity distributions in the images of two and three fainter groups at the 65 and 140 $\mu$m bands do not seem to follow the PSF (Figures 3.3d, e and 3.5d). In case of the 65 $\mu$m band, the r.m.s. fluctuations of the background surface brightnesses of the stacked images for the brighter three groups (Figures 3.3a, b, c) are

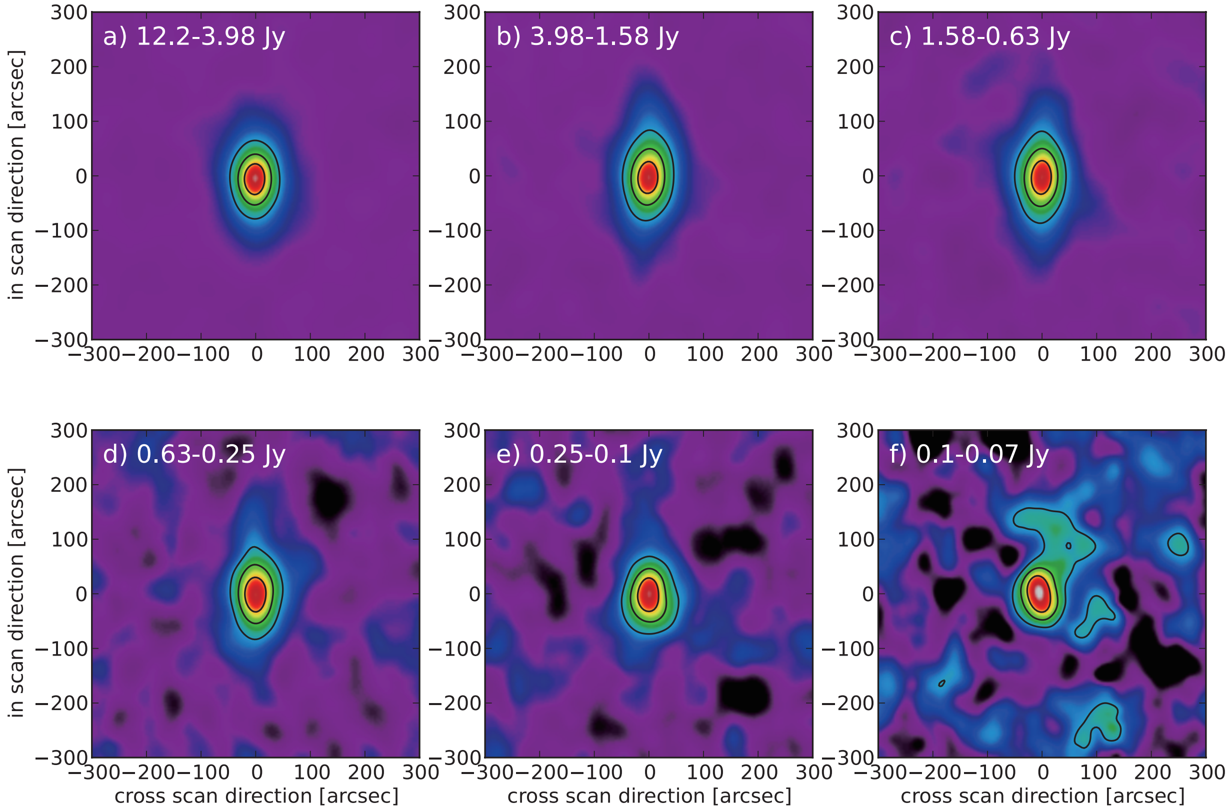


Figure3.4 Same as figure 3.3, but for the 90 $\mu$m band. The 1$\sigma$ background fluctuation levels are 0.7, 1.0, 1.4, 4.0, 4.3, and 9.6% of the peak intensity for a, b, c, d, e, and f, respectively.

2, 5, and 7 % of the peak intensity, respectively. On the other hand, the fainter group images (Figures 3.3d, e) have larger background fluctuation levels, which reach 25 and 27 % of the peak, respectively. The background fluctuations are also clearly seen in the 140 $\mu$m band stacks (Figure 3.5c, and d). Especially, the background fluctuation level of Figure 3.5d is quite high; 57 % of the peak intensity. The amplitude of the aberrations between the stacked sources and the PSFs are similar to the background fluctuations. In conclusion, I cannot exclude possibility that the shape of the PSF changes in these aberration levels.

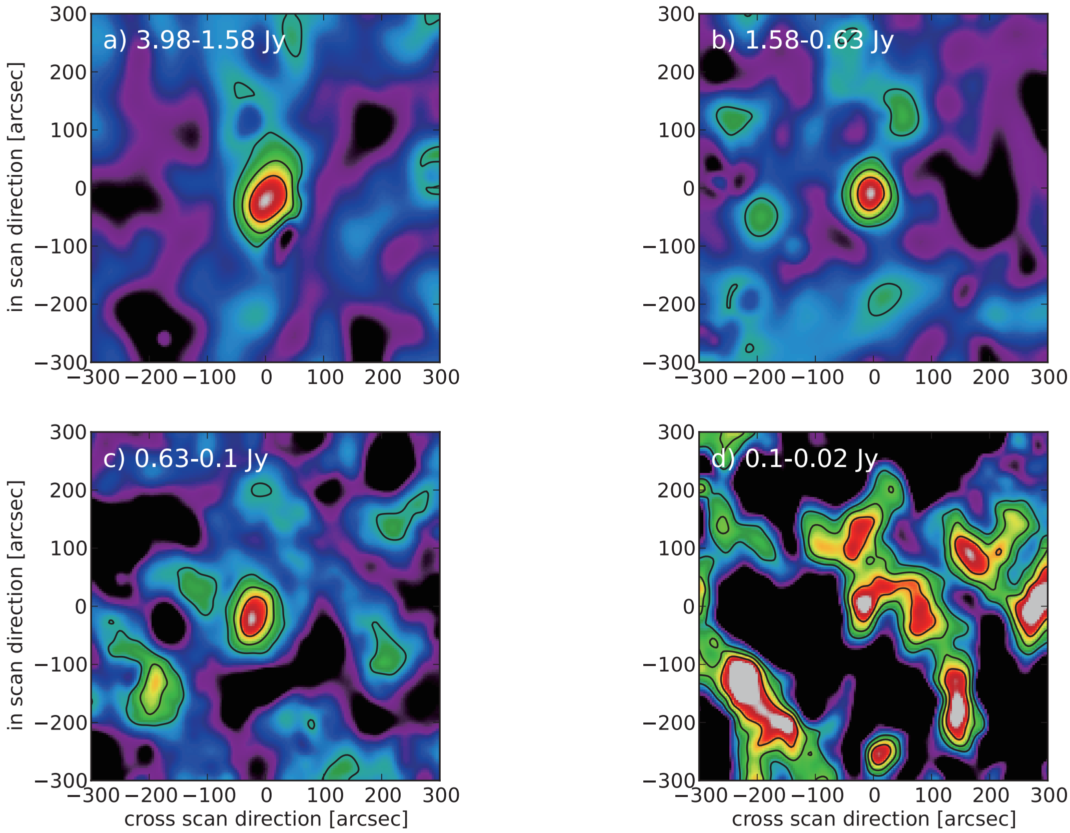


Figure3.5 Same as figure 3.3, but for the 140 $\mu$m band. The $1\sigma$ background fluctuation levels are 9.4, 13, 20, and 57% of the peak intensity for a, b, c, and d, respectively. The stacked source in the panel d is severely contaminated with background structures.

### 3.3.4 RBPs of point sources with different fluxes

To make a further constraint on the PSF for the fainter sources, the surface brightnesses of the stacked images are azimuthally averaged to derive RBPs. The RBPs for the brightest (dashed line) to faintest groups (dot-dashed line) are compared with the RBPs of the PSF stacks in Figure 3.6 (thick-solid line). At the 90 $\mu$m bands, all of the profiles are well consistent with that for the PSF with fluctuations smaller than 5% of the peak intensity; the $1\sigma$ deviations of these RBPs from the PSF profile are 1.6%, 0.5%, 0.5%, 0.6%, 1.0% and 3.2% of the peak intensity for the flux bins of $12.2 - 3.98$, $3.98 - 1.58$, $1.58 - 0.63$, $0.63 - 0.25$, $0.25 - 0.1$, and $0.1 - 0.07$ Jy, respectively. Therefore the RBP of the 90 $\mu$m PSF is well determined by the stacked image of bright standards (Figure 3.1b) in the investigated flux range ($0.06 - 12$ Jy). On the other hand, significant aberrations from the PSF profiles can be seen in the profiles of several groups at the 65 and 140 $\mu$m bands. At the 65 $\mu$m band, the aberration is significant in the profile for the faintest bin ($0.25 - 0.1$ Jy, dot-dashed red line in Figure 3.6a); the profile is dropped with an amplitude of $\sim 20\%$ of the peak at $\sim 100''$ from the center. Though any gradual change of the RBPs as a function of the fluxes is not confirmed in brighter bins, I cannot exclude a possibility that the profiles can change for point sources with fluxes below 0.25 Jy at the 65 $\mu$m band. Aberrations are also seen in the profiles of the most flux bins at the 140 $\mu$m band (see Figure 3.6c). The aberrations do not seem to be a function of the flux, but their amplitude reaches $\sim 20\%$ of the peak intensity at most. The RBP of the 140 $\mu$m PSF is not determined with a precision better than this aberration level in the present study.

### 3.3.5 Absolute Flux Calibration

In order to derive the calibration factor for point-source photometry, I compared the fluxes obtained by aperture photometry with their model prediction. Aperture photometry of stacked point sources is performed on the stacked images with the $90''$ aperture, which is presented in figure 3.6. The sky background is measured in the annulus with the inner and outer radii of $120''$ and $300''$. Uncertainties of the fluxes are derived from the scatter of the values measured in four areas with the same aperture radius of $90''$ in the background annulus. The derived fluxes are divided by the aperture correction factors, $A(226'')$ (see Section 3.3.2) to derive a total flux from the stacked sources.

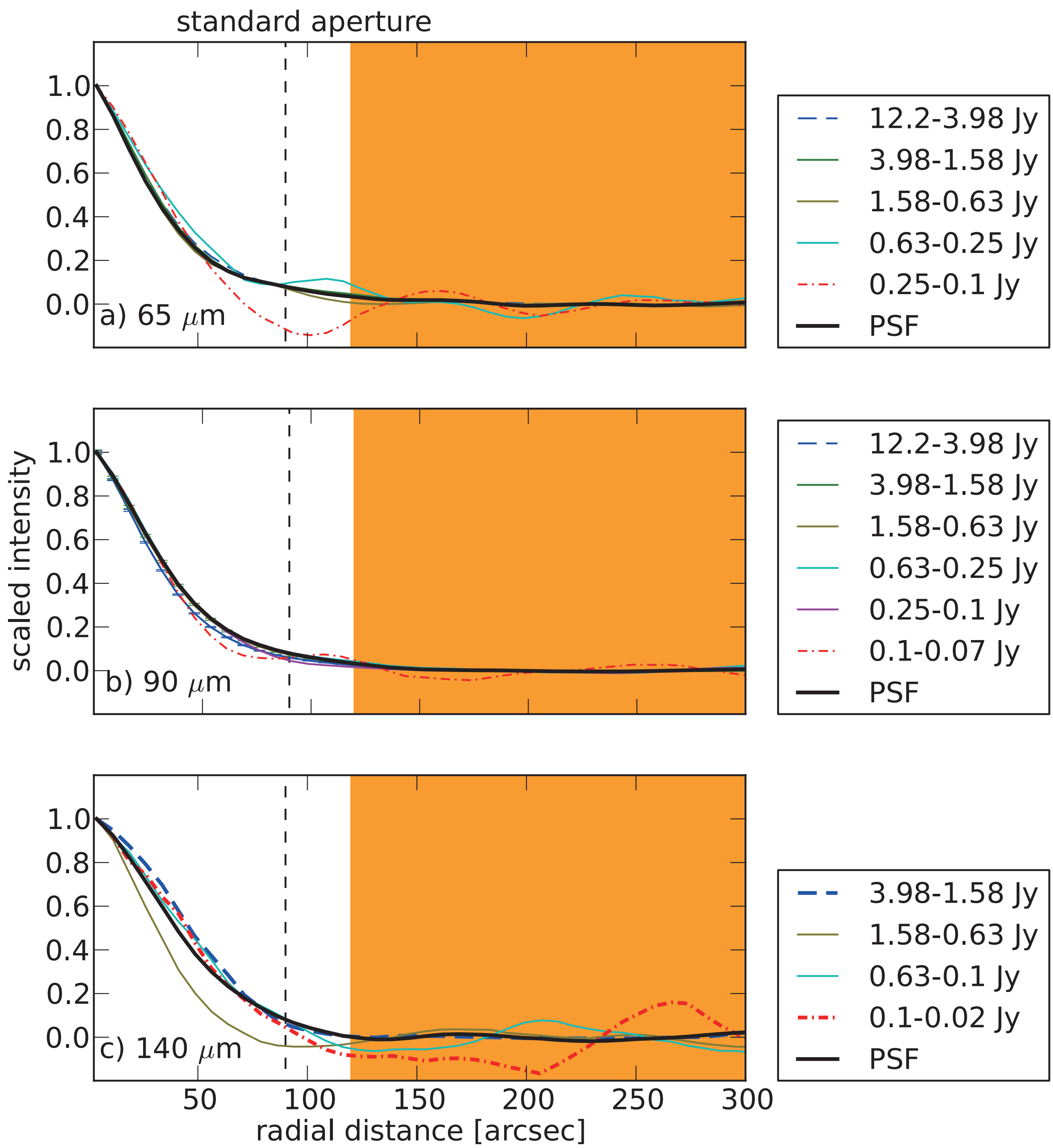


Figure3.6 Normalized radial intensity profiles of a point source derived by the stacking image at the FIS a) 65, b) 90, and c) 140 $\mu$m bands. The lines in the individual figures are the profiles for the standard stars with different fluxes. The bold dashed and dot-dashed lines in each panel are the stars for the maximum and minimum flux groups, respectively. The bold solid lines represent the profiles of the PSFs shown in figure 3.1. An aperture radius ($90''$) for photometry is shown as the vertical dashed line, and the background annulus ($120'' - 300''$) is also shown as the orange area.

Figure 3.7 shows the observed-to-expected flux ratio for the stacked calibration standards as a function of the average expected flux in each flux bin. The ratio between the observed and expected fluxes represents the calibration factor for point-source photometry. The calibration factors are always lower than the unity at the three bands. This means that the observed fluxes are always lower than the expected ones at the three bands.

A possible reason for the obtained result is that the observed fluxes are underestimated due to missing fluxes from the point sources. The missing signals can be induced via the slow transient response of the detector (Shirahata et al., 2009). As already noted in Chapter 1, the transient response of the FIS detectors is a major cause to decrease the signals of the point sources. A typical transient timescale of the FIS detectors is known to be a few to 20 seconds (Kaneda et al., 2002). On the other hand, taking the scan speed ($3'.6$ sec$^{-1}$) and the cross-scan FWHMs of the PSFs (33, 55, and $70''$ for the 65, 90, and 140 $\mu$m, respectively) into consideration, a point source is scanned in only $0.2 - 0.3$ sec, which is much smaller than the transient timescales. This short scan timescale of the point sources is not enough for the detectors to reach a constant output level, and resulting in the relatively smaller output signals for point sources.

Missing signals also can be induced by scattered photons inside optical instruments and detectors. It is possible that photons from the point sources are scattered in the entire detectors, and can be missed, because they can be too extended and too faint (with brightness levels of down to smaller than $10^{-3}$ of the peak intensity of the PSFs; Arimatsu et al. 2011b) to detect the present RBPs of the stacked point sources (Figure 3.2).

The flux ratios do not seem to show a flux-dependent trend, and can be approximated by a constant value. The weighted means of the ratios are derived to be

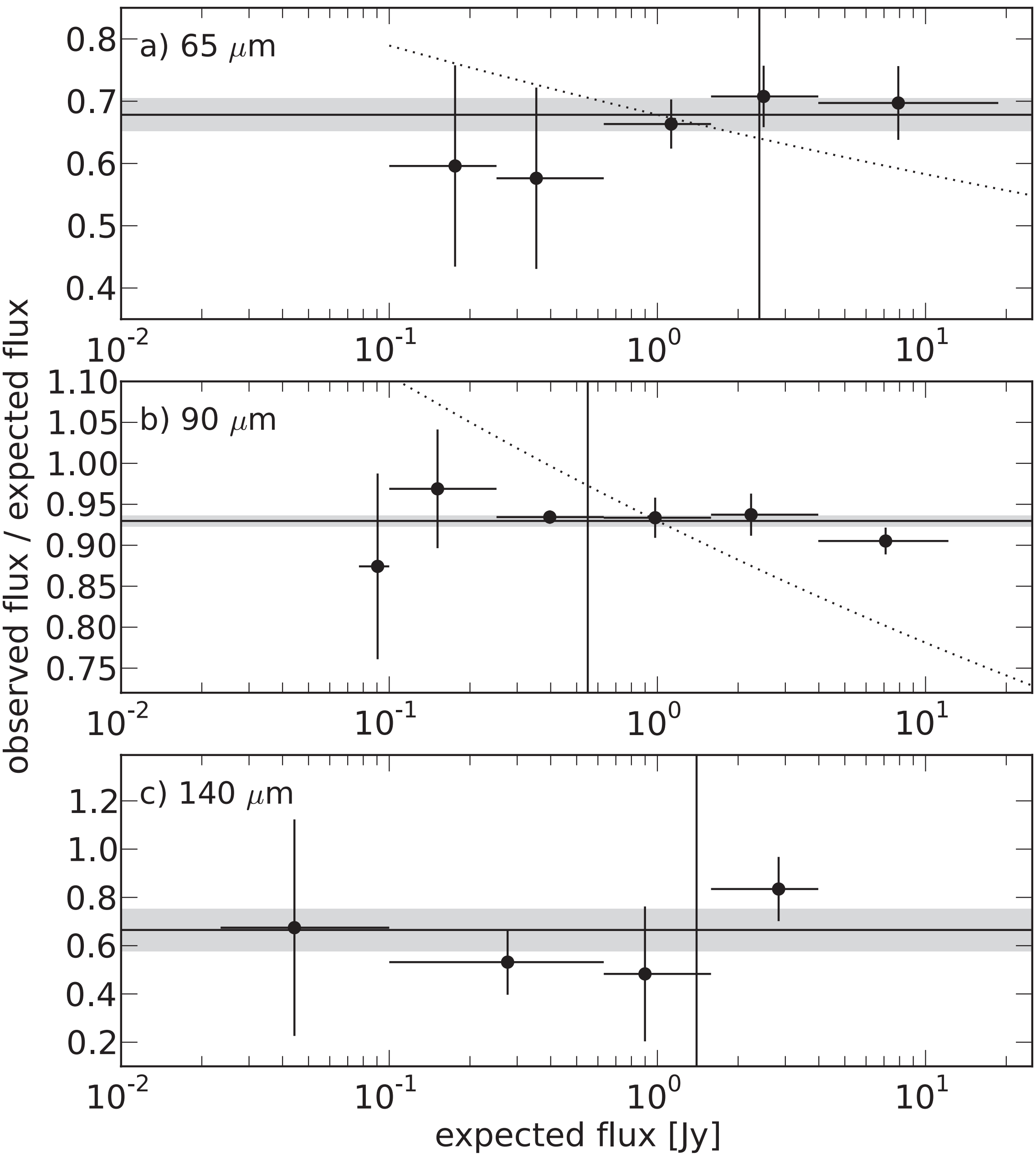


Figure3.7 The observed-to-expected flux ratio as a function of the expected flux at the FIS a) 65 , b) 90, and c) 140 $\mu$m. The error bars on the $y$-axis represent the 1$\sigma$ photometry uncertainties. The solid lines with gray areas are the weighted averages with the 1$\sigma$ uncertainties. The vertical line represents the 5$\sigma$ detection limit of the All-Sky Survey at each band (Kawada et al., 2007). The dotted lines in panels a and b indicate the correction factors derived by the slow-scan mode observations (Shirahata et al., 2009), which are normalized by the weighted averages at the expected flux of 1 Jy.

$0.760 \pm 0.019$, $0.930 \pm 0.007$, and $0.67 \pm 0.09$, for the 65, 90, and 140 $\mu$m bands, respectively. The deviations of the observed fluxes from the weighted means are 9, 3.2, and 21 % for the 65, 90, and 140 $\mu$m, respectively. The 140 $\mu$m deviation is relatively higher than the other two bands. Taking the large error bars of photometry, as shown in Figure 3.7c, into consideration, the deviation at the 140 $\mu$m is mainly due to the large flux uncertainties. These results present photometry for sources at the 65, 90, and 140 $\mu$m band can be performed by using the calibration factors approximated to be constant with accuracies of these deviations throughout the flux ranges of $19-0.1$, $12-0.06$, and $0.02-3.7$Jy, respectively.

## 3.4 Discussions

### 3.4.1 Comparison with the FIS Pointed Observations

In addition to the all-sky survey used in the present study, *AKARI*/FIS had performed slow-scan observations for the pointing mode, and their data characteristics were investigated in the previous studies (Kawada et al., 2007; Shirahata et al., 2009). In the previous studies, the ratios between the observed fluxes and those expected from model spectra show a clear flux-dependence at the 65 and 90 $\mu$m bands (Shirahata et al., 2009). In the flux range of $0.1-10$ Jy, the calibration factor decreases with source fluxes by $\sim 20\%$, and 30% for the 65 and 90 $\mu$m, respectively (see dotted lines in Figure 3.7; Shirahata et al. 2009). On the other hand, the corresponding flux-dependences do not seem to appear in the present calibrations for the all-sky maps (Figure 3.7).

One of the major differences between the slow-scan and all-sky observations is scan speeds during the observations. The flux-dependence calibration trend seen in the slow-scan observations was thought to be due to an input-flux dependence of the transient response function of the FIS detector. According to the laboratory tests, the response function depends on the input fluxes in a timescale of $1 - 20$ seconds (Shirahata et al., 2004). This means that the output signal intensity at a time within this timescale range is not linearly correlated with the input flux. In the slow-scan observations, the detector sweeps the sky with a scan speed of 7 or $15''\,\mathrm{sec}^{-1}$, and thus the integration times of the point sources correspond to 7.9 or 3.7 seconds, respectively, assuming an angular size of the point sources is comparable to the cross-scan FWHM of the $90\,\mu$m band PSF ($55''$, see table 3.2). These timescales are comparable to the flux-dependent transient timescale. The observed flux ratio is thus thought to show the clear flux-dependence in the slow-scan observations.

On the other hand, the detector sweeps the sky with a much higher scan speed ($3'.6\ \mathrm{sec}^{-1}$) in the all-sky observations. A point source is scanned in only about 0.25 second. The transient functions within this short timescale (initial pulse; with a timescale of $\sim 0.1$ second) are known to be flux-independent (Shirahata et al., 2004); the output signal intensity at a time within this timescale range is proportional to the input flux. Therefore the flux-dependent transient effect is expected to be less severe for the all-sky observations.

While the deviations of the fluxes after applying the calibration factors at the 65 and $140\,\mu$m bands (9 and 21%) are similar to, or slightly larger than that derived by pointed observations ($\sim 15\%$, Shirahata et al. 2009), the deviation for the $90\,\mu$m band (3%) is much smaller than the slow-scan value (13%, Shirahata et al. 2009). However, I should note that the present results can be missed possible variations of the calibration factors due to spectral variations of the objects. The present study only uses the stars, whereas previous studies also used asteroids, which have different spectra at FIR. For the FIS detectors, each pixel of the detector array has a different spectral response (Kawada et al., 2007), which may result in the variations of the fluxes. This uncertainty would be included in the uncertainty of the calibration factors derived by Shirahata et al. (2009), but would not be included in the present results. Especially for the 90 $\mu$m and the 140 $\mu$m bands, the wavelength ranges of the spectral responsivity are broader than the other bands (Kawada et al., 2007), and the flux variations due to the spectral variations thus can be more significant. According to Verdugo et al. (2007), the error in photometry variation of the spectral responsivity can be $\sim$ 10%. Therefore, I assume the typical error in photometry due to infrared color of the object is 10%, and adopt the total error of the aperture correction factor at the 90 $\mu$m band to be 10 % in the following study.

### 3.4.2 Possible applications of the calibration factors for fainter sources

Since signals in the FIS all-sky data are dominated by the background emission, such as the zodiacal light, the diffuse galactic interstellar emission, and the extragalactic background light, it seems to be possible that the constant calibration factors are allowed to be extrapolated to flux ranges fainter than the sources used in the present study. According to the empirical model for the FIS detector established by Kaneda et al. (2002), the slow transient response should depend on the total photo-current, which includes background light and signal from the target. Typical surface brightnesses at the high ecliptic and galactic latitudes, where the background zodiacal and diffuse galactic emission intensity reaches minimal level, are $\sim 4, 4$, and $2\,\mathrm{MJy\,sr^{-1}}$ at the 65, 90, and 140 $\mu$m bands, respectively (Matsuura et al., 2011). Taking beam solid angles for the FIS bands (4, 5, and $10 \times 10^{-8}$sr; Shirahata et al. 2009) into consideration, fluxes of the background emission in a beam are expected to be larger than $\sim 0.2$ Jy at the three bands, which are 2, 3, and 10 times brighter than point sources in the faintest flux ranges investigated in the present study. Since the zodiacal and the diffuse galactic emission are stronger in most of the sky, photons in a beam are typically dominated by the background light than the fainter point sources. It is thus unlikely that the calibration factors would be a function of the fluxes of the fainter point sources. Therefore, these flux-independent calibrations can be performed for objects with fluxes smaller than the investigated flux ranges.

## 3.5 Summary of this chapter

In this chapter, determinations of the RBPs and flux calibrations for faint point sources in the *AKARI*/FIS all-sky 65, 90, and 140 $\mu$m maps have been performed with infrared calibration stars. By stacking the bright sources the PSFs are determined. The RBP of the PSF is determined over a $12 - 0.06$ Jy flux range at the 90 $\mu$m map with precisions better than 5% of a peak intensity, but is not determined with precisions better than 20% at the 65 and 140 $\mu$m maps. The calibration factors are derived by comparing the measured photometry values of the stacked stars to the emission model values. The deviations of the observed photometry for the stacked stars with different fluxes from the calibration factor were estimated to be better than 20% for the three bands within flux ranges of $19 - 0.1$, $12 - 0.06$, and $3.7 - 0.02$ Jy at the 65, 90, and 140 $\mu$m bands, respectively. Any flux dependence in the calibration factors with amplitude larger than the deviations is not seen on the investigated flux ranges at the three bands.

# Chapter4

# Stacking analysis of the nearby A-type main-sequence stars

Part of this chapter will be submitted to Astrophysical Journal as:
Ko Arimatsu, Yasuo Doi, Takehiko Wada, Satoshi Takita, & Hirokazu Kataza
"Evidence for the extended dust emission around nearby A-type stars"

## 4.1 Introduction

This chapter describes the results of spatial and spectral studies on nearby A-type stars in the *AKARI*/FIS all-sky maps. Whatever is in the exo-CSPs around the stars, such as debris and dust grains, would emit far-infrared radiation (Stern et al. 1991; see chapter 2), which is the analogue of the infrared emission from debris disks. The FIR emission from the exo-CSPs can be distinguished from the debris disk emission because the exo-CSPs of the present interest are expected to extend ($>$ 1000 AU, see Chapter 1) farther than typical debris disks (smaller than an order of 100 AU, Wyatt 2008). I thus have searched for the extended FIR emission around nearby A-type stars, where the emission from the exo-CSPs is expected to be strong (see chapter 2). In order to search for the faint exo-CSP emission, a stacking analysis for the A-type stars is carried out. In Chapter 3, I found stacked point sources in the *AKARI* FIS 65, 90, 140 $\mu$m all-sky maps are well calibrated by the calibration factors, and the radial profile of the stacked point sources is well determined at the 90 $\mu$m. Therefore one can perform accurate photometry and investigations of the radial properties of the FIR emission using the stacked images.

In this chapter, section 2 describes a selection method of targets and a stacking method used in the present study. In section 3, I report results of photometry of the A-type stars using the stacked image. The SEDs of the measured fluxes are fitted to simple thermal spectra. Section 4 describes the RBPs of the FIR emission that are averaged from the stacked images. The RBPs are compared with the PSF and a simple profile model. Section 5 offers a short summary.

## 4.2 Selection of the targets and stacking method

In this study, I use the *AKARI*/FIS all-sky maps (Doi et al., 2009, 2012) at the N60 (65 $\mu$m), Wide-S (90 $\mu$m), and Wide-L (140 $\mu$m) bands. These maps are preliminary version 130401, which went through data reduction procedures that apply to the publicly released dataset. The properties of the point sources in the maps at the three bands are described in chapter 3. I do not use the N160 (160 $\mu$m) band map because the sensitivity is too low for the faint source studies (see chapter 2).

### 4.2.1 Target selection

Targets for this study are selected from the Hipparcos catalogue (Perryman et al., 1997). The Hipparcos catalogue includes nearby stars with their parallaxes (i.e., distances). I adopt stars noted as A-type stars in the Hipparcos catalogue for the targets. In order to select stars close to the main-sequence phase, the targets must confirm the following criterion

$$-0.2 < M_V < 8 \times [B - V] + 2, \tag{4.1}$$

where $B - V$ is the star's color index and $M_V$ is the absolute V-band magnitude. I should note that several A- stars with luminosity classes of IV − III, main-sequence stars with fainter spectral types (typically F0-F1V), and Herbig Ae/ Be stars can be included in the sample with this criterion, because they are negligibly off the MS on an H-R diagram. Especially Herbig Ae/ Be stars can be embedded in the dense interstellar medium that would result in confusions of the extended FIR emission around stars. I thus rejected candidates of the Herbig stars from the sample. The candidates are selected using the Hipparcos catalogue and the near- to mid-infrared All-Sky Source Catalog produced by the Wide-field Infrared Survey Explorer (WISE, Wright et al. 2010), and the following spectral selection criteria proposed by Vieira et al. (2003);

$$0.75 \log \left( \frac{F_{12}}{F_V} \right) - 1 \leq 2, \tag{4.2}$$

where $F_V$ is the flux at the $V$ band, and $F_{12}$ is that at the WISE 12 $\mu$m band. Several positions of the stars are severely contaminated with the interstellar dust emission. I thus exclude stars at positions with the background surface brightnesses of more than $\sim 20\,\mathrm{M\,Jy\,sr^{-1}}$ at the FIS $90\,\mu$m band from the following analysis. This is the same criterion as that adopted for the standard star investigations (see Chapter 2), and allows us to select samples located at regions with typical background fluctuations below $\sim 1\,\mathrm{MJy\,sr^{-1}}$ at the $90\,\mu$m band. I also exclude images that severely contaminate with detector-induced noises (see Chapter 3) from the targets.

Finally, I have selected 63 A-type stars within 15.8 – 39.8 pc from the Sun from the Hipparcos catalogue, which are listed in Table 4.1. In addition, 3520 stars within 39.8-158 pc (listed in Appendix A) are selected to compare the stacking results with the closer samples. The sample targets are divided into three distance bins, a, $15.8 < d < 39.8$ (group 1), b, $39.8 < d < 100$ (group 2), and c, $100 < d < 158$ pc (group 3). Average distances of the stars in the three bins are 29.4, 78.4, and 131 pc, respectively. The positions of the selected stars that are overlaid on the FIS $90\,\mu$m band all-sky map are shown in Figure 4.1. The target stars are isotropically distributed in the whole sky, except for the Galactic disk region, where the background diffuse infrared emission is severely contaminated. The typical background fluctuations of the selected regions are comparable to or smaller than 0.5 $\mathrm{M\,Jy\,sr^{-1}}$ (see Table 4.1).

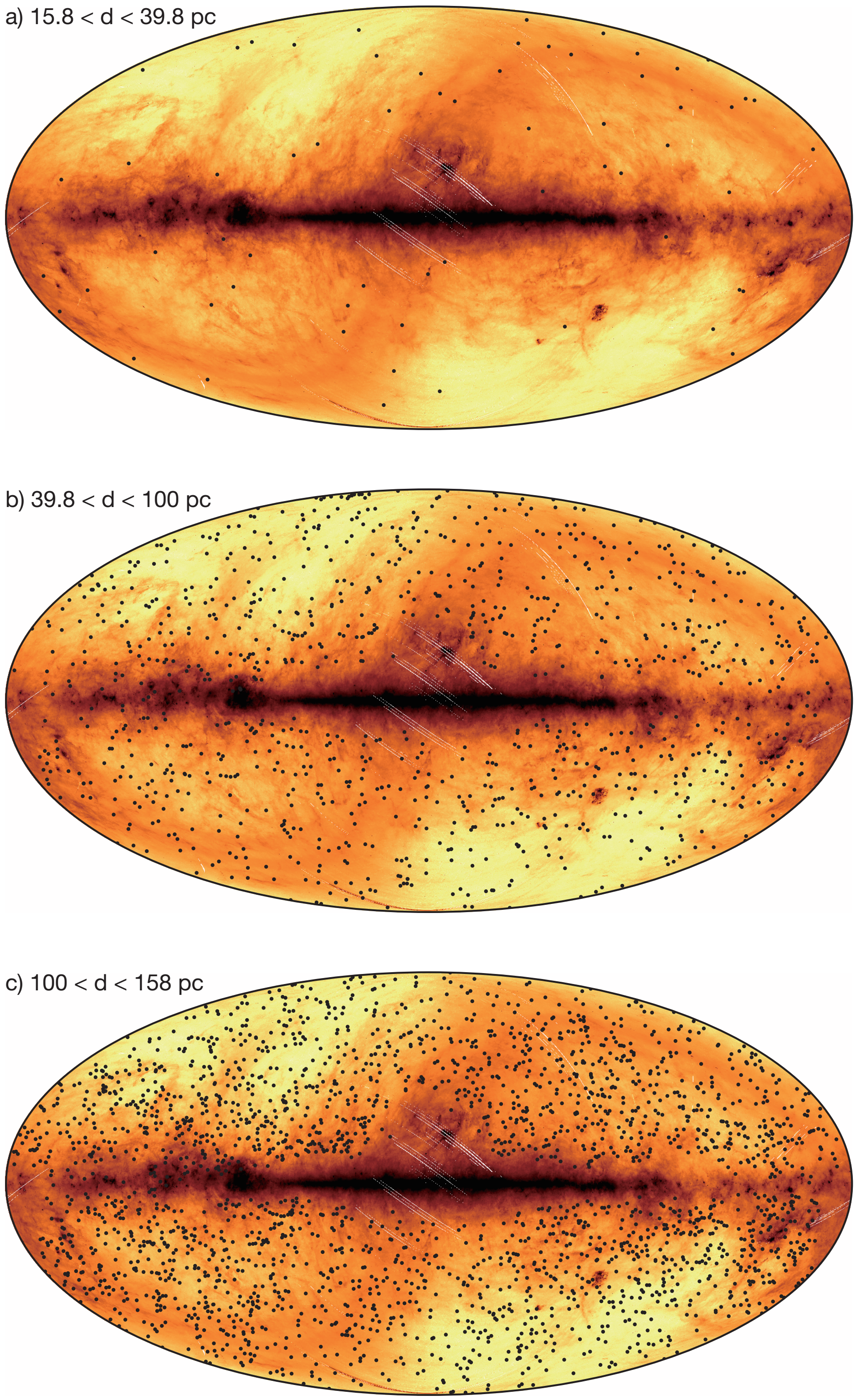


Figure4.1 The positions of the stars grouped into 0.4 dex distance bins: a), $15.8 < d < 39.8$ (group 1), b), $39.8 < d < 100$ (group 2), and c), $100 < d < 158$ pc (group 3), overlaid on the FIS 90 $\mu$m band map.

Table4.1: Selected A-type stars located at $15.8 < d < 39.8$ pc (group 1)

| Hipparcos ID | parallax [mas] | stellar type | K flux [Jy] | 90 $\mu$m expected flux [Jy] | background r.m.s. [MJy sr$^{-1}$] | $L_*$ [$L_\odot$] |
|---|---|---|---|---|---|---|
| 2072 | 42.51 | A5IVn*1 | 24.43 | 0.0252 | 0.24 | 10.9 |
| 8903 | 54.74 | kA4hA5mA5Va*2 | 82.4 | 0.0851 | 0.33 | 21.1 |
| 9480 | 27.91 | A5V*3 | 13.25 | 0.0137 | 0.30 | 16.5 |
| 10064 | 26.24 | A5IV*2 | 56.59 | 0.0585 | 0.32 | 69.0 |
| 10670 | 27.73 | A1Vnn*4 | 17.41 | 0.018 | 0.38 | 20.9 |
| 12706 | 39.78 | A2Vn*2 | 39.22 | 0.0405 | 0.32 | 15.0 |
| 14146 | 37.85 | A4V*5 | 24.82 | 0.0256 | 0.35 | 9.9 |
| 15197 | 27.18 | kA4hA9mA9V*1 | 13.61 | 0.0141 | 0.56 | 11.0 |
| 18907 | 25.24 | A0.5Va*1 | 20.45 | 0.0211 | 0.38 | 30.7 |
| 22845 | 27.04 | A3Va*2 | 11.42 | 0.0118 | 0.47 | 12.5 |
| 23875 | 36.71 | A3IV*2 | 73.3 | 0.0757 | 0.32 | 38.5 |
| 27321 | 51.87 | A6V*1 | 25.91 | 0.0268 | 0.38 | 7.8 |
| 32607 | 32.96 | A8VnkA6*1 | 62.51 | 0.0646 | 0.17 | 29.5 |
| 33705 | 25.57 | A4/A5IV*6 | 4.34 | 0.0045 | 0.46 | 2.4 |
| 35350 | 34.59 | A3V*7 | 25.7 | 0.0265 | 0.45 | 30.0 |
| 35643 | 28.99 | F2VkF1mF0*2 | 7.66 | 0.0079 | 0.39 | 4.1 |

| | | | | | | |
|---|---|---|---|---|---|---|
| 41307 | 26.09 | A0V*8 | 15.57 | 0.0161 | 0.24 | 41.7 |
| 42913 | 40.9 | A1Va(n)*1 | 136.88 | 0.1414 | 0.43 | 65.8 |
| 44382 | 26.24 | kA3hA5mA5V*1 | 18.65 | 0.0193 | 0.17 | 31.6 |
| 44901 | 34.12 | Am*9 | 16.11 | 0.0166 | 0.31 | 11.8 |
| 45075 | 26.79 | kA5hF0mF5II*2 | 17.33 | 0.0179 | 0.32 | 15.5 |
| 45493 | 27.55 | A5V*3 | 12.81 | 0.0132 | 0.46 | 11.1 |
| 48926 | 30.67 | A8IV*6 | 10.79 | 0.0111 | 0.31 | 5.5 |
| 49593 | 35.78 | A7V(n)*2 | 16.69 | 0.0172 | 0.34 | 7.7 |
| 51658 | 29.13 | A7V*10 | 13.97 | 0.0144 | 0.33 | 10.1 |
| 53910 | 41.07 | A1IVps*2 | 81.27 | 0.084 | 0.28 | 54.0 |
| 53954 | 26.37 | A1V*2 | 12.53 | 0.0129 | 0.39 | 17.5 |
| 54872 | 56.52 | A5IV(n)*2 | 92.54 | 0.0956 | 0.38 | 17.8 |
| 57328 | 27.29 | A4V*3 | 11.49 | 0.0119 | 0.40 | 10.5 |
| 58001 | 38.99 | A0Ve+K2V*11 | 71.18 | 0.0735 | 0.27 | 72.7 |
| 58684 | 29.48 | F0Vam*2 | 10.06 | 0.0104 | 0.28 | 7.1 |
| 59504 | 29.7 | kA6hF0mF0*2 | 11.9 | 0.0123 | 0.27 | 7.1 |
| 61468 | 28.92 | A7V*1 | 9.9 | 0.0102 | 0.34 | 7.5 |
| 61960 | 27.1 | A3Va*4 | 8.97 | 0.0093 | 0.36 | 10.1 |
| 63076 | 34.67 | F1VmA7(n)*2 | 11.32 | 0.0117 | 0.19 | 4.3 |
| 63125 | 29.6 | A0spe*12 | 36.81 | 0.038 | 0.27 | 71.9 |

| | | | | | | |
|---|---|---|---|---|---|---|
| 65109 | 55.64 | kA15hA3mA3va[*1] | 52.62 | 0.0544 | 0.44 | 21.3 |
| 66249 | 44.55 | A2Van[*2] | 34.26 | 0.0354 | 0.73 | 17.5 |
| 69713 | 33.54 | A7IV-[*13] | 12.79 | 0.0132 | 0.25 | 6.8 |
| 69732 | 33.58 | A3Va[*2] | 18.19 | 0.0188 | 0.39 | 11.6 |
| 71075 | 38.29 | A7IV+(n)[*13] | 66.0 | 0.0682 | 0.23 | 24.8 |
| 72220 | 25.35 | A0V[*14] | 23.2 | 0.024 | 0.44 | 34.4 |
| 72622 | 42.25 | A3IV[*5] | 70.46 | 0.0728 | 0.53 | 32.1 |
| 75761 | 26.68 | A6III[*3] | 9.73 | 0.01 | 0.32 | 8.9 |
| 76267 | 43.65 | A1V[*15] | 87.4 | 0.0903 | 0.35 | 69.6 |
| 77622 | 46.39 | kA2hA5mA7V[*2] | 28.44 | 0.0294 | 0.30 | 10.4 |
| 84379 | 41.55 | A1IVn[*2] | 50.2 | 0.0519 | 0.26 | 20.7 |
| 85819 | 32.96 | kA3hF0mF0[*3] | 13.39 | 0.0138 | 0.19 | 6.5 |
| 85829 | 32.64 | kA3hF1mF0[*3] | 14.47 | 0.0149 | 0.20 | 6.7 |
| 92024 | 34.21 | A7V[*1] | 12.73 | 0.0131 | 0.40 | 6.8 |
| 92161 | 35.17 | A3IV[*3] | 15.57 | 0.0161 | 0.58 | 13.8 |
| 93408 | 25.54 | A6IV[*3] | 10.52 | 0.0109 | 0.21 | 10.1 |
| 93506 | 36.61 | A2.5Va[*1] | 80.67 | 0.0833 | 0.46 | 40.8 |
| 94083 | 36.64 | A7V[*16] | 12.55 | 0.013 | 0.19 | 4.6 |
| 94114 | 25.15 | A0/A1V[*6] | 16.01 | 0.0165 | 0.54 | 25.2 |
| 95853 | 26.63 | A4Vn[*3] | 24.25 | 0.0251 | 0.28 | 43.1 |

| | | | | | | |
|---|---|---|---|---|---|---|
| 98495 | 30.73 | A0Va*[1] | 20.13 | 0.0208 | 0.39 | 15.3 |
| 102333 | 41.38 | A9IV*[1] | 19.77 | 0.0204 | 0.34 | 5.9 |
| 109427 | 33.77 | A1Va*[1] | 29.73 | 0.0307 | 0.40 | 26.2 |
| 110618 | 34.6 | G9VFe-3.1CH-1.5*[1] | 25.51 | 0.0264 | 0.24 | 6.9 |
| 111169 | 31.86 | A1.5V*[15] | 19.21 | 0.0198 | 0.27 | 34.4 |
| 112623 | 25.16 | A2IVn*[1] | 35.35 | 0.0365 | 0.26 | 40.9 |
| 113860 | 34.98 | A9V*[6] | 12.11 | 0.0125 | 0.39 | 4.7 |

*1 Gray et al. (2006)
*2 Gray et al. (2003)
*3 Helmut & Nidia (1995)
*4 Phillips et al. (2010)
*5 Houk & Smith-Moore (1988)
*6 Houk (1982)
*7 Boyajian et al. (2013)
*8 Seifahrt et al. (2010)
*9 Ginestet et al. (1997)
*10 Helmut (2008)
*11 Eggl et al. (2013)
*12 Robrade & Schmitt (2011)
*13 Gray et al. (2001)
*14 Malagnini & Morossi (1990)
*15 Zorec et al. (2009)
*16 van Belle & von Braun (2009)

### 4.2.2 Stacking Analysis

To investigate average FIR emission properties associated with the A-type stars with sufficient sensitivities, I stack the FIS maps centered at the positions of the selected stars over the distance bins. I evaluate values on finer pixels ($3''.75 \times 3''.75$ grids) over $24' \times 24'$ images by cloud-in-cell interpolation of four nearest neighbors in the original pixels (see Chapter 3). The vertical axis of each image is aligned with the scan-direction of the survey. Then the median value of the pixel values is subtracted from each image as the background surface brightness. Pixels with pixel values more than $3\sigma$ above the background fluctuations are masked (see details in Chapter 3). After these procedures, I combine these images by averaging to make a stacked image.

### 4.2.3 Stacking images

Figure 4.2 shows the stacked images of the selected stars that are grouped into three distance bins at the 65, 90, and 140 $\mu$m bands. An emission located at the position of the stars is seen in each stacked image.

## 4.3 Photometry results

### 4.3.1 Aperture photometry

Since the exo-CSPs with sizes comparable to the outer SD (astrocentric distances of $\sim 4000$ AU) and the inner OC ($1000 - 5000$ AU) can be spatially resolved for the stars located within $\sim 50$ pc from the Sun (see Chapter 2), the exo-CSP emission

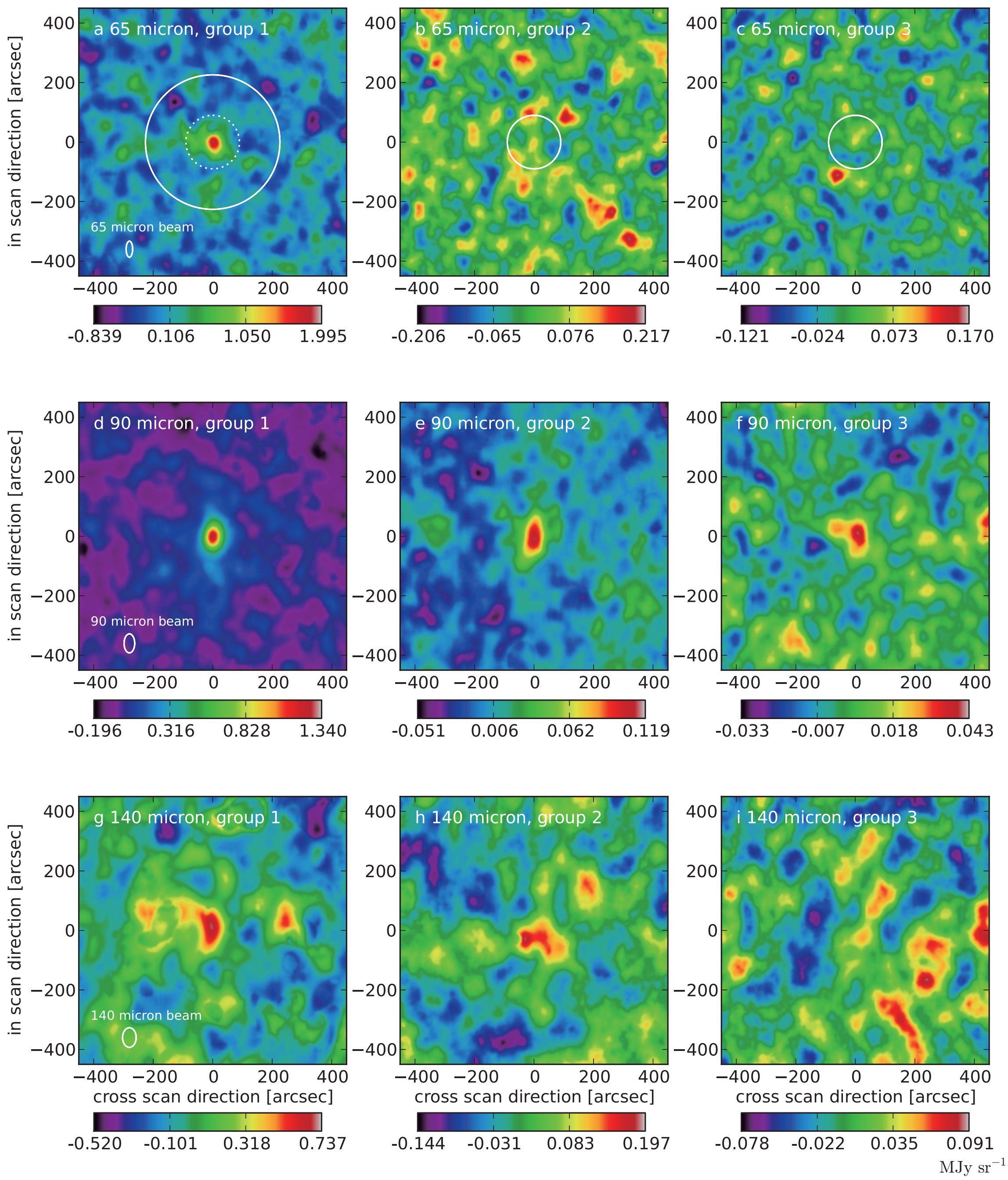


Figure4.2 Stacked images of the selected nearby A-type stars in the *AKARI* FIS maps. Panels in the upper, middle and lower rows represent *AKARI* 65 (blue), 90 (green), and 140 (red) $\mu$m stacked maps, respectively. Panels in the left, middle, and right columns represent stacked images of the stars with distances $d$ of $15.8 < d < 39.8$ (group1), $39.8 < d < 100$ (group2), and $100 < d < 158$ pc (group3), respectively. The solid circles in the panels a, b, and c show apertures I use to extract the signal inside 226, 90, and 90$''$, respectively. The dotted circle in the panel a indicates another aperture with a radius of 90$''$. The ellipses at the bottom left corner of the panels a, d, and g indicate the beam size at the 65, 90, and 140 $\mu$m, respectively (see Chapter 3).

can be resolved in the stacked images of the group 1. Therefore, to extract both the extended emission, and the unresolved emission from the stellar photospheres and from the debris disks, I performed aperture photometry of the stacked images of the group 1 with two apertures; an aperture radius of $90''$ with a background annulus between radii of $120 - 300''$, and an aperture radius of $226''$ with a background annulus between radii of $251 - 703''$. The corresponding physical radii of the $90''$ and $226''$ apertures are $\sim 2600$, and 6600 AU, respectively. Fluxes with the both apertures are divided by the flux calibration factors derived in Chapter 3. Fluxes measured with the $90''$ aperture are also divided by the aperture correction factor $A(226'')$ (see Chapter 3). After that, I derived fluxes in an annulus between radii of $90-226''$ by subtracting fluxes derived with the $90''$ aperture from those with the $226''$ aperture. Uncertainties of the photometry are obtained with standard deviations of fluxes measured from stacked images centered at the same number of randomly chosen blank positions (see Chapter 5). Then $1\sigma$ errors of the photometry are derived by the square root of the square sum of these flux deviations, and the uncertainties of the flux calibration factors and aperture correction factors (see Chapter 3). The $90''$ aperture is also used for photometry of the two distant stacked groups (groups 2 and 3). The corresponding physical radii of the aperture radius are $\sim 6700$ and $\sim 11000$ AU for groups 2 and 3, respectively. The estimated fluxes are tabulated in Table 4.2.

Table4.2 Observed fluxes.

| Observation | Band | Wavelength [$\mu$m] | Flux [Jy] group1, $< 90''$ | group1, $90'' - 226''$ | group2 | group3 |
|---|---|---|---|---|---|---|
| | J | 1.235 | $68.0 \pm 1.2$ | | $9.75 \pm 0.15$ | $3.05 \pm 0.05$ |
| 2MASS[*1] | H | 1.662 | $45.3 \pm 0.9$ | | $6.57 \pm 0.12$ | $2.02 \pm 0.04$ |
| | Ks | 2.159 | $30.7 \pm 0.6$ | | $4.24 \pm 0.08$ | $1.37 \pm 0.03$ |
| WISE[*2] | band 3 | 11.56 | $1.36 \pm 0.14$ | | $0.182 \pm 0.018$ | $0.058 \pm 0.006$ |
| | band 4 | 22.09 | $0.54 \pm 0.05$ | | $0.060 \pm 0.006$ | $0.0186 \pm 0.0019$ |
| | N60 | 65 | $0.46 \pm 0.10$ | $0.12 \pm 0.16$ | $0.023 \pm 0.027$ | $0.013 \pm 0.021$ |
| *AKARI*[*3] | WIDE-S | 90 | $0.24 \pm 0.04$ | $0.27 \pm 0.11$ | $0.037 \pm 0.007$ | $0.013 \pm 0.005$ |
| | WIDE-L | 140 | $0.22 \pm 0.11$ | $0.65 \pm 0.31$ | $0.062 \pm 0.025$ | $0.010 \pm 0.016$ |

[*1] Uncertainties correspond to the absolute calibration error of the 2MASS all-sky survey (1.7%, 2.0%, and 1.9% for the J, H, and Ks bands; from *The 2MASS All-Sky Data Release and Extended Mission Ancillary Products*)

[*2] Uncertainties correspond to the absolute calibration error of the WISE data (10% for the band 3 and 4; from *Explanatory Supplement to the WISE All-Sky Data Release Products*)

[*3] Uncertainties correspond to the square root of the square sum of the flux deviations measured from a set of the blank stack images and the uncertainties of the flux calibration factors aperture correction factors (see text)

### 4.3.2 SED fit to the closest stacks

Figure 4.3 displays the SED of the observed fluxes measured with the 90″ aperture photometry on the stacked images of the group 1. The observed SED shows a clear FIR excess against the Rayleigh-Jeans limit of the photospheric emission (dotted curve in Figure 4.3). In order to interpret the spectral features of the fluxes, a simple infrared emission model consisting of a photospheric component and a blackbody component is employed. First of all, I derive the best-fit results of the model fitting by minimizing $\chi^2$ defined by the following function;

$$\chi^2 = \sum_{i=1}^{6} \frac{(F_\nu^{\rm obs}(\lambda_i) - A\, f_\nu^{\rm ph}(\lambda_i) - C\, B_\nu(\lambda_i, T_{\rm warm}))^2}{\sigma_i^2}, \tag{4.3}$$

where $F_{\rm obs}(\lambda_i)$ is the observed flux at the wavelength $\lambda_i$: $i = 1, 2, 3, 4, 5$, and 6 corresponding to 2MASS Ks (2.17 $\mu$m), WISE band 3 (12 $\mu$m), band 4 (22 $\mu$m), and *AKARI* N60 (65 $\mu$m), WIDE-S (90 $\mu$m), and WIDE-L (140 $\mu$m) bands, respectively. These fluxes are normalized by the 2MASS 2.17 $\mu$m band flux. $\sigma_i$ is the uncertainty of $F_{\rm obs}(\lambda_i)$. $B_\nu(\lambda_i, T_{\rm warm})$ is the Planck function of temperature $T_{\rm warm}$, and $f_\nu^{\rm ph}(\lambda_i)$ is a model photospheric emission spectrum for A5V stars adopted from Kurucz (1992). In this fitting procedure, $A$, $C$, and $T$ are the fitting parameters. Note that if I adopt models of other spectral types (A0- F0), the best-fit values of the parameters $C$ and $T$ do not change with amplitudes greater than 5%. This is because all of the model spectra are quite similar to each other at wavelengths $\lambda > 2\mu$m, where the spectra reach the Rayleigh-Jeans limit ($f_\nu^{\rm ph}(\lambda) \propto \lambda^{-2}$).

In the fitting procedure, the observed fluxes should be compared with model flux values that are derived by taking a model spectrum and response functions of the bands into consideration. Since the flux of the AKARI/FIS data refers to the spectrum $\lambda F_\lambda$ = constant, a model flux value at the band $i$, $F_\lambda^{\rm FIS}(\lambda_i)$, is derived from a model spectrum $F_\lambda^{\rm model}(\lambda)$ and a response function $R(\lambda)$ of the FIS bands;

$$F_\lambda^{\rm FIS}(\lambda_i) = \frac{\int F_\lambda^{\rm model}(\lambda) R(\lambda) d\lambda}{\int (\lambda_i/\lambda) R(\lambda) d\lambda}. \tag{4.4}$$

I use $R(\lambda)$ for the FIS bands measured in the laboratory (see Kawada et al. 2007). On the other hand, the calibration of the WISE data uses the spectrum with $F_\lambda$ = constant. I therefore apply the following correction;

$$F_\lambda^{\rm WISE}(\lambda_i) = \frac{\int F_\lambda^{\rm model}(\lambda) R(\lambda) d\lambda}{\int R(\lambda) d\lambda}. \tag{4.5}$$

As shown in Figure 4.3, the excess feature can be approximated by a blackbody model spectrum with the temperature of $T_{\rm warm} = 122 \pm 12$ K (dotted-dashed curve in Figure 4.3). The excess temperature is marginally in agreement with a median cold disk temperature of nearby A-type stars obtained by the recent *Herschel* results ($T \sim 110$ K; Thureau et al. 2014). From the fitting results, the fractional luminosity ($f_{\rm warm}$, the energy contribution of the excess to that of the photospheric emission) is obtained by the following equation;

$$f_{\rm warm} = \frac{C \int (\nu/c) B_\nu(\nu, T) d\nu}{A \int f_\nu^{\rm ph}(\nu) d\nu}. \tag{4.6}$$

The fractional luminosity is derived to be $f_{\rm warm} = 4.6^{+1.5}_{-1.1} \times 10^{-5}$. According to the recent *Herschel* results (Thureau et al., 2014), an occurrence rate and an average fractional luminosity of detected debris disks around A-type stars are $\sim 24\%$ and $\sim 2 \times 10^{-4}$. If the contribution of undetected debris disks is ignored, an average fractional luminosity of the debris disks around A-stars is deduced to be $\sim 5 \times 10^{-5}$, which is comparable to $f_{\rm warm}$. Therefore the spectral properties of the obtained

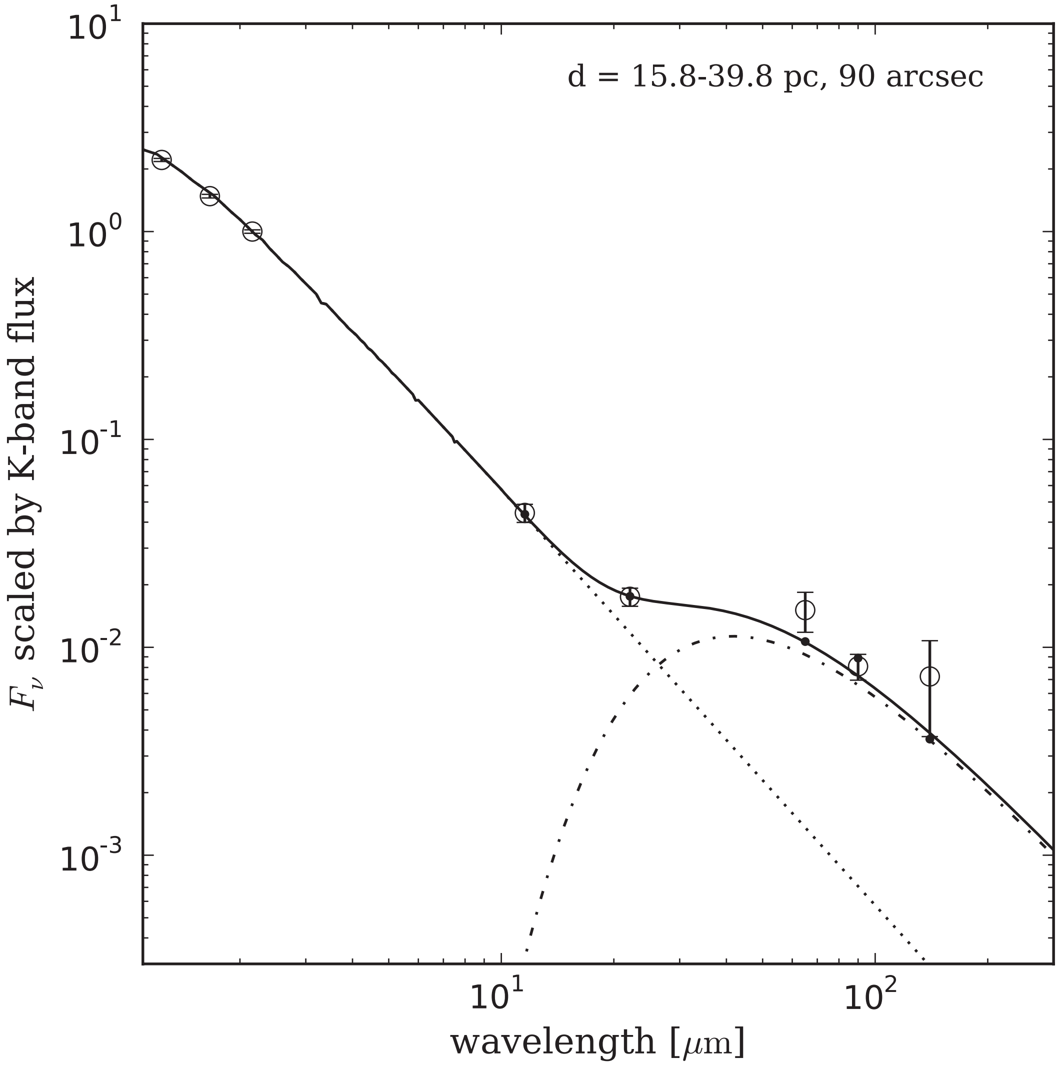


Figure4.3 The obtained fluxes of the group1 measured with the 90″ aperture (physical scale of 2600 AU) and the SED fit results. Open black circles with error bars show the measured fluxes and the near- to mid-infrared fluxes obtained by averaging the 2MASS (wavelength at 1.25, 1.65, and 2.17 $\mu$m) and the WISE (12 and 22 $\mu$m) catalogue values scaled by the 2.17 $\mu$m flux. Black points represent model flux values that take the spectral response functions of the bands into consideration, which are derived by the equations 4.4 and 4.5. The solid, dotted, and dot-dashed curves are the SED fit results, which are derived by the equation 4.3.

excess in the 90″ aperture is consistent with that of the known debris disks.

The SED of the group 1 fluxes measured with the 90″ − 226″ annulus is presented in Figure 4.4. FIR emission is detected in this annulus. Since the corresponding physical scale of the annulus is $\sim 2600 - 6600$ AU, and is larger than those characteristics for known debris disks (smaller than 1000 AU, Wyatt 2008), it is difficult to consider the FIR emission as the debris disk emission. The SED is fitted to a model consisting of a modified blackbody spectrum, in a manner that minimizes the following $\chi^2$;

$$\chi^2 = \sum_{i=4}^{6} \frac{(F_\nu^{\rm obs}(\lambda_i) - E\,\lambda_i^{-1} B_\nu(\lambda_i, T_{\rm cold}))^2}{\sigma_i^2}. \quad (4.7)$$

In this fitting procedure, $E$ and $T_{\rm cold}$ are the fitting parameters. In this model, the emissivity $\epsilon$ of the grain is assumed to be proportional to $\lambda^{-1}$.

The fit result is shown as a solid curve in Figure 4.4. The corresponding temperature and the fractional luminosity of the emission is estimated to be $T_{\rm cold} = 22.8 \pm 5.2$ K and $f_{\rm cold} = 2.0^{+6.3}_{-1.5} \times 10^{-5}$, respectively. The obtained temperature $T_{\rm cold}$ is lower than the typical debris disk temperature obtained in the present result ($T_{\rm warm} = 122 \pm 12$ K).

### 4.3.3 SEDs of distant samples

For comparison with the stacked SEDs of the group 1, fluxes of more distant two groups , $39.8 < d < 100$ pc (group2), and $100 < d < 158$ pc groups (group3), are shown in Figure 4.5. These fluxes are measured with a 90″ aperture, which corresponds to apertures with physical radii of 6700 and 11000 AU, respectively. The SED of the group 2 stack (Figure 4.5a) seems to follow the total SED of the group 1 (crosses in Figure 4.5a). However, the excess intensities are relatively smaller than that of the group 1. Taking the results of the group1 into consideration, I fit the SED with a spectral model consisting of a photospheric, blackbody, and additional modified blackbody components. The best-fit parameters for the two-temperature model are derived in a manner that minimizes the following $\chi^2$;

$$\chi^2 = \sum_{i=1}^{6} \frac{(F_\nu^{\rm obs}(\lambda_i) - A\, f_\nu^{\rm ph}(\lambda_i) - C\, B_\nu(\lambda_i, T_{\rm warm}) - E\, \lambda_i^{-1} B_\nu(\lambda_i, T_{\rm cold}))^2}{\sigma_i^2}. \quad (4.8)$$

In this fitting procedure, $T_{\rm warm}$, and $T_{\rm cold}$ are set to be 122 K and 23 K, respectively, and $A$, $C$, and $E$ are the fitting parameters.

The best-fit result is shown as solid curve in Figure 4.5a. The corresponding $f_{\rm warm}$ for the group 2 is $1.7^{+1.3}_{-0.7} \times 10^{-5}$, which is smaller than the results of the group 1 ($\sim 4 \times 10^{-5}$). On the other hand, the corresponding $f_{\rm cold}$ is $1.1^{+0.5}_{-0.3} \times 10^{-5}$, which is in agreement with the results of the group 1 ($2.0^{+6.3}_{-1.5} \times 10^{-5}$).

It is much more harder to understand properties of the group 3 SED (Figure 4.5b), because the error of the photometry is larger than the closer two groups. If performed the same fitting procedure, the $f_{\rm warm}$ and $f_{\rm cold}$ are derived to be $1.8^{+1.4}_{-0.7} \times 10^{-5}$ and $0.9^{+0.8}_{-0.4} \times 10^{-5}$, respectively, which is in agreement with the results of the group 2. Therefore, the observed SEDs of these groups are consistent with the assumption of the existence of the cold emission component seen in the group 1 stack.

## 4.4 Radial brightness profiles

In order to investigate the spatial characteristics of the extended cold excess component, I have further investigated the stars in the map at the 90 $\mu$m, where the RBP of the PSFs is well determined (see Chapter 3). The RBP of the group 1 stack is shown in Figure 4.6a. The profile follows the RBPs of the PSF (shown as a dotted curve in Figure 4.6a), except for that at a radial range of $\sim 120'' - 220''$; an excess of the profile against the PSF is seen in this range. Taking the average distance of the stacked samples (29.4 pc) into consideration, this angular radial range corresponds to a physical radius of $\sim 3500 - 6500$ AU.

For providing an example of interpretation, the obtained RBP is compared with a simple model profile. The model profile consists of two components; an unresolved component, which can be approximated by a point source and is represented by the PSF, and a resolved shell component. The shell component assumes that each stacked star has an optically thin shell with a fixed physical radius. The model profile is composed of the individual shell integrated along the line of sight, angularly scaled according to the distance of the stacked stars, and convolved with the PSF to assess the observed profile directly. In the fitting, amplitudes of the unresolved and shell components and radial distance of the shell are free parameters. Figure 4.6b shows the best-fit result of the model profile overlaid on the observed RBP. The observed RBP is approximated by the model of the shell with a radius of $6.1^{+0.1}_{-0.2} \times 10^3$ AU.

For comparison to the group 1 RBP, a RBP of the stack for the group 2, where a signal-to-noise ratio is still sufficient ($\sim 5$), is derived (Figure 4.7). As shown in Figure 4.7a, the excess seen in the group1 profile does not appear in this profile; the RBP is consistent with the PSF in the radial range of $120'' - 200''$. Instead, a slight excess appears at an angular radial range $50'' - 120''$. This radial range corresponds to the distance of $\sim 4000 - 8000$ AU. The RBP is fitted in the same the same manner as that for the group 1. According to the fit, this RBP is approximated by the model of the shell with a radius of $6.3^{+1.9}_{-2.0} \times 10^3$ AU (see solid curve in Figure 4.7). The best-fit radius is consistent with that derived from the group 1 RBPs.

These results are consistent with an assumption that typical A-type star systems are surrounded by a common extended FIR emission structure. The corresponding radius is far larger than that of the known debris disks around A-type stars ($<$

1000 AU; Wyatt 2008), but comparable to that of the detached scattered disk, or the inner OC radius of our solar system (1000-10000 AU; Dones et al. 2004).

## 4.5 Summary of this chapter

In this chapter, stacking analyses of nearby 3583 A-type stars located within 158 pc from the Sun are performed with the *AKARI*/FIS FIR all-sky map with three appropriate distance bins ($15.8-39.8$ pc, $39.8-100$ pc, and $100-158$ pc bins). The photometry of the stacked image presents a FIR excess emission that comes from closer than 2600 AU from the parent stars, and corresponds a $\sim 120$ K blackbody with a fractional luminosity (the energy contribution of the excess to the stellar photospheric emission) of $\sim 5 \times 10^{-5}$. These properties are in agreement with the average properties of known debris disks around A-type stars. In addition to the debris disk component, a colder excess component corresponding to the $\sim 23$ K modified blackbody emission with a fractional luminosity of an order of $10^{-5}$ is seen in the annulus corresponding physical radii of $2600 - 6600$ AU. In order to make a constraint on a spatial distribution of the cold excess component, RBPs are derived from the stacked images at the $90\,\mu$m band. The RBPs indicate that the emission structure extends to approximately 5000 AU, which is larger than the typical debris-disk sizes (smaller than 1000 AU).

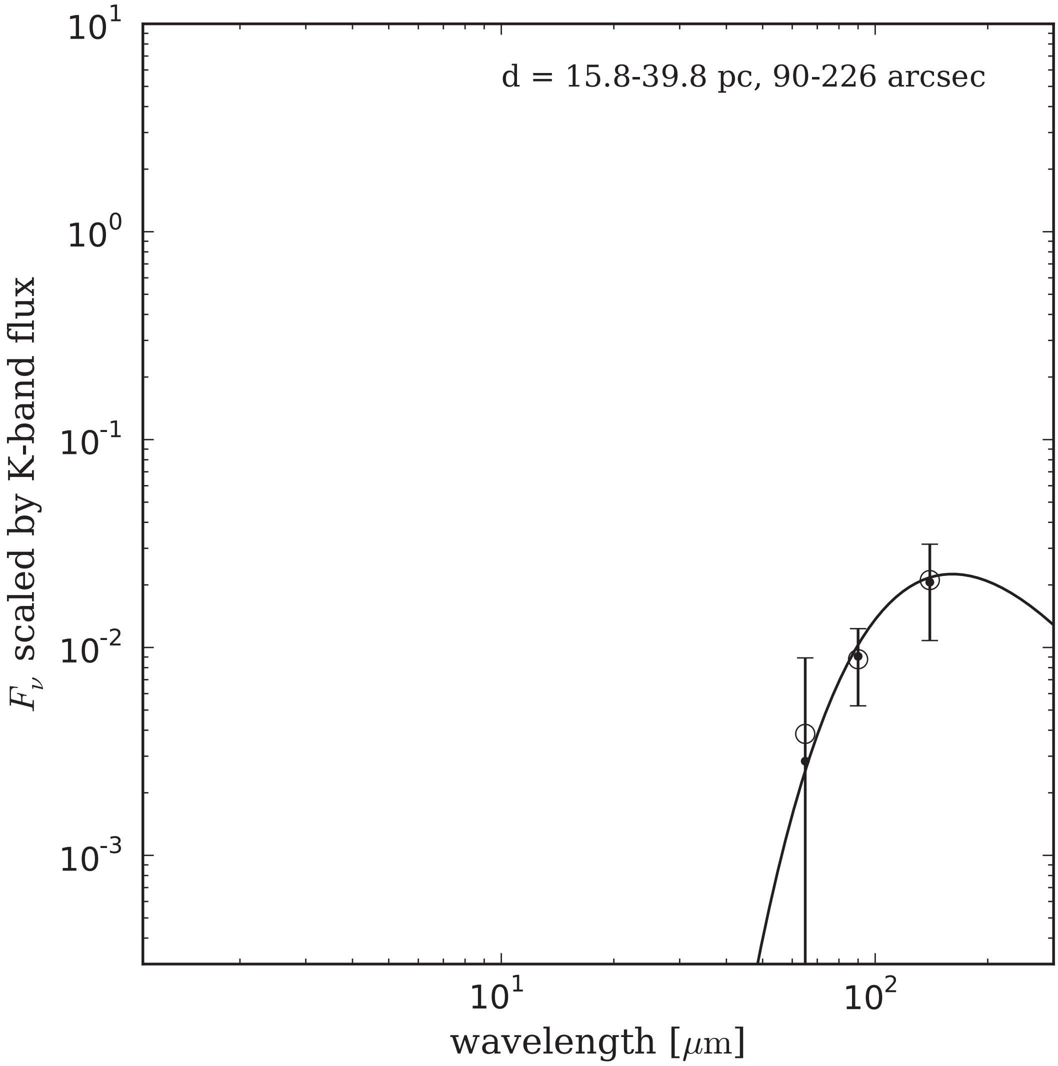


Figure4.4 Same as Figure 4.3, but for the fluxes measured with an $90'' - 226''$ annulus (physical scale of 2600-6600 AU) overlaid with the best-fit model spectrum derive by the equation 4.7.

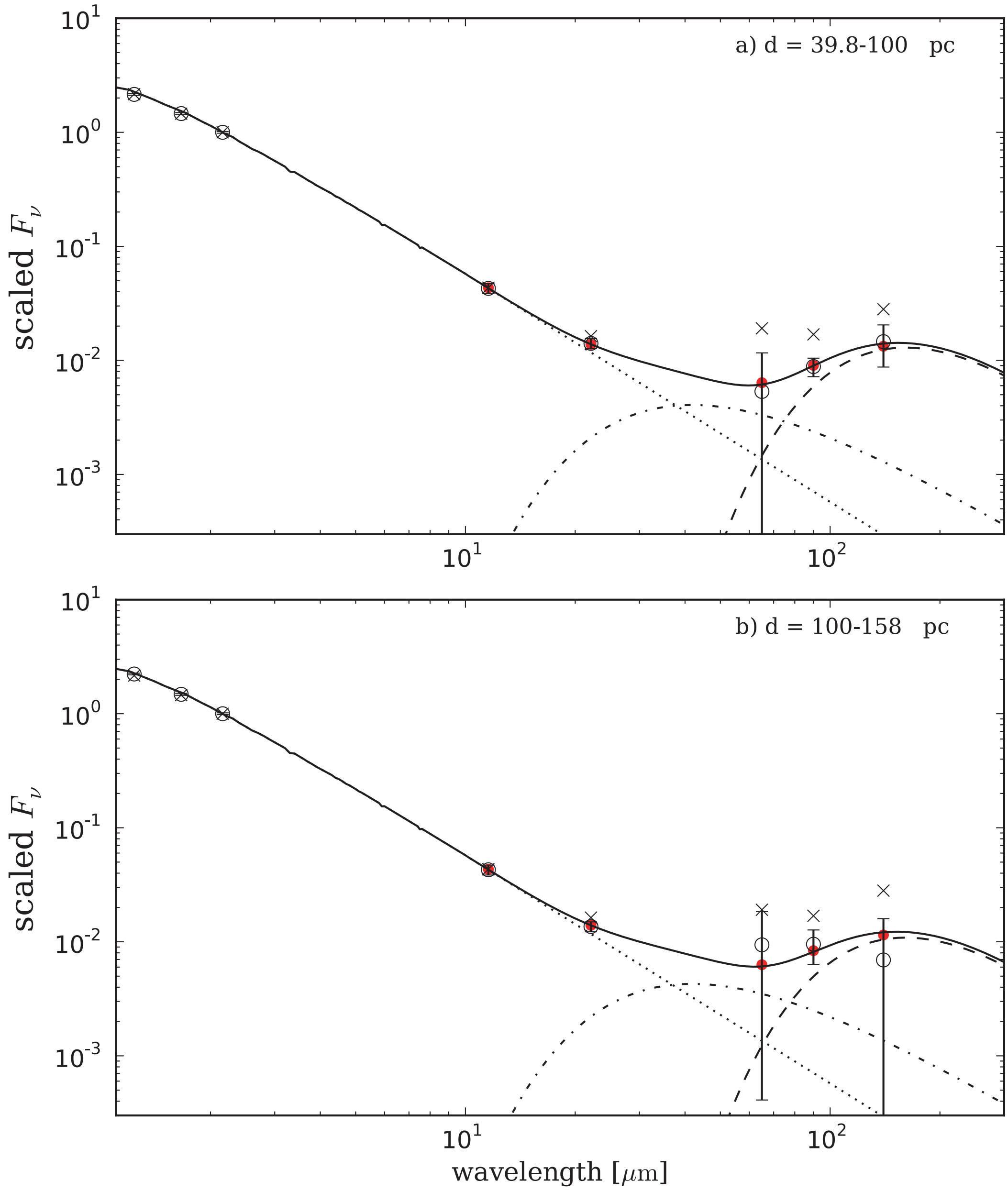


Figure4.5 The fluxes and the SED fit results for (a) the $39.8 < d < 100$ pc (group2), and (b) $100 < d < 158$ pc groups (group3). The fluxes are measured with a $90''$ aperture, which corresponds to physical radial scales of (a) 6700, and (b) 11000 AU, respectively. The best-fit model SEDs derived by the equation 4.8 are plotted as solid curves and the individual model components are presented as dotted, dot-dashed, and dashed curves. The fluxes of the group1 is plotted as crosses for comparison.

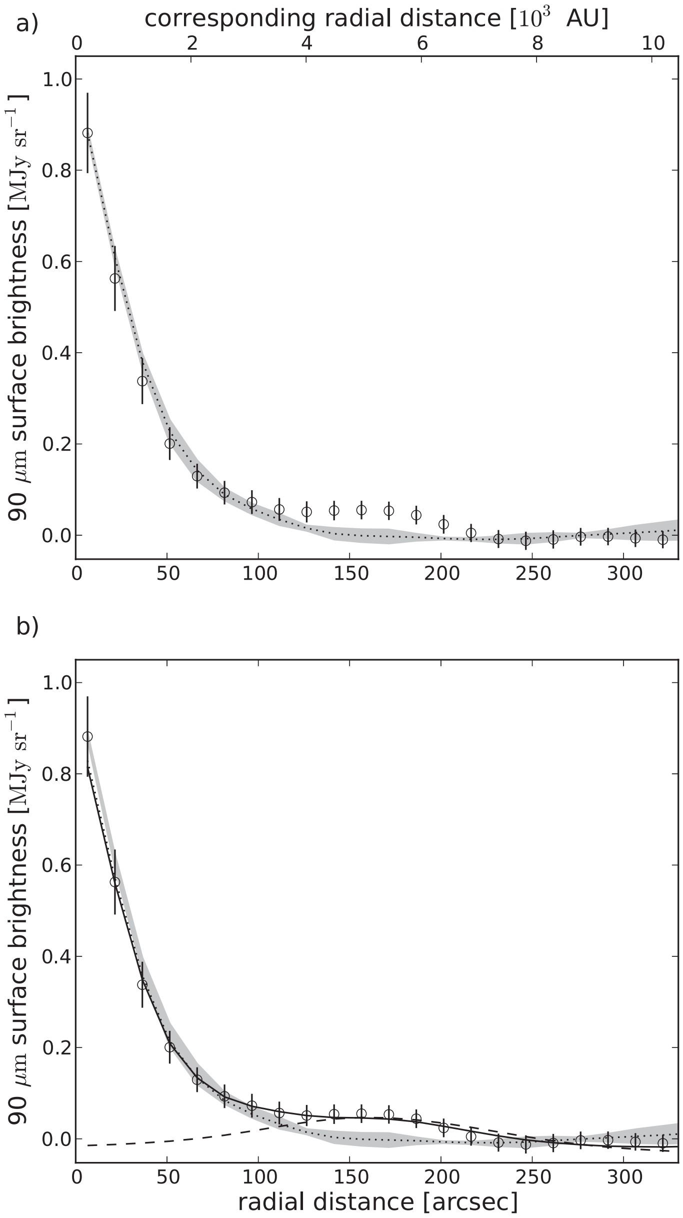


Figure4.6 a) The RBP of the stacked A-type stars located at 25.1-39.8 pc (gropu1) at the 90 $\mu$m band is shown as circles with error bars. The dotted curve indicates the RBP of the PSF at the 90 $\mu$m (Arimatsu et al., 2014), which is normalized to match the peak intensity. The errors are estimated from the variance of the intensity in each annulus. The gray region represents the uncertainty of the PSF, which is derived from the variance of the RBPs of the stacked standard stars with different flux bins (see Figure 3.6 and Chapter 3) . b) The same as a), but overlaid with the best fit model profile, which is shown as a solid curve. The model profile consists of two components; an unresolved component (black dotted line), which can be approximated by a point source and is represented by the PSF, and a resolved shell component (black dashed line). The shell component assumes that each stacked star has an optically thin shell with a fixed radius derived by the profile fit, $r = 6100$ AU. Note that the surface brightness value at each distance bin is correlated with those of the neighboring bins due to PSF scattering of the signal.

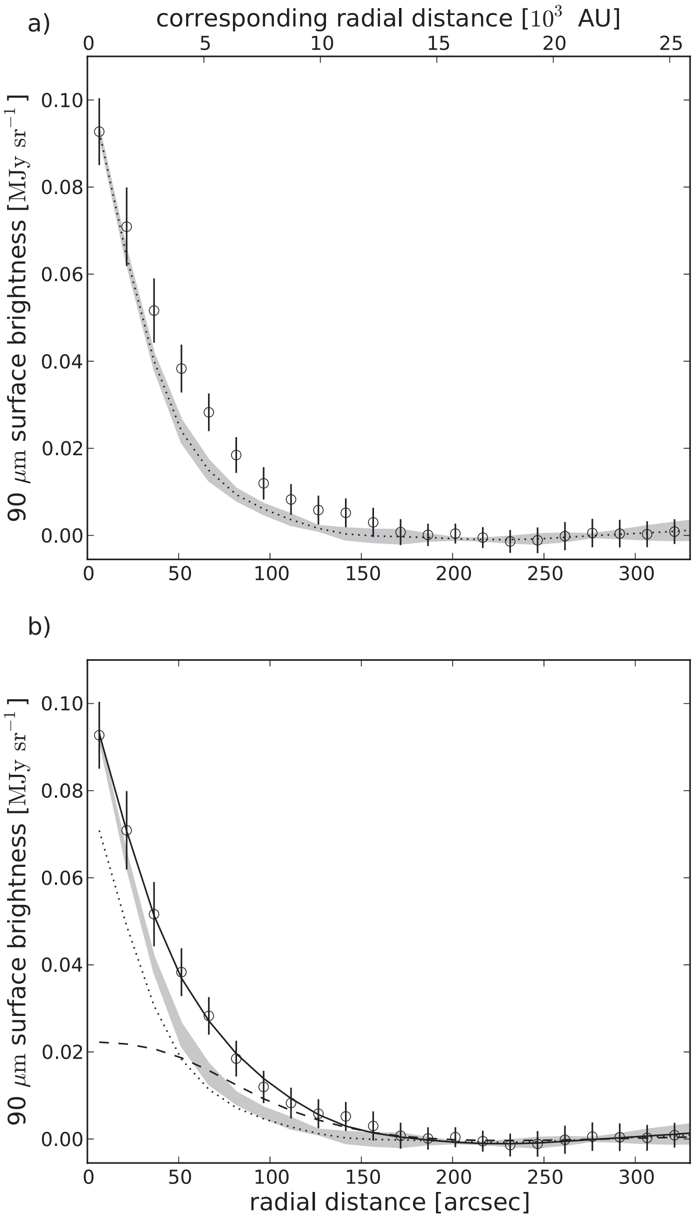


Figure4.7 The same as Figure4.6, but for the stacks of the stars located at 39.8-100 pc (group 2), the best-fit radius derived by the fit is $r = 6300$ AU.

# Chapter5

# Discussions

Part of this chapter will be submitted to Astrophysical Journal as:
Ko Arimatsu, Yasuo Doi, Takehiko Wada, Satoshi Takita, & Hirokazu Kataza
"Evidence for the extended dust emission around nearby A-type stars"

## 5.1 Possibilities of false detection

### 5.1.1 SED derived from median stacking results

The FIS all-sky maps adopted for the present study can be contaminated with background infrared sources. This confusion would affect the photometry derived with the stacked images, especially that for the closest group (group 1: $15.8-39.8$pc), because the number of the allocated objects is relatively small (63 objects), and the adopted aperture size for the photometry is relatively large. The median stacks can help to reduce residual contribution from background objects, especially from background point sources. If the observed emission is due to the point source contamination, the FIR emission should not appear in the median-stacked images. Figure 5.1 shows the fluxes of the group 1, which are obtained by the averaging and the median methods, and are measured in the $90'' - 226''$ annulus. The SED of the median stacks shows a similar distribution to that of the average stacks, corresponding to a modified black-body spectrum with the temperature of $\sim 23$ K. The median fluxes are about 1.5 times smaller than the average values. This difference might reflect the confusion of the sources in the average stacks. However, this difference is difficult to confirm, taking the large error-bars into consideration.

### 5.1.2 SEDs of the split subsamples

In addition to the median stacking, I have also examined the effect of anomalous contaminations from minority of the samples by splitting into two samples (even and odd members of the original sample), and stacking the individual samples. Figure 5.2 shows the stacked SEDs of the subsamples. In both groups, the flux values are consistent with the stacking results of the original sample, and show significant FIR excesses. I thus found no evidence for the observed cold emission from minority of the stacked samples.

### 5.1.3 Blank test

As described in Chapter 4, the uncertainties of the photometry are obtained with deviations of fluxes measured from stacked images of randomly selected blank regions. Figure 5.3 compared the stacked blank images with the stacked object images at the 90 $\mu$m band. In Figure 5.3, the central emission peaks are seen in the stacked images of the selected stars, which are shown in the upper panels. On the other hand, the corresponding peaks are not confirmed in the randomly stacked images shown in the lower panels. This result indicates that the obtained emission is the real emission associated with the stacked stars, not the artifacts generated by the data reduction procedures.

I estimate the probability that the detected cold emission in the annulus of the group 1 is due to statistical fluctuations of the background, by investigating distributions of the fluxes of the stacked blank images. I perform photometry on 150 stacked blank images, each of which is produced by stacking the same number of the blank images as the objects used for the stacks of the group 1 (63 objects). The average background surface brightness values of the selected blank images at the 65, 90, and 140 $\mu$m bands are 7.1, 9.2, and 9.4 MJy sr$^{-1}$, respectively, which are comparable to those of the stacked sample images (6.5, 8.3, and 8.8 MJy sr-1). Photometry in the $90'' - 226''$ annulus region is made with these images. Figure 5.4 shows the histograms of the photometry results of the blank stack images at the a) 65, b) 90, and c) 140 $\mu$m bands. The average fluxes of the blank annulus are $0.006 \pm 0.013$, $-0.007 \pm 0.009$, and $-0.023 \pm 0.021$ Jy at the 65, 90, and 140 $\mu$m bands, respectively, and indicate that any systematic effect accounts of the observed positive detections. On the other hand, as shown in Figure 5.4, probability distributions of the fluxes seem to follow normal distributions with variances of 0.16, 0.10, and 0.25 Jy, respectively. The significances of the excess of the fluxes observed in the group 1 annulus (Table 4.2) thus correspond to 0.8, 2.7, and 2.6$\sigma$ at the 65, 90, and 140 $\mu$m bands, respectively. This result indicates the probabilities of $\sim 30\%$, $\sim 1\%$, and $\sim 1\%$ that excesses are caused by random statistical fluctuations of the background at the 65, 90, and 140 maps, respectively.

### 5.1.4 Flux distributions of the individual sample images

For further calculation of the significances of the excess emission against the background fluctuation, we compare distributions of the fluxes measured in the circumstellar annulus regions of the individual group 1 sample images used for the stacking analysis with those of the blank images. Photometry in the $90'' - 226''$ annulus region is performed with individual extracted 63 images of the group1 sample (on-source population) and 10000 blank region images. The normalized distributions of the fluxes of these two populations are compared in Figure 5.5. While the standard deviations of the fluxes of the on-source images ($\sigma_{\rm source}$) and those of the blank images ($\sigma_{\rm random}$) are similar, the average fluxes of the on-source population (average$_{\rm source}$) are shifted against the average background values (average$_{\rm random}$), as already indicated by the stacked results (see Chapter 4). According to the two-sample $z$ test for the difference between the average values of two populations, the significances of the excess of the average annulus fluxes for the on-source population thus correspond to 0.8, 2.7, and 1.7$\sigma$ at the 65, 90, and 140 $\mu$m bands, respectively.

### 5.1.5 RBPs of four quadrants of the stacked image

In order to check false detections due to spurious features in the stacked image that are mimicking the excess emission seen in the RBPs (see Figure 4.6), I have derived RBPs of four quadrant sub-regions of the stacked image defined in Figure 5.6a; two regions include in-scan directions (quad 1 and 3), and the others include crow-scan directions (quad 2 and 4). Since the stars are stacked regardless of their orbital inclinations, the CSP emission in the stacked images will become spherically symmetric, even if they individually have asymmetric distributions, and will appear as similar excess profiles in the four RBPs.

Figure 5.6b compares the RBPs of the four quadrant regions of the stacked image with those of the PSF. All of the four profiles show similar excess against the PSF profiles at a radial range of $120'' - 200''$. These similar profiles are in agreement with an assumption that the excess comes from real circumstellar CSP emission associated with the stacked stars.

## 5.2 Properties and origin of carriers of the possible FIR excess emission

### 5.2.1 Size and mass derivations of the dust grains

The present study found the cold excess emission that is approximated by the gray-body emission with the temperature of $\sim 23$ K and spatially extended to be $\sim 5000$ AU. The corresponding spatial scale of the excess emission is far larger than those of the known debris disks ($< 1000$ AU, Wyatt 2008), and of protoplanetary disks around Herbig Ae/Be stars (< 1000 AU, e.g., Mannings & Sargent 1997). This spatial scale rather resembles to those of the outer SD and the inner OC in the solar system (a few 1000 AU, Dones et al. 2004). If one assumes that the observed cold excess emission comes from dust grains around the target A-type stars, what kind of dust grains (size and mass) that account for the observed FIR emission? In order to estimate the particle size and total mass of the dust grains, a simple spectral model is fitted to the observed SED. Since the temperature and intensity of the FIR emission depend on luminosities of the parent stars, the stellar luminosities of individual stars are thus taken into consideration. Assuming that the dust grains are isotropically distributed at a radius $R$, and optically depth $\tau$ and grain radius $a$ are identical, the expected spectrum is expressed by the following equation;

$$F^{\rm model} = \tau F^{\rm model}_{\rm scaled} = \frac{\tau}{N}\sum_j 4\pi\left(\frac{R}{d_{\rm star_j}}\right)^2 B_\nu(\lambda, T_{\rm eq}(a, L_j))\left(\frac{\lambda}{100\,\mu{\rm m}}\right)^{-1}, \quad (5.1)$$

where $L_j$ and $d_{\rm star_j}$ are a luminosity and distance from the Sun of a stacked star $j$, and $N$ is the number of the stacked stars. $L_j$ is calculated from the fit to the fluxes at the Hipparcos I-band and the 2MASS J, H, and Ks bands, assuming that the photospheric spectrum follows a single-temperature Planck function. The derived $L_j$ for each star is tabulated in Table 4.1 (see Chapter 4). The equilibrium temperature $T_{\rm eq}(a, L_j)$ for each star $j$ is derived by the equation 2.2 with $L_j$ and $a$.

I derive the best-fit result of the model fitting by minimizing $\chi^2$ defined by the following function;

$$\chi^2 = \sum_{i=1}^{3} \frac{(F_\nu^{\rm obs}(\lambda_i) - \tau\, F^{\rm model}_{\rm scaled})^2}{\sigma_i^2}. \quad (5.2)$$

In this procedure, $a$ and $\tau$ are fitting parameters. The total dust mass $M_d$ is estimated with $\tau$;

$$M_d = N\frac{4}{3}\pi a^3 \rho_m = \tau \frac{16\pi}{3} a \rho_m R^2 \left( \frac{100\mu\mathrm{m}}{\lambda_0} \right), \tag{5.3}$$

where $\rho_m$ is the volume density of the dust grains and $\lambda_0$ is the reference wavelength. In the fitting, $\rho_m$, $\lambda_0$ and $R$ are assumed to be $\rho_m = 1\,\mathrm{g\,cm^{-3}}$, $\lambda_0 \sim 1.5a$, and $R =$ 5000 AU, respectively, The best-fit model spectrum $F^{\mathrm{model}}_{\mathrm{scaled}}$ is shown in Figure 5.7. Through the fitting procedure, $a$ and $M_d$ are derived to be $a = 3^{+8}_{-2}\,\mu$m and $M_d =$ $0.10^{+0.38}_{-0.08}\,M_{\mathrm{earth}}$, respectively.

### 5.2.2 Diffusion timescale of the dust grains

In order to discuss the origin of the emission carriers, one should take possible dynamics that would act on the dust grains in the outer stellar systems into consideration. The stars located within $\sim$ 100 pc from the Sun are sitting in the warm ($T \sim$ 7500 K) tenuous ($n_{\mathrm{H}} \sim 0.24\mathrm{cm}^{-3}$) interstellar medium region called as "local bubble" (Lallement, 1998). In this tenuous environment, dust grains are expected to be photoelectrically charged to a potential of an order of one volt (Draine, 2010). Therefore the interstellar magnetic field interacts with the charged grains. If the stellar system moves in the interstellar medium with speed $-v_w$, the dust grain is expected to get accelerated to a velocity $\sim v_w$ in the stellar system frame on the Larmor period $T_L$ (Belyaev & Rafikov, 2010) for a grain with a radius $a$;

$$T_L = 2\pi \frac{m_g}{a|U|B_\perp} \sim 10^6 \left( \frac{a}{5\mu\mathrm{m}} \right)^2 \;\; [\mathrm{yr}], \tag{5.4}$$

where $m_g$ is the mass of a dust grain, $|U|$ and $B_\perp$ are the electrical potential of the grain and the magnetic flux density perpendicular to the interstellar flow. In the above approximation, the interstellar magnetic flux density is assumed to be $B \sim 2\,\mu$G (Ben-Jaffel & Ratkiewicz, 2012). The diffusion timescale of the micron-sized grains is approximately an order of Myr, which is much shorter than the typical age of A-type stars ($\sim$ 100-1000 Myr). Therefore, the dust observed in thousands AU away from the central stars cannot be primordial. A replenish process is needed to account for the observed emission.

Taking the obtained blown-out timescale ($\sim$ 1 Myr) and the observed dust mass ($0.1\,M_{\rm earth}$) into consideration, the efficiency of the replenishment is required to be greater than $0.1\,M_{\rm earth}/10^6$ yr. This rate should be continued in the typical age of the A-type stars to account for the observed emission. The total mass of the source is thus required to be about $10 - 100M_{\rm earth}$, which is comparable to, or slightly larger than the total mass of the OC of our solar system (up to $40\,M_{\rm earth}$, Dones et al. 2004; Duncan et al. 1987).

### 5.2.3 Possible dust replenishment processes

If the replenishment is true, what is the process that replenishes the grains? Since the FIR emission preferentially highlights smaller grains, a group of larger cometary source objects (i.e., exo-CSP) is the most likely replenishment source. The dust mass supplied by replenishment processes highly depends on the total mass and size distribution of the exo-CSPs (Howe & Rafikov, 2014; Yamamoto & Mukai, 1998). Here I assume that the bulk of mass in the exo-CSPs is concentrated in the smallest objects, and all objects have a radius $r = 1$ m, because particles with sizes equal to or larger than this radius are always bound to the stellar system in various phase of the interstellar medium (Belyaev & Rafikov, 2010). In the following calculations, a bulk mass density of the cometary objects $\rho_m$ is set to be $\rho_m = 1\,{\rm g\,cm^{-3}}$. Under the above assumptions, the total mass of the exo-CSP, $M_{\rm comet}$, is approximated with the number of the cometary objects $N_{\rm comet}$;

$$M_{\rm comet} = N_{\rm comet}\rho_m \frac{4\pi r^3}{3}.$$

In the population, cometary source objects would be disrupted by mutual collisions, eroded by interstellar dust impacts, and sometimes heated by nearby supernovae and passing bright stars, which could result in replenishment of dust (e.g., Stern et al. 2003). In the proposed processes, one may think that the mutual collision is the most plausible replenishment process. In the solar system, mutual collision is thought to be the most efficient process to produce dust in the asteroid belt and Kuiper belt (Yamamoto & Mukai, 1998). Once the objects mutually collide, a large number of small dust grains are produced through the collisional cascade (Stern et al., 1996). However, the collisions in the cometary population may be relatively rare due to lower number densities and lower orbital speeds. For simplicity, I assume that the objects in the exo-CSPs are isotropically distributed (e.g., assuming OC-like populations), and the number density profile $\rho(r)$ follows a power law of the form $\rho(r) \propto r^{-\eta}$, as suggested by numerical calculations of the OC's formation (Duncan et al., 1987; Dones et al., 2004). In the present calculation, the power-law index $\eta$ is set to be $\eta = 3.5$, as suggested by Duncan et al. (1987). In addition, all comets move on circular orbits. The collision speed is therefore approximated by the Keplerian speed. In these conditions, according to Howe & Rafikov (2014), the total dust production rate $dM_{\rm dust}/dt$, i.e., the erosion rate $-dM_{\rm comet}/dt$ at a radius $R_{\rm in}$ is approximated by

$$\frac{dM_{\rm dust}(t)}{dt} = -\frac{dM_{\rm dust}(R_{\rm in}, t)}{dt} \sim \frac{M_{\rm comet}(t=0)}{t_{\rm er}(R_{\rm in})}\left(1 + \frac{t}{t_{\rm er}(R_{\rm in})}\right)^{-2}, \tag{5.5}$$

where $t_{\rm er}(R)$ is the erosion timescale at radius $R$, approximated as

$$t_{\rm er}(R_{\rm in}) \sim 5 \times \left(\frac{r}{1\,{\rm km}}\right)^{0.64} \left(\frac{R_{\rm in}}{1000\,{\rm AU}}\right)^{4.39} \left(\frac{M_{\rm comet}}{10\,M_{\rm earth}}\right)^{-1} \left(\frac{M_{\rm star}}{1\,M_{\rm sun}}\right)^{-1.39} [{\rm Gyr}]. \quad (5.6)$$

In the above equation, $M_{\rm sun}$ is the mass of the Sun and $M_{\rm sun} = 1.99 \times 10^{30}$kg, and $M_{\rm star}$ is the mass of the parent star. Assuming $M_{\rm comet}(t = 0) = 100M_{\rm earth}$, $r = 1$m, and $M_{\rm star} = 2M_{\rm sun}$ (characteristics of A5V stars), I find that the dust production rate $dM_{\rm dust}/dt$ is $\sim 0.05M_{\rm earth}{\rm Myr}^{-1}$, comparable to that required for the observed emission intensity ($0.1M_{\rm earth}{\rm Myr}^{-1}$). and $t_{\rm er}$ is comparable to the A-type MS lifetime ($\sim 10^9$yr). Note that this calculation assumes the isotropic distributions of the cometary objects. If I assume that the objects distribute more like the SD, with typical inclinations of less than 30 deg (Duncan et al., 2004), the squared volume density of the object ($\propto$ collisional rate and thus the dust production rate) can be $\sim 10$ times higher.

Another continuous replenishment process is the interstellar dust impact (Yamamoto & Mukai, 1998). In this process, the production rate is proportional to the total cross section of the cometary source object (Yamamoto & Mukai, 1998), $N_{\rm comet}\pi r^2$, and is proportional to $M_{\rm comet}(t)$, assuming that $r$ is invariant. $dM_{\rm dust}/dt$ is therefore expressed as,

$$\frac{dM_{\rm dust}(t)}{dt} = -\frac{dM_{\rm comet}(t)}{dt} = EM_{\rm comet}(t = 0)e^{-Et}, \quad (5.7)$$

where dust production efficiency $E$ is defined with the mass flux of ejecting dust $F$ (Yamamoto & Mukai, 1998), such as

$$E \equiv F\frac{N_{\rm comet}\pi r^2}{M_{\rm comet}} = F\frac{3}{4r\rho_m}. \quad (5.8)$$

$F$, i.e., $E$ varies substantially with surface conditions of the cometary objects (Yamamoto & Mukai, 1998). If the surfaces are composed of hard icy material, $E$ will be smaller than $4 \times 10^{-5}\,\mathrm{Myr}^{-1}$. The produced dust mass on this efficiency is too small to account for the observed dust mass, assuming $M_{\mathrm{comet}}(t=0) < 500\,M_{\mathrm{earth}}$. On the other hand, if the surfaces are covered by loose icy particles composed with layers of fine grains, $E$ would become $2 \times 10^{-2} - 2 \times 10^{-3}\,\mathrm{Myr}^{-1}$ for $r = 1\,\mathrm{m}$. Assuming $M_{\mathrm{comet}}(t=0) = 100 M_{\mathrm{earth}}$ and $E = 2 \times 10^{-3}\,\mathrm{Myr}^{-1}$, the production rate thus ranges from 0.2 to 0.03 $M_{\mathrm{earth}}\,\mathrm{Myr}^{-1}$ for $t = 100 - 1000\,\mathrm{Myr}$, which is comparable to that accounts for the observed emission $\sim 0.1\,M_{\mathrm{earth}}\,\mathrm{Myr}^{-1}$.

It is possible that other episodic processes can produce dust from the cometary source objects. For example, supernovae explosions occurred closer than 20 pc from the stars will be capable of heating the cometary source objects (Stern et al., 2003). Furthermore, close (< 5 pc) encounters of O-type MS and supergiant stars can also heat the objects well above temperatures capable of removing volatile ices from surface layers (Stern et al., 2003). These encounters are expected to be occurred about eight and 0.2 events in typical A-type MS lifetime ($10^9$ yr), respectively (Stern et al., 2003), and may be intermittently acting on the replenishments.

In all of the proposed cases above, the efficiency of the supply process highly depends on the size distribution and material properties of the cometary objects. Further FIR and sub-mm observations of the outer edge of individual stellar systems, and observations of the solar system objects (Kuiper-belt, SD, OC objects, and comets) are required for more precise discussions of the grain supplement processes.

### 5.2.4 Origin of the CSPs

The possible evidence for the large-scale dust emission gives a direct implication on the universality of the CSP formation in extra stellar systems. In general, the giant planets, such as Jupiter, Saturn, Uranus, and Neptune are thought to play an important role on the formation of the CSPs by scattering the material to the outer solar system (Dones et al., 2004). The present results suggest that not a few A-type stars experienced such a gravitational scattering of their protoplanetary disks. The existence of scattering source in outer stellar systems is thus strongly supported.

If I assume that the exo-CSPs have formed through a scenario similar to that proposed for the solar system OC and SD formation, plants in the outer extrasolar system are proposed for the scattering sources. According to Higuchi et al. (2006), the efficiency of scattering planetesimals to higher-eccentricity bounded orbits can depend on the mass and semimajor axis of the planet, and eccentricities and number density profiles of the planetesimals in the protoplanetary disks. Assuming the standard protoplanetary disks (Hayashi, 1981), i.e., the surface number density of planetesimals is proportional to a power of the semimajor axis $R$, $\propto R^{-3/2}$, the efficiency of the scattering per unit time $K$ is empirically approximated by

$$K \propto R_p^0 \, M_p^2, \tag{5.9}$$

where $R_p$, and $M_p$ are the semimajor axis and the mass of the planet, respectively, and the relation is valid within the range of $1 < R_p < 30$ AU, and $0.1 < M_p < 10 \, M_J$ ($M_J$ is the jovian mass). Therefore, the total mass of the resultant population can be less dependent on the semimajor axes of the planet, whereas it highy depends on the planet mass. According to the microlensing monitoring observations (Cassan et al., 2012), $17^{+6}_{-9}$ % of all-types of the stars host planets with the mass of 0.3 to $10\mathrm{M_J}$ within $0.5 - 10$ AU from the star. In addition, outside 10AU from several nearby stars (including A-type stars), planets comparable to or superior to the jovian mass have been found in recent direct observations (Kalas et al., 2008; Marios et al., 2008; Carson et al., 2012). Therefore, the sputtering objects that cause the CSP formation may be common around stars.

I should note that the present results cannot exclude the possibility that the discovered FIR emission comes from the populations analogues to the detached SD, rather than the OC. In case of the planet-scatter scenario in the solar system (Duncan et al., 1987; Dones et al., 2004), the scattered objects are firstly injected into the SD-like population, and then end up in the Oort cloud via gravitational perturbations by passing stars and the Galactic tides. According to the numerical calculations by Dones et al. (2004), the total mass of the SD component is comparable, or more massive than that of the OC at the present day, until $\sim$ a few 100 Myr after the planet formation, i.e., marginally comparable to typical MS lifetime of the A-type stars. This may not be the case for the typical A-type MS stars, because the mass of the stars and the orbital characteristics of the parent planets should be different from the solar system. Further observations as well as numerical calculations should be required for more precise discussions.

Another possibility is that the CSPs have been formed with a process that does not need giant planets. The CSPs may be ascribed to objects captured from the protoplanetary disks of other stars in their birth clusters (Levison et al., 2010). According to Levison et al. (2010), objects could have been captured from nearby stars during the close encounters, and then formed isotropic populations that extend more than thousands AU. If this is the case, the gravitational "slingshots" are not required inside the stellar systems, and the extended populations universally exist regardless of the structure of planetary systems.

## 5.3 Summary of this chapter

In order to evaluate the significance of the present detection, I have performed four tests. Firstly, the possibilities of contaminations with background objects to the excess is investigated by performing a follow-up median stacking analysis. The median result is consistent with the average results. I thus found no evidence of the observed cold excess emission from the background objects. Secondly, I have performed a stacking analysis of sub-groups of the sample, and found no evidence for any anomalous contribution from minor samples. For the third test, I have performed a stacking analysis of randomly selected blank regions, and found that the cold excess fluxes are above statistical background fluctuations with significance of $\sim 2.5\sigma$. Finally, I have derived the RBPs of four sub-regions of the stacked images, and find no evidence of the contamination of local background inhomogeneities to the observed profile excess.

Assuming the observed cold excess comes from the circumstellar dust grains around the stacked stars, the observed emission can be approximated by the thermal emission from micron-sized dust grains with a total mass of $\sim 10^{-1}\,M_{\rm earth}$. These grains would be diffused by the passing interstellar magnetic field in a timescale of $\sim 10^6$ years. Therefore the grains should be replenished from larger objects in the groups with a total mass of comparable to the OC in the solar system ($\sim$ a few to $10^2\,M_{\rm earth}$), via some replenish processes with efficiencies of $\sim 10^{-1}\,M_{\rm earth}\,{\rm Myr}^{-1}$. The mutual collisions of the objects, the interstellar dust impact, and several episodic events are proposed for possible processes for the dust replenishment. The present results indicate that the cometary populations are natural by-products of typical planetary systems, rather than the exception.

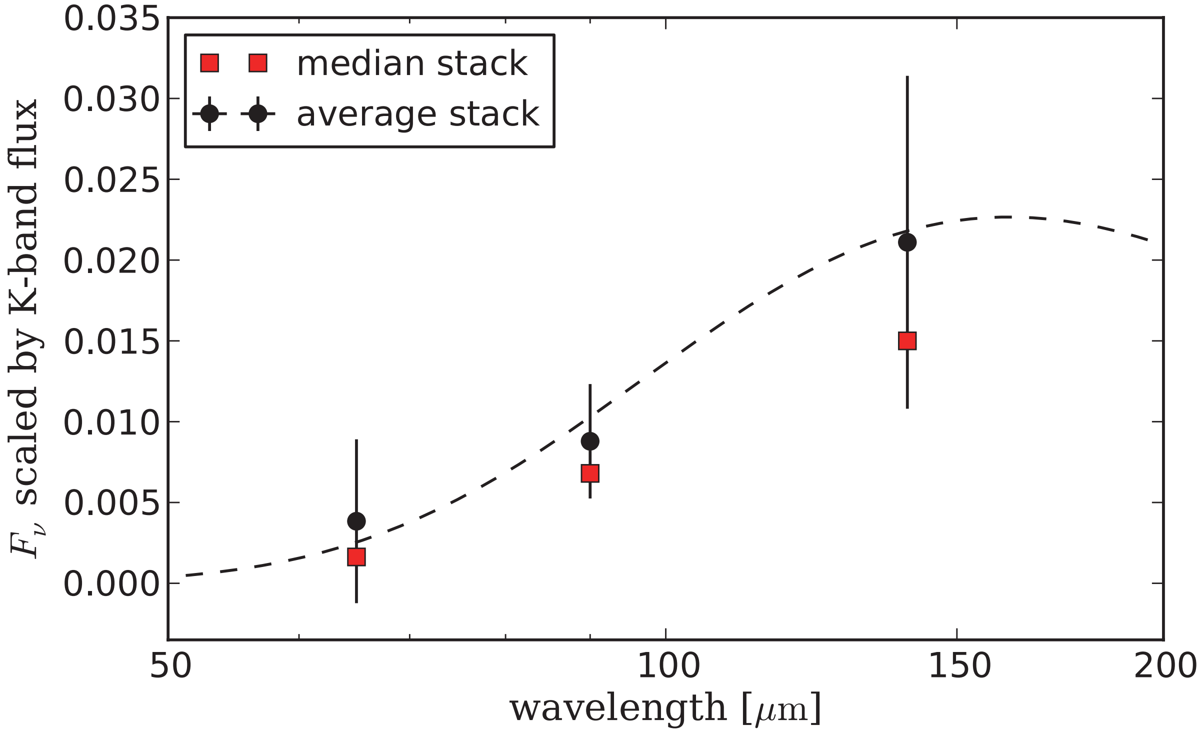


Figure5.1 Black points with error bars show the fluxes obtained from the averaging stacked maps of 63 A-type stars located in the distance range 15.8 – 39.8 pc (group 1), which are measured with the $90'' - 226''$ annulus (the same as Figure 4.4). The red squares present the fluxes obtained from the median stacks of the maps, and measured with the same annulus. The dashed curve shows the spectrum of gray-body emission with the temperature of 23 K.

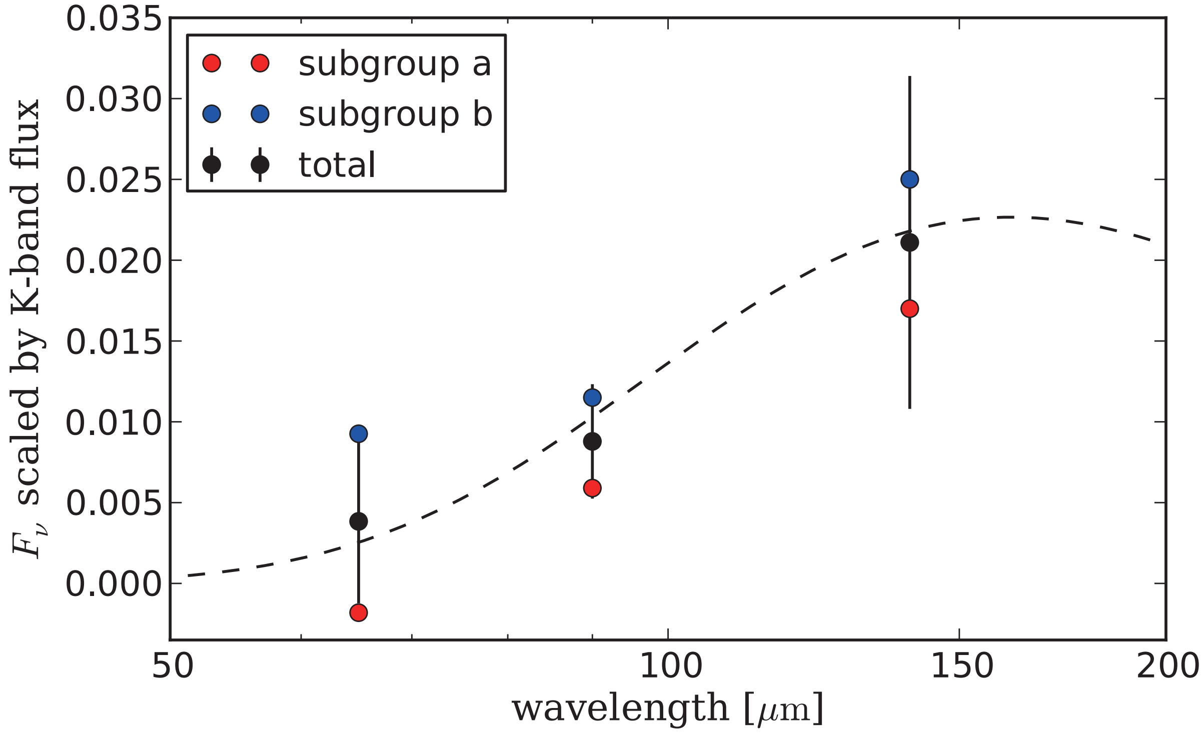


Figure5.2 The same as Figure 5.1, but with the average fluxes of the two subgroups (red and blue circles), instead of the median fluxes.

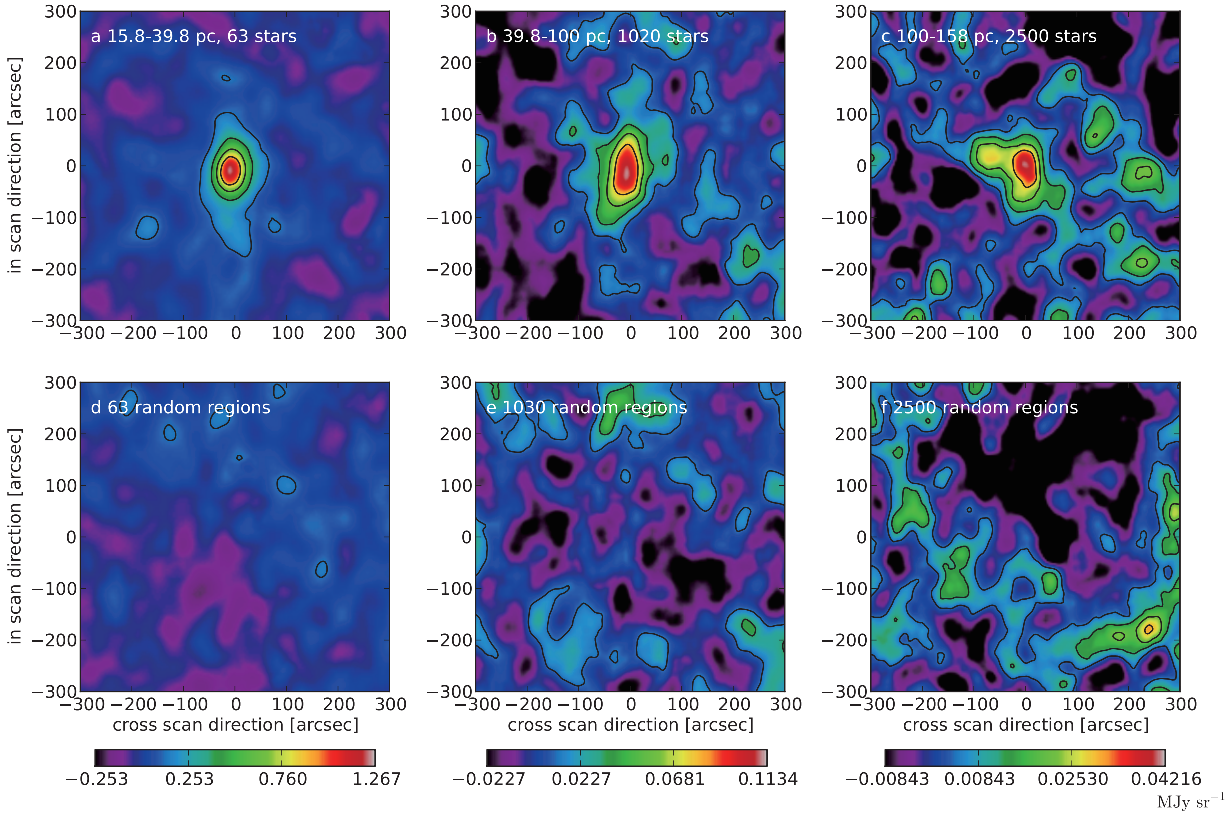


Figure5.3 Upper panels (a, b, and c) are images centered at the positions of the selected A-type stars at the 90 $\mu$m band that are used for the present study (Figure 1). Lower panels (d, e, and f) show the images centered at randomly selected positions. The panels in each column are displayed with the same color scale, whose color bar is displayed at the bottom. Contours are at 70, 50, and 20% of the peak pixel value of the upper panels.

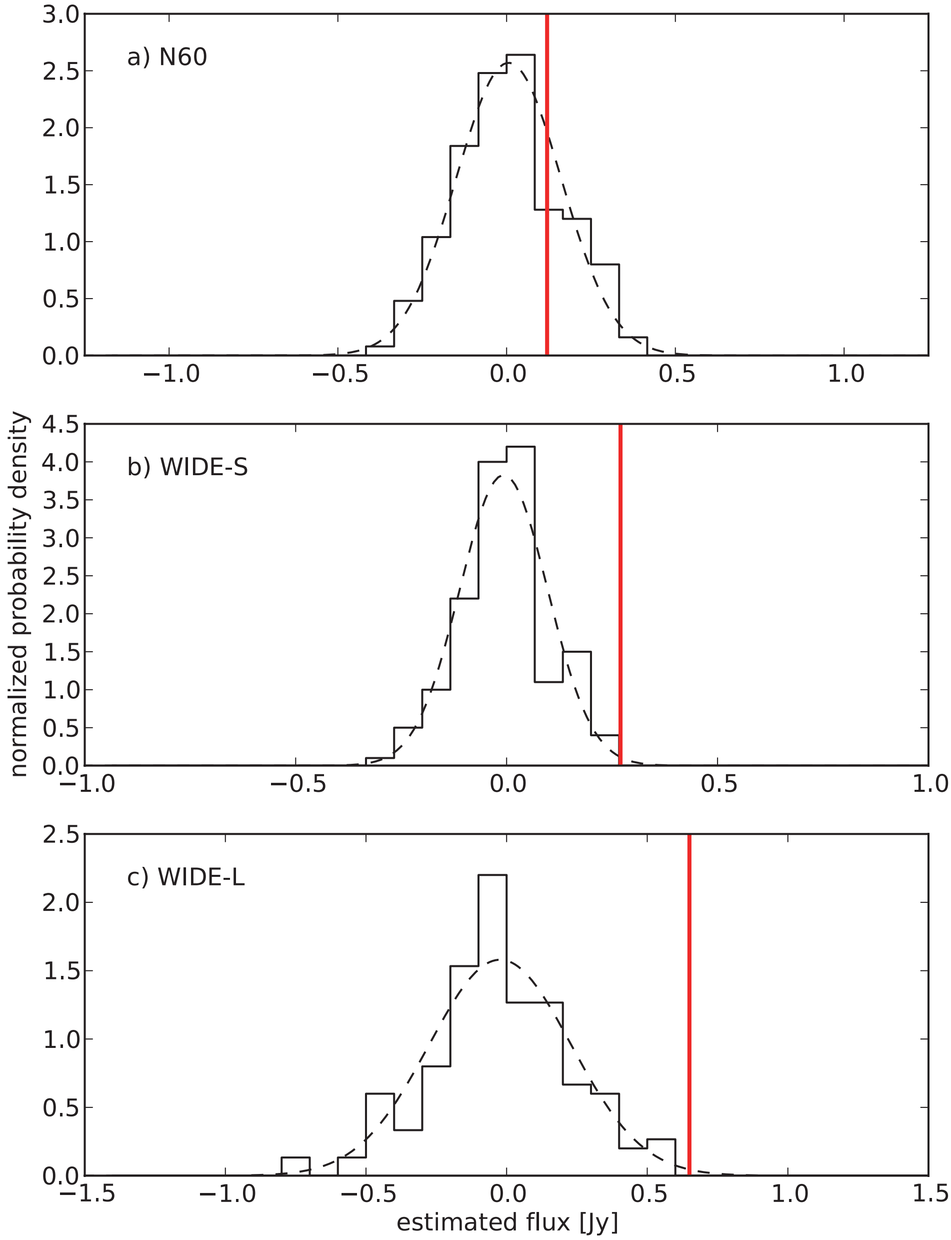


Figure5.4 Histograms of the fluxes obtained from the 150 test stack images that are made by stacking 63 randomly selected regions in the FIS a) 65, b) 90, and c) 140 $\mu$m maps with the $90'' - 226''$ annulus. Dashed curves indicate normal distribution fit to the distribution, and red vertical lines are the measured fluxes of the stacked A-type stars in the group 1 at the individual bands.

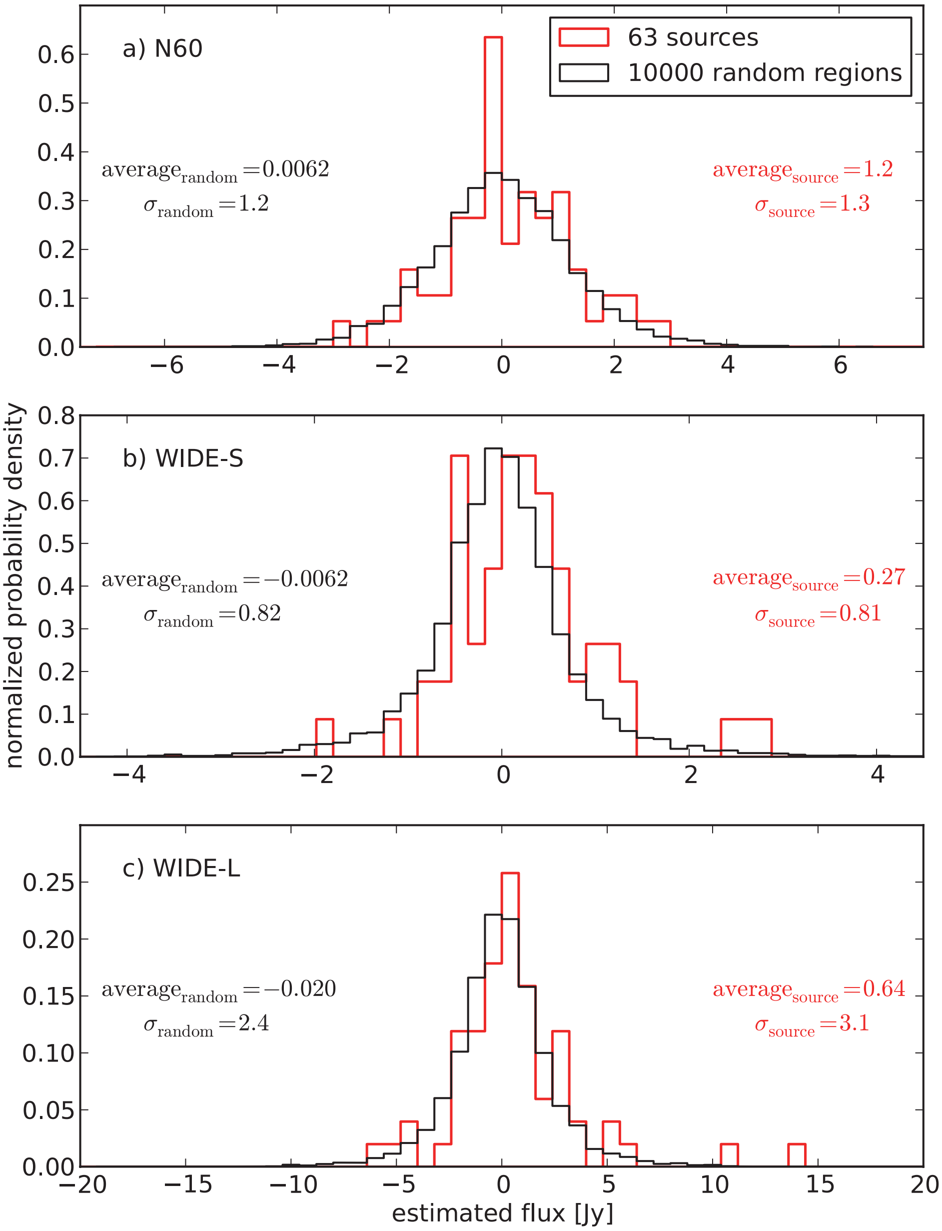


Figure5.5 Histograms of the fluxes of the images of the 63 selected stars in group 1 (red), and of those obtained from the 10000 blank region images (black) at the FIS a) 65, b) 90, and c) 140 $\mu$m maps with the $90'' - 226''$ annulus. The average and the deviation of the fluxes of the on-source and blank images are presented as average$_{source}$, $\sigma_{source}$, and average$_{random}$, $\sigma_{random}$, respectively.

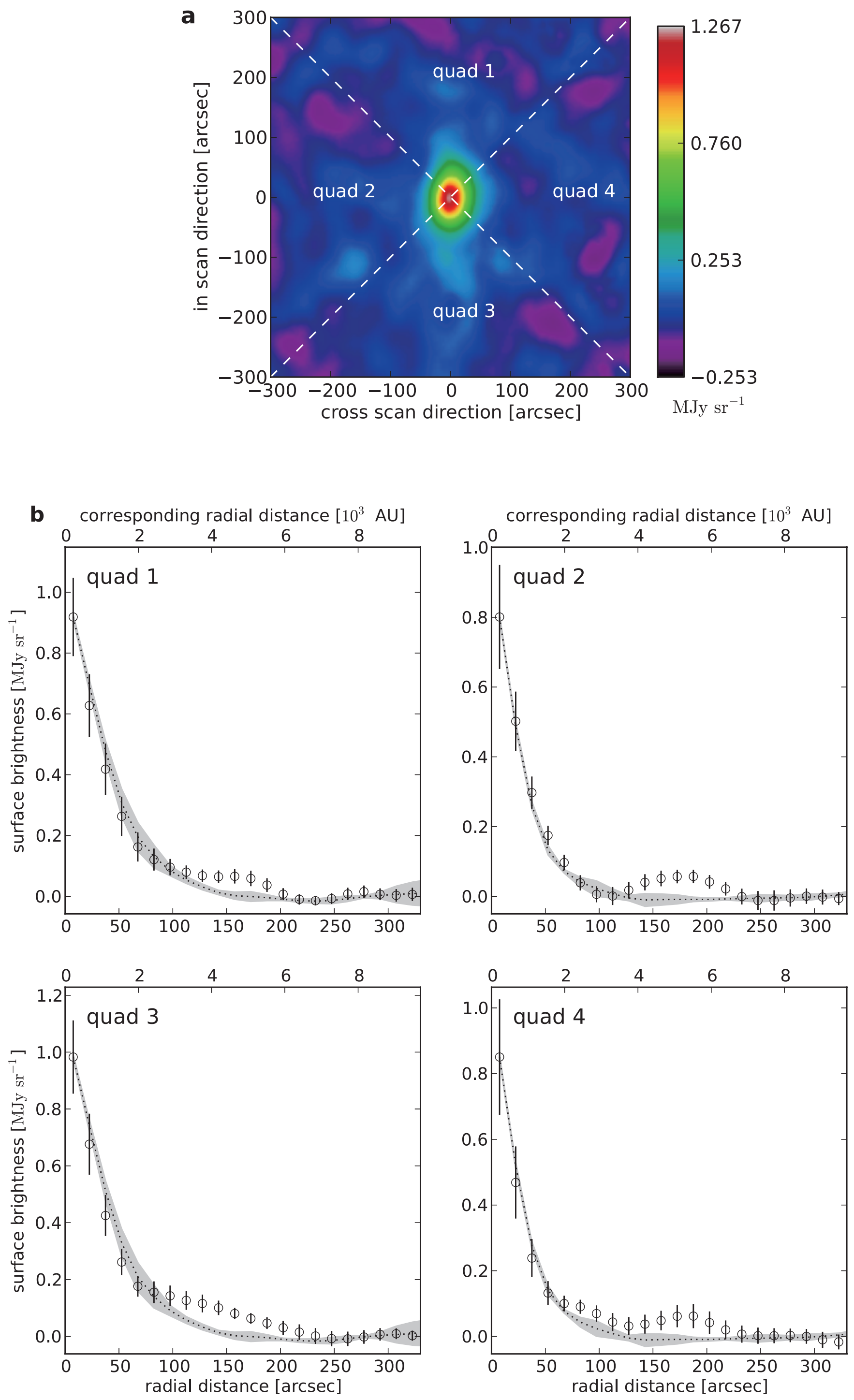


Figure5.6 a) Stacked image of the group 1 at the FIS 90 $\mu$m band, overlaid with the definition of the four quadrant regions. b) RBPs of the four quadrant regions (open circles with error bars) overlaid with the RBPs of PSF of the corresponding quadrant regions (dotted curves with error gray regions) normalized to match the peak intensity.

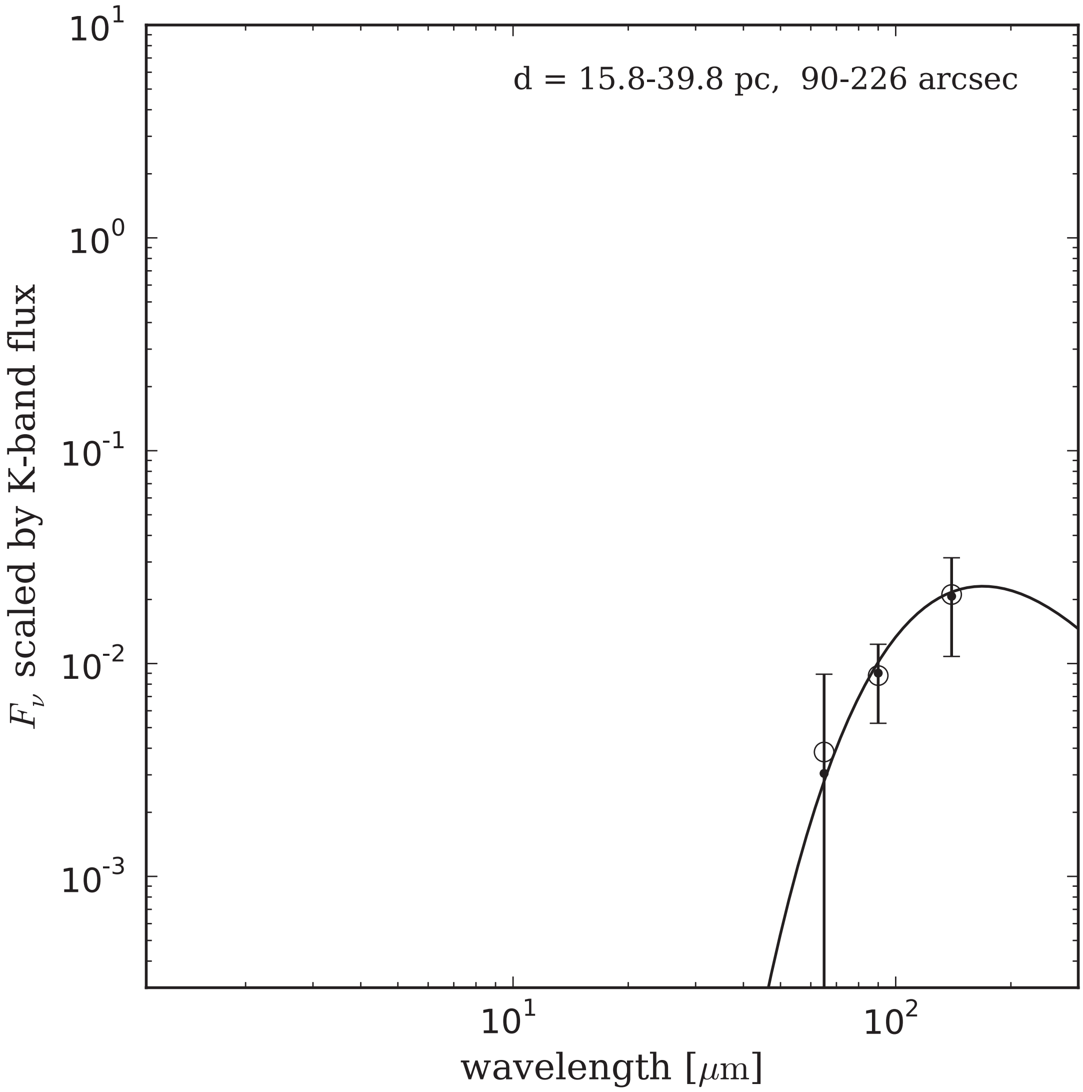


Figure5.7 The same plot as shown in Figure 4.4, but overlaid with the best-fit model spectrum provided in section 5.2.1, which takes the equilibrium temperature of the dust grains around the individual stars of the stacked sample into consideration.

# Chapter6

# Conclusions and future prospects

## 6.1 Conclusions

In this thesis, I searched for extrasolar CSPs around nearby A-type stars using the FIS all-sky maps obtained with the infrared satellite *AKARI*.

In order to obtain accurate spatial and spectral properties of the exo-CSP emission, calibrations for point sources in the FIS all-sky maps are carried out at the 65, 90, and 140 $\mu$m bands. By performing the stacking analysis with the images of the infrared standard stars, I can perform radial properties flux measurements of the point sources fainter than the detection limits of the FIS maps. The RBPs of the stacked point sources are determined, and are confirmed to be stable within the investigated flux range ($0.06 - 12$ Jy) at the 90 $\mu$m band. The aperture photometry of the infrared standard stars is performed, and measured fluxes are compared with emission model values to derive calibration factors. The calibration factors for the point source photometry are determined with uncertainties of 9, 3, and 21% at the 65, 90, and 140 $\mu$m bands, respectively. Any flux dependence in the calibration factors with amplitude larger than $\sim 20\%$ is not found within the investigated flux ranges at the three bands.

Based on a data set of 3583 A-type stars located inside 158 pc from the Sun, stacking analyses have been performed with three appropriate distance bins ($15.8 - 39.8$ pc, $39.8-100$ pc, and $100-158$ pc bins) using the *AKARI*/FIS all-sky map at the 65, 90, and 140 $\mu$m bands. The photometry of the stacked image presents a FIR excess emission that comes from closer than 2600 AU from the parent stars, and corresponds a $\sim 120$ K blackbody with a fractional luminosity (the energy contribution of the excess to the stellar photospheric emission) of $\sim 5 \times 10^{-5}$. These properties are in agreement with the average properties of known debris disks around A-type stars. In addition to the debris disk component, a colder excess component corresponding to the $\sim 23$ K modified blackbody emission with a fractional luminosity of an order of $10^{-5}$ is seen in the annulus corresponding physical radii of $2600 - 6600$ AU. In order to make a constraint on a spatial distribution of the cold excess component, RBPs are derived from the stacked images at the 90 $\mu$m band. The RBPs indicate that the emission structure extends to approximately 5000 AU, which is larger than the typical debris-disk sizes (smaller than 1000 AU).

In order to evaluate the significance of the present detection, I have performed four tests. Firstly, I have carried out median stacking analysis that is thought to be more robust to contamination from background point sources. The median stack and average stack to the same sample give consistent results of the cold excess fluxes. I thus found no evidence of the cold excess emission from the background objects. Secondly, I have performed a stacking analysis of sub-groups of the sample and found that the cold excess fluxes are not due to anomalous contribution from minor samples. For the third test, the cold excess fluxes are compared with those derived from stacks of randomly selected blank regions, and are found to be above the statistical background fluctuations with significances of up to $\sim 2.5\sigma$. Finally, I have derived the RBPs of four sub-regions of the stacked images, and found no evidence of the contamination of local background inhomogeneities to the observed profile.

Assuming the observed cold excess comes from the circumstellar dust grains around the stacked stars, the excess can be explained by the thermal emission from micron-sized grains with the mass of $\sim 0.1\,\mathrm{M_{earth}}$. Taking interstellar diffusion timescales of the grains into consideration, these grains can be supplied form object groups with the total mass of $\sim 10 - 100\,\mathrm{M_{earth}}$, which is comparable to that of the OC of the solar system, via several possible replenish processes. The present results indicate that the CSPs are not exceptional products of typical stellar system formations.

## 6.2 Future Prospects

### 6.2.1 CSPs around other type stars and planet and debris disk host stars

The present study has investigated the FIR emission only from the A-type stars. Further studies of other types of stars including solar-type stars are required in order to understand common properties of the exo-CSPs. In addition, for further discussion on a possible link between the exo-CSPs, and planet and debris disk formation processes, comparisons of characteristics of the FIR extended emission around stars with/without planets and debris disks are required, which are not achieved in the present study due to the lack of sensitivity of the present data sets. For these purposes, FIR to sub-mm imaging observations with higher sensitivities should be performed in future missions, such as SPICA(Nakagawa et al., 2012) and CCAT(Woody et al., 2012).

### 6.2.2 Observations of the SD and OC in the solar system

In the present discussions, the radial distribution and size distribution of the objects in the exo-CSPs are assumed to be simple distributions, based on the numerical simulations of the solar system OC and SD formations (Duncan et al., 1987; Dones et al., 2004). Observational constraints on these properties are quite important not only to understand accurate properties, formation and evolution scenarios of the CSPs, but also to gain accurate discussions on the observational results of the extrasolar CSPs. However, the observational constraints are not available so far. Direct detection of the objects in the outer SD and the OC is impossible because they are extremely faint, and are thus invisible using the latest instruments.

Instead of the direct detection, I planed to detect the stellar occultation events by the SD and OC objects. I will perform serendipitous monitoring observations of a large number ($10^4 - 10^6$) of stars with wide-field optical instruments, such as Hyper Suprime-Cam on Subaru telescope, and newly developed telescope array based on the small-sized (aperture sizes of $\sim$ 30 cm) telescopes and CMOS cameras. By measuring the occurrence rate, the duration, and the amplitude of the occultation events, I will obtain the abundances, sizes, and orbital properties of the CSP objects These observations will provide the observational constraints on the physical properties of the outer SD and the inner OC, and a hint of the detailed formation and evolution scenarios of the CSPs.

# AppendixA

# Tables of the selected A-type stars

TableA.1: Selected A-type MS stars located at $39.8 < d < 100$ pc (group 2)

| Hipparcos ID | parallax [mas] | K flux [Jy] |
|---|---|---|
| 128 | 15.2 | 2.61 |
| 159 | 16.92 | 2.19 |
| 432 | 10.35 | 1.67 |
| 1123 | 11.13 | 2.23 |
| 1302 | 10.75 | 2.6 |
| 1366 | 12.88 | 11.42 |
| 1473 | 23.11 | 10.92 |
| 1721 | 10.13 | 1.13 |
| 2225 | 12.32 | 6.76 |
| 2355 | 17.62 | 10.99 |
| 2381 | 18.08 | 7.8 |
| 2472 | 18.97 | 8.79 |
| 2479 | 13.44 | 1.67 |
| 2578 | 21.52 | 6.76 |
| 2852 | 20.12 | 4.54 |
| 3277 | 15.29 | 3.95 |
| 3405 | 13.57 | 12.61 |
| 3414 | 18.71 | 9.78 |
| 3438 | 12.96 | 2.36 |
| 3521 | 15.01 | 5.66 |
| 3572 | 11.24 | 3.83 |
| 3865 | 11.53 | 3.03 |
| 3903 | 10.31 | 3.26 |
| 3919 | 11.01 | 2.34 |
| 4212 | 11.72 | 2.83 |
| 4283 | 13.3 | 5.24 |

| | | |
|---|---|---|
| 4303 | 10.32 | 0.79 |
| 4329 | 10.4 | 1.4 |
| 4366 | 11.94 | 3.35 |
| 4436 | 23.93 | 23.42 |
| 4852 | 14.39 | 5.42 |
| 5131 | 13.67 | 5.22 |
| 5132 | 14.67 | 3.8 |
| 5231 | 10.04 | 0.74 |
| 5259 | 13.96 | 3.27 |
| 5300 | 16.48 | 8.19 |
| 5317 | 16.61 | 8.25 |
| 5321 | 10.3 | 1.33 |
| 5363 | 11.5 | 2.26 |
| 5518 | 10.26 | 5.02 |
| 5542 | 23.73 | 14.88 |
| 5626 | 11.98 | 4.23 |
| 5661 | 13.62 | 5.52 |
| 5674 | 12.94 | 1.88 |
| 5737 | 22.09 | 9.93 |
| 6061 | 14.83 | 7.17 |
| 6108 | 11.41 | 1.66 |
| 6347 | 10.09 | 1.7 |
| 6369 | 12.26 | 1.97 |
| 6507 | 11.16 | 2.4 |
| 6514 | 15.43 | 6.87 |
| 6794 | 17.91 | 3.51 |
| 6888 | 11.44 | 3.41 |
| 6897 | 10.77 | 1.83 |
| 6960 | 14.72 | 6.9 |
| 7108 | 11.42 | 2.18 |
| 7113 | 10.5 | 1.91 |
| 7115 | 10.21 | 2.65 |
| 7262 | 13.7 | 1.66 |
| 7283 | 10.15 | 2.2 |
| 7298 | 12.89 | 2.32 |
| 7345 | 16.32 | 4.37 |
| 7364 | 12.0 | 1.27 |
| 7663 | 10.51 | 0.96 |
| 7825 | 12.15 | 6.2 |
| 7941 | 10.71 | 3.55 |
| 7987 | 10.41 | 1.63 |
| 8122 | 13.95 | 2.27 |
| 8151 | 11.95 | 1.1 |
| 8194 | 10.43 | 1.32 |
| 8241 | 17.54 | 6.89 |
| 8296 | 10.08 | 1.77 |
| 8454 | 10.29 | 1.33 |
| 8593 | 13.37 | 4.52 |
| 8847 | 13.61 | 2.48 |
| 8882 | 10.55 | 5.69 |
| 9295 | 12.12 | 3.74 |
| 9358 | 10.34 | 2.43 |

| | | |
|---|---|---|
| 9563 | 10.46 | 1.74 |
| 9589 | 11.31 | 6.7 |
| 9598 | 20.12 | 18.01 |
| 9836 | 17.4 | 8.47 |
| 9858 | 14.09 | 2.02 |
| 9951 | 11.47 | 2.74 |
| 9977 | 16.48 | 11.32 |
| 10054 | 14.61 | 3.53 |
| 10099 | 11.31 | 1.94 |
| 10559 | 11.13 | 5.4 |
| 10819 | 12.77 | 5.19 |
| 11001 | 24.1 | 17.42 |
| 11102 | 16.3 | 4.45 |
| 11138 | 13.37 | 2.3 |
| 11348 | 15.24 | 3.71 |
| 11477 | 21.35 | 7.02 |
| 11578 | 12.33 | 2.93 |
| 11622 | 11.66 | 1.91 |
| 11678 | 14.44 | 4.26 |
| 11687 | 11.87 | 3.84 |
| 11821 | 11.39 | 1.2 |
| 11904 | 11.73 | 2.24 |
| 12225 | 22.49 | 10.33 |
| 12489 | 13.97 | 6.23 |
| 12725 | 12.39 | 2.55 |
| 12876 | 11.06 | 9.65 |
| 12990 | 21.24 | 5.05 |
| 13141 | 19.73 | 6.85 |
| 13271 | 10.02 | 2.26 |
| 13569 | 13.89 | 2.18 |
| 13579 | 10.41 | 2.16 |
| 13628 | 10.56 | 0.51 |
| 13717 | 17.28 | 7.6 |
| 13765 | 13.21 | 3.23 |
| 13782 | 20.54 | 7.21 |
| 13874 | 10.2 | 6.11 |
| 13883 | 11.11 | 3.84 |
| 13884 | 10.4 | 9.5 |
| 14109 | 15.24 | 3.98 |
| 14293 | 23.22 | 8.46 |
| 14479 | 13.21 | 2.02 |
| 14551 | 17.35 | 3.27 |
| 14554 | 10.13 | 0.89 |
| 14619 | 15.23 | 2.79 |
| 14751 | 10.57 | 1.12 |
| 14791 | 12.75 | 2.47 |
| 14844 | 16.13 | 4.09 |
| 14862 | 20.15 | 8.68 |
| 15039 | 14.16 | 1.78 |
| 15204 | 14.96 | 3.89 |
| 15239 | 11.99 | 1.46 |
| 15279 | 11.88 | 1.87 |

| | | |
|---|---|---|
| 15353 | 17.24 | 3.53 |
| 15568 | 11.54 | 1.76 |
| 15614 | 12.38 | 1.99 |
| 15648 | 21.0 | 8.19 |
| 15660 | 11.62 | 1.46 |
| 15870 | 10.76 | 2.33 |
| 15886 | 10.62 | 1.93 |
| 15987 | 10.01 | 2.23 |
| 16285 | 16.04 | 5.62 |
| 16378 | 10.82 | 0.74 |
| 16449 | 13.55 | 2.42 |
| 16591 | 18.29 | 4.23 |
| 16835 | 14.98 | 3.16 |
| 16924 | 13.52 | 2.61 |
| 17395 | 23.3 | 6.21 |
| 17552 | 11.21 | 0.79 |
| 17717 | 11.98 | 6.2 |
| 17763 | 11.94 | 0.72 |
| 17846 | 14.43 | 5.51 |
| 17854 | 10.02 | 5.55 |
| 17891 | 14.11 | 5.24 |
| 17954 | 16.96 | 7.92 |
| 18153 | 10.91 | 2.18 |
| 18217 | 19.14 | 4.73 |
| 18286 | 10.69 | 1.67 |
| 18339 | 20.41 | 5.24 |
| 18438 | 16.64 | 4.18 |
| 18481 | 13.26 | 2.84 |
| 18492 | 11.29 | 1.39 |
| 18547 | 16.32 | 2.71 |
| 19121 | 12.26 | 2.34 |
| 19515 | 18.61 | 17.58 |
| 19571 | 13.06 | 4.37 |
| 19688 | 11.29 | 1.7 |
| 19718 | 10.81 | 2.25 |
| 20106 | 10.86 | 4.13 |
| 20109 | 13.49 | 7.35 |
| 20144 | 10.09 | 1.64 |
| 20257 | 11.25 | 2.45 |
| 20281 | 10.17 | 2.36 |
| 20380 | 10.53 | 4.01 |
| 20446 | 10.05 | 2.22 |
| 20507 | 15.66 | 7.14 |
| 20529 | 10.2 | 2.18 |
| 20576 | 10.64 | 1.32 |
| 21402 | 21.68 | 22.22 |
| 21618 | 10.67 | 1.7 |
| 21644 | 14.34 | 8.32 |
| 21670 | 19.44 | 7.96 |
| 21849 | 11.12 | 1.49 |
| 21915 | 13.9 | 2.86 |
| 21928 | 12.02 | 5.53 |

| | | |
|---|---|---|
| 22028 | 11.06 | 4.45 |
| 22040 | 14.66 | 8.58 |
| 22137 | 11.0 | 1.72 |
| 22189 | 11.76 | 2.19 |
| 22192 | 17.4 | 3.45 |
| 22287 | 20.12 | 8.59 |
| 22361 | 21.92 | 5.44 |
| 22509 | 16.84 | 14.37 |
| 22573 | 11.39 | 4.13 |
| 22701 | 14.39 | 21.59 |
| 22833 | 13.54 | 7.77 |
| 22897 | 11.39 | 2.46 |
| 22926 | 12.45 | 2.0 |
| 23296 | 20.17 | 3.9 |
| 23554 | 16.65 | 4.89 |
| 23585 | 17.52 | 2.7 |
| 23879 | 16.84 | 10.21 |
| 23983 | 18.54 | 7.58 |
| 24009 | 11.81 | 2.54 |
| 24093 | 10.09 | 0.94 |
| 24348 | 12.16 | 2.75 |
| 24362 | 13.46 | 1.5 |
| 24394 | 13.31 | 5.04 |
| 24478 | 11.49 | 1.6 |
| 24528 | 11.65 | 1.79 |
| 25205 | 13.32 | 2.74 |
| 25280 | 14.84 | 3.67 |
| 25488 | 10.52 | 4.82 |
| 25517 | 12.41 | 1.39 |
| 25608 | 11.1 | 4.2 |
| 25807 | 11.7 | 1.91 |
| 25853 | 12.0 | 4.15 |
| 25911 | 10.05 | 3.36 |
| 26161 | 10.43 | 0.93 |
| 26309 | 17.68 | 3.01 |
| 26395 | 15.14 | 2.73 |
| 26410 | 12.6 | 3.94 |
| 26966 | 14.45 | 3.24 |
| 27192 | 16.29 | 2.99 |
| 27249 | 16.89 | 4.15 |
| 27259 | 10.6 | 1.45 |
| 27924 | 10.69 | 1.54 |
| 27949 | 13.54 | 8.28 |
| 28230 | 11.12 | 1.18 |
| 28484 | 15.82 | 5.73 |
| 28654 | 11.91 | 1.92 |
| 28778 | 10.74 | 1.18 |
| 28855 | 12.4 | 3.38 |
| 28878 | 10.23 | 1.0 |
| 28899 | 12.25 | 3.56 |
| 28910 | 19.14 | 10.35 |
| 28957 | 10.13 | 3.92 |

| | | |
|---|---|---|
| 29064 | 12.48 | 4.35 |
| 29150 | 12.77 | 4.39 |
| 29357 | 11.85 | 1.76 |
| 29852 | 16.1 | 4.44 |
| 29857 | 11.9 | 1.26 |
| 30060 | 21.88 | 12.17 |
| 30165 | 11.72 | 1.19 |
| 30167 | 14.38 | 2.34 |
| 30252 | 13.84 | 2.12 |
| 30275 | 10.93 | 1.16 |
| 30342 | 19.87 | 6.48 |
| 30381 | 10.61 | 1.82 |
| 30423 | 10.22 | 2.23 |
| 30463 | 11.37 | 3.33 |
| 30651 | 12.01 | 6.71 |
| 30666 | 14.26 | 3.69 |
| 30760 | 12.66 | 1.9 |
| 30762 | 10.41 | 1.5 |
| 31092 | 10.74 | 2.9 |
| 31173 | 11.86 | 4.28 |
| 31386 | 12.02 | 1.01 |
| 31427 | 13.57 | 1.76 |
| 31472 | 10.99 | 0.92 |
| 31665 | 10.12 | 3.19 |
| 32104 | 23.41 | 6.6 |
| 32296 | 14.48 | 2.37 |
| 32319 | 11.21 | 1.72 |
| 32438 | 14.26 | 7.91 |
| 32594 | 11.07 | 1.09 |
| 32886 | 10.16 | 1.5 |
| 32938 | 18.14 | 4.16 |
| 33081 | 10.4 | 2.0 |
| 33477 | 10.24 | 1.21 |
| 33485 | 14.49 | 8.07 |
| 33584 | 13.69 | 2.71 |
| 34002 | 12.59 | 3.93 |
| 34059 | 16.98 | 9.93 |
| 34081 | 10.34 | 8.45 |
| 34276 | 10.77 | 1.71 |
| 34417 | 16.81 | 2.5 |
| 34589 | 15.76 | 3.23 |
| 34782 | 21.02 | 4.67 |
| 34897 | 15.07 | 2.68 |
| 34899 | 17.97 | 7.49 |
| 34952 | 10.22 | 2.22 |
| 35180 | 11.79 | 5.21 |
| 35229 | 10.38 | 1.36 |
| 35341 | 12.18 | 4.91 |
| 35384 | 10.97 | 9.47 |
| 35467 | 11.42 | 2.62 |
| 35543 | 10.9 | 1.8 |
| 35567 | 14.25 | 2.04 |

| | | |
|---|---|---|
| 35578 | 11.08 | 2.42 |
| 35735 | 14.23 | 3.34 |
| 35842 | 10.46 | 2.28 |
| 35946 | 12.9 | 2.28 |
| 35987 | 10.28 | 6.3 |
| 36145 | 13.11 | 9.89 |
| 36624 | 10.61 | 1.81 |
| 36807 | 11.37 | 4.74 |
| 36922 | 10.1 | 1.6 |
| 37133 | 10.43 | 1.73 |
| 37140 | 12.44 | 4.37 |
| 37372 | 11.15 | 2.32 |
| 37394 | 10.51 | 3.94 |
| 37495 | 12.36 | 2.22 |
| 37519 | 13.93 | 2.13 |
| 37609 | 13.75 | 9.38 |
| 37921 | 10.44 | 5.93 |
| 38017 | 11.77 | 1.66 |
| 38083 | 14.33 | 1.79 |
| 38235 | 15.67 | 3.02 |
| 38266 | 10.82 | 1.39 |
| 38319 | 15.69 | 3.55 |
| 38393 | 11.87 | 1.57 |
| 38538 | 12.82 | 9.14 |
| 38723 | 16.55 | 4.63 |
| 39017 | 16.2 | 2.15 |
| 39095 | 13.69 | 12.6 |
| 39346 | 12.67 | 1.71 |
| 39567 | 15.49 | 6.09 |
| 39847 | 14.96 | 9.11 |
| 40293 | 10.31 | 2.11 |
| 40514 | 10.44 | 1.53 |
| 40646 | 10.73 | 5.86 |
| 40699 | 10.34 | 2.94 |
| 40791 | 15.19 | 2.04 |
| 40896 | 10.44 | 1.19 |
| 41036 | 15.36 | 3.85 |
| 41152 | 19.46 | 5.3 |
| 41336 | 10.21 | 2.24 |
| 41375 | 18.83 | 6.72 |
| 41451 | 11.43 | 4.02 |
| 41483 | 16.01 | 11.17 |
| 41564 | 11.73 | 3.9 |
| 41578 | 10.6 | 4.72 |
| 41754 | 11.93 | 1.82 |
| 41765 | 10.55 | 1.19 |
| 41893 | 14.1 | 3.6 |
| 42080 | 20.63 | 7.08 |
| 42090 | 10.17 | 4.04 |
| 42146 | 12.15 | 3.53 |
| 42197 | 13.08 | 1.67 |
| 42313 | 18.21 | 16.25 |

| | | |
|---|---|---|
| 42334 | 13.49 | 4.96 |
| 42466 | 11.71 | 1.78 |
| 42794 | 10.23 | 3.04 |
| 42806 | 20.58 | 9.31 |
| 42874 | 10.95 | 1.97 |
| 42895 | 16.49 | 4.32 |
| 42928 | 12.78 | 3.91 |
| 42931 | 15.78 | 3.83 |
| 42989 | 12.01 | 2.5 |
| 43121 | 16.38 | 4.02 |
| 43330 | 11.86 | 2.13 |
| 43338 | 12.47 | 3.01 |
| 43620 | 11.01 | 2.55 |
| 43853 | 14.24 | 2.65 |
| 43932 | 16.73 | 6.52 |
| 43970 | 20.39 | 7.55 |
| 43976 | 12.14 | 1.84 |
| 44238 | 12.01 | 1.28 |
| 44331 | 15.24 | 4.05 |
| 44342 | 17.03 | 4.47 |
| 44393 | 11.16 | 1.02 |
| 44574 | 12.6 | 2.99 |
| 44578 | 10.99 | 1.73 |
| 44683 | 10.19 | 1.81 |
| 44714 | 10.36 | 0.76 |
| 44806 | 10.69 | 1.61 |
| 44923 | 12.52 | 3.55 |
| 45001 | 15.35 | 5.85 |
| 45150 | 19.65 | 3.98 |
| 45184 | 12.1 | 4.04 |
| 45257 | 11.48 | 1.54 |
| 45510 | 12.03 | 2.18 |
| 45511 | 12.3 | 2.02 |
| 45585 | 12.37 | 3.01 |
| 45667 | 10.51 | 1.3 |
| 45758 | 10.19 | 2.75 |
| 45892 | 11.37 | 1.85 |
| 45910 | 10.27 | 1.83 |
| 45938 | 10.26 | 1.29 |
| 46065 | 10.18 | 1.71 |
| 46081 | 10.42 | 1.76 |
| 46130 | 10.53 | 1.31 |
| 46223 | 14.29 | 2.12 |
| 46297 | 10.87 | 4.27 |
| 46328 | 14.65 | 3.68 |
| 46460 | 12.17 | 3.45 |
| 46517 | 16.04 | 4.01 |
| 46522 | 10.93 | 1.91 |
| 46546 | 10.38 | 2.1 |
| 46873 | 10.98 | 1.71 |
| 46891 | 10.85 | 2.38 |
| 47006 | 12.21 | 12.19 |

| | | |
|---|---|---|
| 47070 | 11.5 | 2.32 |
| 47115 | 12.04 | 2.09 |
| 47335 | 11.66 | 1.36 |
| 47363 | 12.43 | 2.31 |
| 47664 | 10.9 | 2.17 |
| 47701 | 20.48 | 4.64 |
| 48164 | 11.17 | 1.49 |
| 48212 | 13.33 | 2.11 |
| 48266 | 10.65 | 4.2 |
| 48341 | 16.31 | 3.7 |
| 48390 | 24.9 | 9.1 |
| 48437 | 12.47 | 7.08 |
| 48590 | 10.79 | 0.64 |
| 48613 | 10.22 | 3.38 |
| 48682 | 14.65 | 6.19 |
| 48763 | 14.39 | 3.54 |
| 48977 | 10.18 | 2.1 |
| 49125 | 11.71 | 1.59 |
| 49165 | 14.13 | 1.82 |
| 49259 | 10.85 | 2.58 |
| 49802 | 12.57 | 3.04 |
| 49839 | 13.02 | 1.77 |
| 50070 | 20.06 | 9.5 |
| 50078 | 10.25 | 4.54 |
| 50083 | 10.74 | 9.28 |
| 50097 | 10.5 | 2.86 |
| 50196 | 12.37 | 2.52 |
| 50303 | 12.67 | 4.67 |
| 50320 | 10.89 | 2.0 |
| 50372 | 24.27 | 28.62 |
| 50391 | 16.07 | 3.68 |
| 50417 | 10.09 | 1.52 |
| 50448 | 13.07 | 4.9 |
| 50536 | 15.01 | 4.88 |
| 50649 | 10.46 | 1.67 |
| 50857 | 12.31 | 1.56 |
| 50860 | 14.18 | 4.18 |
| 50868 | 18.63 | 4.5 |
| 50888 | 24.7 | 8.9 |
| 50933 | 10.84 | 6.68 |
| 51194 | 14.22 | 3.23 |
| 51200 | 15.09 | 4.08 |
| 51295 | 10.16 | 1.22 |
| 51302 | 13.38 | 2.81 |
| 51438 | 12.6 | 9.95 |
| 51448 | 11.27 | 3.7 |
| 51556 | 13.33 | 4.14 |
| 51852 | 13.87 | 2.77 |
| 52131 | 10.47 | 1.89 |
| 52216 | 10.69 | 1.27 |
| 52352 | 11.04 | 1.94 |
| 52422 | 22.0 | 6.36 |

| | | |
|---|---|---|
| 52455 | 10.21 | 0.98 |
| 52457 | 15.72 | 7.18 |
| 52513 | 15.37 | 3.28 |
| 52709 | 13.33 | 3.12 |
| 52737 | 14.88 | 6.04 |
| 52763 | 10.47 | 1.29 |
| 52913 | 10.43 | 2.56 |
| 52920 | 10.21 | 0.78 |
| 53005 | 15.82 | 3.09 |
| 53062 | 12.12 | 1.45 |
| 53295 | 12.22 | 8.84 |
| 53411 | 10.19 | 2.28 |
| 53524 | 10.92 | 1.28 |
| 53530 | 10.3 | 4.57 |
| 53771 | 16.7 | 3.29 |
| 53773 | 15.99 | 15.69 |
| 53824 | 21.61 | 9.51 |
| 53860 | 11.47 | 2.46 |
| 53963 | 18.84 | 4.56 |
| 54063 | 16.17 | 2.08 |
| 54136 | 12.41 | 3.89 |
| 54137 | 11.69 | 6.8 |
| 54315 | 10.67 | 3.6 |
| 54360 | 11.5 | 6.89 |
| 54388 | 13.23 | 2.6 |
| 54477 | 17.21 | 5.37 |
| 54515 | 13.07 | 1.8 |
| 54605 | 10.8 | 1.58 |
| 54674 | 11.22 | 2.37 |
| 54682 | 12.26 | 12.28 |
| 54688 | 16.43 | 3.3 |
| 54718 | 10.11 | 3.39 |
| 54721 | 10.87 | 2.56 |
| 54746 | 20.02 | 6.85 |
| 54854 | 12.13 | 2.16 |
| 54960 | 10.9 | 1.41 |
| 55002 | 11.84 | 1.72 |
| 55060 | 10.88 | 1.89 |
| 55081 | 11.27 | 1.9 |
| 55130 | 13.96 | 2.67 |
| 55266 | 17.82 | 10.96 |
| 55485 | 12.79 | 2.69 |
| 55488 | 12.4 | 2.83 |
| 55497 | 13.4 | 2.73 |
| 55564 | 11.58 | 3.13 |
| 55700 | 13.35 | 1.41 |
| 55740 | 10.02 | 1.86 |
| 55769 | 10.1 | 2.22 |
| 55781 | 10.17 | 1.48 |
| 55861 | 11.7 | 1.22 |
| 56034 | 15.59 | 5.02 |
| 56083 | 14.73 | 2.82 |

| | | |
|---|---|---|
| 56253 | 16.72 | 3.98 |
| 56444 | 12.37 | 2.68 |
| 56573 | 17.24 | 9.29 |
| 56797 | 11.15 | 1.54 |
| 56920 | 13.93 | 2.32 |
| 57013 | 15.58 | 4.44 |
| 57253 | 11.18 | 1.7 |
| 57562 | 16.97 | 5.29 |
| 57646 | 15.96 | 4.84 |
| 57779 | 18.08 | 3.46 |
| 57805 | 15.87 | 3.84 |
| 57971 | 13.23 | 2.69 |
| 58188 | 11.42 | 5.67 |
| 58327 | 10.14 | 2.94 |
| 58510 | 11.8 | 4.89 |
| 58551 | 13.21 | 0.92 |
| 58591 | 11.0 | 1.59 |
| 58678 | 10.66 | 1.08 |
| 58823 | 10.55 | 1.01 |
| 59002 | 12.86 | 1.05 |
| 59203 | 10.32 | 1.1 |
| 59243 | 10.48 | 2.27 |
| 59309 | 22.81 | 6.74 |
| 59353 | 13.96 | 3.88 |
| 59364 | 10.6 | 3.84 |
| 59366 | 10.09 | 2.48 |
| 59451 | 10.31 | 1.54 |
| 59608 | 20.18 | 5.36 |
| 59676 | 12.04 | 2.91 |
| 59819 | 16.49 | 7.36 |
| 59868 | 10.53 | 1.25 |
| 59923 | 18.74 | 4.79 |
| 60014 | 11.85 | 2.6 |
| 60018 | 18.06 | 4.77 |
| 60044 | 11.29 | 5.26 |
| 60060 | 10.12 | 1.35 |
| 60066 | 13.14 | 2.7 |
| 60087 | 11.43 | 2.89 |
| 60123 | 11.01 | 2.34 |
| 60134 | 12.32 | 1.54 |
| 60266 | 11.2 | 1.44 |
| 60360 | 10.07 | 0.64 |
| 60490 | 11.57 | 2.53 |
| 60503 | 12.89 | 2.27 |
| 60514 | 11.47 | 7.34 |
| 60561 | 10.83 | 1.5 |
| 60746 | 11.56 | 9.21 |
| 60797 | 10.9 | 2.16 |
| 60891 | 12.66 | 2.52 |
| 60904 | 12.06 | 5.11 |
| 60957 | 12.84 | 4.5 |
| 60978 | 11.88 | 7.58 |

| | | |
|---|---|---|
| 61071 | 10.49 | 5.2 |
| 61082 | 10.13 | 0.89 |
| 61280 | 11.81 | 2.36 |
| 61347 | 13.32 | 1.74 |
| 61498 | 14.91 | 3.28 |
| 61558 | 14.54 | 3.49 |
| 61622 | 24.77 | 21.81 |
| 61692 | 15.27 | 3.15 |
| 61782 | 10.01 | 0.62 |
| 61902 | 11.36 | 2.35 |
| 61937 | 14.6 | 3.65 |
| 61968 | 13.37 | 4.04 |
| 62081 | 13.9 | 3.19 |
| 62102 | 10.16 | 1.2 |
| 62140 | 10.77 | 2.01 |
| 62209 | 10.79 | 0.94 |
| 62267 | 13.36 | 10.9 |
| 62394 | 13.41 | 3.52 |
| 62402 | 15.85 | 4.69 |
| 62788 | 16.62 | 4.61 |
| 62896 | 21.03 | 21.79 |
| 62933 | 16.4 | 4.34 |
| 62972 | 13.43 | 3.57 |
| 62983 | 14.98 | 3.12 |
| 63123 | 10.08 | 1.31 |
| 63280 | 11.39 | 1.39 |
| 63320 | 13.39 | 1.86 |
| 63414 | 10.95 | 5.2 |
| 63453 | 10.79 | 1.24 |
| 63491 | 18.23 | 3.25 |
| 63531 | 11.5 | 1.51 |
| 63724 | 14.97 | 8.49 |
| 64003 | 14.22 | 3.97 |
| 64111 | 10.67 | 2.47 |
| 64246 | 16.12 | 6.08 |
| 64527 | 11.36 | 2.07 |
| 64692 | 13.32 | 5.44 |
| 64822 | 17.12 | 4.48 |
| 64882 | 11.81 | 1.79 |
| 64906 | 11.85 | 5.33 |
| 64921 | 11.71 | 1.57 |
| 65183 | 11.28 | 2.67 |
| 65198 | 15.32 | 4.17 |
| 65224 | 11.11 | 1.66 |
| 65241 | 15.7 | 3.76 |
| 65466 | 12.82 | 4.2 |
| 65728 | 13.79 | 4.47 |
| 65969 | 11.48 | 2.11 |
| 66015 | 13.94 | 4.22 |
| 66065 | 15.25 | 3.85 |
| 66198 | 11.77 | 3.71 |
| 66234 | 17.12 | 13.02 |

| | | |
|---|---|---|
| 66376 | 10.99 | 2.02 |
| 66433 | 11.41 | 1.94 |
| 66522 | 13.95 | 3.04 |
| 66586 | 10.61 | 0.77 |
| 66634 | 19.27 | 5.68 |
| 66700 | 11.32 | 2.21 |
| 66729 | 10.14 | 1.4 |
| 66753 | 12.71 | 6.07 |
| 66798 | 14.74 | 3.68 |
| 66908 | 10.05 | 1.21 |
| 67143 | 11.35 | 3.46 |
| 67194 | 19.48 | 4.89 |
| 67270 | 10.35 | 2.63 |
| 67289 | 10.33 | 2.04 |
| 67292 | 16.64 | 5.12 |
| 67461 | 10.54 | 1.65 |
| 67483 | 15.41 | 3.77 |
| 67495 | 10.06 | 2.17 |
| 67548 | 12.12 | 2.24 |
| 67596 | 11.24 | 1.92 |
| 67630 | 12.73 | 1.8 |
| 67714 | 10.03 | 2.76 |
| 67782 | 15.46 | 4.34 |
| 68110 | 10.49 | 1.8 |
| 68414 | 13.03 | 2.66 |
| 68498 | 11.33 | 3.51 |
| 68520 | 14.94 | 15.4 |
| 68637 | 10.4 | 2.41 |
| 69200 | 11.55 | 0.76 |
| 69265 | 10.76 | 1.68 |
| 69592 | 16.95 | 2.97 |
| 69650 | 10.83 | 1.89 |
| 69658 | 12.49 | 4.01 |
| 69727 | 19.19 | 3.54 |
| 69828 | 12.49 | 2.21 |
| 69896 | 23.36 | 11.52 |
| 69904 | 10.2 | 3.23 |
| 69923 | 12.07 | 1.71 |
| 69929 | 11.08 | 3.08 |
| 69951 | 13.61 | 1.89 |
| 69974 | 17.47 | 13.41 |
| 69995 | 14.6 | 3.28 |
| 70022 | 14.29 | 3.46 |
| 70051 | 11.52 | 2.43 |
| 70400 | 21.56 | 8.23 |
| 70510 | 10.36 | 0.63 |
| 70556 | 10.19 | 0.84 |
| 70663 | 17.16 | 6.04 |
| 70680 | 13.83 | 2.85 |
| 70894 | 13.1 | 4.01 |
| 71077 | 10.08 | 1.37 |
| 71094 | 14.03 | 4.73 |

| | | |
|---|---|---|
| 71206 | 12.9 | 2.52 |
| 71316 | 10.85 | 1.41 |
| 71618 | 16.56 | 5.25 |
| 71795 | 18.07 | 22.14 |
| 72104 | 15.76 | 8.18 |
| 72293 | 10.22 | 1.43 |
| 72552 | 11.06 | 3.88 |
| 72814 | 10.08 | 1.46 |
| 72940 | 10.63 | 1.47 |
| 73049 | 13.2 | 5.9 |
| 73535 | 11.9 | 0.98 |
| 73566 | 10.04 | 4.88 |
| 73587 | 10.56 | 2.28 |
| 73608 | 10.68 | 2.51 |
| 73841 | 12.55 | 3.81 |
| 73937 | 10.44 | 2.53 |
| 73990 | 10.29 | 0.79 |
| 74000 | 13.35 | 2.99 |
| 74144 | 12.47 | 1.47 |
| 74145 | 10.92 | 1.43 |
| 74149 | 10.59 | 1.21 |
| 74488 | 12.24 | 2.47 |
| 74505 | 11.58 | 2.42 |
| 74596 | 14.4 | 6.02 |
| 74689 | 20.2 | 5.66 |
| 74875 | 12.45 | 2.81 |
| 75000 | 11.72 | 3.23 |
| 75043 | 15.32 | 4.9 |
| 75164 | 10.23 | 2.71 |
| 75678 | 12.01 | 2.1 |
| 75729 | 11.09 | 1.05 |
| 75736 | 15.54 | 3.27 |
| 75788 | 10.89 | 2.07 |
| 75848 | 11.21 | 2.11 |
| 76251 | 11.38 | 1.37 |
| 76376 | 13.24 | 3.75 |
| 76736 | 12.94 | 2.07 |
| 76866 | 14.28 | 5.54 |
| 76878 | 18.78 | 5.08 |
| 76952 | 22.48 | 22.7 |
| 76996 | 15.02 | 5.9 |
| 77060 | 22.21 | 7.9 |
| 77089 | 10.8 | 0.69 |
| 77111 | 10.16 | 2.35 |
| 77277 | 12.0 | 6.29 |
| 77336 | 12.95 | 4.7 |
| 77370 | 12.56 | 4.79 |
| 77464 | 20.34 | 5.27 |
| 77516 | 20.94 | 22.04 |
| 77532 | 12.21 | 2.12 |
| 77660 | 20.47 | 8.8 |
| 77910 | 13.54 | 3.2 |

| | | |
|---|---|---|
| 78553 | 14.93 | 2.42 |
| 78554 | 18.42 | 9.47 |
| 78583 | 10.3 | 1.21 |
| 78817 | 10.54 | 1.69 |
| 78893 | 11.92 | 4.48 |
| 79007 | 12.12 | 6.11 |
| 79036 | 10.47 | 1.87 |
| 79387 | 13.05 | 6.36 |
| 79472 | 11.21 | 1.85 |
| 79503 | 11.95 | 2.06 |
| 79781 | 21.0 | 4.87 |
| 79797 | 18.13 | 3.64 |
| 80170 | 16.69 | 44.29 |
| 80460 | 12.73 | 6.99 |
| 80939 | 12.18 | 1.04 |
| 80953 | 14.48 | 4.94 |
| 81016 | 10.97 | 1.46 |
| 81073 | 11.31 | 2.39 |
| 81248 | 10.62 | 1.11 |
| 81560 | 10.73 | 1.25 |
| 81634 | 10.73 | 1.45 |
| 81641 | 10.76 | 3.38 |
| 81840 | 11.04 | 2.65 |
| 81846 | 10.08 | 1.42 |
| 81873 | 10.7 | 2.93 |
| 81971 | 10.7 | 1.03 |
| 82312 | 10.03 | 1.1 |
| 82350 | 11.34 | 3.03 |
| 82402 | 17.3 | 5.41 |
| 82475 | 10.1 | 0.75 |
| 82779 | 11.49 | 1.41 |
| 82892 | 10.6 | 1.55 |
| 83207 | 20.04 | 18.09 |
| 83223 | 13.69 | 2.93 |
| 83313 | 11.05 | 5.71 |
| 83388 | 10.15 | 1.71 |
| 83478 | 12.38 | 2.85 |
| 83480 | 10.54 | 2.17 |
| 83494 | 18.5 | 3.83 |
| 83613 | 22.68 | 9.52 |
| 83738 | 11.38 | 3.34 |
| 83774 | 11.67 | 2.14 |
| 83853 | 12.0 | 3.29 |
| 84054 | 11.41 | 3.77 |
| 84433 | 11.28 | 1.14 |
| 84510 | 10.06 | 2.17 |
| 84606 | 18.34 | 11.19 |
| 85038 | 15.63 | 2.13 |
| 85086 | 10.09 | 3.29 |
| 85382 | 11.63 | 2.87 |
| 85463 | 10.37 | 1.26 |
| 85537 | 15.86 | 7.98 |

| | | |
|---|---|---|
| 85666 | 10.55 | 1.9 |
| 85699 | 20.88 | 5.09 |
| 85790 | 11.86 | 3.69 |
| 85822 | 17.85 | 13.2 |
| 85840 | 13.18 | 1.9 |
| 86178 | 15.07 | 3.6 |
| 86179 | 11.14 | 1.77 |
| 86254 | 13.59 | 4.86 |
| 86378 | 10.29 | 1.72 |
| 87149 | 10.02 | 1.03 |
| 87174 | 19.58 | 4.74 |
| 87212 | 15.03 | 7.48 |
| 87247 | 10.82 | 1.67 |
| 87341 | 10.25 | 4.41 |
| 87386 | 16.64 | 2.88 |
| 87486 | 11.65 | 1.52 |
| 87875 | 10.46 | 3.77 |
| 87896 | 11.02 | 1.22 |
| 87960 | 10.4 | 1.17 |
| 88290 | 12.31 | 13.51 |
| 88349 | 11.2 | 1.55 |
| 88726 | 22.79 | 11.74 |
| 88866 | 23.55 | 20.06 |
| 88899 | 10.16 | 9.5 |
| 89056 | 11.45 | 1.05 |
| 89925 | 17.36 | 6.7 |
| 89935 | 11.79 | 10.79 |
| 89936 | 14.57 | 2.39 |
| 90089 | 11.35 | 2.22 |
| 90133 | 16.59 | 4.77 |
| 90304 | 14.03 | 3.97 |
| 91752 | 10.74 | 1.24 |
| 91775 | 13.91 | 2.09 |
| 91875 | 16.15 | 7.57 |
| 92040 | 11.33 | 3.6 |
| 92112 | 10.73 | 5.51 |
| 92269 | 17.81 | 3.84 |
| 92294 | 14.45 | 6.15 |
| 92312 | 11.63 | 3.13 |
| 92598 | 10.4 | 1.34 |
| 92676 | 11.26 | 3.06 |
| 93074 | 16.21 | 3.37 |
| 93266 | 10.32 | 1.78 |
| 93542 | 17.75 | 8.37 |
| 94140 | 10.15 | 2.09 |
| 94789 | 11.0 | 6.22 |
| 95077 | 17.52 | 7.16 |
| 95081 | 14.52 | 11.07 |
| 95167 | 10.56 | 3.27 |
| 95626 | 10.49 | 0.59 |
| 95720 | 12.87 | 1.72 |
| 95823 | 17.42 | 6.06 |

| | | |
|---|---|---|
| 96286 | 10.94 | 2.44 |
| 96406 | 11.23 | 5.16 |
| 96534 | 13.04 | 1.61 |
| 96721 | 10.05 | 4.09 |
| 96739 | 11.84 | 2.45 |
| 96807 | 11.44 | 5.09 |
| 96907 | 12.0 | 3.44 |
| 97018 | 14.25 | 2.27 |
| 97086 | 10.62 | 1.12 |
| 97145 | 10.48 | 1.19 |
| 97229 | 18.48 | 4.38 |
| 97421 | 19.19 | 7.28 |
| 97423 | 16.0 | 3.44 |
| 97534 | 24.08 | 8.04 |
| 97581 | 12.27 | 1.46 |
| 97646 | 12.55 | 5.78 |
| 97871 | 11.79 | 4.25 |
| 97971 | 10.72 | 3.33 |
| 98055 | 11.3 | 10.64 |
| 98103 | 15.84 | 5.26 |
| 98111 | 11.67 | 2.88 |
| 98152 | 10.84 | 2.47 |
| 98258 | 11.18 | 7.91 |
| 98294 | 11.1 | 1.2 |
| 98382 | 11.11 | 1.69 |
| 98406 | 10.34 | 1.66 |
| 98421 | 20.81 | 7.56 |
| 98579 | 11.65 | 2.55 |
| 98633 | 10.54 | 4.24 |
| 98689 | 10.85 | 1.28 |
| 98705 | 11.47 | 1.52 |
| 99077 | 12.17 | 1.24 |
| 99149 | 10.55 | 1.87 |
| 99655 | 21.41 | 15.59 |
| 99742 | 21.24 | 8.26 |
| 99892 | 11.38 | 1.36 |
| 99994 | 13.89 | 2.31 |
| 100073 | 10.66 | 1.87 |
| 100118 | 10.16 | 1.26 |
| 100256 | 11.09 | 5.33 |
| 100305 | 10.39 | 1.23 |
| 100469 | 13.35 | 4.02 |
| 100526 | 14.44 | 2.22 |
| 100697 | 12.95 | 3.79 |
| 100787 | 16.52 | 2.31 |
| 100933 | 11.8 | 2.21 |
| 101044 | 11.77 | 3.17 |
| 101070 | 13.36 | 2.55 |
| 101093 | 24.04 | 21.69 |
| 101123 | 13.65 | 3.43 |
| 101300 | 12.33 | 3.58 |
| 101469 | 13.11 | 2.02 |

| | | |
|---|---|---|
| 101483 | 18.85 | 5.33 |
| 101558 | 14.94 | 3.27 |
| 101589 | 14.36 | 12.05 |
| 101608 | 13.9 | 3.63 |
| 101800 | 18.4 | 5.04 |
| 101808 | 19.86 | 4.24 |
| 101867 | 15.27 | 7.63 |
| 102205 | 11.89 | 1.76 |
| 102253 | 23.49 | 6.31 |
| 102281 | 16.03 | 19.57 |
| 102373 | 11.38 | 1.62 |
| 102395 | 23.71 | 50.62 |
| 102878 | 10.09 | 1.64 |
| 102959 | 10.22 | 2.06 |
| 103045 | 21.01 | 17.34 |
| 103261 | 12.59 | 3.12 |
| 103298 | 16.35 | 5.61 |
| 103460 | 17.58 | 4.25 |
| 103545 | 11.83 | 4.77 |
| 103640 | 10.21 | 2.32 |
| 103652 | 13.85 | 5.5 |
| 103752 | 12.0 | 2.54 |
| 103777 | 10.94 | 2.88 |
| 104139 | 20.61 | 15.27 |
| 104293 | 12.73 | 1.92 |
| 104296 | 10.57 | 3.2 |
| 104308 | 15.05 | 2.5 |
| 104338 | 12.07 | 2.1 |
| 104365 | 17.06 | 5.03 |
| 104771 | 11.17 | 3.55 |
| 104772 | 10.51 | 1.9 |
| 104983 | 10.28 | 1.08 |
| 105140 | 19.76 | 10.63 |
| 105331 | 10.79 | 1.1 |
| 105685 | 10.39 | 3.09 |
| 105703 | 14.84 | 8.15 |
| 105819 | 11.46 | 2.75 |
| 105860 | 21.72 | 4.18 |
| 105913 | 18.57 | 8.72 |
| 105931 | 13.8 | 1.17 |
| 105966 | 17.96 | 5.1 |
| 105984 | 10.62 | 1.45 |
| 106310 | 11.34 | 1.34 |
| 106363 | 14.42 | 2.79 |
| 106654 | 18.57 | 5.48 |
| 106703 | 13.76 | 4.13 |
| 106783 | 12.68 | 2.39 |
| 106786 | 18.26 | 13.28 |
| 106856 | 18.74 | 6.62 |
| 106985 | 23.48 | 39.62 |
| 107100 | 13.74 | 2.04 |
| 107253 | 11.97 | 3.64 |

| | | |
|---|---|---|
| 107302 | 19.08 | 4.57 |
| 107326 | 12.99 | 2.7 |
| 107334 | 10.76 | 1.92 |
| 107517 | 11.1 | 3.95 |
| 107573 | 11.01 | 1.43 |
| 107596 | 12.74 | 3.74 |
| 107763 | 10.78 | 6.25 |
| 107919 | 13.96 | 2.53 |
| 107925 | 10.01 | 0.97 |
| 107995 | 11.51 | 1.86 |
| 108060 | 14.18 | 3.73 |
| 108166 | 11.71 | 1.15 |
| 108220 | 10.34 | 1.63 |
| 108232 | 10.65 | 2.73 |
| 108294 | 10.35 | 5.72 |
| 108552 | 10.48 | 1.13 |
| 108759 | 10.48 | 3.39 |
| 108812 | 11.37 | 2.11 |
| 108991 | 14.1 | 8.14 |
| 109121 | 10.09 | 2.73 |
| 109147 | 11.08 | 1.47 |
| 109285 | 25.01 | 12.6 |
| 109306 | 12.7 | 3.44 |
| 109349 | 11.25 | 1.77 |
| 109404 | 15.35 | 8.38 |
| 109521 | 18.24 | 6.92 |
| 109667 | 17.22 | 3.39 |
| 109745 | 13.0 | 4.31 |
| 109831 | 11.67 | 3.63 |
| 109984 | 12.44 | 3.62 |
| 110166 | 10.01 | 1.59 |
| 110171 | 15.19 | 4.13 |
| 110395 | 20.67 | 16.43 |
| 110657 | 10.05 | 1.43 |
| 110658 | 10.02 | 1.28 |
| 110786 | 12.23 | 1.98 |
| 110787 | 15.98 | 4.04 |
| 110935 | 22.96 | 6.39 |
| 111056 | 13.75 | 5.39 |
| 111123 | 12.29 | 7.34 |
| 111188 | 21.99 | 13.27 |
| 111200 | 14.49 | 4.07 |
| 111314 | 13.11 | 5.5 |
| 111594 | 14.41 | 2.65 |
| 111622 | 10.48 | 0.92 |
| 111643 | 14.86 | 3.67 |
| 111659 | 11.37 | 1.85 |
| 111807 | 11.41 | 2.0 |
| 111898 | 10.15 | 2.85 |
| 112051 | 10.7 | 8.4 |
| 112346 | 11.82 | 1.1 |
| 112362 | 10.75 | 2.7 |

| | | |
|---|---|---|
| 112405 | 23.23 | 21.77 |
| 112449 | 13.51 | 2.86 |
| 112548 | 10.2 | 1.5 |
| 112904 | 10.06 | 1.02 |
| 113048 | 19.22 | 6.41 |
| 113167 | 10.61 | 3.87 |
| 113186 | 11.55 | 7.73 |
| 113195 | 11.92 | 1.38 |
| 113307 | 11.98 | 5.24 |
| 113331 | 11.76 | 2.29 |
| 113465 | 10.41 | 2.35 |
| 113542 | 10.83 | 0.51 |
| 113629 | 10.65 | 1.54 |
| 113647 | 10.54 | 1.81 |
| 113711 | 10.49 | 1.48 |
| 114132 | 11.09 | 4.38 |
| 114224 | 10.7 | 0.91 |
| 114258 | 13.44 | 3.22 |
| 114373 | 10.08 | 2.35 |
| 114428 | 10.79 | 2.02 |
| 114448 | 11.45 | 1.62 |
| 114520 | 12.89 | 8.49 |
| 114822 | 14.09 | 4.6 |
| 115115 | 13.1 | 6.89 |
| 115250 | 19.5 | 15.49 |
| 115261 | 12.5 | 3.0 |
| 115288 | 15.11 | 3.14 |
| 115678 | 10.02 | 2.55 |
| 115723 | 10.05 | 1.37 |
| 115770 | 15.81 | 5.74 |
| 116323 | 14.17 | 5.25 |
| 116354 | 13.97 | 5.14 |
| 116370 | 13.64 | 2.43 |
| 116389 | 11.92 | 10.91 |
| 116482 | 15.51 | 2.85 |
| 116510 | 11.75 | 1.8 |
| 116602 | 16.26 | 10.37 |
| 116611 | 13.65 | 4.53 |
| 116714 | 12.4 | 3.72 |
| 116758 | 24.38 | 12.22 |
| 117173 | 13.24 | 2.37 |
| 117219 | 15.32 | 3.1 |
| 117254 | 12.91 | 1.58 |
| 117452 | 22.73 | 10.26 |
| 117500 | 12.22 | 4.22 |
| 117515 | 10.3 | 1.33 |
| 117558 | 10.03 | 1.03 |
| 117569 | 10.9 | 1.54 |
| 117629 | 10.16 | 4.19 |
| 117730 | 17.31 | 8.68 |
| 117734 | 12.09 | 1.55 |
| 117797 | 10.88 | 3.49 |

| | | |
|---|---|---|
| 117990 | 12.44 | 2.78 |
| 118027 | 10.84 | 1.76 |
| 118092 | 15.91 | 3.49 |
| 118121 | 20.53 | 7.84 |
| 118256 | 11.46 | 2.03 |
| 118259 | 11.26 | 1.38 |

TableA.2: Selected A-type MS stars located at $100 < d < 158$ pc (group 3)

| Hipparcos ID | parallax [mas] | K flux [Jy] |
|---|---|---|
| 69 | 6.35 | 0.405 |
| 186 | 7.55 | 3.07 |
| 297 | 6.42 | 1.472 |
| 345 | 7.75 | 2.091 |
| 424 | 6.66 | 1.775 |
| 445 | 9.55 | 0.963 |
| 474 | 7.0 | 0.555 |
| 497 | 7.05 | 1.388 |
| 581 | 7.12 | 1.07 |
| 594 | 6.51 | 0.247 |
| 609 | 7.19 | 0.536 |
| 648 | 8.95 | 1.304 |
| 652 | 8.19 | 1.436 |
| 701 | 6.36 | 0.666 |
| 727 | 7.7 | 0.97 |
| 728 | 8.65 | 2.834 |
| 760 | 8.56 | 4.446 |
| 798 | 7.37 | 2.779 |
| 859 | 7.1 | 0.698 |
| 905 | 7.22 | 0.471 |
| 935 | 6.73 | 0.363 |
| 1043 | 8.09 | 1.388 |
| 1090 | 7.03 | 0.699 |
| 1101 | 9.78 | 1.616 |
| 1193 | 9.18 | 2.161 |
| 1215 | 7.92 | 1.962 |
| 1272 | 7.32 | 1.018 |
| 1318 | 7.65 | 1.54 |
| 1320 | 9.88 | 0.764 |
| 1333 | 7.18 | 1.27 |
| 1377 | 7.02 | 0.569 |
| 1409 | 7.31 | 0.487 |
| 1410 | 6.34 | 0.789 |
| 1413 | 8.06 | 1.047 |
| 1488 | 8.17 | 0.892 |
| 1496 | 9.28 | 1.366 |
| 1524 | 8.25 | 0.796 |
| 1677 | 7.87 | 1.733 |
| 1688 | 9.71 | 1.214 |
| 1714 | 7.25 | 0.734 |
| 1755 | 6.57 | 1.38 |
| 1777 | 7.4 | 0.844 |
| 1799 | 7.45 | 1.667 |
| 1916 | 6.46 | 0.765 |
| 1928 | 6.35 | 0.483 |
| 1979 | 7.33 | 0.472 |
| 2023 | 7.81 | 0.781 |
| 2071 | 7.58 | 0.277 |
| 2178 | 7.7 | 3.265 |

| | | |
|---|---|---|
| 2184 | 8.63 | 2.359 |
| 2228 | 6.83 | 0.747 |
| 2243 | 6.59 | 1.344 |
| 2335 | 6.94 | 0.425 |
| 2395 | 6.77 | 0.383 |
| 2406 | 6.94 | 1.034 |
| 2415 | 8.46 | 1.598 |
| 2419 | 7.21 | 0.574 |
| 2420 | 7.14 | 0.853 |
| 2431 | 7.01 | 2.057 |
| 2488 | 7.95 | 0.339 |
| 2496 | 9.86 | 1.174 |
| 2500 | 7.6 | 0.56 |
| 2539 | 9.62 | 1.921 |
| 2629 | 6.65 | 5.325 |
| 2641 | 7.93 | 1.841 |
| 2658 | 7.02 | 0.991 |
| 2701 | 8.21 | 1.758 |
| 2782 | 8.57 | 1.339 |
| 2788 | 7.21 | 0.668 |
| 2850 | 9.61 | 0.832 |
| 2936 | 8.26 | 2.008 |
| 2993 | 7.76 | 0.675 |
| 3018 | 7.53 | 0.845 |
| 3042 | 7.58 | 1.626 |
| 3064 | 9.25 | 0.849 |
| 3080 | 7.8 | 0.709 |
| 3149 | 7.33 | 0.729 |
| 3227 | 6.53 | 0.976 |
| 3240 | 8.73 | 1.564 |
| 3269 | 7.06 | 4.324 |
| 3275 | 7.04 | 0.483 |
| 3351 | 6.41 | 1.563 |
| 3459 | 9.56 | 1.598 |
| 3516 | 6.86 | 0.391 |
| 3544 | 9.28 | 5.267 |
| 3672 | 6.68 | 1.098 |
| 3805 | 7.45 | 0.985 |
| 3896 | 6.33 | 0.475 |
| 3964 | 8.66 | 2.357 |
| 4059 | 9.72 | 0.774 |
| 4089 | 7.57 | 0.828 |
| 4115 | 6.89 | 0.526 |
| 4160 | 8.94 | 1.088 |
| 4267 | 8.88 | 3.203 |
| 4296 | 6.54 | 0.677 |
| 4390 | 6.41 | 1.443 |
| 4442 | 7.38 | 1.121 |
| 4470 | 7.65 | 0.777 |
| 4496 | 7.64 | 1.395 |
| 4519 | 6.64 | 0.863 |
| 4555 | 6.86 | 1.328 |

| | | |
|---|---|---|
| 4558 | 7.62 | 2.21 |
| 4630 | 8.93 | 0.894 |
| 4695 | 7.8 | 0.774 |
| 4710 | 6.74 | 1.181 |
| 4863 | 6.85 | 0.857 |
| 4903 | 9.49 | 3.868 |
| 4911 | 9.68 | 3.179 |
| 4978 | 6.93 | 1.099 |
| 5035 | 7.56 | 0.455 |
| 5174 | 6.53 | 0.296 |
| 5188 | 6.94 | 0.885 |
| 5216 | 8.94 | 1.214 |
| 5233 | 8.91 | 2.041 |
| 5252 | 7.05 | 0.714 |
| 5425 | 6.39 | 1.022 |
| 5429 | 6.49 | 0.777 |
| 5442 | 8.3 | 0.99 |
| 5595 | 6.54 | 0.583 |
| 5615 | 6.49 | 0.31 |
| 5702 | 8.51 | 0.784 |
| 5886 | 7.47 | 1.843 |
| 5907 | 9.94 | 1.91 |
| 5991 | 7.34 | 0.486 |
| 5992 | 9.69 | 2.511 |
| 6048 | 9.75 | 2.828 |
| 6076 | 8.32 | 1.244 |
| 6082 | 6.34 | 1.034 |
| 6096 | 7.11 | 1.339 |
| 6256 | 9.78 | 1.488 |
| 6302 | 9.02 | 1.341 |
| 6349 | 8.28 | 0.745 |
| 6393 | 7.29 | 2.507 |
| 6513 | 6.47 | 0.608 |
| 6533 | 7.87 | 0.389 |
| 6606 | 9.15 | 1.235 |
| 6648 | 8.09 | 0.49 |
| 6663 | 6.45 | 0.597 |
| 6685 | 6.34 | 2.124 |
| 6850 | 6.81 | 0.891 |
| 6966 | 7.07 | 1.622 |
| 6981 | 8.61 | 4.149 |
| 7003 | 6.65 | 0.342 |
| 7004 | 7.11 | 0.591 |
| 7051 | 7.72 | 0.587 |
| 7125 | 7.04 | 1.084 |
| 7148 | 9.61 | 1.912 |
| 7160 | 7.44 | 0.679 |
| 7222 | 8.06 | 1.395 |
| 7331 | 7.55 | 0.65 |
| 7382 | 6.93 | 1.011 |
| 7383 | 7.61 | 0.707 |
| 7462 | 7.18 | 0.613 |

| | | |
|---|---|---|
| 7552 | 6.4 | 0.656 |
| 7644 | 7.27 | 0.669 |
| 7724 | 9.4 | 1.203 |
| 7911 | 7.04 | 2.106 |
| 7957 | 7.97 | 1.051 |
| 7965 | 7.34 | 3.525 |
| 8009 | 7.42 | 0.902 |
| 8138 | 7.29 | 1.392 |
| 8168 | 9.2 | 1.115 |
| 8211 | 7.85 | 1.432 |
| 8466 | 6.66 | 0.549 |
| 8531 | 6.93 | 0.454 |
| 8754 | 6.4 | 0.847 |
| 8756 | 6.55 | 0.626 |
| 8784 | 7.01 | 0.693 |
| 8866 | 6.62 | 2.187 |
| 8877 | 7.28 | 0.629 |
| 8986 | 7.65 | 2.13 |
| 9075 | 9.31 | 0.805 |
| 9112 | 6.54 | 2.04 |
| 9154 | 6.56 | 0.705 |
| 9165 | 6.64 | 2.491 |
| 9166 | 6.39 | 0.919 |
| 9190 | 6.42 | 0.56 |
| 9285 | 7.36 | 1.339 |
| 9521 | 7.22 | 2.502 |
| 9570 | 8.81 | 4.897 |
| 9587 | 7.48 | 0.321 |
| 9690 | 9.78 | 1.589 |
| 9800 | 7.41 | 2.348 |
| 9881 | 6.97 | 0.73 |
| 9925 | 7.5 | 0.491 |
| 9955 | 9.43 | 1.589 |
| 10167 | 8.05 | 1.433 |
| 10194 | 7.68 | 1.596 |
| 10205 | 6.44 | 0.624 |
| 10220 | 6.76 | 2.79 |
| 10242 | 8.58 | 2.322 |
| 10253 | 6.71 | 0.302 |
| 10285 | 7.83 | 1.604 |
| 10309 | 7.95 | 2.989 |
| 10320 | 9.82 | 5.515 |
| 10355 | 9.79 | 1.04 |
| 10415 | 6.37 | 0.596 |
| 10432 | 8.35 | 0.687 |
| 10512 | 6.39 | 1.757 |
| 10549 | 7.44 | 0.377 |
| 10554 | 6.71 | 0.975 |
| 10730 | 6.68 | 1.01 |
| 10731 | 8.32 | 1.083 |
| 10732 | 8.42 | 4.655 |
| 10740 | 8.36 | 0.624 |

| | | |
|---|---|---|
| 10793 | 9.31 | 5.775 |
| 10795 | 9.51 | 4.118 |
| 10814 | 7.22 | 3.544 |
| 10862 | 6.82 | 1.252 |
| 11075 | 9.34 | 1.907 |
| 11109 | 7.01 | 0.424 |
| 11112 | 6.97 | 1.108 |
| 11133 | 7.42 | 1.009 |
| 11145 | 6.36 | 0.647 |
| 11165 | 8.26 | 0.708 |
| 11256 | 6.91 | 1.305 |
| 11339 | 8.0 | 1.101 |
| 11397 | 8.61 | 0.687 |
| 11436 | 6.95 | 0.437 |
| 11456 | 6.69 | 0.605 |
| 11479 | 8.47 | 1.818 |
| 11525 | 7.05 | 0.324 |
| 11554 | 6.48 | 0.482 |
| 11635 | 7.17 | 0.469 |
| 11642 | 7.8 | 0.643 |
| 11643 | 8.51 | 1.017 |
| 11664 | 8.34 | 0.666 |
| 11690 | 8.46 | 0.667 |
| 11719 | 8.72 | 1.546 |
| 11744 | 8.46 | 1.31 |
| 11808 | 6.77 | 0.423 |
| 11959 | 7.54 | 1.015 |
| 11971 | 7.9 | 1.051 |
| 11980 | 6.49 | 0.621 |
| 12036 | 7.04 | 0.691 |
| 12113 | 9.04 | 2.204 |
| 12164 | 6.47 | 0.521 |
| 12229 | 9.6 | 0.986 |
| 12276 | 6.84 | 0.882 |
| 12332 | 9.41 | 6.917 |
| 12333 | 8.97 | 0.643 |
| 12441 | 7.6 | 1.024 |
| 12452 | 6.54 | 0.826 |
| 12571 | 7.57 | 0.486 |
| 12630 | 7.83 | 1.455 |
| 12640 | 9.64 | 3.429 |
| 12647 | 7.66 | 2.361 |
| 12733 | 7.29 | 0.77 |
| 12744 | 9.27 | 2.34 |
| 12775 | 8.06 | 2.973 |
| 12786 | 9.34 | 2.432 |
| 12821 | 8.02 | 3.677 |
| 12858 | 9.47 | 1.034 |
| 12899 | 6.42 | 0.9 |
| 12901 | 6.77 | 0.705 |
| 12937 | 7.09 | 1.062 |
| 12952 | 6.47 | 0.61 |

| | | |
|---|---|---|
| 12959 | 9.92 | 1.412 |
| 12975 | 6.81 | 0.81 |
| 13063 | 8.39 | 1.498 |
| 13073 | 8.17 | 0.562 |
| 13121 | 7.08 | 2.886 |
| 13174 | 6.91 | 0.771 |
| 13175 | 8.74 | 1.38 |
| 13233 | 7.12 | 1.177 |
| 13259 | 7.01 | 0.643 |
| 13272 | 8.86 | 1.129 |
| 13304 | 6.96 | 0.565 |
| 13409 | 6.56 | 1.034 |
| 13413 | 7.0 | 0.861 |
| 13414 | 7.74 | 2.337 |
| 13421 | 9.94 | 3.05 |
| 13422 | 6.39 | 0.356 |
| 13488 | 6.86 | 0.615 |
| 13526 | 7.97 | 0.853 |
| 13545 | 6.5 | 1.03 |
| 13675 | 7.89 | 1.178 |
| 13682 | 7.98 | 0.557 |
| 13723 | 6.66 | 0.45 |
| 13742 | 6.85 | 0.615 |
| 13789 | 9.01 | 1.725 |
| 13821 | 7.74 | 0.949 |
| 13872 | 8.82 | 0.729 |
| 13947 | 7.9 | 2.089 |
| 14021 | 7.79 | 1.598 |
| 14051 | 7.18 | 0.875 |
| 14266 | 6.98 | 0.83 |
| 14312 | 6.45 | 0.333 |
| 14363 | 7.61 | 0.973 |
| 14375 | 7.37 | 0.473 |
| 14378 | 7.78 | 1.085 |
| 14385 | 6.55 | 0.747 |
| 14408 | 6.87 | 0.999 |
| 14557 | 7.47 | 1.53 |
| 14567 | 6.97 | 0.763 |
| 14643 | 6.95 | 0.77 |
| 14661 | 6.72 | 0.48 |
| 14664 | 6.77 | 0.497 |
| 14712 | 8.54 | 0.932 |
| 14758 | 7.85 | 1.512 |
| 14773 | 8.08 | 1.487 |
| 14790 | 8.11 | 1.647 |
| 14811 | 8.73 | 0.881 |
| 14867 | 7.66 | 0.609 |
| 14910 | 7.68 | 1.143 |
| 14956 | 6.77 | 0.601 |
| 15021 | 9.77 | 1.094 |
| 15064 | 7.46 | 1.083 |
| 15130 | 8.78 | 0.774 |

| | | |
|---|---|---|
| 15154 | 7.52 | 4.273 |
| 15177 | 6.37 | 0.894 |
| 15193 | 7.9 | 2.452 |
| 15232 | 6.91 | 1.574 |
| 15277 | 7.23 | 0.751 |
| 15327 | 7.65 | 1.015 |
| 15365 | 8.12 | 0.76 |
| 15373 | 8.49 | 0.521 |
| 15392 | 7.78 | 0.537 |
| 15399 | 8.19 | 1.44 |
| 15400 | 7.19 | 0.812 |
| 15445 | 9.39 | 1.099 |
| 15659 | 6.93 | 0.402 |
| 15684 | 6.41 | 0.383 |
| 15697 | 8.13 | 1.179 |
| 15700 | 7.25 | 2.002 |
| 15882 | 7.74 | 1.561 |
| 15883 | 8.39 | 1.791 |
| 15884 | 7.49 | 1.793 |
| 15933 | 9.6 | 1.195 |
| 15978 | 6.68 | 0.785 |
| 16015 | 7.39 | 2.195 |
| 16077 | 7.78 | 2.589 |
| 16081 | 6.7 | 0.453 |
| 16086 | 8.62 | 0.932 |
| 16124 | 7.75 | 1.094 |
| 16156 | 9.01 | 2.083 |
| 16168 | 9.51 | 4.021 |
| 16201 | 6.59 | 0.83 |
| 16253 | 6.56 | 1.054 |
| 16263 | 7.76 | 6.503 |
| 16289 | 9.49 | 1.246 |
| 16300 | 6.63 | 0.911 |
| 16339 | 8.81 | 4.107 |
| 16384 | 6.5 | 0.41 |
| 16394 | 6.74 | 1.296 |
| 16403 | 6.78 | 0.388 |
| 16407 | 7.62 | 0.694 |
| 16424 | 6.97 | 2.684 |
| 16425 | 7.48 | 2.981 |
| 16444 | 7.45 | 0.866 |
| 16564 | 6.82 | 0.432 |
| 16596 | 7.06 | 1.35 |
| 16661 | 9.13 | 2.12 |
| 16682 | 8.54 | 1.576 |
| 16704 | 7.74 | 0.578 |
| 16795 | 9.1 | 0.943 |
| 16859 | 7.46 | 1.794 |
| 16868 | 7.02 | 1.039 |
| 16876 | 7.26 | 0.901 |
| 16961 | 8.17 | 1.175 |
| 16972 | 6.88 | 1.355 |

| | | |
|---|---|---|
| 17000 | 7.88 | 1.429 |
| 17007 | 7.81 | 2.635 |
| 17026 | 6.6 | 2.425 |
| 17034 | 6.87 | 1.026 |
| 17081 | 6.91 | 0.676 |
| 17101 | 9.1 | 1.464 |
| 17142 | 9.52 | 1.266 |
| 17223 | 7.74 | 2.026 |
| 17227 | 9.7 | 0.899 |
| 17256 | 9.02 | 1.754 |
| 17273 | 7.51 | 0.669 |
| 17333 | 6.99 | 0.633 |
| 17337 | 7.07 | 1.819 |
| 17388 | 8.57 | 1.068 |
| 17428 | 7.81 | 0.756 |
| 17547 | 8.27 | 0.979 |
| 17549 | 7.33 | 1.134 |
| 17577 | 6.35 | 0.728 |
| 17618 | 9.9 | 3.966 |
| 17658 | 7.65 | 0.728 |
| 17694 | 9.87 | 0.655 |
| 17720 | 7.65 | 1.217 |
| 17729 | 7.61 | 0.551 |
| 17744 | 9.25 | 1.855 |
| 17872 | 6.43 | 1.186 |
| 17999 | 9.83 | 1.556 |
| 18026 | 6.44 | 0.366 |
| 18037 | 6.32 | 0.336 |
| 18066 | 6.56 | 2.669 |
| 18070 | 7.39 | 1.111 |
| 18072 | 8.16 | 0.577 |
| 18094 | 7.93 | 3.664 |
| 18109 | 9.3 | 2.025 |
| 18120 | 6.79 | 0.35 |
| 18146 | 8.77 | 0.806 |
| 18194 | 7.29 | 0.819 |
| 18201 | 6.82 | 2.852 |
| 18233 | 8.04 | 0.915 |
| 18254 | 6.93 | 1.543 |
| 18275 | 9.33 | 2.618 |
| 18297 | 8.98 | 0.888 |
| 18431 | 8.66 | 0.566 |
| 18437 | 9.66 | 1.201 |
| 18499 | 9.46 | 1.429 |
| 18507 | 8.26 | 0.84 |
| 18549 | 7.28 | 0.376 |
| 18602 | 7.49 | 1.301 |
| 18640 | 7.54 | 0.587 |
| 18650 | 6.91 | 0.934 |
| 18689 | 7.39 | 0.86 |
| 18715 | 7.2 | 0.477 |
| 18723 | 9.09 | 3.191 |

| | | |
|---|---|---|
| 18729 | 9.86 | 1.928 |
| 18731 | 6.56 | 1.259 |
| 18756 | 7.06 | 0.815 |
| 18760 | 7.23 | 0.321 |
| 18777 | 7.0 | 1.026 |
| 18804 | 6.8 | 0.425 |
| 18863 | 7.44 | 1.208 |
| 18868 | 7.33 | 0.562 |
| 18905 | 7.39 | 0.282 |
| 18950 | 7.53 | 2.47 |
| 18956 | 7.32 | 1.814 |
| 18959 | 7.63 | 0.878 |
| 18969 | 7.45 | 0.893 |
| 18979 | 7.23 | 0.834 |
| 19047 | 6.57 | 1.043 |
| 19049 | 7.36 | 0.972 |
| 19086 | 7.17 | 0.667 |
| 19106 | 6.98 | 0.367 |
| 19177 | 7.13 | 3.238 |
| 19202 | 7.18 | 2.472 |
| 19241 | 6.6 | 0.519 |
| 19249 | 7.6 | 1.533 |
| 19305 | 7.68 | 1.235 |
| 19306 | 7.46 | 0.959 |
| 19317 | 8.7 | 0.575 |
| 19366 | 6.65 | 1.298 |
| 19399 | 6.46 | 1.416 |
| 19436 | 8.13 | 1.241 |
| 19440 | 6.78 | 1.415 |
| 19608 | 7.4 | 0.647 |
| 19704 | 8.73 | 2.255 |
| 19726 | 7.48 | 1.275 |
| 19760 | 6.87 | 0.715 |
| 19761 | 8.04 | 0.617 |
| 19824 | 7.21 | 0.775 |
| 19830 | 8.65 | 0.863 |
| 19831 | 6.93 | 0.703 |
| 19839 | 6.73 | 0.585 |
| 19857 | 8.03 | 1.221 |
| 19867 | 9.42 | 0.933 |
| 19878 | 9.41 | 1.686 |
| 19881 | 9.82 | 1.241 |
| 19917 | 8.41 | 2.278 |
| 19923 | 7.26 | 1.439 |
| 19972 | 9.42 | 0.725 |
| 20004 | 6.94 | 1.541 |
| 20046 | 7.55 | 1.323 |
| 20072 | 7.68 | 1.121 |
| 20096 | 6.37 | 1.173 |
| 20117 | 8.56 | 1.145 |
| 20121 | 6.39 | 0.338 |
| 20153 | 7.44 | 0.499 |

| | | |
|---|---|---|
| 20173 | 8.27 | 0.928 |
| 20190 | 8.06 | 0.775 |
| 20289 | 6.81 | 0.901 |
| 20300 | 8.82 | 1.158 |
| 20306 | 6.58 | 0.82 |
| 20309 | 8.59 | 1.086 |
| 20315 | 6.48 | 0.756 |
| 20328 | 7.27 | 0.442 |
| 20358 | 7.78 | 0.703 |
| 20360 | 6.54 | 2.179 |
| 20405 | 7.31 | 0.514 |
| 20409 | 6.64 | 0.467 |
| 20456 | 8.62 | 3.206 |
| 20474 | 6.71 | 1.505 |
| 20510 | 6.94 | 0.494 |
| 20515 | 7.21 | 0.481 |
| 20521 | 9.69 | 0.822 |
| 20543 | 7.58 | 0.77 |
| 20603 | 6.32 | 0.924 |
| 20735 | 8.2 | 1.576 |
| 20765 | 9.0 | 3.354 |
| 20784 | 7.26 | 1.189 |
| 20799 | 8.17 | 0.807 |
| 20845 | 9.35 | 1.215 |
| 20957 | 8.12 | 1.153 |
| 20980 | 7.46 | 0.759 |
| 21020 | 7.5 | 0.796 |
| 21024 | 6.46 | 0.865 |
| 21032 | 7.06 | 2.025 |
| 21049 | 7.02 | 0.455 |
| 21050 | 6.32 | 0.452 |
| 21061 | 6.37 | 0.555 |
| 21087 | 7.93 | 0.876 |
| 21106 | 8.47 | 1.706 |
| 21110 | 8.16 | 2.563 |
| 21161 | 8.18 | 0.792 |
| 21193 | 7.14 | 0.768 |
| 21213 | 7.45 | 0.998 |
| 21219 | 7.51 | 1.706 |
| 21247 | 8.74 | 5.071 |
| 21266 | 6.39 | 0.707 |
| 21285 | 7.43 | 0.428 |
| 21295 | 7.99 | 4.273 |
| 21315 | 6.77 | 1.814 |
| 21316 | 7.57 | 0.364 |
| 21330 | 8.42 | 0.446 |
| 21370 | 6.99 | 0.379 |
| 21376 | 7.56 | 0.524 |
| 21419 | 6.57 | 0.291 |
| 21452 | 7.36 | 2.924 |
| 21485 | 6.96 | 0.754 |
| 21486 | 8.28 | 1.744 |

| | | |
|---|---|---|
| 21560 | 7.67 | 0.464 |
| 21634 | 6.84 | 2.118 |
| 21653 | 7.43 | 0.867 |
| 21657 | 9.14 | 1.022 |
| 21775 | 8.31 | 0.59 |
| 21787 | 8.59 | 1.116 |
| 21957 | 6.56 | 1.022 |
| 22057 | 6.52 | 0.366 |
| 22093 | 6.55 | 1.533 |
| 22114 | 7.68 | 0.667 |
| 22163 | 8.3 | 0.748 |
| 22372 | 9.39 | 0.879 |
| 22476 | 8.4 | 1.202 |
| 22520 | 7.76 | 1.682 |
| 22590 | 6.89 | 0.881 |
| 22605 | 6.39 | 0.432 |
| 22640 | 6.49 | 0.632 |
| 22652 | 7.23 | 0.854 |
| 22709 | 8.33 | 0.794 |
| 22722 | 7.33 | 0.924 |
| 22818 | 7.83 | 0.672 |
| 22842 | 9.59 | 2.405 |
| 22923 | 6.66 | 1.808 |
| 22927 | 7.2 | 0.579 |
| 22936 | 6.82 | 4.483 |
| 22941 | 6.73 | 1.006 |
| 22984 | 6.34 | 1.168 |
| 23011 | 6.33 | 2.477 |
| 23012 | 8.43 | 0.667 |
| 23014 | 7.9 | 0.931 |
| 23024 | 6.55 | 0.462 |
| 23028 | 8.4 | 1.059 |
| 23090 | 7.36 | 1.767 |
| 23092 | 7.18 | 2.579 |
| 23129 | 6.73 | 1.274 |
| 23169 | 6.79 | 0.39 |
| 23192 | 6.74 | 1.077 |
| 23239 | 7.59 | 0.868 |
| 23262 | 6.31 | 0.431 |
| 23386 | 6.57 | 0.401 |
| 23451 | 8.92 | 0.611 |
| 23737 | 7.7 | 2.179 |
| 23746 | 6.31 | 0.3 |
| 23778 | 8.78 | 0.9 |
| 23891 | 6.49 | 0.732 |
| 23899 | 6.95 | 1.127 |
| 23901 | 9.21 | 1.325 |
| 23964 | 9.37 | 2.625 |
| 24036 | 6.65 | 0.903 |
| 24057 | 6.84 | 0.615 |
| 24106 | 8.85 | 0.999 |
| 24152 | 7.97 | 0.728 |

| | | |
|---|---|---|
| 24311 | 6.31 | 0.583 |
| 24313 | 6.83 | 2.47 |
| 24401 | 7.09 | 1.115 |
| 24404 | 9.16 | 1.223 |
| 24440 | 7.75 | 2.051 |
| 24483 | 7.32 | 1.074 |
| 24507 | 9.09 | 2.394 |
| 24519 | 7.94 | 0.479 |
| 24530 | 6.71 | 0.6 |
| 24532 | 8.21 | 1.93 |
| 24576 | 7.31 | 0.638 |
| 24592 | 7.26 | 0.813 |
| 24599 | 8.81 | 1.418 |
| 24732 | 9.09 | 2.918 |
| 24741 | 6.63 | 0.699 |
| 24746 | 7.11 | 1.024 |
| 24831 | 7.31 | 2.596 |
| 24946 | 7.04 | 0.392 |
| 24961 | 6.37 | 0.841 |
| 24967 | 9.03 | 2.514 |
| 25010 | 8.41 | 1.344 |
| 25026 | 6.75 | 0.647 |
| 25058 | 7.25 | 1.238 |
| 25095 | 8.21 | 0.54 |
| 25136 | 7.65 | 1.889 |
| 25172 | 7.35 | 1.059 |
| 25197 | 9.59 | 5.764 |
| 25227 | 7.3 | 0.701 |
| 25259 | 7.98 | 1.141 |
| 25271 | 7.06 | 0.891 |
| 25298 | 6.75 | 1.706 |
| 25406 | 7.64 | 0.91 |
| 25437 | 8.85 | 1.142 |
| 25543 | 8.09 | 1.27 |
| 25602 | 7.25 | 0.741 |
| 25645 | 9.63 | 1.385 |
| 25727 | 8.06 | 1.437 |
| 25748 | 6.39 | 1.483 |
| 25776 | 9.35 | 2.383 |
| 25907 | 6.99 | 0.64 |
| 25933 | 7.16 | 0.753 |
| 25998 | 9.4 | 0.775 |
| 26107 | 6.66 | 0.72 |
| 26126 | 9.45 | 6.222 |
| 26146 | 8.35 | 0.709 |
| 26164 | 6.88 | 1.187 |
| 26195 | 6.51 | 0.606 |
| 26408 | 8.77 | 2.589 |
| 26429 | 7.05 | 0.84 |
| 26454 | 6.32 | 0.977 |
| 26555 | 9.42 | 0.415 |
| 26805 | 7.15 | 0.913 |

| | | |
|---|---|---|
| 26831 | 8.92 | 1.226 |
| 26873 | 8.29 | 0.814 |
| 26895 | 6.57 | 0.284 |
| 26896 | 6.65 | 0.68 |
| 27015 | 6.9 | 1.506 |
| 27076 | 8.45 | 1.368 |
| 27121 | 6.86 | 1.428 |
| 27294 | 7.96 | 0.663 |
| 27462 | 7.3 | 1.129 |
| 27472 | 7.91 | 3.07 |
| 27577 | 6.79 | 0.509 |
| 27592 | 7.4 | 2.151 |
| 27598 | 7.37 | 0.841 |
| 27599 | 6.96 | 0.683 |
| 27674 | 7.9 | 0.849 |
| 27698 | 9.95 | 1.235 |
| 27701 | 8.33 | 1.429 |
| 27792 | 7.71 | 0.943 |
| 27822 | 6.58 | 1.468 |
| 27873 | 6.68 | 1.305 |
| 27942 | 6.97 | 1.063 |
| 28013 | 9.75 | 0.68 |
| 28043 | 6.42 | 1.56 |
| 28071 | 6.79 | 0.474 |
| 28078 | 8.16 | 0.95 |
| 28081 | 9.96 | 1.475 |
| 28096 | 6.85 | 0.807 |
| 28248 | 6.52 | 1.057 |
| 28325 | 9.93 | 9.426 |
| 28350 | 6.58 | 0.738 |
| 28385 | 9.54 | 3.65 |
| 28397 | 6.55 | 0.619 |
| 28464 | 9.87 | 1.398 |
| 28520 | 8.99 | 2.841 |
| 28523 | 6.79 | 2.739 |
| 28542 | 6.62 | 0.879 |
| 28601 | 6.68 | 0.608 |
| 28686 | 6.79 | 2.448 |
| 28758 | 7.05 | 0.382 |
| 28765 | 8.28 | 2.834 |
| 28836 | 7.75 | 0.802 |
| 28946 | 8.57 | 8.347 |
| 28971 | 7.17 | 0.961 |
| 28989 | 8.89 | 0.883 |
| 29152 | 6.45 | 0.505 |
| 29175 | 7.07 | 0.615 |
| 29307 | 7.48 | 0.797 |
| 29363 | 6.73 | 0.874 |
| 29365 | 7.36 | 1.91 |
| 29370 | 7.67 | 0.846 |
| 29375 | 8.18 | 1.123 |
| 29404 | 9.97 | 2.652 |

| | | |
|---|---|---|
| 29455 | 6.47 | 0.549 |
| 29471 | 7.15 | 0.49 |
| 29487 | 6.88 | 1.706 |
| 29507 | 7.12 | 0.862 |
| 29527 | 6.78 | 0.627 |
| 29561 | 9.17 | 1.431 |
| 29590 | 7.86 | 0.917 |
| 29606 | 9.52 | 0.798 |
| 29633 | 7.34 | 0.627 |
| 29658 | 9.55 | 1.163 |
| 29671 | 9.04 | 0.858 |
| 29684 | 8.3 | 0.849 |
| 29699 | 6.71 | 2.066 |
| 29808 | 8.35 | 3.617 |
| 29816 | 6.6 | 0.779 |
| 29848 | 7.93 | 0.903 |
| 29851 | 9.34 | 1.049 |
| 29859 | 6.68 | 1.048 |
| 29965 | 6.58 | 0.553 |
| 29975 | 8.67 | 1.217 |
| 29998 | 6.8 | 0.8 |
| 30007 | 6.76 | 0.606 |
| 30105 | 8.67 | 2.253 |
| 30119 | 8.35 | 1.728 |
| 30121 | 7.0 | 0.684 |
| 30173 | 6.84 | 1.013 |
| 30194 | 8.1 | 0.541 |
| 30217 | 9.76 | 3.554 |
| 30265 | 6.9 | 0.662 |
| 30328 | 8.72 | 1.509 |
| 30372 | 7.37 | 1.324 |
| 30387 | 8.37 | 1.706 |
| 30491 | 6.45 | 1.169 |
| 30596 | 7.41 | 0.252 |
| 30602 | 7.18 | 2.177 |
| 30617 | 6.61 | 0.608 |
| 30675 | 7.97 | 1.754 |
| 30727 | 6.48 | 0.891 |
| 30797 | 6.35 | 0.426 |
| 30929 | 7.94 | 0.851 |
| 30933 | 6.64 | 0.744 |
| 31074 | 7.25 | 0.976 |
| 31150 | 9.86 | 1.379 |
| 31186 | 9.99 | 1.195 |
| 31194 | 8.29 | 0.767 |
| 31206 | 7.45 | 0.728 |
| 31282 | 6.8 | 0.57 |
| 31290 | 7.35 | 1.951 |
| 31316 | 9.06 | 1.969 |
| 31320 | 8.01 | 0.678 |
| 31323 | 8.83 | 1.527 |
| 31325 | 7.98 | 1.662 |

| | | |
|---|---|---|
| 31355 | 8.64 | 0.868 |
| 31357 | 6.36 | 0.638 |
| 31479 | 8.85 | 0.753 |
| 31519 | 8.23 | 1.041 |
| 31531 | 8.76 | 1.523 |
| 31614 | 8.73 | 0.605 |
| 31673 | 7.21 | 1.07 |
| 31710 | 8.7 | 0.644 |
| 31741 | 6.44 | 0.373 |
| 31758 | 7.08 | 3.11 |
| 31871 | 7.8 | 1.088 |
| 31897 | 8.07 | 7.065 |
| 31904 | 6.75 | 0.77 |
| 31922 | 8.73 | 1.656 |
| 31944 | 9.41 | 2.171 |
| 31948 | 9.58 | 1.112 |
| 32029 | 8.93 | 0.602 |
| 32055 | 6.52 | 1.579 |
| 32061 | 9.19 | 1.246 |
| 32278 | 7.26 | 0.288 |
| 32295 | 6.53 | 1.071 |
| 32361 | 6.97 | 0.445 |
| 32379 | 7.87 | 0.856 |
| 32411 | 8.19 | 6.485 |
| 32453 | 7.01 | 0.513 |
| 32466 | 8.68 | 1.833 |
| 32493 | 8.18 | 0.814 |
| 32532 | 6.56 | 1.015 |
| 32539 | 7.56 | 2.247 |
| 32579 | 9.56 | 1.125 |
| 32615 | 7.2 | 1.074 |
| 32619 | 6.84 | 0.591 |
| 32629 | 6.72 | 0.517 |
| 32632 | 9.35 | 1.0 |
| 32643 | 7.33 | 0.609 |
| 32689 | 7.69 | 2.023 |
| 32691 | 7.75 | 0.778 |
| 32697 | 9.3 | 2.085 |
| 32793 | 9.94 | 2.686 |
| 32838 | 9.89 | 2.146 |
| 32884 | 6.98 | 1.065 |
| 32903 | 7.62 | 0.415 |
| 32905 | 6.66 | 0.717 |
| 32959 | 8.22 | 0.841 |
| 32964 | 7.18 | 1.919 |
| 32992 | 6.79 | 0.425 |
| 33012 | 6.94 | 2.635 |
| 33054 | 6.63 | 1.381 |
| 33056 | 9.08 | 3.742 |
| 33075 | 6.71 | 0.504 |
| 33077 | 9.9 | 7.091 |
| 33079 | 7.12 | 3.348 |

| | | |
|---|---|---|
| 33126 | 6.91 | 2.344 |
| 33186 | 6.6 | 0.714 |
| 33218 | 7.6 | 1.035 |
| 33245 | 6.63 | 0.543 |
| 33297 | 9.74 | 2.353 |
| 33326 | 8.66 | 0.994 |
| 33360 | 7.95 | 1.096 |
| 33476 | 8.5 | 1.319 |
| 33502 | 8.1 | 1.053 |
| 33525 | 8.54 | 1.348 |
| 33574 | 7.05 | 1.576 |
| 33590 | 7.68 | 2.257 |
| 33609 | 7.13 | 0.818 |
| 33679 | 6.81 | 0.459 |
| 33784 | 6.62 | 1.098 |
| 33812 | 6.34 | 1.39 |
| 33823 | 7.64 | 3.15 |
| 33893 | 6.71 | 1.355 |
| 33909 | 7.99 | 1.659 |
| 33921 | 9.21 | 1.31 |
| 33984 | 9.71 | 1.335 |
| 34016 | 6.95 | 1.102 |
| 34246 | 7.03 | 0.819 |
| 34264 | 6.35 | 1.047 |
| 34439 | 6.65 | 1.192 |
| 34570 | 8.15 | 0.584 |
| 34621 | 8.99 | 1.432 |
| 34643 | 8.86 | 0.762 |
| 34657 | 7.61 | 0.85 |
| 34721 | 9.72 | 1.553 |
| 34722 | 8.36 | 4.759 |
| 34806 | 8.01 | 0.761 |
| 34881 | 6.54 | 1.356 |
| 35029 | 7.67 | 2.772 |
| 35095 | 7.18 | 2.542 |
| 35183 | 6.62 | 0.584 |
| 35194 | 8.33 | 0.762 |
| 35241 | 6.78 | 3.098 |
| 35244 | 7.63 | 1.22 |
| 35277 | 7.35 | 0.68 |
| 35400 | 6.38 | 0.399 |
| 35498 | 8.22 | 0.779 |
| 35540 | 6.53 | 0.607 |
| 35603 | 7.29 | 1.741 |
| 35610 | 8.99 | 1.641 |
| 35624 | 8.01 | 0.362 |
| 35676 | 6.51 | 0.981 |
| 35690 | 7.06 | 1.118 |
| 35770 | 9.59 | 0.909 |
| 35787 | 6.61 | 0.658 |
| 35866 | 9.35 | 1.329 |
| 35894 | 8.26 | 0.91 |

| | | |
|---|---|---|
| 35953 | 7.05 | 0.926 |
| 35995 | 6.85 | 1.486 |
| 36087 | 7.66 | 1.067 |
| 36130 | 6.44 | 1.335 |
| 36281 | 8.8 | 1.557 |
| 36304 | 9.43 | 2.072 |
| 36305 | 8.83 | 1.12 |
| 36331 | 6.98 | 0.805 |
| 36371 | 9.61 | 2.719 |
| 36381 | 9.84 | 1.286 |
| 36384 | 8.66 | 1.006 |
| 36489 | 8.55 | 1.54 |
| 36506 | 6.99 | 1.168 |
| 36536 | 9.36 | 2.01 |
| 36595 | 6.47 | 1.249 |
| 36636 | 7.78 | 1.346 |
| 36687 | 6.4 | 1.132 |
| 36760 | 8.69 | 6.698 |
| 36780 | 7.46 | 2.782 |
| 36796 | 7.76 | 2.269 |
| 36811 | 9.08 | 0.9 |
| 36837 | 9.65 | 1.452 |
| 36869 | 6.98 | 2.897 |
| 36919 | 9.39 | 1.718 |
| 37004 | 9.27 | 1.038 |
| 37009 | 8.02 | 0.869 |
| 37056 | 7.68 | 0.571 |
| 37111 | 7.98 | 1.163 |
| 37116 | 7.8 | 0.76 |
| 37264 | 6.88 | 0.677 |
| 37269 | 7.5 | 2.463 |
| 37365 | 8.19 | 1.169 |
| 37371 | 9.94 | 1.01 |
| 37478 | 6.47 | 2.862 |
| 37593 | 8.42 | 1.11 |
| 37611 | 9.14 | 1.675 |
| 37679 | 7.02 | 0.768 |
| 37720 | 8.09 | 2.167 |
| 37811 | 7.08 | 1.676 |
| 37817 | 9.44 | 1.275 |
| 37861 | 7.31 | 0.749 |
| 37940 | 6.33 | 0.88 |
| 37980 | 8.16 | 0.99 |
| 38098 | 8.99 | 0.849 |
| 38199 | 8.02 | 0.449 |
| 38249 | 8.22 | 1.776 |
| 38274 | 8.0 | 1.46 |
| 38299 | 7.47 | 1.004 |
| 38403 | 9.6 | 2.601 |
| 38410 | 8.68 | 1.896 |
| 38578 | 7.15 | 1.294 |
| 38626 | 8.4 | 0.618 |

| | | |
|---|---|---|
| 38722 | 9.61 | 4.711 |
| 38885 | 7.57 | 0.959 |
| 38891 | 8.61 | 1.59 |
| 39041 | 7.97 | 2.981 |
| 39062 | 9.9 | 1.298 |
| 39108 | 8.01 | 0.711 |
| 39121 | 8.98 | 0.703 |
| 39122 | 8.65 | 2.836 |
| 39134 | 9.17 | 1.509 |
| 39197 | 7.14 | 1.55 |
| 39207 | 7.9 | 1.563 |
| 39213 | 9.42 | 3.836 |
| 39214 | 7.02 | 1.574 |
| 39266 | 6.43 | 0.473 |
| 39288 | 7.49 | 1.622 |
| 39291 | 7.59 | 0.606 |
| 39358 | 6.32 | 1.701 |
| 39363 | 9.05 | 0.872 |
| 39488 | 7.32 | 0.615 |
| 39510 | 8.74 | 0.963 |
| 39520 | 9.31 | 0.941 |
| 39538 | 9.88 | 4.516 |
| 39643 | 6.58 | 0.499 |
| 39722 | 6.9 | 1.907 |
| 39833 | 7.81 | 0.958 |
| 40013 | 7.6 | 0.687 |
| 40194 | 9.11 | 0.566 |
| 40211 | 6.8 | 2.081 |
| 40237 | 9.76 | 0.843 |
| 40246 | 8.2 | 0.936 |
| 40342 | 9.91 | 3.385 |
| 40376 | 7.18 | 1.024 |
| 40386 | 8.67 | 2.441 |
| 40404 | 7.92 | 0.455 |
| 40474 | 6.53 | 3.039 |
| 40533 | 7.22 | 0.783 |
| 40621 | 7.36 | 1.048 |
| 40834 | 8.25 | 3.067 |
| 40901 | 8.7 | 1.406 |
| 40941 | 6.77 | 1.725 |
| 40984 | 8.04 | 0.71 |
| 40989 | 7.39 | 0.685 |
| 41003 | 9.16 | 5.855 |
| 41084 | 7.59 | 0.514 |
| 41140 | 7.29 | 0.641 |
| 41173 | 8.42 | 0.856 |
| 41213 | 6.93 | 0.478 |
| 41252 | 8.43 | 2.026 |
| 41328 | 9.79 | 4.099 |
| 41430 | 6.53 | 1.599 |
| 41478 | 8.42 | 1.669 |
| 41493 | 7.85 | 0.479 |

| | | |
|---|---|---|
| 41504 | 9.89 | 2.149 |
| 41577 | 7.37 | 0.945 |
| 41630 | 7.04 | 0.68 |
| 41648 | 6.71 | 0.455 |
| 41782 | 6.81 | 1.437 |
| 41791 | 7.95 | 0.401 |
| 41960 | 6.88 | 0.531 |
| 42029 | 9.05 | 1.416 |
| 42101 | 6.8 | 1.935 |
| 42160 | 7.22 | 0.443 |
| 42164 | 7.01 | 0.949 |
| 42201 | 7.11 | 0.903 |
| 42225 | 6.76 | 0.423 |
| 42265 | 7.07 | 3.805 |
| 42274 | 6.56 | 0.572 |
| 42300 | 6.97 | 0.539 |
| 42330 | 6.97 | 0.874 |
| 42342 | 7.01 | 2.721 |
| 42348 | 8.92 | 1.419 |
| 42353 | 8.74 | 1.637 |
| 42374 | 7.02 | 0.689 |
| 42378 | 9.68 | 0.611 |
| 42412 | 7.01 | 0.982 |
| 42419 | 6.41 | 0.54 |
| 42434 | 9.05 | 1.978 |
| 42440 | 7.46 | 2.008 |
| 42511 | 9.39 | 1.435 |
| 42542 | 6.75 | 2.546 |
| 42578 | 6.44 | 1.96 |
| 42588 | 6.55 | 0.772 |
| 42606 | 7.63 | 1.497 |
| 42705 | 7.64 | 0.763 |
| 42766 | 7.9 | 0.397 |
| 42769 | 9.23 | 1.681 |
| 42770 | 6.61 | 0.662 |
| 42775 | 7.43 | 1.962 |
| 42899 | 8.18 | 1.441 |
| 42917 | 8.0 | 3.133 |
| 42994 | 7.74 | 0.848 |
| 43002 | 9.14 | 3.073 |
| 43043 | 8.77 | 0.87 |
| 43061 | 7.91 | 1.14 |
| 43078 | 6.99 | 0.588 |
| 43118 | 7.21 | 0.655 |
| 43142 | 9.61 | 6.432 |
| 43147 | 7.33 | 0.758 |
| 43201 | 6.75 | 0.842 |
| 43211 | 6.61 | 0.24 |
| 43385 | 7.03 | 0.676 |
| 43417 | 9.26 | 1.804 |
| 43456 | 6.37 | 0.501 |
| 43461 | 7.67 | 0.847 |

| | | |
|---|---|---|
| 43480 | 6.78 | 0.407 |
| 43539 | 8.03 | 1.237 |
| 43551 | 6.38 | 0.542 |
| 43571 | 7.05 | 1.427 |
| 43666 | 7.97 | 1.619 |
| 43774 | 8.28 | 1.57 |
| 43775 | 6.5 | 0.963 |
| 43805 | 6.49 | 1.905 |
| 43817 | 6.53 | 0.841 |
| 43879 | 7.33 | 0.641 |
| 43962 | 6.58 | 0.904 |
| 43994 | 6.79 | 0.443 |
| 44006 | 6.65 | 0.454 |
| 44009 | 7.02 | 0.426 |
| 44017 | 8.45 | 1.375 |
| 44042 | 9.42 | 1.828 |
| 44056 | 7.51 | 1.676 |
| 44078 | 7.07 | 0.924 |
| 44085 | 7.11 | 0.807 |
| 44120 | 7.67 | 0.519 |
| 44135 | 7.58 | 1.284 |
| 44180 | 9.78 | 2.305 |
| 44249 | 6.56 | 0.507 |
| 44277 | 7.2 | 0.794 |
| 44280 | 7.01 | 0.827 |
| 44307 | 6.4 | 3.441 |
| 44325 | 6.79 | 1.04 |
| 44360 | 6.81 | 0.657 |
| 44380 | 6.87 | 0.672 |
| 44400 | 6.5 | 0.28 |
| 44421 | 7.64 | 1.441 |
| 44426 | 6.49 | 0.832 |
| 44450 | 8.19 | 0.854 |
| 44453 | 7.71 | 0.639 |
| 44459 | 6.56 | 0.416 |
| 44552 | 8.77 | 1.106 |
| 44635 | 6.71 | 0.615 |
| 44740 | 7.78 | 0.613 |
| 44764 | 7.48 | 0.658 |
| 44787 | 7.28 | 1.12 |
| 44876 | 9.79 | 1.153 |
| 44887 | 8.74 | 3.654 |
| 44967 | 9.67 | 0.789 |
| 45017 | 6.58 | 0.732 |
| 45037 | 7.85 | 1.692 |
| 45047 | 8.74 | 0.947 |
| 45152 | 8.41 | 1.501 |
| 45153 | 6.94 | 1.39 |
| 45167 | 8.68 | 2.379 |
| 45272 | 6.57 | 1.903 |
| 45286 | 9.27 | 0.689 |
| 45293 | 6.79 | 0.324 |

| | | |
|---|---|---|
| 45354 | 6.65 | 1.05 |
| 45424 | 9.38 | 2.116 |
| 45440 | 8.33 | 0.848 |
| 45453 | 6.43 | 0.677 |
| 45550 | 7.35 | 1.322 |
| 45575 | 9.95 | 0.622 |
| 45590 | 8.89 | 3.215 |
| 45592 | 9.5 | 1.62 |
| 45640 | 7.59 | 1.296 |
| 45654 | 8.06 | 0.734 |
| 45658 | 7.48 | 0.637 |
| 45676 | 6.92 | 0.413 |
| 45710 | 6.95 | 0.946 |
| 45744 | 7.26 | 1.909 |
| 45813 | 8.06 | 2.087 |
| 45894 | 7.84 | 2.041 |
| 45895 | 6.73 | 0.737 |
| 45961 | 8.08 | 1.419 |
| 45999 | 7.2 | 2.307 |
| 46068 | 8.68 | 1.798 |
| 46075 | 9.92 | 2.511 |
| 46182 | 9.35 | 0.822 |
| 46208 | 8.47 | 2.167 |
| 46211 | 7.6 | 0.736 |
| 46258 | 9.68 | 1.572 |
| 46262 | 7.06 | 0.615 |
| 46279 | 7.99 | 0.986 |
| 46304 | 7.28 | 1.061 |
| 46313 | 7.03 | 1.184 |
| 46335 | 9.35 | 1.04 |
| 46336 | 7.4 | 1.788 |
| 46351 | 9.45 | 1.105 |
| 46376 | 7.13 | 0.898 |
| 46378 | 7.79 | 0.392 |
| 46396 | 8.72 | 2.596 |
| 46410 | 6.88 | 2.943 |
| 46498 | 6.82 | 0.701 |
| 46571 | 6.31 | 1.126 |
| 46621 | 8.34 | 0.799 |
| 46642 | 6.97 | 1.201 |
| 46681 | 6.49 | 0.687 |
| 46704 | 7.11 | 1.791 |
| 46727 | 7.43 | 1.095 |
| 46734 | 8.71 | 5.722 |
| 46758 | 7.13 | 0.854 |
| 46808 | 7.78 | 1.142 |
| 46812 | 6.48 | 0.688 |
| 46813 | 9.28 | 4.888 |
| 46856 | 9.76 | 0.982 |
| 46881 | 6.61 | 1.928 |
| 46890 | 7.6 | 1.622 |
| 46936 | 8.14 | 0.85 |

| | | |
|---|---|---|
| 47082 | 7.02 | 1.345 |
| 47083 | 8.1 | 1.207 |
| 47096 | 6.39 | 2.335 |
| 47134 | 8.06 | 1.389 |
| 47151 | 7.85 | 0.607 |
| 47169 | 7.95 | 1.432 |
| 47194 | 6.84 | 0.469 |
| 47208 | 9.39 | 1.093 |
| 47249 | 8.7 | 1.717 |
| 47303 | 7.54 | 1.365 |
| 47336 | 9.68 | 1.96 |
| 47405 | 9.7 | 1.318 |
| 47439 | 7.36 | 0.826 |
| 47556 | 7.86 | 1.107 |
| 47571 | 9.57 | 1.227 |
| 47633 | 7.49 | 2.179 |
| 47636 | 8.46 | 2.676 |
| 47647 | 6.97 | 0.973 |
| 47670 | 6.34 | 0.484 |
| 47813 | 6.34 | 0.429 |
| 47822 | 7.83 | 1.058 |
| 47922 | 7.38 | 0.724 |
| 47953 | 6.77 | 0.313 |
| 47999 | 7.4 | 1.203 |
| 48098 | 7.17 | 1.219 |
| 48129 | 6.66 | 0.67 |
| 48218 | 6.34 | 4.344 |
| 48234 | 7.25 | 0.716 |
| 48278 | 7.65 | 0.848 |
| 48301 | 7.9 | 0.778 |
| 48403 | 7.05 | 0.507 |
| 48532 | 6.95 | 1.087 |
| 48584 | 7.13 | 2.57 |
| 48687 | 8.7 | 2.746 |
| 48776 | 6.49 | 3.182 |
| 48817 | 8.9 | 0.57 |
| 48849 | 6.63 | 1.015 |
| 48925 | 7.89 | 0.889 |
| 48960 | 7.76 | 0.919 |
| 48972 | 7.77 | 0.589 |
| 48994 | 6.51 | 0.586 |
| 49036 | 7.82 | 0.532 |
| 49047 | 7.98 | 1.165 |
| 49065 | 8.17 | 4.537 |
| 49099 | 6.86 | 0.604 |
| 49113 | 6.81 | 0.724 |
| 49200 | 7.1 | 0.653 |
| 49207 | 7.11 | 0.515 |
| 49209 | 9.25 | 2.128 |
| 49225 | 7.24 | 0.504 |
| 49328 | 6.8 | 1.695 |
| 49356 | 7.53 | 0.738 |

| | | |
|---|---|---|
| 49362 | 7.56 | 0.871 |
| 49408 | 9.88 | 2.826 |
| 49416 | 6.93 | 1.499 |
| 49437 | 7.69 | 0.734 |
| 49458 | 6.35 | 0.52 |
| 49466 | 9.2 | 1.282 |
| 49518 | 7.23 | 1.251 |
| 49541 | 7.73 | 2.421 |
| 49567 | 6.35 | 0.448 |
| 49590 | 7.13 | 0.86 |
| 49647 | 8.3 | 0.812 |
| 49670 | 9.0 | 1.32 |
| 49726 | 6.82 | 0.401 |
| 49836 | 9.05 | 1.274 |
| 49900 | 6.74 | 2.439 |
| 50066 | 7.98 | 4.207 |
| 50187 | 6.61 | 0.924 |
| 50188 | 6.56 | 0.715 |
| 50305 | 9.5 | 3.351 |
| 50308 | 7.95 | 1.57 |
| 50459 | 7.83 | 1.522 |
| 50463 | 6.86 | 0.846 |
| 50508 | 9.05 | 1.364 |
| 50574 | 7.54 | 1.771 |
| 50593 | 7.38 | 1.048 |
| 50602 | 7.67 | 0.904 |
| 50612 | 6.34 | 0.756 |
| 50629 | 6.85 | 0.308 |
| 50658 | 9.81 | 1.374 |
| 50685 | 7.95 | 5.669 |
| 50698 | 9.31 | 1.091 |
| 50705 | 9.84 | 2.093 |
| 50728 | 8.73 | 2.787 |
| 50739 | 7.66 | 2.102 |
| 50755 | 6.85 | 2.439 |
| 50787 | 6.46 | 1.174 |
| 50901 | 9.16 | 0.754 |
| 50945 | 7.29 | 0.635 |
| 50974 | 6.7 | 0.371 |
| 50976 | 7.4 | 2.8 |
| 50990 | 7.28 | 0.794 |
| 51050 | 7.4 | 0.702 |
| 51061 | 6.37 | 1.243 |
| 51075 | 8.02 | 2.045 |
| 51122 | 7.25 | 0.521 |
| 51173 | 6.69 | 1.173 |
| 51213 | 8.47 | 2.563 |
| 51274 | 8.89 | 0.616 |
| 51458 | 8.98 | 0.645 |
| 51472 | 8.68 | 1.874 |
| 51501 | 6.88 | 1.381 |
| 51532 | 6.47 | 0.474 |

| | | |
|---|---|---|
| 51603 | 8.16 | 1.223 |
| 51649 | 6.58 | 0.211 |
| 51788 | 9.64 | 0.883 |
| 51802 | 7.05 | 4.437 |
| 51837 | 8.34 | 1.165 |
| 51843 | 6.84 | 0.566 |
| 51937 | 6.91 | 1.128 |
| 52025 | 6.35 | 0.575 |
| 52035 | 8.15 | 0.886 |
| 52069 | 7.31 | 0.922 |
| 52109 | 8.77 | 1.11 |
| 52113 | 9.09 | 2.681 |
| 52280 | 6.51 | 0.469 |
| 52324 | 8.12 | 1.345 |
| 52344 | 8.48 | 0.995 |
| 52413 | 9.47 | 1.298 |
| 52478 | 8.87 | 3.07 |
| 52496 | 6.92 | 0.303 |
| 52520 | 9.43 | 3.627 |
| 52530 | 9.78 | 1.1 |
| 52537 | 9.2 | 3.093 |
| 52540 | 9.16 | 0.506 |
| 52602 | 9.42 | 1.941 |
| 52614 | 7.19 | 0.728 |
| 52638 | 8.64 | 4.617 |
| 52650 | 8.99 | 1.809 |
| 52683 | 8.0 | 1.61 |
| 52743 | 6.55 | 1.004 |
| 52814 | 8.2 | 1.004 |
| 52841 | 7.65 | 3.438 |
| 52844 | 6.95 | 0.623 |
| 52877 | 7.76 | 1.78 |
| 52883 | 7.26 | 1.863 |
| 52893 | 9.58 | 1.305 |
| 52911 | 9.76 | 6.222 |
| 52919 | 7.42 | 0.837 |
| 52965 | 9.41 | 4.324 |
| 52980 | 8.9 | 4.875 |
| 53258 | 6.38 | 0.644 |
| 53290 | 9.01 | 1.593 |
| 53329 | 6.69 | 0.763 |
| 53355 | 8.04 | 4.583 |
| 53379 | 6.58 | 2.35 |
| 53395 | 8.55 | 1.207 |
| 53409 | 7.31 | 0.292 |
| 53485 | 8.39 | 0.732 |
| 53501 | 7.73 | 0.91 |
| 53510 | 8.43 | 0.601 |
| 53571 | 8.02 | 0.668 |
| 53605 | 7.77 | 1.39 |
| 53659 | 6.81 | 0.773 |
| 53694 | 8.13 | 0.572 |

| | | |
|---|---|---|
| 53702 | 9.17 | 3.305 |
| 53703 | 7.88 | 0.882 |
| 53722 | 9.43 | 0.402 |
| 53727 | 6.59 | 1.39 |
| 53741 | 6.67 | 1.155 |
| 53794 | 7.62 | 0.84 |
| 53857 | 6.51 | 1.028 |
| 53925 | 6.55 | 1.043 |
| 53977 | 8.62 | 1.115 |
| 54106 | 8.58 | 1.696 |
| 54107 | 8.77 | 1.52 |
| 54141 | 6.96 | 1.293 |
| 54157 | 7.32 | 0.674 |
| 54166 | 7.35 | 1.433 |
| 54220 | 8.07 | 0.475 |
| 54231 | 9.23 | 1.307 |
| 54302 | 7.74 | 0.907 |
| 54329 | 8.56 | 1.115 |
| 54430 | 7.13 | 1.919 |
| 54487 | 7.99 | 4.458 |
| 54561 | 9.54 | 3.705 |
| 54706 | 8.06 | 0.835 |
| 54716 | 8.55 | 1.135 |
| 54719 | 8.82 | 0.615 |
| 54736 | 6.66 | 0.345 |
| 54742 | 6.81 | 2.514 |
| 54752 | 8.51 | 0.819 |
| 54765 | 9.95 | 1.877 |
| 54807 | 6.5 | 2.973 |
| 54843 | 7.23 | 1.381 |
| 54983 | 9.27 | 0.953 |
| 54987 | 8.42 | 0.667 |
| 55019 | 6.31 | 1.643 |
| 55063 | 9.16 | 1.879 |
| 55106 | 7.75 | 3.535 |
| 55107 | 6.94 | 0.687 |
| 55133 | 8.13 | 1.912 |
| 55166 | 8.77 | 1.037 |
| 55170 | 9.13 | 1.809 |
| 55271 | 6.64 | 1.369 |
| 55332 | 6.71 | 1.882 |
| 55382 | 6.34 | 1.229 |
| 55443 | 6.87 | 1.007 |
| 55490 | 6.67 | 0.77 |
| 55531 | 7.77 | 1.533 |
| 55570 | 9.13 | 1.019 |
| 55679 | 8.03 | 0.699 |
| 55802 | 9.85 | 2.047 |
| 55851 | 8.1 | 0.476 |
| 55899 | 7.02 | 0.988 |
| 55960 | 8.38 | 0.902 |
| 56005 | 7.58 | 1.917 |

| | | |
|---|---|---|
| 56059 | 7.55 | 0.33 |
| 56077 | 8.69 | 1.741 |
| 56098 | 6.35 | 0.556 |
| 56110 | 7.09 | 0.707 |
| 56207 | 6.75 | 0.778 |
| 56275 | 9.24 | 0.937 |
| 56324 | 7.56 | 0.667 |
| 56339 | 6.46 | 1.219 |
| 56378 | 6.49 | 0.279 |
| 56391 | 8.86 | 6.32 |
| 56395 | 8.23 | 0.739 |
| 56486 | 6.52 | 0.605 |
| 56543 | 7.31 | 0.522 |
| 56553 | 8.21 | 2.374 |
| 56597 | 8.71 | 0.509 |
| 56625 | 7.61 | 1.052 |
| 56631 | 7.42 | 0.89 |
| 56632 | 7.54 | 2.518 |
| 56649 | 7.4 | 1.261 |
| 56732 | 7.19 | 0.581 |
| 56746 | 6.97 | 0.817 |
| 56780 | 7.87 | 0.397 |
| 56893 | 7.04 | 0.842 |
| 56904 | 6.48 | 1.701 |
| 56925 | 7.8 | 1.248 |
| 56941 | 9.68 | 1.98 |
| 56963 | 8.89 | 0.694 |
| 56968 | 8.99 | 1.213 |
| 57014 | 6.93 | 0.592 |
| 57133 | 7.15 | 0.647 |
| 57158 | 6.71 | 0.666 |
| 57189 | 7.36 | 2.736 |
| 57234 | 7.77 | 0.77 |
| 57246 | 8.96 | 0.648 |
| 57258 | 8.55 | 0.67 |
| 57302 | 6.68 | 0.491 |
| 57446 | 7.21 | 0.719 |
| 57470 | 7.3 | 1.011 |
| 57515 | 8.71 | 1.368 |
| 57528 | 8.56 | 0.819 |
| 57567 | 8.03 | 0.776 |
| 57604 | 6.42 | 1.237 |
| 57710 | 8.41 | 0.532 |
| 57809 | 7.54 | 1.471 |
| 57813 | 8.78 | 1.236 |
| 57816 | 8.18 | 0.709 |
| 57910 | 7.45 | 0.326 |
| 57920 | 9.68 | 2.023 |
| 58039 | 8.59 | 1.169 |
| 58113 | 8.68 | 0.925 |
| 58131 | 8.37 | 1.266 |
| 58137 | 8.28 | 1.419 |

| | | |
|---|---|---|
| 58297 | 6.34 | 0.424 |
| 58316 | 8.14 | 1.001 |
| 58396 | 6.49 | 0.344 |
| 58410 | 9.46 | 2.394 |
| 58416 | 8.64 | 1.327 |
| 58458 | 7.3 | 0.93 |
| 58505 | 6.68 | 0.502 |
| 58512 | 8.71 | 2.962 |
| 58525 | 8.74 | 0.456 |
| 58616 | 9.93 | 1.541 |
| 58637 | 9.3 | 0.519 |
| 58650 | 9.71 | 1.696 |
| 58674 | 9.53 | 1.352 |
| 58765 | 7.36 | 2.644 |
| 58797 | 8.42 | 1.193 |
| 58830 | 8.64 | 3.107 |
| 58851 | 8.05 | 0.88 |
| 58884 | 9.61 | 4.902 |
| 58937 | 6.57 | 0.354 |
| 59093 | 9.43 | 1.424 |
| 59100 | 7.15 | 1.52 |
| 59119 | 6.82 | 0.755 |
| 59167 | 6.62 | 0.475 |
| 59174 | 7.54 | 0.759 |
| 59229 | 9.99 | 5.669 |
| 59271 | 8.56 | 1.439 |
| 59275 | 6.47 | 0.656 |
| 59293 | 7.62 | 0.721 |
| 59346 | 9.05 | 2.839 |
| 59403 | 6.32 | 0.277 |
| 59505 | 9.21 | 0.554 |
| 59531 | 7.24 | 1.325 |
| 59541 | 7.64 | 1.02 |
| 59622 | 8.03 | 2.385 |
| 59636 | 7.09 | 1.066 |
| 59659 | 7.16 | 1.399 |
| 59675 | 6.33 | 0.626 |
| 59702 | 9.18 | 0.763 |
| 59724 | 9.11 | 0.72 |
| 59729 | 7.71 | 1.088 |
| 59825 | 6.47 | 0.677 |
| 59851 | 9.78 | 2.193 |
| 59852 | 7.3 | 0.573 |
| 59911 | 6.42 | 0.488 |
| 59950 | 6.68 | 2.301 |
| 60084 | 6.77 | 0.634 |
| 60133 | 9.27 | 1.574 |
| 60219 | 7.23 | 1.781 |
| 60313 | 8.3 | 1.544 |
| 60327 | 9.97 | 2.276 |
| 60334 | 7.97 | 1.9 |
| 60382 | 7.91 | 0.972 |

| | | |
|---|---|---|
| 60426 | 7.48 | 1.097 |
| 60577 | 9.05 | 0.952 |
| 60667 | 7.12 | 0.857 |
| 60712 | 6.9 | 1.311 |
| 60726 | 8.29 | 1.127 |
| 60775 | 9.88 | 1.617 |
| 60805 | 6.9 | 1.091 |
| 60850 | 8.17 | 2.136 |
| 60880 | 9.76 | 2.669 |
| 60883 | 8.1 | 1.388 |
| 60939 | 9.98 | 0.15 |
| 61017 | 9.26 | 1.852 |
| 61034 | 6.95 | 0.964 |
| 61064 | 6.85 | 1.376 |
| 61077 | 6.45 | 0.524 |
| 61111 | 7.04 | 0.549 |
| 61122 | 7.62 | 0.695 |
| 61197 | 9.77 | 0.872 |
| 61214 | 9.35 | 1.067 |
| 61295 | 9.41 | 2.681 |
| 61342 | 8.86 | 1.138 |
| 61350 | 6.43 | 0.689 |
| 61353 | 9.43 | 1.476 |
| 61557 | 9.09 | 2.387 |
| 61579 | 6.78 | 2.479 |
| 61593 | 9.89 | 0.894 |
| 61628 | 9.28 | 1.286 |
| 61684 | 9.44 | 0.876 |
| 61711 | 7.55 | 0.961 |
| 61748 | 6.45 | 1.957 |
| 61814 | 7.83 | 0.429 |
| 61847 | 6.41 | 1.412 |
| 61989 | 9.45 | 1.879 |
| 62005 | 6.87 | 0.323 |
| 62096 | 6.64 | 1.077 |
| 62122 | 8.54 | 0.766 |
| 62170 | 7.05 | 2.865 |
| 62232 | 7.34 | 2.195 |
| 62478 | 8.01 | 1.891 |
| 62516 | 7.04 | 3.165 |
| 62541 | 8.1 | 3.958 |
| 62576 | 9.97 | 3.777 |
| 62641 | 8.43 | 5.133 |
| 62691 | 6.72 | 0.532 |
| 62703 | 8.53 | 4.803 |
| 62781 | 7.46 | 0.697 |
| 62792 | 7.42 | 0.623 |
| 62799 | 6.81 | 2.153 |
| 62810 | 8.72 | 0.868 |
| 62825 | 8.95 | 3.354 |
| 62907 | 8.05 | 1.416 |
| 62991 | 6.83 | 0.566 |

| | | |
|---|---|---|
| 63096 | 6.68 | 1.464 |
| 63111 | 8.93 | 0.703 |
| 63120 | 7.35 | 0.826 |
| 63227 | 9.59 | 1.451 |
| 63236 | 8.97 | 1.453 |
| 63238 | 7.5 | 0.685 |
| 63331 | 7.22 | 1.804 |
| 63350 | 7.11 | 1.195 |
| 63459 | 6.74 | 1.251 |
| 63575 | 6.47 | 0.533 |
| 63592 | 7.58 | 1.52 |
| 63606 | 6.61 | 0.535 |
| 63654 | 6.83 | 0.563 |
| 63677 | 6.59 | 1.464 |
| 63775 | 6.91 | 1.298 |
| 63783 | 8.03 | 1.06 |
| 64023 | 7.72 | 0.74 |
| 64055 | 9.25 | 1.181 |
| 64086 | 6.33 | 0.334 |
| 64090 | 7.21 | 0.699 |
| 64093 | 8.69 | 0.571 |
| 64108 | 7.26 | 1.811 |
| 64364 | 8.19 | 0.775 |
| 64375 | 8.88 | 2.637 |
| 64525 | 6.86 | 0.333 |
| 64648 | 7.15 | 1.978 |
| 64752 | 6.91 | 0.508 |
| 64789 | 9.68 | 1.195 |
| 64828 | 8.39 | 2.463 |
| 64883 | 7.06 | 0.482 |
| 64925 | 9.87 | 1.183 |
| 64936 | 7.53 | 0.922 |
| 64954 | 7.32 | 1.799 |
| 65089 | 9.75 | 0.771 |
| 65119 | 7.97 | 2.689 |
| 65203 | 7.12 | 1.925 |
| 65219 | 7.77 | 1.595 |
| 65229 | 7.91 | 1.2 |
| 65230 | 7.12 | 3.777 |
| 65304 | 8.1 | 0.675 |
| 65348 | 7.67 | 0.402 |
| 65405 | 8.14 | 1.359 |
| 65426 | 9.44 | 1.305 |
| 65463 | 8.42 | 0.943 |
| 65522 | 7.03 | 3.58 |
| 65551 | 8.79 | 1.455 |
| 65822 | 7.36 | 1.416 |
| 65933 | 9.27 | 1.486 |
| 65942 | 9.51 | 1.314 |
| 66004 | 7.84 | 1.776 |
| 66063 | 8.37 | 0.615 |
| 66068 | 7.77 | 0.984 |

| | | |
|---|---|---|
| 66094 | 9.3 | 2.114 |
| 66171 | 6.39 | 2.392 |
| 66235 | 8.2 | 1.051 |
| 66247 | 6.43 | 2.978 |
| 66330 | 7.1 | 0.808 |
| 66349 | 8.83 | 0.566 |
| 66394 | 9.5 | 1.561 |
| 66400 | 8.44 | 6.211 |
| 66424 | 6.48 | 0.835 |
| 66447 | 8.08 | 0.899 |
| 66463 | 6.85 | 1.034 |
| 66566 | 8.62 | 0.775 |
| 66684 | 6.49 | 0.971 |
| 66722 | 8.25 | 1.935 |
| 66728 | 8.57 | 2.297 |
| 66756 | 6.44 | 0.473 |
| 66857 | 7.48 | 2.305 |
| 66932 | 9.75 | 1.804 |
| 67002 | 8.15 | 1.194 |
| 67004 | 7.87 | 1.986 |
| 67005 | 9.46 | 2.684 |
| 67028 | 9.85 | 1.788 |
| 67036 | 8.88 | 1.384 |
| 67099 | 8.64 | 0.606 |
| 67139 | 9.63 | 2.596 |
| 67256 | 6.46 | 0.976 |
| 67318 | 6.82 | 0.256 |
| 67321 | 6.87 | 1.144 |
| 67481 | 6.97 | 2.189 |
| 67523 | 9.02 | 2.22 |
| 67581 | 7.92 | 0.839 |
| 67775 | 9.39 | 1.314 |
| 67848 | 7.35 | 3.571 |
| 67865 | 6.63 | 0.837 |
| 67893 | 8.39 | 1.357 |
| 67910 | 9.22 | 0.785 |
| 68055 | 7.69 | 1.226 |
| 68196 | 6.94 | 1.632 |
| 68219 | 6.32 | 0.441 |
| 68234 | 7.71 | 1.189 |
| 68276 | 6.79 | 3.486 |
| 68304 | 6.95 | 1.57 |
| 68440 | 6.62 | 0.508 |
| 68454 | 7.32 | 0.622 |
| 68466 | 8.13 | 0.945 |
| 68478 | 9.59 | 3.489 |
| 68615 | 9.12 | 1.385 |
| 68713 | 6.76 | 0.376 |
| 68722 | 6.71 | 0.543 |
| 68752 | 8.16 | 1.626 |
| 68771 | 8.11 | 0.636 |
| 68781 | 9.37 | 0.772 |

| | | |
|---|---|---|
| 68808 | 8.56 | 2.13 |
| 68888 | 9.25 | 1.758 |
| 68891 | 7.7 | 1.64 |
| 68953 | 7.31 | 0.437 |
| 68956 | 7.45 | 2.537 |
| 68989 | 6.92 | 0.374 |
| 69092 | 8.83 | 1.511 |
| 69213 | 8.51 | 1.928 |
| 69302 | 6.78 | 0.552 |
| 69361 | 7.88 | 1.077 |
| 69455 | 8.08 | 0.402 |
| 69489 | 8.33 | 1.209 |
| 69575 | 7.96 | 0.924 |
| 69602 | 6.45 | 0.652 |
| 69698 | 9.16 | 1.42 |
| 69818 | 9.84 | 2.711 |
| 69858 | 6.7 | 0.487 |
| 69859 | 6.85 | 1.352 |
| 69917 | 9.84 | 1.589 |
| 69933 | 7.37 | 1.087 |
| 69948 | 6.68 | 0.699 |
| 69958 | 9.75 | 2.594 |
| 69983 | 9.52 | 0.79 |
| 70006 | 7.18 | 0.59 |
| 70029 | 7.3 | 2.414 |
| 70041 | 7.77 | 1.075 |
| 70050 | 7.3 | 1.047 |
| 70089 | 7.25 | 0.934 |
| 70120 | 6.36 | 1.276 |
| 70121 | 6.91 | 1.178 |
| 70141 | 7.42 | 1.031 |
| 70149 | 8.72 | 0.381 |
| 70183 | 7.78 | 0.829 |
| 70220 | 8.16 | 1.948 |
| 70282 | 7.58 | 1.599 |
| 70287 | 7.38 | 1.388 |
| 70375 | 8.22 | 1.747 |
| 70384 | 8.49 | 3.432 |
| 70429 | 8.17 | 0.589 |
| 70441 | 7.09 | 0.782 |
| 70443 | 6.75 | 0.848 |
| 70483 | 9.25 | 2.167 |
| 70518 | 7.01 | 2.126 |
| 70549 | 6.43 | 0.992 |
| 70553 | 7.07 | 0.922 |
| 70652 | 7.4 | 0.627 |
| 70697 | 7.88 | 0.879 |
| 70716 | 8.72 | 1.335 |
| 70765 | 8.62 | 0.6 |
| 70809 | 6.64 | 1.607 |
| 70814 | 7.14 | 0.687 |
| 70819 | 7.7 | 0.876 |

| | | |
|---|---|---|
| 70822 | 6.38 | 0.436 |
| 70892 | 9.35 | 2.441 |
| 70918 | 6.92 | 1.914 |
| 70963 | 7.55 | 1.381 |
| 71008 | 9.2 | 1.64 |
| 71140 | 8.02 | 0.958 |
| 71199 | 6.35 | 0.664 |
| 71222 | 6.55 | 1.094 |
| 71234 | 6.41 | 1.221 |
| 71235 | 7.53 | 2.028 |
| 71237 | 8.25 | 0.586 |
| 71321 | 8.53 | 0.919 |
| 71379 | 8.27 | 1.119 |
| 71573 | 7.61 | 3.323 |
| 71585 | 8.62 | 2.004 |
| 71614 | 7.88 | 0.568 |
| 71708 | 7.76 | 0.512 |
| 71820 | 8.15 | 0.695 |
| 71925 | 8.45 | 1.153 |
| 71973 | 6.5 | 0.838 |
| 72015 | 7.78 | 1.48 |
| 72158 | 9.93 | 0.894 |
| 72192 | 7.72 | 1.411 |
| 72250 | 9.59 | 4.077 |
| 72299 | 7.2 | 0.76 |
| 72307 | 8.89 | 1.188 |
| 72316 | 8.22 | 0.369 |
| 72321 | 7.11 | 0.652 |
| 72330 | 9.07 | 1.588 |
| 72350 | 7.37 | 1.16 |
| 72514 | 7.77 | 0.432 |
| 72534 | 7.28 | 1.154 |
| 72627 | 7.8 | 1.722 |
| 72644 | 7.37 | 0.584 |
| 72725 | 9.12 | 1.67 |
| 72768 | 6.99 | 1.829 |
| 72802 | 6.9 | 1.015 |
| 72895 | 9.16 | 1.415 |
| 73028 | 9.08 | 1.428 |
| 73043 | 7.96 | 0.873 |
| 73051 | 7.08 | 0.736 |
| 73070 | 9.24 | 1.649 |
| 73102 | 7.47 | 1.515 |
| 73116 | 8.3 | 2.303 |
| 73125 | 7.86 | 0.625 |
| 73145 | 9.0 | 0.652 |
| 73150 | 8.24 | 1.331 |
| 73156 | 7.34 | 1.799 |
| 73174 | 7.52 | 1.17 |
| 73189 | 8.21 | 1.914 |
| 73200 | 6.46 | 0.62 |
| 73206 | 6.92 | 1.067 |

| | | |
|---|---|---|
| 73215 | 9.03 | 1.509 |
| 73216 | 6.31 | 0.31 |
| 73249 | 8.67 | 1.573 |
| 73284 | 9.32 | 7.052 |
| 73393 | 6.64 | 0.873 |
| 73450 | 6.87 | 0.639 |
| 73507 | 9.98 | 3.929 |
| 73559 | 8.3 | 4.126 |
| 73635 | 7.54 | 1.339 |
| 73645 | 7.82 | 1.106 |
| 73672 | 8.97 | 2.425 |
| 73706 | 7.03 | 2.5 |
| 73730 | 9.33 | 1.068 |
| 73741 | 7.1 | 0.596 |
| 73808 | 7.57 | 0.78 |
| 73913 | 7.08 | 0.494 |
| 73987 | 8.25 | 1.027 |
| 74115 | 7.68 | 1.265 |
| 74154 | 8.17 | 0.557 |
| 74272 | 6.47 | 3.441 |
| 74284 | 7.18 | 0.923 |
| 74319 | 6.77 | 0.953 |
| 74328 | 7.99 | 0.974 |
| 74359 | 8.21 | 1.279 |
| 74382 | 6.83 | 0.434 |
| 74458 | 9.15 | 1.063 |
| 74468 | 9.97 | 0.555 |
| 74529 | 7.46 | 0.531 |
| 74551 | 7.31 | 1.1 |
| 74553 | 9.29 | 2.396 |
| 74574 | 8.1 | 1.054 |
| 74592 | 8.36 | 1.557 |
| 74659 | 6.36 | 0.633 |
| 74743 | 7.07 | 0.774 |
| 74749 | 9.35 | 2.868 |
| 74810 | 7.6 | 1.497 |
| 74923 | 8.65 | 0.876 |
| 74973 | 7.45 | 0.22 |
| 75031 | 6.43 | 0.961 |
| 75163 | 7.55 | 0.966 |
| 75216 | 7.24 | 1.067 |
| 75230 | 7.33 | 2.112 |
| 75256 | 7.07 | 2.599 |
| 75402 | 6.88 | 0.454 |
| 75439 | 8.48 | 4.226 |
| 75476 | 6.82 | 1.203 |
| 75492 | 6.88 | 0.539 |
| 75514 | 8.58 | 0.522 |
| 75587 | 8.99 | 2.072 |
| 75613 | 6.56 | 1.188 |
| 75622 | 7.51 | 0.641 |
| 75688 | 6.83 | 0.575 |

| | | |
|---|---|---|
| 75756 | 9.8 | 2.049 |
| 75770 | 6.81 | 3.042 |
| 75825 | 7.04 | 1.432 |
| 75875 | 7.91 | 0.974 |
| 75896 | 7.3 | 0.911 |
| 75906 | 6.85 | 0.492 |
| 75911 | 9.36 | 0.53 |
| 75919 | 7.09 | 3.162 |
| 75953 | 9.14 | 1.388 |
| 75965 | 8.84 | 0.581 |
| 76043 | 8.21 | 1.024 |
| 76080 | 6.66 | 0.796 |
| 76138 | 7.43 | 0.816 |
| 76176 | 6.86 | 0.399 |
| 76196 | 8.21 | 2.318 |
| 76269 | 7.97 | 0.678 |
| 76305 | 9.01 | 0.856 |
| 76369 | 6.45 | 0.521 |
| 76438 | 7.23 | 1.112 |
| 76485 | 8.74 | 0.988 |
| 76517 | 8.57 | 0.962 |
| 76579 | 7.72 | 2.026 |
| 76610 | 8.9 | 1.519 |
| 76632 | 7.97 | 1.833 |
| 76637 | 6.44 | 1.65 |
| 76699 | 9.61 | 2.238 |
| 76773 | 7.36 | 0.925 |
| 76815 | 8.33 | 0.758 |
| 76892 | 6.61 | 1.457 |
| 76994 | 8.36 | 0.608 |
| 77013 | 6.86 | 1.069 |
| 77115 | 9.2 | 1.24 |
| 77163 | 8.49 | 4.495 |
| 77283 | 8.54 | 1.479 |
| 77570 | 8.96 | 1.238 |
| 77652 | 7.69 | 1.465 |
| 77755 | 6.46 | 1.975 |
| 77785 | 7.89 | 2.544 |
| 77849 | 7.13 | 0.801 |
| 77933 | 6.64 | 1.355 |
| 77975 | 6.61 | 0.667 |
| 78017 | 7.01 | 1.819 |
| 78116 | 7.23 | 0.508 |
| 78121 | 6.72 | 0.866 |
| 78124 | 8.51 | 1.339 |
| 78134 | 7.58 | 1.366 |
| 78196 | 8.98 | 1.026 |
| 78376 | 7.39 | 0.991 |
| 78448 | 8.04 | 1.707 |
| 78520 | 7.54 | 0.395 |
| 78545 | 7.9 | 1.513 |
| 78570 | 8.02 | 0.914 |

| | | |
|---|---|---|
| 78590 | 7.56 | 1.392 |
| 78654 | 8.4 | 0.831 |
| 78722 | 6.96 | 1.704 |
| 78761 | 7.04 | 1.625 |
| 78763 | 7.99 | 0.762 |
| 78829 | 8.49 | 0.949 |
| 78840 | 8.1 | 2.671 |
| 78909 | 6.63 | 0.78 |
| 78958 | 9.75 | 0.989 |
| 79047 | 9.18 | 1.893 |
| 79102 | 8.88 | 2.457 |
| 79125 | 8.13 | 2.31 |
| 79204 | 6.34 | 1.561 |
| 79208 | 9.58 | 2.873 |
| 79217 | 6.4 | 0.709 |
| 79289 | 7.72 | 0.808 |
| 79332 | 7.41 | 2.575 |
| 79436 | 6.62 | 0.744 |
| 79465 | 7.26 | 1.928 |
| 79493 | 6.82 | 0.938 |
| 79841 | 6.84 | 0.7 |
| 79998 | 9.15 | 1.673 |
| 80005 | 6.98 | 1.373 |
| 80051 | 7.89 | 1.85 |
| 80152 | 8.98 | 1.573 |
| 80184 | 7.24 | 0.712 |
| 80231 | 6.93 | 0.705 |
| 80247 | 6.33 | 2.301 |
| 80261 | 7.85 | 1.638 |
| 80335 | 7.36 | 0.839 |
| 80351 | 9.55 | 3.344 |
| 80375 | 8.9 | 3.438 |
| 80379 | 7.59 | 1.338 |
| 80406 | 7.13 | 0.952 |
| 80409 | 6.47 | 0.51 |
| 80427 | 8.63 | 1.246 |
| 80457 | 7.25 | 0.798 |
| 80527 | 8.81 | 1.884 |
| 80641 | 6.49 | 2.058 |
| 80809 | 9.0 | 1.862 |
| 80814 | 9.53 | 1.585 |
| 80952 | 7.74 | 0.651 |
| 80971 | 6.35 | 1.497 |
| 80985 | 7.66 | 0.743 |
| 80991 | 9.72 | 3.235 |
| 80994 | 8.75 | 1.092 |
| 81115 | 9.32 | 0.952 |
| 81189 | 6.65 | 0.503 |
| 81230 | 6.55 | 0.991 |
| 81259 | 6.78 | 1.746 |
| 81320 | 6.92 | 1.263 |
| 81345 | 7.69 | 0.956 |

| | | |
|---|---|---|
| 81401 | 6.59 | 1.136 |
| 81430 | 6.88 | 0.607 |
| 81440 | 7.92 | 4.13 |
| 81627 | 7.34 | 0.849 |
| 81630 | 6.56 | 0.435 |
| 81673 | 8.47 | 1.424 |
| 81717 | 7.99 | 1.631 |
| 81757 | 8.26 | 1.966 |
| 81940 | 6.73 | 0.621 |
| 82078 | 7.94 | 1.726 |
| 82104 | 7.69 | 0.49 |
| 82147 | 9.16 | 2.844 |
| 82162 | 6.62 | 3.973 |
| 82240 | 7.81 | 0.579 |
| 82253 | 8.7 | 1.534 |
| 82308 | 8.26 | 0.909 |
| 82415 | 6.73 | 0.824 |
| 82449 | 7.48 | 0.916 |
| 82480 | 9.45 | 4.92 |
| 82518 | 7.07 | 0.927 |
| 82556 | 6.78 | 0.546 |
| 82702 | 8.08 | 1.613 |
| 82806 | 7.27 | 3.489 |
| 82864 | 9.43 | 1.966 |
| 82884 | 7.06 | 1.527 |
| 82891 | 6.54 | 1.452 |
| 83128 | 8.26 | 1.346 |
| 83168 | 7.14 | 1.635 |
| 83210 | 6.36 | 0.424 |
| 83285 | 8.07 | 1.54 |
| 83342 | 8.6 | 2.459 |
| 83383 | 8.21 | 0.951 |
| 83384 | 7.92 | 1.254 |
| 83593 | 6.94 | 2.286 |
| 83640 | 6.38 | 1.131 |
| 83665 | 8.52 | 1.246 |
| 83724 | 7.04 | 0.785 |
| 83816 | 6.82 | 2.21 |
| 83876 | 8.9 | 1.689 |
| 83946 | 9.4 | 0.671 |
| 84036 | 8.57 | 1.939 |
| 84146 | 7.53 | 0.497 |
| 84273 | 7.0 | 0.666 |
| 84384 | 8.69 | 0.785 |
| 84432 | 6.39 | 0.479 |
| 84480 | 7.37 | 0.6 |
| 84495 | 6.95 | 1.175 |
| 84631 | 8.12 | 2.868 |
| 84644 | 6.9 | 0.62 |
| 84711 | 6.88 | 1.051 |
| 84732 | 8.12 | 1.141 |
| 84878 | 6.91 | 0.886 |

| | | |
|---|---|---|
| 85021 | 8.81 | 1.041 |
| 85067 | 8.25 | 0.641 |
| 85070 | 6.55 | 0.166 |
| 85146 | 6.69 | 0.75 |
| 85185 | 7.55 | 4.214 |
| 85279 | 7.12 | 0.88 |
| 85290 | 9.58 | 4.214 |
| 85317 | 9.15 | 2.322 |
| 85368 | 6.76 | 1.37 |
| 85379 | 8.98 | 4.685 |
| 85432 | 7.28 | 1.019 |
| 85759 | 9.62 | 1.197 |
| 85821 | 7.0 | 0.425 |
| 85981 | 9.65 | 1.338 |
| 85998 | 9.54 | 3.718 |
| 86009 | 6.97 | 1.062 |
| 86012 | 7.85 | 1.131 |
| 86041 | 8.38 | 1.002 |
| 86118 | 8.5 | 3.627 |
| 86148 | 7.15 | 0.863 |
| 86215 | 8.88 | 0.88 |
| 86306 | 8.87 | 1.248 |
| 86422 | 8.74 | 1.416 |
| 86443 | 8.35 | 0.266 |
| 86442 | 6.42 | 0.621 |
| 86446 | 7.49 | 1.559 |
| 86514 | 6.82 | 0.618 |
| 86546 | 7.76 | 2.072 |
| 86627 | 8.59 | 1.957 |
| 86648 | 6.72 | 0.95 |
| 86660 | 7.43 | 1.124 |
| 86679 | 8.86 | 2.784 |
| 86782 | 7.9 | 3.89 |
| 86806 | 7.29 | 0.54 |
| 86809 | 6.93 | 3.664 |
| 86908 | 8.23 | 0.794 |
| 86982 | 8.39 | 0.826 |
| 87021 | 6.61 | 1.184 |
| 87044 | 8.86 | 4.397 |
| 87045 | 7.6 | 2.295 |
| 87069 | 7.54 | 1.785 |
| 87146 | 7.26 | 1.449 |
| 87210 | 9.01 | 2.488 |
| 87297 | 6.36 | 1.776 |
| 87352 | 8.11 | 1.539 |
| 87405 | 7.34 | 1.826 |
| 87480 | 6.61 | 1.211 |
| 87507 | 7.93 | 0.56 |
| 87531 | 8.56 | 1.054 |
| 87610 | 7.69 | 1.07 |
| 87766 | 6.79 | 1.112 |
| 87825 | 8.66 | 1.355 |

| | | |
|---|---|---|
| 87910 | 9.36 | 2.908 |
| 87976 | 7.11 | 0.434 |
| 88056 | 7.71 | 0.672 |
| 88132 | 6.34 | 1.828 |
| 88148 | 8.26 | 2.924 |
| 88283 | 6.72 | 0.894 |
| 88373 | 6.63 | 0.954 |
| 88379 | 7.43 | 1.244 |
| 88423 | 6.36 | 0.852 |
| 88429 | 8.01 | 2.053 |
| 88436 | 9.66 | 1.318 |
| 88547 | 8.3 | 0.708 |
| 88555 | 8.74 | 1.19 |
| 88664 | 7.64 | 0.955 |
| 88834 | 9.55 | 0.945 |
| 88841 | 7.24 | 2.247 |
| 88880 | 7.11 | 0.43 |
| 88975 | 6.79 | 1.313 |
| 88983 | 9.5 | 0.895 |
| 88997 | 8.05 | 0.622 |
| 89033 | 7.57 | 0.554 |
| 89070 | 7.34 | 1.424 |
| 89104 | 7.11 | 1.793 |
| 89171 | 7.19 | 1.21 |
| 89265 | 6.53 | 0.368 |
| 89277 | 8.52 | 1.628 |
| 89342 | 9.8 | 1.374 |
| 89368 | 6.55 | 1.566 |
| 89565 | 7.81 | 1.322 |
| 89572 | 8.12 | 0.621 |
| 89612 | 7.05 | 0.852 |
| 89819 | 6.88 | 0.4 |
| 90031 | 6.73 | 1.841 |
| 90052 | 6.81 | 3.289 |
| 90070 | 6.94 | 1.094 |
| 90105 | 7.45 | 1.471 |
| 90146 | 9.59 | 2.767 |
| 90187 | 9.81 | 1.87 |
| 90256 | 8.41 | 2.461 |
| 90262 | 6.66 | 0.586 |
| 90342 | 7.63 | 3.908 |
| 90429 | 6.9 | 0.428 |
| 90453 | 6.55 | 0.463 |
| 90557 | 9.17 | 1.048 |
| 90635 | 6.9 | 0.867 |
| 90716 | 7.08 | 0.802 |
| 90758 | 6.35 | 0.599 |
| 90762 | 7.88 | 4.289 |
| 90780 | 7.37 | 3.006 |
| 90929 | 7.49 | 0.67 |
| 91041 | 7.14 | 2.208 |
| 91052 | 6.39 | 1.384 |

| | | |
|---|---|---|
| 91088 | 7.32 | 1.053 |
| 91144 | 6.74 | 0.694 |
| 91166 | 7.67 | 0.857 |
| 91242 | 8.79 | 0.554 |
| 91274 | 6.43 | 0.57 |
| 91315 | 7.66 | 3.332 |
| 91319 | 6.88 | 0.581 |
| 91378 | 6.41 | 0.644 |
| 91467 | 6.64 | 0.516 |
| 91534 | 6.54 | 0.882 |
| 91552 | 6.51 | 2.754 |
| 91575 | 8.74 | 1.256 |
| 91589 | 7.39 | 1.504 |
| 91670 | 8.5 | 0.614 |
| 91899 | 6.9 | 0.78 |
| 92015 | 7.26 | 1.368 |
| 92047 | 9.7 | 2.31 |
| 92143 | 9.13 | 1.498 |
| 92219 | 6.92 | 1.768 |
| 92268 | 6.42 | 1.957 |
| 92336 | 8.89 | 1.556 |
| 92346 | 9.6 | 1.64 |
| 92359 | 7.33 | 1.381 |
| 92544 | 8.68 | 0.689 |
| 92545 | 7.45 | 0.745 |
| 92583 | 7.75 | 0.489 |
| 92659 | 7.1 | 0.62 |
| 92672 | 6.65 | 1.646 |
| 92738 | 6.4 | 1.213 |
| 92954 | 7.09 | 0.992 |
| 92978 | 7.58 | 1.333 |
| 93068 | 8.59 | 2.101 |
| 93161 | 6.43 | 1.115 |
| 93470 | 9.25 | 2.151 |
| 93630 | 6.31 | 0.563 |
| 93640 | 8.33 | 0.732 |
| 93713 | 9.34 | 4.553 |
| 93775 | 7.25 | 0.728 |
| 93845 | 9.82 | 4.176 |
| 93862 | 9.33 | 2.744 |
| 93915 | 6.89 | 1.316 |
| 93965 | 9.3 | 1.025 |
| 94174 | 9.1 | 1.26 |
| 94177 | 6.67 | 1.577 |
| 94280 | 6.92 | 2.862 |
| 94288 | 6.5 | 0.487 |
| 94403 | 8.8 | 0.967 |
| 94510 | 7.39 | 1.325 |
| 94604 | 6.63 | 2.276 |
| 94690 | 8.03 | 1.096 |
| 94742 | 7.01 | 0.583 |
| 94921 | 8.87 | 1.925 |

| | | |
|---|---|---|
| 94924 | 8.15 | 1.112 |
| 94974 | 7.25 | 2.403 |
| 94975 | 7.55 | 1.923 |
| 95091 | 6.92 | 1.15 |
| 95551 | 7.47 | 0.368 |
| 95574 | 7.82 | 1.689 |
| 95656 | 9.02 | 3.584 |
| 95671 | 8.42 | 0.708 |
| 95992 | 6.36 | 0.775 |
| 96010 | 6.72 | 0.778 |
| 96098 | 6.76 | 0.708 |
| 96141 | 8.05 | 6.402 |
| 96161 | 6.77 | 0.758 |
| 96178 | 7.47 | 4.111 |
| 96189 | 7.66 | 1.611 |
| 96195 | 7.76 | 2.068 |
| 96201 | 7.22 | 0.792 |
| 96234 | 7.49 | 3.847 |
| 96252 | 7.1 | 1.464 |
| 96328 | 8.23 | 0.949 |
| 96583 | 8.43 | 0.507 |
| 96603 | 9.96 | 1.714 |
| 96610 | 9.13 | 1.467 |
| 96718 | 9.32 | 1.173 |
| 96724 | 6.88 | 3.422 |
| 96729 | 8.03 | 2.146 |
| 96734 | 9.72 | 2.112 |
| 96749 | 7.73 | 0.635 |
| 96771 | 8.33 | 3.124 |
| 96777 | 8.98 | 1.335 |
| 96779 | 6.51 | 0.336 |
| 96848 | 7.13 | 0.611 |
| 96896 | 6.54 | 0.885 |
| 96910 | 6.76 | 0.402 |
| 97122 | 7.37 | 3.47 |
| 97134 | 7.27 | 0.793 |
| 97155 | 7.1 | 0.666 |
| 97367 | 8.16 | 0.943 |
| 97441 | 6.43 | 0.991 |
| 97502 | 7.08 | 0.703 |
| 97510 | 6.4 | 1.108 |
| 97511 | 7.84 | 0.978 |
| 97697 | 8.58 | 2.902 |
| 97749 | 9.62 | 4.483 |
| 97777 | 6.76 | 0.737 |
| 97892 | 9.61 | 2.726 |
| 97980 | 9.45 | 5.489 |
| 98028 | 6.93 | 1.237 |
| 98040 | 9.5 | 0.756 |
| 98144 | 6.83 | 0.391 |
| 98146 | 9.31 | 1.7 |
| 98191 | 9.38 | 1.267 |

| | | |
|---|---|---|
| 98308 | 7.58 | 2.57 |
| 98342 | 7.39 | 1.445 |
| 98357 | 6.65 | 1.018 |
| 98361 | 7.3 | 0.626 |
| 98512 | 9.07 | 6.569 |
| 98643 | 8.28 | 2.058 |
| 98712 | 6.51 | 0.542 |
| 98733 | 6.61 | 1.057 |
| 98756 | 7.53 | 1.308 |
| 98924 | 6.74 | 0.249 |
| 98930 | 7.49 | 0.78 |
| 98951 | 6.37 | 1.135 |
| 99013 | 7.76 | 0.766 |
| 99054 | 7.94 | 0.922 |
| 99055 | 7.51 | 1.333 |
| 99125 | 8.76 | 0.905 |
| 99147 | 8.98 | 0.792 |
| 99282 | 6.59 | 0.178 |
| 99371 | 6.98 | 1.44 |
| 99426 | 6.94 | 0.854 |
| 99453 | 7.21 | 2.181 |
| 99650 | 7.87 | 0.709 |
| 99807 | 7.26 | 1.068 |
| 99860 | 8.73 | 1.166 |
| 99869 | 7.58 | 0.847 |
| 99978 | 6.76 | 0.492 |
| 99984 | 7.64 | 1.24 |
| 100014 | 7.49 | 1.279 |
| 100121 | 9.99 | 1.789 |
| 100128 | 8.3 | 1.689 |
| 100147 | 7.04 | 0.889 |
| 100162 | 7.75 | 0.953 |
| 100201 | 8.21 | 2.9 |
| 100206 | 7.43 | 0.832 |
| 100237 | 7.06 | 0.899 |
| 100253 | 7.51 | 1.617 |
| 100333 | 6.48 | 0.494 |
| 100349 | 6.74 | 1.138 |
| 100365 | 8.23 | 1.653 |
| 100376 | 9.53 | 0.316 |
| 100416 | 6.78 | 0.64 |
| 100481 | 6.69 | 0.813 |
| 100491 | 8.8 | 1.532 |
| 100495 | 6.64 | 0.568 |
| 100505 | 6.94 | 0.397 |
| 100547 | 8.47 | 0.937 |
| 100591 | 8.8 | 6.036 |
| 100594 | 8.18 | 1.061 |
| 100617 | 6.37 | 1.072 |
| 100636 | 7.02 | 0.652 |
| 100678 | 6.72 | 0.745 |
| 100696 | 6.99 | 0.894 |

| | | |
|---|---|---|
| 100709 | 7.13 | 0.845 |
| 100716 | 6.89 | 1.549 |
| 100825 | 7.13 | 0.543 |
| 100845 | 7.93 | 0.604 |
| 100930 | 7.11 | 0.842 |
| 101189 | 9.26 | 0.721 |
| 101196 | 7.54 | 0.669 |
| 101213 | 9.43 | 2.862 |
| 101255 | 9.24 | 0.977 |
| 101294 | 7.37 | 0.664 |
| 101309 | 6.48 | 0.706 |
| 101384 | 9.31 | 1.935 |
| 101387 | 6.93 | 0.707 |
| 101397 | 8.64 | 0.714 |
| 101449 | 8.5 | 0.685 |
| 101460 | 8.18 | 1.003 |
| 101473 | 8.13 | 2.189 |
| 101492 | 7.67 | 1.56 |
| 101580 | 6.96 | 0.868 |
| 101646 | 7.46 | 0.756 |
| 101671 | 8.71 | 1.776 |
| 101758 | 7.05 | 0.56 |
| 101771 | 8.02 | 1.313 |
| 101823 | 7.62 | 1.731 |
| 101975 | 7.5 | 0.606 |
| 102030 | 7.85 | 0.858 |
| 102070 | 7.52 | 0.492 |
| 102114 | 6.32 | 1.799 |
| 102144 | 9.51 | 1.283 |
| 102165 | 8.17 | 0.687 |
| 102183 | 6.84 | 1.589 |
| 102208 | 9.11 | 3.567 |
| 102310 | 7.57 | 0.558 |
| 102324 | 6.96 | 0.559 |
| 102331 | 9.07 | 1.184 |
| 102384 | 7.58 | 1.939 |
| 102436 | 6.48 | 0.235 |
| 102565 | 7.35 | 0.596 |
| 102584 | 8.45 | 1.583 |
| 102627 | 8.85 | 1.295 |
| 102631 | 6.98 | 1.95 |
| 102694 | 7.6 | 0.95 |
| 102697 | 7.06 | 0.833 |
| 102876 | 7.03 | 2.502 |
| 102880 | 8.67 | 0.889 |
| 102946 | 6.55 | 0.776 |
| 102982 | 8.57 | 1.154 |
| 103043 | 7.0 | 0.822 |
| 103085 | 8.67 | 1.069 |
| 103105 | 8.48 | 1.495 |
| 103116 | 7.95 | 2.394 |
| 103164 | 9.92 | 2.472 |

| | | |
|---|---|---|
| 103197 | 6.37 | 0.281 |
| 103335 | 6.78 | 0.978 |
| 103377 | 7.69 | 0.807 |
| 103400 | 7.2 | 0.383 |
| 103405 | 7.69 | 1.335 |
| 103435 | 6.65 | 0.939 |
| 103453 | 6.4 | 0.629 |
| 103468 | 9.35 | 1.488 |
| 103508 | 6.41 | 0.524 |
| 103529 | 9.72 | 0.833 |
| 103561 | 6.93 | 0.359 |
| 103616 | 7.58 | 1.718 |
| 103720 | 7.56 | 1.395 |
| 103797 | 6.88 | 0.411 |
| 103878 | 6.64 | 0.388 |
| 103924 | 6.84 | 0.606 |
| 103979 | 8.87 | 1.152 |
| 104014 | 6.68 | 0.657 |
| 104254 | 7.22 | 0.801 |
| 104272 | 7.5 | 1.684 |
| 104313 | 8.39 | 1.334 |
| 104317 | 9.85 | 1.053 |
| 104326 | 6.53 | 0.997 |
| 104430 | 9.75 | 2.087 |
| 104501 | 8.01 | 1.858 |
| 104538 | 6.81 | 2.805 |
| 104588 | 7.75 | 0.736 |
| 104615 | 9.36 | 1.456 |
| 104629 | 7.07 | 0.302 |
| 104670 | 8.04 | 1.031 |
| 104717 | 8.85 | 1.525 |
| 104743 | 8.5 | 1.046 |
| 104756 | 6.37 | 3.165 |
| 104793 | 7.07 | 0.463 |
| 104808 | 8.05 | 0.431 |
| 104810 | 7.19 | 1.1 |
| 104847 | 8.05 | 0.801 |
| 104978 | 8.22 | 5.474 |
| 105013 | 8.11 | 0.254 |
| 105093 | 7.47 | 0.459 |
| 105161 | 9.58 | 1.755 |
| 105169 | 8.61 | 1.611 |
| 105237 | 7.02 | 1.31 |
| 105365 | 6.34 | 0.263 |
| 105526 | 7.12 | 1.818 |
| 105570 | 9.06 | 7.19 |
| 105608 | 8.76 | 1.323 |
| 105674 | 6.62 | 0.813 |
| 105696 | 7.04 | 2.984 |
| 105779 | 6.57 | 1.629 |
| 105880 | 6.49 | 0.743 |
| 106037 | 7.53 | 1.119 |

| | | |
|---|---|---|
| 106067 | 8.65 | 1.799 |
| 106148 | 6.58 | 0.535 |
| 106163 | 8.38 | 0.965 |
| 106184 | 8.15 | 2.625 |
| 106223 | 6.7 | 0.643 |
| 106258 | 9.39 | 1.811 |
| 106259 | 9.0 | 1.447 |
| 106371 | 6.42 | 0.426 |
| 106424 | 9.05 | 1.946 |
| 106464 | 9.05 | 0.896 |
| 106553 | 8.5 | 0.883 |
| 106597 | 6.38 | 0.371 |
| 106755 | 8.99 | 3.522 |
| 106758 | 8.18 | 2.539 |
| 106871 | 7.25 | 0.599 |
| 106953 | 7.01 | 0.404 |
| 106969 | 9.65 | 1.874 |
| 106981 | 7.61 | 1.464 |
| 107063 | 8.13 | 1.23 |
| 107083 | 6.53 | 0.631 |
| 107084 | 6.79 | 1.258 |
| 107097 | 7.16 | 3.101 |
| 107127 | 6.72 | 0.818 |
| 107232 | 7.97 | 5.54 |
| 107238 | 9.06 | 3.426 |
| 107268 | 8.86 | 1.31 |
| 107311 | 6.8 | 0.972 |
| 107324 | 9.08 | 0.973 |
| 107336 | 9.24 | 1.821 |
| 107386 | 7.54 | 0.761 |
| 107410 | 9.09 | 1.06 |
| 107498 | 7.61 | 1.175 |
| 107531 | 7.76 | 2.181 |
| 107555 | 6.62 | 1.808 |
| 107575 | 6.98 | 4.289 |
| 107606 | 6.31 | 0.791 |
| 107608 | 9.63 | 7.655 |
| 107610 | 8.17 | 1.284 |
| 107627 | 7.05 | 0.874 |
| 107683 | 9.94 | 1.504 |
| 107697 | 9.47 | 1.062 |
| 107724 | 8.65 | 1.237 |
| 107750 | 6.44 | 3.209 |
| 107766 | 7.95 | 1.068 |
| 108024 | 7.46 | 0.914 |
| 108084 | 9.16 | 2.34 |
| 108086 | 6.9 | 0.549 |
| 108180 | 6.49 | 0.852 |
| 108312 | 7.31 | 0.411 |
| 108327 | 6.51 | 1.617 |
| 108339 | 7.41 | 4.79 |
| 108340 | 6.83 | 1.222 |

| | | |
|---|---|---|
| 108401 | 7.18 | 0.844 |
| 108414 | 7.59 | 0.952 |
| 108415 | 6.47 | 1.204 |
| 108482 | 7.33 | 0.491 |
| 108485 | 8.13 | 0.499 |
| 108622 | 6.99 | 0.982 |
| 108746 | 7.77 | 1.057 |
| 108786 | 7.03 | 0.282 |
| 108830 | 6.83 | 0.405 |
| 108856 | 6.48 | 0.788 |
| 108862 | 6.4 | 0.89 |
| 108976 | 8.19 | 1.38 |
| 109145 | 8.32 | 1.04 |
| 109167 | 7.86 | 0.582 |
| 109234 | 7.94 | 0.522 |
| 109251 | 6.52 | 0.962 |
| 109257 | 7.35 | 0.543 |
| 109277 | 7.02 | 0.887 |
| 109412 | 9.24 | 2.475 |
| 109418 | 7.94 | 1.641 |
| 109442 | 9.0 | 2.185 |
| 109493 | 7.8 | 3.366 |
| 109523 | 8.35 | 0.628 |
| 109546 | 6.63 | 0.865 |
| 109682 | 6.41 | 0.845 |
| 109755 | 8.99 | 1.201 |
| 109775 | 6.89 | 0.791 |
| 109819 | 8.88 | 0.749 |
| 109893 | 6.34 | 0.627 |
| 109939 | 8.25 | 2.452 |
| 109952 | 9.6 | 1.226 |
| 109969 | 6.99 | 0.472 |
| 109992 | 8.51 | 1.509 |
| 110036 | 7.63 | 1.559 |
| 110121 | 7.25 | 0.685 |
| 110152 | 6.88 | 0.848 |
| 110203 | 7.6 | 0.708 |
| 110372 | 6.35 | 1.162 |
| 110378 | 6.64 | 1.059 |
| 110383 | 7.4 | 2.091 |
| 110390 | 6.55 | 0.51 |
| 110422 | 9.95 | 0.908 |
| 110434 | 6.93 | 1.419 |
| 110465 | 9.78 | 1.523 |
| 110479 | 7.69 | 0.754 |
| 110507 | 7.25 | 0.546 |
| 110517 | 6.76 | 0.45 |
| 110522 | 8.96 | 1.818 |
| 110578 | 7.69 | 3.098 |
| 110584 | 6.73 | 0.712 |
| 110624 | 8.89 | 1.48 |
| 110746 | 6.59 | 2.041 |

| | | |
|---|---|---|
| 110792 | 8.09 | 0.621 |
| 110829 | 6.52 | 0.457 |
| 110842 | 7.81 | 1.876 |
| 110982 | 7.4 | 0.606 |
| 111018 | 6.61 | 1.245 |
| 111032 | 8.61 | 1.119 |
| 111041 | 8.69 | 1.798 |
| 111127 | 8.64 | 1.3 |
| 111132 | 6.36 | 0.4 |
| 111142 | 9.43 | 0.957 |
| 111167 | 7.37 | 0.957 |
| 111191 | 8.0 | 3.107 |
| 111212 | 6.91 | 0.549 |
| 111307 | 6.83 | 0.857 |
| 111392 | 8.67 | 0.583 |
| 111411 | 8.4 | 1.359 |
| 111527 | 7.53 | 0.842 |
| 111583 | 7.39 | 0.683 |
| 111601 | 8.68 | 1.948 |
| 111619 | 6.72 | 0.783 |
| 111684 | 9.2 | 0.929 |
| 111789 | 6.45 | 1.02 |
| 111809 | 7.5 | 4.077 |
| 111837 | 6.4 | 0.314 |
| 112003 | 6.38 | 0.435 |
| 112071 | 6.64 | 0.682 |
| 112079 | 8.93 | 0.957 |
| 112099 | 7.77 | 1.249 |
| 112140 | 9.87 | 1.218 |
| 112179 | 8.87 | 1.706 |
| 112258 | 7.03 | 0.383 |
| 112281 | 9.88 | 1.411 |
| 112355 | 9.99 | 3.136 |
| 112500 | 6.92 | 1.9 |
| 112502 | 7.56 | 0.831 |
| 112518 | 6.74 | 1.437 |
| 112525 | 7.79 | 2.381 |
| 112582 | 6.61 | 0.564 |
| 112671 | 7.09 | 0.733 |
| 112674 | 6.78 | 0.611 |
| 112694 | 9.98 | 2.261 |
| 112705 | 9.13 | 0.793 |
| 112725 | 9.81 | 1.725 |
| 112754 | 6.32 | 0.374 |
| 112769 | 8.01 | 0.723 |
| 112775 | 7.25 | 0.703 |
| 112883 | 7.57 | 1.468 |
| 112900 | 7.26 | 1.352 |
| 113028 | 9.19 | 2.074 |
| 113039 | 7.73 | 0.987 |
| 113211 | 7.45 | 1.241 |
| 113300 | 7.04 | 0.355 |

| | | |
|---|---|---|
| 113351 | 6.76 | 1.895 |
| 113391 | 7.79 | 0.517 |
| 113487 | 6.31 | 1.143 |
| 113564 | 7.49 | 1.473 |
| 113606 | 7.48 | 0.662 |
| 113649 | 7.24 | 0.77 |
| 113656 | 6.34 | 0.605 |
| 113664 | 7.26 | 2.511 |
| 113665 | 7.16 | 1.882 |
| 113673 | 9.97 | 2.945 |
| 113672 | 7.62 | 0.615 |
| 113788 | 9.33 | 8.886 |
| 113960 | 7.19 | 0.712 |
| 113967 | 9.72 | 1.741 |
| 114019 | 6.73 | 0.912 |
| 114031 | 8.09 | 1.302 |
| 114051 | 9.23 | 0.764 |
| 114164 | 8.26 | 0.886 |
| 114182 | 6.66 | 1.136 |
| 114184 | 8.85 | 1.07 |
| 114185 | 6.52 | 0.483 |
| 114187 | 6.64 | 2.514 |
| 114194 | 6.59 | 1.126 |
| 114262 | 7.25 | 0.773 |
| 114351 | 7.33 | 0.5 |
| 114358 | 6.95 | 0.891 |
| 114371 | 9.45 | 1.889 |
| 114547 | 7.46 | 0.353 |
| 114700 | 7.38 | 1.736 |
| 114705 | 9.06 | 0.81 |
| 114714 | 7.94 | 1.975 |
| 114745 | 7.16 | 2.986 |
| 114752 | 9.25 | 1.272 |
| 114774 | 7.48 | 0.965 |
| 114802 | 7.63 | 1.18 |
| 114804 | 7.7 | 1.062 |
| 114991 | 6.37 | 0.747 |
| 115015 | 8.37 | 2.39 |
| 115034 | 7.67 | 0.633 |
| 115065 | 6.9 | 4.478 |
| 115110 | 8.47 | 0.872 |
| 115120 | 7.96 | 2.589 |
| 115128 | 7.32 | 1.54 |
| 115209 | 6.4 | 0.461 |
| 115238 | 6.85 | 0.6 |
| 115255 | 7.97 | 1.102 |
| 115263 | 8.73 | 0.763 |
| 115316 | 7.07 | 1.803 |
| 115326 | 6.56 | 0.43 |
| 115394 | 8.03 | 0.341 |
| 115428 | 7.54 | 1.07 |
| 115627 | 7.34 | 0.938 |

| | | |
|---|---|---|
| 115646 | 6.52 | 1.995 |
| 115667 | 6.76 | 1.058 |
| 115698 | 6.54 | 0.872 |
| 115711 | 7.38 | 0.636 |
| 115742 | 8.46 | 1.916 |
| 115796 | 9.61 | 1.308 |
| 115806 | 8.89 | 2.445 |
| 115820 | 7.22 | 1.262 |
| 115858 | 8.29 | 1.762 |
| 115908 | 8.58 | 2.654 |
| 115927 | 6.89 | 0.462 |
| 116065 | 7.37 | 0.904 |
| 116078 | 9.12 | 0.655 |
| 116088 | 6.96 | 0.538 |
| 116119 | 6.78 | 1.997 |
| 116204 | 6.51 | 1.649 |
| 116205 | 6.71 | 0.567 |
| 116225 | 7.58 | 1.226 |
| 116233 | 8.83 | 0.855 |
| 116245 | 8.55 | 1.38 |
| 116265 | 6.58 | 1.953 |
| 116321 | 8.1 | 1.21 |
| 116434 | 8.45 | 1.198 |
| 116592 | 8.97 | 2.314 |
| 116695 | 6.69 | 0.882 |
| 116715 | 6.85 | 1.009 |
| 116761 | 8.68 | 1.306 |
| 116835 | 6.49 | 0.752 |
| 116860 | 8.19 | 0.691 |
| 116998 | 6.55 | 1.266 |
| 117092 | 7.35 | 0.771 |
| 117127 | 7.24 | 0.586 |
| 117129 | 6.56 | 1.394 |
| 117208 | 7.21 | 0.507 |
| 117214 | 7.23 | 0.509 |
| 117231 | 8.12 | 0.724 |
| 117345 | 7.45 | 0.763 |
| 117346 | 6.34 | 0.375 |
| 117352 | 8.04 | 1.086 |
| 117442 | 7.29 | 0.619 |
| 117479 | 8.88 | 1.184 |
| 117510 | 8.24 | 2.234 |
| 117535 | 6.93 | 0.798 |
| 117746 | 7.87 | 0.945 |
| 117754 | 7.53 | 0.968 |
| 117774 | 7.06 | 2.124 |
| 117838 | 7.68 | 0.326 |
| 117856 | 6.47 | 0.85 |
| 117892 | 8.18 | 0.708 |
| 117897 | 7.02 | 0.658 |
| 117962 | 7.51 | 1.301 |
| 117998 | 7.32 | 0.628 |

| | | |
|---|---|---|
| 118007 | 6.86 | 1.884 |
| 118177 | 7.55 | 2.535 |
| 118198 | 6.53 | 0.773 |
| 118241 | 9.44 | 0.415 |
| 118253 | 7.85 | 0.62 |
| 118257 | 7.36 | 0.887 |
| 118275 | 8.11 | 0.791 |

# acknowledge

My deepest appreciation goes to Prof. Hirokazu Kataza who provided helpful comments and suggestions as my supervisor. I would also particularly like to thank Dr. Takehiko Wada whose opinions and information have helped me very much throughout the production of this study. I thank Dr. Shuji Matsuura, Takao Nakagawa, Mitsunobu Kawada, Satoshi Takita, and the other members of Laboratory of Infrared Astrophysics/ Institute of Space and Astronautical Science for supporting my work. I also appreciate Dr. Yasuo Doi for giving me an opportunity to make this work. Finally, I wish to thank my family and friends for their support.

# References


Akeson, R. L. et al. 2009, A&A, 474, 653

Andrews, S. M., & Williams, J. P. 2007, ApJ, 671, 1800

Arimatsu, K., Izumiura, H., Ueta, T., Yamamura, I., Onaka, T. 2011, ApJ, 729, 19

Arimatsu, K., et al. 2011, PASP, 123, 906

Arimatsu, K., et al. 2012, Proceedings of the International Astronomical Union, IAU Symposium, 284, 210

Arimatsu, K., et al. 2014, PASJ, 66, 47

Aumann, H. H., Beichman, C. A., Gillett, F. C. et al., 1984, ApJ, 278, L23

Backman, D. E., Dasgupta. A., & Stencel, R. E. 1995, ApJ, 450, L35

Beichman, C. A., Neugebauer, G., Habing, H. J., Clegg, P. E., & Chester, T. J. 1988, Infrared Astronomical Satellite (IRAS) Catalogs and Atlases. Volume 1: Explanatory Supplement (Washington, DC: US GPO)

Ben-Jaffel, L., & Ratkiewicz, R. 2012, A&A, 546, 78

Belyaev M., & Rafikov R. 2010, ApJ, 723, 1718

Bernstein, G. M. et al. AJ, 128, 1364

Bournaud, F. et al. 2012, ApJ, 757, 19

Boyajian, T. S., et al., 2013, ApJ, 771, 40

Brown, M. E., Trujillo, C., & Rabinowitz, D. 2004, ApJ, 617, 645

Brown, M. 2008, In *The Solar System Beyond Neptune* Barucci, M.A., Boehnhardt, H., Cruikshank, D.P., Morbidelli, A. Ed, 335

Cantalupo, C., Borrill, J. D., Jaffe, A. H., et al. 2010, ApJS, 187, 212

Carson J. et al. 2012, ApJ, 763, L32

Cassan, A. et al. 2012, Nature, 481, 167

Cohen, M., Walker, R. G., Carter, B., Hammersley, P., Kidger, M., & Noguchi, K. 1999, AJ, 117, 1864

Doi, Y., et al. 2009, Astronomical Society of the Pacific Conference Series, 418, 387

Doi, Y., et al. 2012, PKAS, 27, 111

Dones, L., Weissman, P. R., Levison, H. F., and Duncan, M. J. 2004, In Michel C. Festou; H. Uwe Keller; Harold A. Weaver. Comets II. University of Arizona Press.,

Draine, B. T. & Li, A. 2007, ApJ, 657, 810

Draine, B. T. 2010, *Physics of the Interstellar and Intergalactic Medium Princeton*, Princeton Univ. Press

Duncan M., Quinn T., and Tremaine S. 1987, AJ, 94, 1330

Duncan M., Quinn T., & Tremaine S. 1988, ApJ, 328, L69

Duncan, M. J., & Levison, H. F. 1997, Science, 276, 1670

Duncan M. J., Levison H. F., and Dones L. In Michel C. Festou; H. Uwe Keller; Harold A. Weaver. Comets II. University of Arizona Press., 153

Eggl, S., Pilat-Lohinger, E., Funk, B., Georgakarakos, N., Haghighipour, N. 2013, MNRAS, 428, 3104

Eiroa, C., et al. 2011, A&A, 536, L4

Eiroa, C., et al. 2013, A&A, 536, id.11

Fernández J. A. 1980 MNRAS, 192, 481

Fernández J. A., Gallardo, T., & Brunini, A. 2004, Icarus, 172, 372

Frisch, P. C., Dorschner, J. M., Geiss, J., et al. 1999, ApJ, 525, 492

Frisch, P. C., et al. 2009, Space Sci. Rev., 146, 235

Giard, M., Montier, L., Pointecouteau, E., & Simmat, E. 2008, A&A, 490, 547

Ginestet, N., Carquillat, J. M., Jaschek, C., & Jaschek, M. 1997, A&AS, 123, 135

Gomes, R. S., Fern Ndez, J. A., Gallardo, T., & Brunini, A. 2008, In *The Solar System Beyond Neptune* Barucci, M.A., Boehnhardt, H., Cruikshank, D.P., Morbidelli, A. Ed, 259

Gorjian, V., Wright, E. L., & Chary, R. R. 2000, ApJ, 536, 550

Gray, R. O., Napier, M. G., Winkler, L. I. 2001, AJ, 121, 2148

Gray, R. O. et al., 2003, AJ, 126, 2048

Gray, R. O. et al., 2006, AJ, 132, 161

Greenwood, J. P., Itoh S., Sakamoto, N., Warren, P., Taylor, L., & Yurimoto, H. 2011, Nature Geoscience, 4, 79

Harrington, R. S. 1985, Icarus, 61, 60

Hayashi, C. 1981, Prog. Theor. Phys. Suppl., 70, 35

Heisler, J., & Tremaine, S. 1986, Icarus, 65, 13

Helmut, A. A., & Nidia, M. I. 1995, ApJS, 99, 135

Helmut, A. A. 2008, ApJS, 176, 216

Higuchi, A., Kokubo, E., & Mukai, T. 2006, AJ, 131, 1119

Hills J. G. 1981, AJ, 86, 1730

Holmberg J. & Flynn C. 2000, MNRAS, 313, 209

Houk, N. 1982, Michigan Catalog of Two-dimensional Spectral Types for HD Stars, Vol. 3 (Ann Arbor: Univ. Michigan Dept. Astron.)

Houk, N., & Smith-Moore, M. 1988, Michigan Catalog of Two-dimensional Spectral Types for HD Stars, Vol. 4 (Ann Arbor: Univ. Michigan Dept. Astron.)

Howard, A. W. 2013, Science, 340, 572

Howe, A. R., Rafikov, R. R. 2014, ApJ, 781, id 52

Ibar E. et al., 2010, MNRAS, 409, 38

Jauzac, M. et al. 2011, A&A, 525, 52

Jewitt, D. & Luu, J. 1993, Nature, 362, 730

Jewitt, D. C. & Delsanti A. 2006, In *Solar System Update : Topical and Timely Reviews in Solar System Sciences.* Springer-Praxis Ed, 267

Joss P. C. 1973, A&A, 25, 271

Kalas, P. et al. 2008. Science, 322, 1345

Kaneda, H., Okamura, Y., Nakagawa, T., & Shibai, H. 2002, Adv. Space Res., 30, 2105

Kashiwagi, T., Yahata, T., & Suto, Y. et al. 2012, PASJ, 65, 12

Kawada, M. et al. 2007, PASJ, 59, 389

Kenyon, S. J., Bromley, B. C., O'Brien, D. P., & Davis, D. R., 2008, In *The Solar System Beyond Neptune* Barucci, M.A., Boehnhardt, H., Cruikshank, D.P., Morbidelli, A. Ed, 293

Kerschbaum, F., et al. 2010, A&A, 48, L140

Kurucz, R. L. 1992, IAU Symposium, 149, 225

Lallement, R. 1998, in IAU Colloq. 166, The Local Bubble and Beyond, ed. D. Breitschwerdt, M. J. Freyberg, & J. Truemper (New York: Springer), 19

Landgraf, M., Baggaley, W. J., Grun, E., Kruger, H., & Linkert, G. 2000, J. Geophys. Res., 105, 10343

Laor, A., & Draine, B.T. 1993, ApJ, 402, 2, 441

Lejeune, T., & Schaerer, D. 2001, A&A, 366, 538

Levison H. F., Dones L., & Duncan M. J. 2001, AJ, 121, 2253

Levison, H.F., Duncan, M.J., Brasser, R., & Kaufmann, D.E. 2010, Science 329, 187

Liu, Q., Tinggui, W., Peng, J. 2014, AJ, 148, 3

Malagnini, M. L., & Morossi, C. 1990, A&AS, 85, 1015

Mannings, V., Sargent, A., I. 1997, ApJ, 490, 792

Mannings V, Barlow M. J. 1998, ApJ, 497, 330

Marios, C. et al. 2008, Science, 322, 1348

Marshall, J. P., et al. 2014, A&A, 565, id.A15

Mathis, J. S., Mezger, P. G., and Panagia, N. 1983, A&A, 128, 212

Matsuura, S., et al. 2011, ApJ, 737, 2

Ménard, B., Kilbinger, M., Scranton, R. 2010, MNRAS, 406, 1815

Morales, F. Y., Rieke, G. H., Werner, M. W., et al. 2011, ApJ, 730, L29

Murakami, H. et al. 2007, PASJ, 59, S369

Neugebauer, G., et al. 1984, ApJ, 278, L1

Nakagawa, T., Matsuhara, H., & Kawakatsu, Y. 2012, Proc. SPIE, 8442

Oort, J. H. 1950, Bull. Astron. Inst. Neth. 11, 91

Oudmaijer, R. D., van der Veen, W. E. C. J., Waters, L. B. F. M., et al. 1992, A&AS, 96, 625

Perryman, M. A. C., et al., 1997, A&A, 23, L49

Petit, J.-M., Kavelaars, J. J., Gladman, B. J., et al. 2011, AJ, 142, 131

Phillips, N. M., Greaves, J. S., Dent, W. R. F., Matthews, B. C., Holland, W. S., Wyatt, M. C., & Sibthorpe, B. 2010, MNRAS, 403, 1089

Pilbratt, G. L., Riedinger, J. R., Passvogel, T., et al. 2010, A&A, 518, L1

Poglitsch, A., Waelkens, C., Geis, N., et al. 2010, A&A, 518, L2

PRISM Collaboration, 2013, arXiv:1310.1554

Robrade, J., & Schmitt, J. H. M. M. 2011, A&A, 531, 58

Roussel, H. 2013, PASP, 125, 1126

Schlichting, H. E., Ofek, E. O., Wenz, M., et al. 2009, Nature, 462, 895

Schlichting, H. E., Ofek, E. O., Sari, R., et al. 2012, ApJ, 761, 150

Schwamb, M., Brown, M., & Rabinowitz, D. 2009, ApJ, 694, L45

Schwamb, M., Brown, M., Rabinowitz, D., & Ragozzine, D. 2010, ApJ, 720, 1691

Seifahrt, A. et al., 2010, A&A, 524, 11

Shirahata, M. et al. 2009, PASJ, 61, 737

Shirahata, M., et al. 2004, Proc. SPIE, 5487, 369

Smith, B. A., & Terrile, R. J. 1984. Science 226, 1421

Spitzer, L. 1978, in *Physical Processes in the Interstellar Medium*, Wiley-Interscience

Stansberry, J. A., et al. 2007, PASP, 119, 1038

Stern, S. A. 1995, AJ, 110, 856

Stern, S. A. 1996, A&A, 310, 999

Stern, S. A. 2003, Nature, 424, 639

Stern S. A., Stocke, J., Weissman P. R. 1991, Icarus, 91, 65

Su K. Y. L., et al., 2006, ApJ, 653, 675

Suzuki, T., Kaneda, H., Matsuura, S., et al. 2008, PASP, 120, 895

Tanner, A., Beichman, C., Bryden, G., Lisse, C., & Lawler, S. 2009, ApJ,704, 109

Thompson, M. A., et al. 2010. A&A, 518, L34

Thureau, N. D., et al. 2014, MNRAS, 445, 2558

Trujillo, C., & Brown, M. 2003, Earth Moon Planet, 92, 99

van Belle, G. T. & von Braun, K. 2009, ApJ, 694, 1085

Verdugo, E., Yamamura, I., & Pearson, C. 2007
*AKARI FIS Data User Manual Version 1.3*
`http://www.ir.isas.jaxa.jp/AKARI/Observation/IDUM/FIS_IDUM_1.3.pdf`

Vicente, S. M., & Alves, J. 2005, A&A, 441, 195

Vieira, S. L. A., Corradi, W. J. B., Alencar, S. H. P., Mendes, L. T. S., Torres, C. A. O., Quast, G. R., Guimar es, M. M., & da Silva, L. 2003, AJ, 131, 1163

Volk, K. & Malhotra, R. 2008, ApJ, 687, 714

Weidenschilling S. 2003, In Michel C. Festou; H. Uwe Keller; Harold A. Weaver. Comets II. University of Arizona Press., Weingartner, J. C., & Draine, B. T. 2001, ApJ, 548, 296

Weissman P. R. 1996, ASP Conference Series 107, 265

Werner M. W., et al. 2004. ApJS, 154,1

Woody, D., et al. 2012, Proc. SPIE, 8444

Wright, E. L., et al. 2010, AJ, 140, 1868

Wyatt, M. C. 2008, Annu. Rev. Astronomy and Astrophysics, 46, 339

Yamamoto, S., & Mukai, T. 1998, Earth Planets Space, 50, 531

Yamamura, I., et al. 2009, Astronomical Society of the Pacific Conference Series, 418, 3

Yamamura, I., Makiuti, S., Ikeda, N., Fukuda, Y., Oyabu, S., Koga, T. & White, G. J. 2010 *AKARI/FIS All-Sky Survey Bright Source Catalogue Version 1.0 Release Note* `http://irsa.ipac.caltech.edu/data/AKARI/documentation/AKARI-FIS\_BSC\_V1\_RN.pdf`

Zhang, Z.-W. et al. 2013, AJ, 146, 14

Zorec, J., et al., 2009, A&A, 501, 297